Probability-based strength reassessment of corroded FPSOs using monitored loads

Francesco Petillo

Delft University of Technology

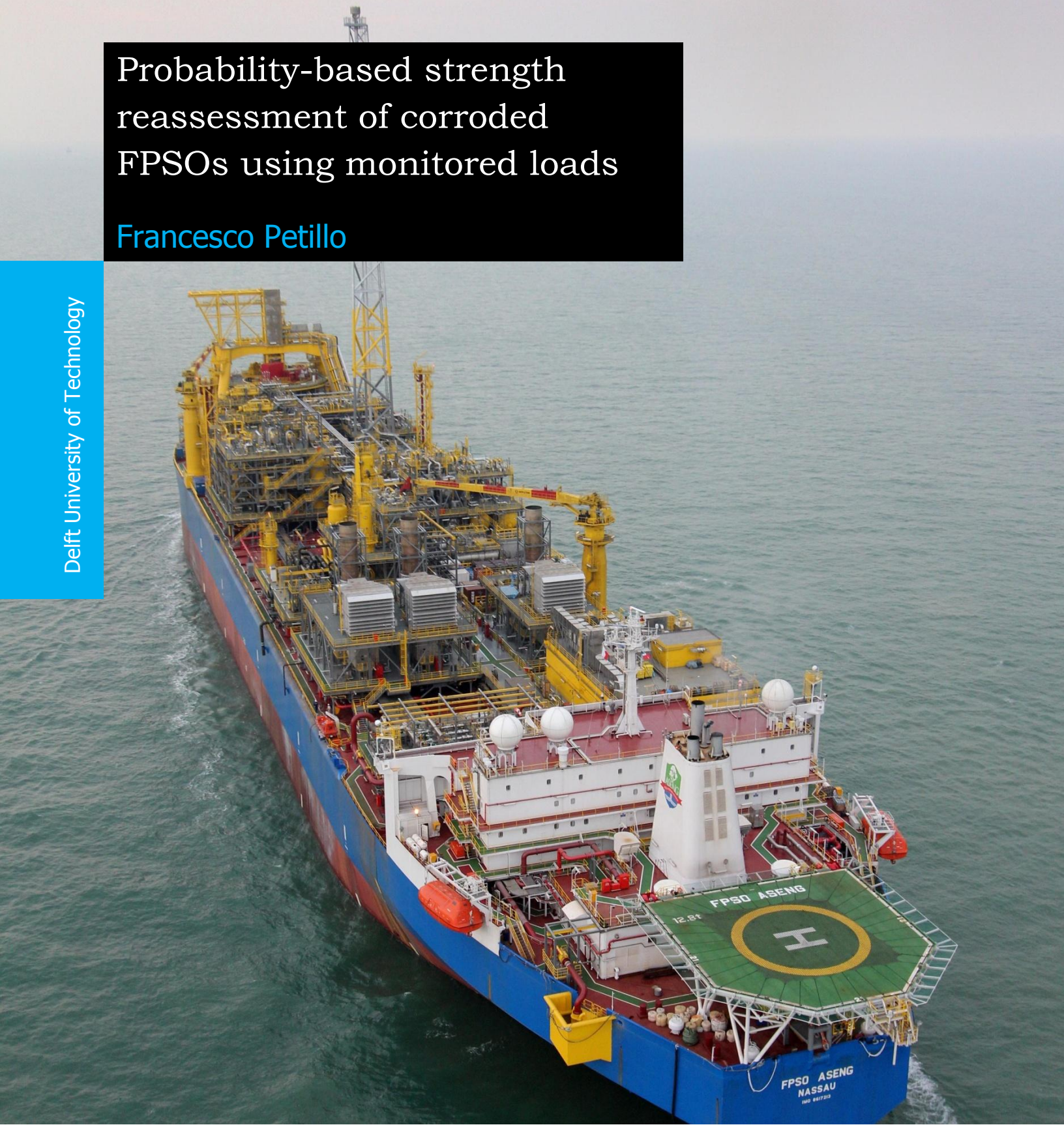

TU Delft Delft University of Technology

Challenge the future

Probability-based strength reassessment of corroded FPSOs using measured loads

by

Francesco Petillo

in partial fulfilment of the requirements for the degree of

Master of Science

in Maritime Technology - Ship and Offshore Structures

at the Delft University of Technology,

to be defended publicly on Wednesday February 25th, 2015 at 4:00 PM.

Supervisors:	Prof. dr. ir. L. M. Kaminski	TU Delft
	Ir. R. Hagemann	MARIN
Thesis committee:	Prof. dr. ir. P. Van Gelder	TU Delft
	Ir. M. Tammer	TU Delft

This thesis is not confidential.

An electronic version of this thesis is available at http://repository.tudelft.nl/.

TU Delft Delft University of Technology

Abstract

FPSOs are nowadays a common practice in the production of oil at sea. These ship-type offshore units, however, cannot have regular dry-docking as they have to be on field sometimes even for their entire lifetime. This is the reason why structural monitoring systems may play an important role in the safety of these units. The structural degradation mechanisms which affect FPSOs are two: fatigue and corrosion. The MONITAS JIP was started in 2005 in order to deal with fatigue. One of the goal of this JIP was the development of a monitoring system able to continuously calculate the fatigue lifetime consumption of the FPSO using some measured loads. However, these extensive measurements can be used for other purposes as well. In this work, the strength reassessment of a corroded FPSO tank has been addressed. For this purpose, thickness measurements coming from the inspections and the loads measured by the MONITAS system have been combined in a new probability-based model, which is able to calculate the probability of failure for the inspected structure. Both the thickness measurements and the MONITAS data have to be properly processed before entering the structural reliability model. Different failure criteria (yielding, elasto-plastic buckling, brittle fracture) have been identified, and for any of them a closed-form limit state function has been written down. To write down the limit state functions, analytical models (simple beam theory, classical plate theory, large deflection analysis, membrane stress-based method and others) and empirical formulae (Johnson-Ostenfeld formula) have been used. The result is a reassessment tool which – if properly combined with a corrosion prediction model - can be used by FPSO operators in order to avoid unnecessary maintenance of a corroded plate, to optimize repair intervention or to justify extra-maintenance. The present work contains also a case study with sensitivity analysis and some ideas for further developments. For the case study, the Monte Carlo simulation method was used to run the reliability analysis.

Table of contents

Abstract 5
Table of contents 7
List of symbols 12
List of abbreviations 17
1. INTRODUCTION 18
1.1. FPSO degradation mechanisms 18
1.2 MONITAS systems 20
1.3 Goal of the master thesis and project set up 21
1.4 Corrosion 23
1.5 Inspections 23
1.6 Structure to analyze 24
1.7 Loads 26
1.8 Failure criteria 27
1.9 Reliability analysis 28
1.10 Summary of main assumptions 28
1.11 Structure of this report 28
References 29
2. THICKNESS MEASUREMENTS PROCESSING 30
2.1 Mean corroded thickness for the different structures 31
2.2 Corrosion trend as a function of the position on the vertical axis 32
2.3 Probability and statistics theoretical background 36
2.3.1 Truncated distribution 36
2.3.2 Methods for estimating parameters and distributions 37
2.3.3 Method of moments for the considered distribution type 38
2.3.4 Method of the maximum likelihood for the considered distribution type 40
2.3.5 Kolmogorov-Smirnov test 43
2.3.6 Least squares method 44
2.3.7 Linearization of the cumulative distribution function 45
2.3.8 Quantile-quantile plot 47
2.4 Results of the distribution estimation 47

2.4.1 Deck plate 48
2.4.2 Web deck longitudinals 54
2.4.3 Flange deck longitudinals 57
2.4.3 Summary of the results 58
References 58
3. MODELLING LOAD VARIABLES 59
3.1 MONITAS monitored data 59
3.2 Long term distribution for wave induced loads 60
3.3 Modelling uncertainties for traditional cargo ships 60
3.3.1 Statistical uncertainties 61
3.3.2 Modelling uncertainties 62
3.4 Loads combination 64
3.5 Loads identification for FPSOs endowed with AHMS 65
3.5.1 Still water bending moment 65
3.5.2 Vertical wave bending moment 66
3.5.3 Horizontal wave bending moment 67
3.5.4 Static sea pressure 67
3.5.5 Dynamic sea pressure on the side 67
3.5.6 Cargo/ballast static pressure 68
3.5.7 Cargo/ballast dynamic pressure 68
3.5.8 Load combination factor 68
3.5.9 Material properties and constructional parameters 69
3.5.10 Corroded thickness 70
References 71
4. LIMIT STATE FUNCTIONS 73
4.1 Introduction 73
4.1.1 Sign convention and reference system 74
4.2 Effective width and effective breadth 74
4.3 Unstiffened plate limit state functions 75
4.3.1 Yielding of unstiffened plates 76
4.3.2 Plastic hinges formation in unstiffened plates 79

4.3.3 Ultimate collapse of unstiffened plates 84
4.4 Stiffened panel limit state functions 90
4.4.1 First yielding of stiffeners 91
4.4.2 Plastic hinge formation in stiffeners 92
4.4.3 Elasto-plastic buckling of stiffened panels 97
4.4.4 Collapse mode I for a stiffened panels: overall collapse of the plating and stiffeners as a unit 99
4.4.5 Collapse mode II for stiffened panels: yielding along the plate-stiffener intersection .. 105
4.4.6 Collapse mode III for stiffened panels: beam-column type collapse 105
4.4.7 Collapse mode IV for stiffened panels: local buckling of the stiffener web 106
4.4.8 Collapse mode V: flexural-torsional buckling of the stiffeners 109
4.5 Fracture mechanics 112
4.6 ALPS-ULSAP validation 113
4.7 Conclusion and recommendations 115
References 115
5. MONITORED DATA PROCESSING 118
5.1 The loads 118
5.2 Probability and statistics theoretical background 119
5.2.1 Maximum likelihood estimation 119
5.2.2 Linearization of the cumulative distribution function 122
5.3 The SWBM 124
5.4 The VWBM 130
5.5 The HWBM 137
5.6 Correlation between loads 143
5.7 Summary of the results 145
References 145
6. RELIABILITY ANALYSIS 147
6.1 The vessels 147
6.2 Monte-Carlo simulation 149
6.2.1 Generation of random variable for the Monte-Carlo simulation 150
6.3 Correlation between random variables 151
6.4 Load cases 152

6.5 Corrosion prediction model 152
References 155
7. RESULTS AND SENSITIVITY ANALYSIS 156
7.1 Sensitivity analysis 156
7.1.1 Analytical method vs. Jonshon-Ostenfeld formula 156
7.1.2 Effects of the initial corroded thickness on the structural reliability 158
7.1.3 Effects of the load combinations method on the structural reliability 163
7.1.4 Corrosion of the plate vs. Corrosion of the stiffeners 164
7.1.5 Effects of the correlation coefficients on the structural reliability 166
7.1.6 Time-dependent reliability analysis 167
7.2 Comparison with some target reliability indices 168
References 169
8. CONCLUSIONS AND RECOMMENDATIONS 171
8.1 Main findings 171
8.2 Future developments 172
8.2.1 Further improvements 172
8.2.2 Implementation of the reassessment procedure 173
8.2.3 Utilization of the model for research purposes 175
References 176
9. ANNEX A 177
9.1 Kolmogorov-Smirnov tables 177
10. ANNEX B 179
10.1 Statistical uncertainties for FPSO with AHMS 179
10.2 Modelling uncertainties for FPSO with AHMS 180
11. ANNEX C 181
11.1 Generation of uncorrelated random variables 181
11.2 Generation of correlated random variables 182
References 183
12. ANNEX D 184
12.1 Results 184

12.1.1 Analytical method vs. Jonshon-Ostenfeld formula 184
12.1.2 Effects of the initial corroded thickness on the structural reliability 184
12.1.3 Effects of the load combinations method on the structural reliability 188
12.1.4 Corrosion of the plate vs. Corrosion of the stiffeners 192
12.1.5 Effects of the correlation coefficients on the structural reliability 192
12.1.6 Time-dependent reliability analysis 193
12.1.7 Comparison with some target reliability indices 193
References for figures 194

List of symbols

Few symbols have more than one meaning. When these symbols will be used in the text, the actual meaning will be always specified (even when it is already quite clear from the context), so to avoid any ambiguity.

a: in a truncated random variable, one of the two truncation values *or* one of the two dimension of a plate (not necessarily the longest/shortest one) *or* in fracture mechanics, half-length of the crack.

a_{Gumbel}: location parameter Gumbel distribution

$a_{Weibull}$: shape parameter Weibull distribution

b: in a truncated random variable, one of the two truncation values *or* stiffeners spacing *or* one of the two dimension of a plate (not necessarily the longest/shortest one)

b_{eff}: effective breadth *or* effective width (see paragraph 4.2)

b_f: stiffener flange width

b_{Gumbel}: scale parameter Gumbel distribution

$b_{Weibull}$: scale parameter Weibull distribution

c: ratio between σ_y over σ_x *or* in an orthotropic plate analysis, correction $\nu/0.86$

$c.o.v.$: coefficient of variation (i.e. ratio of the standard deviation to the mean)

d_∞: thickness loss for long term corrosion

f: corroded thickness multiplicator factor

f_{plate}: corroded thickness multiplicator factor for the plating

$f_{stiffeners}$: corroded thickness multiplicator factor for stiffeners

$g(x)$: limit state function

h_w: stiffener web height

k: shape parameter gamma distribution *or* buckling coefficient

l: stiffener length

m: buckling half-wave numbers in the *x* direction

n: total number of observations *or* buckling half-wave numbers in the *y* direction

n_F: in the Monte Carlo simulation, number of failures

n_S: number of stiffeners *or* total number of samples in the Monte Carlo simulation

p: significance level (Kolmogorov-Smirnov test)

q: lateral pressure

q_l: equivalent line pressure

s: standard deviation of the observed material

t: time

t_{corr}: corroded thickness

t_f: stiffener flange gross thickness

t_p: plate gross thickness

t_w: stiffener web gross thickness

w: section modulus *or* plate/stiffeners lateral deflection

w: horizontal section modulus

x: coordinate of the plastic neutral axis

$\bar{x}$: mean value of the observed material

x_1: in calculating of the plastic section modulus, coordinate of the local centroid of one of the two area

y_{KS}: Kolmogorov-Smirnov test quantity

z: in calculating of the plastic section modulus, coordinate of the local centroid of one of the two area

A: amplitude of the lateral deflection

A_S: cross sectional area of the stiffener without the attached plate

B: width of the orthotropic plate

B_i: modelling uncertainties for the random variable i

C: capacity of the structure

C_B: block coefficient

D: flexural rigidity of the plate

D_x, D_y: flexural rigidity of the porthotropic late in the x/y direction

E: elasticity modulus

E_x, E_y: elasticity modulus of the orthotropic plate in the x/y direction

F: stress function

$F_X(x)$: cumulative distribution function

$\widehat{F_X}(x)$: empirical cumulative distribution function

G_{xy}: elastic shear modulus of the orthotropic plate

H: effective torsional rigidity of the orthotropic plate

I: moment of inertia

I_{eff}: mass moment of inertia using the effective width

K: stress intensity factor

K_1: in fracture mechanics, stress intensity factor for mode I

K_C: critical fracture toughness

L: loads acting on the structure *or* likelihood function *or* stiffened/unstiffened plate length

M_{max}: maximum bending moment

M_{pm}: plastic bending moment

N_x, N_y: axial load in the x/y direction

P_f: probability of failure

R: correlation matrix

T: shear force

U: standard normal distributed uncorrelated variable

V: uniform distributed uncorrelated variable

X: random variable

Z_{pe}, Z_{pm}: plastic section modulus at the end/middle of the beam

Z_s: section modulus of the stiffener with attached plate

β: plate-slenderness coefficient *or* reliability index

γ: Euler-Mascheroni constant

ϵ_x, ϵ_y: normal strain in the x/y direction

θ: scale parameter gamma distribution

λ: inverse scale parameter of the exponential distribution

μ: mean

$\mu_{t_{corr,flange}}$: mean value corroded thickness of stiffener flange

$\mu_{t_{corr,plate}}$: mean value corroded thickness of the plating

$\mu_{t_{corr,web}}$: mean value corroded thickness of stiffener web

ν: Poisson's ratio

ν_x, ν_y: Poisson's ratio of the orthotropic plate in the x/y direction

ρ: correlation coefficient

$\rho_{plate,web}$: correlation coefficient between the corroded thickness of the plating and the corroded thickness of the stiffener web

$\rho_{plate,flange}$: correlation coefficient between the corroded thickness of the plating and the corroded thickness of the stiffener flange

$\rho_{flange,web}$: correlation coefficient between the corroded thickness of the stiffener flange and the corroded thickness of the stiffener web

σ: standard deviation *or* in fracture mechanics, remote stress.

σ_a: applied stress

σ_E: elastic buckling strength

σ_E^W: elastic buckling strength of the stiffener web

σ_{eq}: equivalent (Von Mises) stress

σ_F: reference yield stress (in the Johnson-Ostenfeld formula)

σ_{ij}: in fracture mechanism, stress acting on a plate element at a distance r from crack tip and at angle θ from crack plane (see chapter 4, fig. 20)

σ_n: stress induced by an axial load N_x/N_y

σ_{perm}: permissible stress

σ_u: ultimate strength

σ_u^T: ultimate strength of the stiffener bracuse of lateral-torsional buckling or tripping

σ_u^W: ultimate strength of the stiffener because of web buckling

$\sigma_x,\ \sigma_y$: stress in the x/y direction

σ_{x1}, σ_{x2}: in a stiffened panel, stresses in the x direction at the corners of the plate

$\sigma_{xav},\ \sigma_{yav}$: average stress in the x/y direction

σ_{xu}: ultimate strength in the x direction

σ_{xu}^P: ultimate strength of the plating between stiffeners

σ_{y1}, σ_{y2}: in a stiffened panel, stresses in the y direction at the corners of the plate

σ_Y: yielding stress

$\sigma_Y{}'$: equivalent yielding stress (if shear stress would be considered)

σ_{Yeq}: equivalent yielding stress (if the stiffeners and the plate have different yielding stress)

σ_{Yp}: yielding stress plate

σ_{Ys}: yielding stress stiffener

τ_c: lifetime of the coating

τ_t: transition time

τ_{xy}: shear stress

$\Gamma(k)$: gamma function

Φ: standard normal cumulative distribution function

List of abbreviations

AHMS: Advisory Hull Monitoring System

ALPS: Analysis of Large Plated Structures

CDF: Cumulative Distribution Function

C.O.V.: Coefficient of variance

CS: Class society

DNV: Det Norske Veritas (international class societies)

FORM: First order reliability method

FPSO: Floating Production Storage Offloading

HWBM: Horizontal Wave Bending Moment

IRM: Inspection Repair Maintenance

KV: Kolmogorov-Smirnov

LBSG: Long Base Strain Gauge

LSF: Limit state function

MCS: Monte Carlo Simulation

MLE: Maximum likelihood estimation

Pdf: probability density function

RBI: Risk Based Inspection

RV: Random variable

RWA: Relative wave amplitude

SLS: Serviceability limit state

SORM: Second order reliability method

SS: Sum of squares

SWBM: Still Water Bending Moment

ULS: Ultimate limit state

ULSAP: Ultimate Limit State Assessment Program

VWBM: Vertical Wave Bending Moment

1

Introduction

In the recent years, improvements in the sensor technology, data acquisition, data communication, GPS and data storage, led to the development of more and more sophisticated structural monitoring systems for offshore structures. These systems can be used to rationally extend the lifetime of the monitored structure, to prevent failures, to improve the Inspection, Repair & Maintenance (IRM) plan, to get useful knowledge for future designs and, in case of structural failure, can be used as "black box" in a post-event analysis.

The present work introduces a new way to estimate the structural reliability of a corroded FPSO, combining thickness measurements coming from inspections and loads measured by an already operative fatigue monitoring system, the Advisory Hull Monitoring System MONITAS.

1.1. FPSO degradation mechanisms

Ship-type offshore units are nowadays a common practice in the production and storage of oil at sea. They are usually preferred to other kinds of production facilities for the simplicity of the installation procedures and for their storage capacity (which does not make necessary the installation of a pipeline infrastructure). They can be either new-built structures, or converted tankers. In August 2012, 156 FPSO were operative worldwide ([1]).

FPSOs are endowed with a processing equipment to separate crude oil, water and gas. Treated oil is then transferred to cargo tanks in the ship's hull, while gas is either used as fuel on-board or re-injected into the reservoir or exported to shore via pipeline. The stored oil is then transferred to a shuttle tanker, which brings it to refineries.

Figure 1 - FPSO

Due to the fact that FPSOs have to be for years at the same location (sometimes even for its whole lifetime) without regular dry-docking, a good structural monitoring system plays an important role in their safety. In particular, it becomes critical to monitor the vessel with respect to its main two structural degradation mechanisms: fatigue and corrosion.

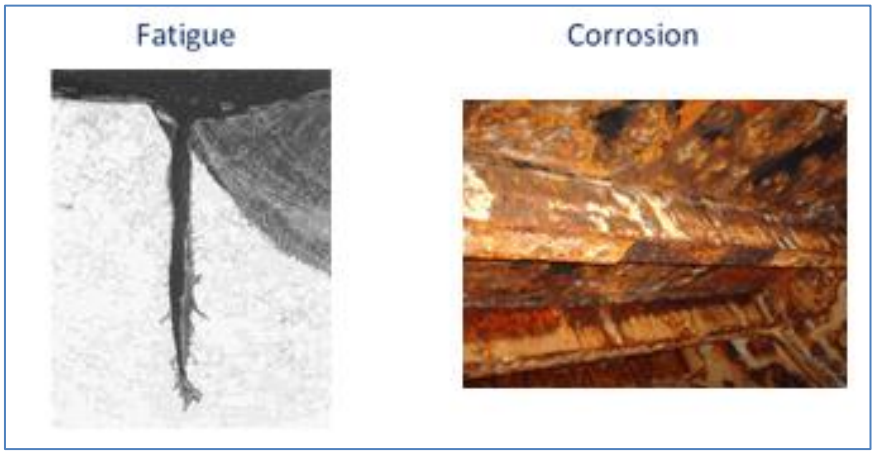

Figure 2 - FPSO hull degradation mechanisms

The former is the phenomenon by which a crack may originate and propagate in the structure under the action of a cyclic load. FPSO designers are always very concerned with fatigue, as the magnitude of uncertainties, in both the fatigue resistance and fatigue loads, is very high (Kaminski, [2]). This is one of the reason why the MONITAS JIP was set up by MARIN together with other international companies. This system is able to predict the fatigue lifetime of the unit, to compare it with the design estimated lifetime, and also to explain “why” the first one is different from the second.

On the other hand, the way by which the effects of corrosions are taken into account by designers is through some extra thickness to add to the structural elements as corrosion allowance. The corrosion allowances are typically in the range of 0.5-2.0 millimeters, depending on the importance of the structural element and on the environment that it is facing.

1.2 MONITAS systems

The MONITAS system is a fatigue monitoring system which is able to monitor some loads acting on the structure, and to use them to recalculate the fatigue lifetime consumption, using the same fatigue tool used in the design. The factors which are monitored by the MONITAS system and which are used to recalculate the fatigue lifetime consumption are given below:

1. draft;
2. wave height and peak period, for both wind-sea and swell;
3. 6 DOF motions of the vessel and accelerations;
4. FPSO orientation;
5. relative wave height.

The MONITAS is then able to compare the design lifetime consumption with the new calculated lifetime consumption. Furthermore, MONITAS is also able to say "why" there is such a difference. In order to do that, it calculates the fatigue lifetime consumption using the measured data for all input parameter's except one, where it keeps the design assumed value. This procedure is iterated for all input parameters. In this way we are able to say which of the "wrong" assumption made during the design has a major influence on the difference between design lifetime consumption and calculated design consumption.

Besides that, also stresses (in location free of stress concentration and preferably caused by one dominant mechanism) are recorded by some strain gauges. These stresses are then processed (rainflow counting) in order to transform them into a simple set of stress ranges. Fatigue lifetime consumption is then calculated one more time using these stress cycles as a input. A comparison between this new lifetime consumption ("measured lifetime consumption") and the calculated lifetime consumption is giving us feedback on the precision of the fatigue design tool.

To sum up, in the MONITAS system we compare the followings:

1. the "design fatigue": lifetime consumption calculated using design assumed value;
2. the "calculated fatigue": lifetime consumption calculated using measured loads;
3. the "measured fatigue": lifetime consumption calculated from measurements of strain cycles.

An example of a MONITAS output is given in figure 3.

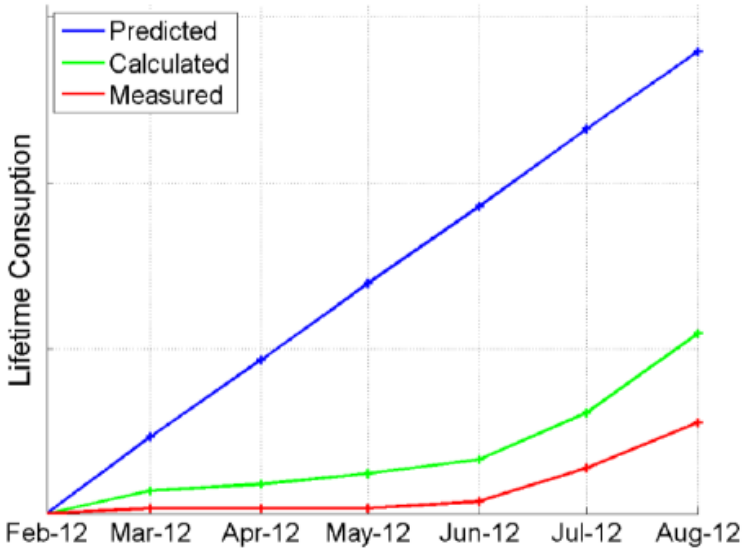

Figure 3 - MONITAS output

1.3 Goal of the master thesis and project set up

The current practice to check the structural reliability of a corroded FPSO is based on the comparison between the average of the measured thicknesses of a corroded plate and a certain threshold value (net thickness, or net thickness plus a percentage of the corrosion allowance). There are then quite large margins of improvements in the reassessment of a corroded FPSO, and this is indeed the procedure which this thesis is going to improve.

An improvement of this reassessment can be done by using:

1. the MONITAS data for loads;
2. a probability distribution of thicknesses for each plate rather than the average value;
3. a probability-based approach.

In other words, the goal of this Master Thesis is to find a way to evaluate the strength of a corroded FPSO using the real thicknesses, coming from inspections, and the real loads, coming from the MONITAS monitoring system. These two sets of data – after having been properly processed – will constitute the input to a structural reliability analysis, the output of which will be a new safety index (see figure 4). The data processing will focus on the estimation of the statistical properties (mean value, standard deviation and type of probability distribution) of the measured or monitored data.

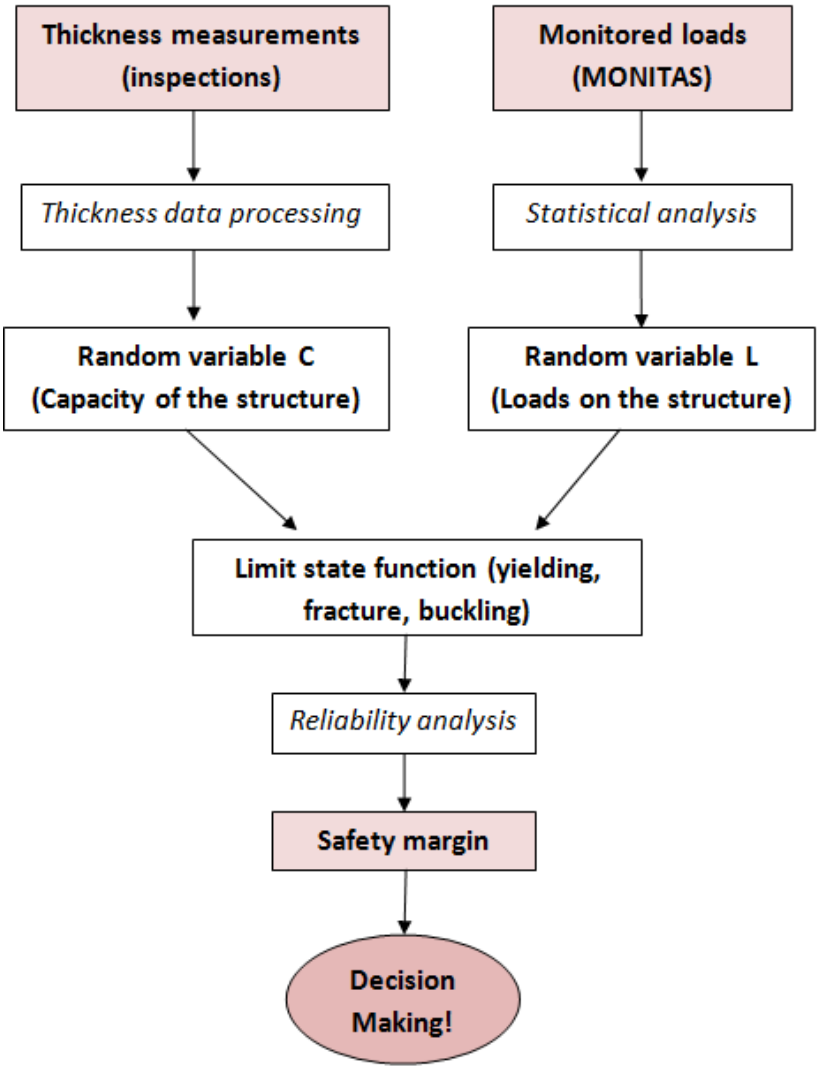

Figure 4 - Thesis flow scheme

Some of the advantages of this new approach are quite evident, namely:

1) less uncertainties in loads, thanks to the MONITAS monitored loads;
2) less uncertainties in the capacity of the structure, thanks to the real thickness measurements coming from inspections;
3) probability-based approach, which will tell us not only "if" the structure is safe but also "how" safe it is;
4) more rational approach, since we are using the real capacity and real loads of the structure to actually recalculate the ultimate strength.

In the following paragraphs more information will be given on the corrosion effects, the inspection procedure and the failure criteria considered. Furthermore some of the main assumptions will be introduced and justified.

1.4 Corrosion

On a FPSO we usually have two main corrosion mechanisms: general and pitting corrosion.

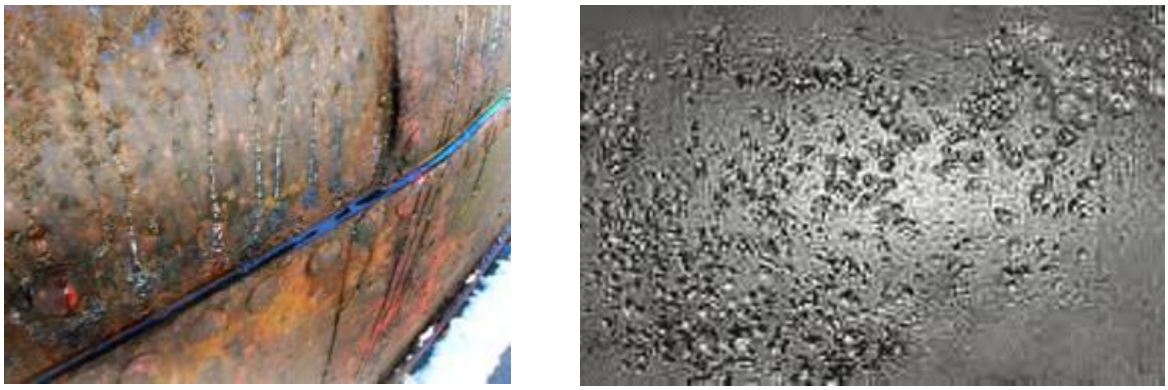

Figure 5 – General corrosion (left) and pitting corrosion (right) in steel

The former occurs when we have corrosion distributed over an entire surface or a big fraction of it, the latter is a very localized corrosion phenomenon. Often we have a coexistence of both.

In this work we will focus just on the general corrosion. Pitting is also important, but usually it does not affect the in-plane stress distribution, due to its very localized nature. Moreover, a plate with aggressive pitting corrosion will generally be soon replaced, as it is a plate with high probability of crack initiation. Furthermore, for mild and low alloy steels corrosion usually approximates a near-uniform loss (Melchers, [3]).

It has been shown that the material properties themselves, such as elastic moduli and yield strength are not influenced by the corrosion of the adjacent material (Melchers, [3]). Therefore it is reasonable to consider the effect of uniform corrosion on the strength of the structure just through the reduction of the actual thicknesses.

1.5 Inspections

In general, two kinds of inspections are carried out on FPSOs: the ones for Classification Societies, and the ones for the operator/ship-owner which are usually based on the RBI plan. The rules from Classification Societies ask for a 5 years cycle of inspection ([4]). The locations for thickness measurements are based on rules from tankers. Any inspections carried out involves thicknesses of the plate, of the stiffener web and of the stiffener flange. In the present work, thickness measurements coming from a standard inspection report will be used in the case study. However, in the final chapter, some small modifications to the inspection procedure are suggested, in order to increase the precision of the reassessment tool.

Figure 6 - Thickness measurements

It is important to point out that in this work no prediction in time of the corrosion waste thickness is made. Furthermore the analysis will only focus on the parts of the vessel which have been directly inspected and of which we know some measured thicknesses. However we should keep in mind that when inspections are carried out according to the RBI plan, the tank to examine is chosen in such a way that this tank is supposed to be the most likely to corrosion damage. There are plans for the future to incorporate in this strength analysis also a corrosion prediction model and a way to infer the corroded thicknesses for those tanks which have not been directly inspected as well. A more detailed discussion on the possible future developments of the current work is given in chapter 8.

1.6 Structure to analyze

Ships and structures are composed of many structural elements, that may be classified as follows ([8]):

1. hull girder;
2. primary structures;
3. stiffened panels;
4. unstiffened plates;
5. structural details.

In our strength reassessment it was decided to focus only on stiffened plates and unstiffened panels (see fig. 7), neglecting any hull girder reassessment. The reason for such a choice is that it is much more likely to have severe corrosion just on one plate or stiffener rather than on all plates and stiffeners on the same cross section.

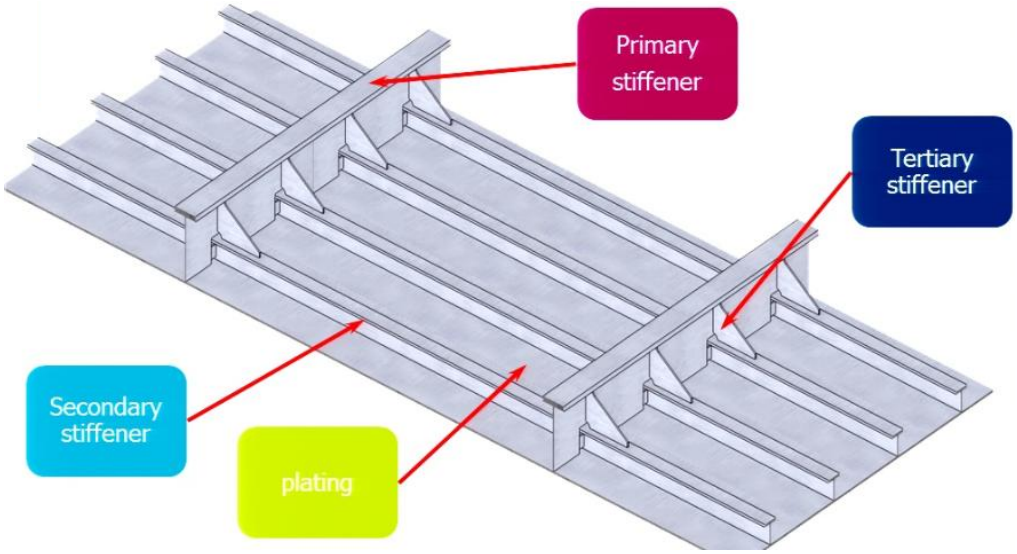

Figure 7 – Stiffened panel, basic structural elements

Figures 8 is giving the structural hierarchy valid for any kind of vessel (terminology is specific for offshore structures): the plating is supported by secondary stiffeners (longitudinals), which in turn are supported by primary stiffeners (web frames, girders). Primary stiffeners support themselves. Tertiary stiffeners are used to strengthen locally the primary stiffeners.

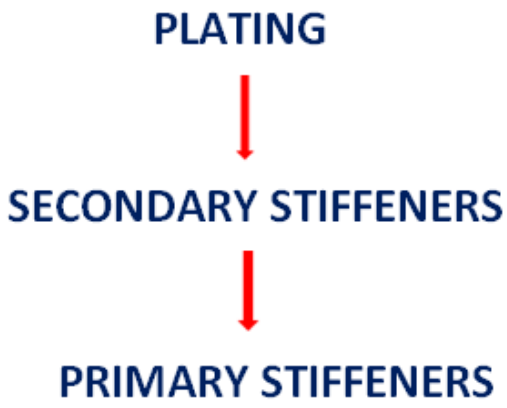

Figure 8 - Structural hierarchy in a ship

Hull structures of FPSOs experiences structural failures typically seen in trading tankers. The areas of an oil tanker which are more prone to corrosion damage are then ([4]):

- structure in the ballast tanks;

- under-deck areas in cargo oil tanks;
- inner bottom (bottom of cargo tanks).

However, in the reassessment procedure we should consider the availability of the thicknesses measurements. They not always are made at the locations listed above.

The location for thickness measurements are chosen on both the Class Regulation and on the RBI plan. Reasonably, both standards will give more attention to the structures more prone to corrosion damage. Therefore at the moment thickness measurements are carried out, we can already assume that a choice of the most critical areas to be checked has been made, and thus a degree of conservativeness has already been included.

During inspections, a (either ballast or cargo oil) tank is emptied, and the thicknesses of the following structures are examined:

- side plate;
- transverse bulkheads;
- longitudinal bulkheads;
- bottom plate;
- deck plate.

Hence, a model and a strength criteria for all this structures is needed.

However in this model this has been done only for the deck, but it can be easily extended to the other structures.

1.7 Loads

All the loads acting on the deck structure of a FPSO are:

- in plane stress due to vertical bending moment;
- in plane stress due to horizontal bending moment;
- topsides loads;
- green water lateral pressure (static pressure + dynamic pressure + impact pressure);
- horizontal shear force;
- lateral internal pressure (static pressure + dynamic pressure + impact pressure).

The lateral pressure due to its small magnitude can be reasonably neglected. Also the topsides loads, which usually are concentrated loads, have not been considered. FPSO topsides are generally supported by some stools which are welded to the deck. It is a good design practice to locate these stool over some bulkheads, girders or web frames. Finally, the horizontal shear force has also been disregarded due to its small magnitude (especially in turret moored FPSO).

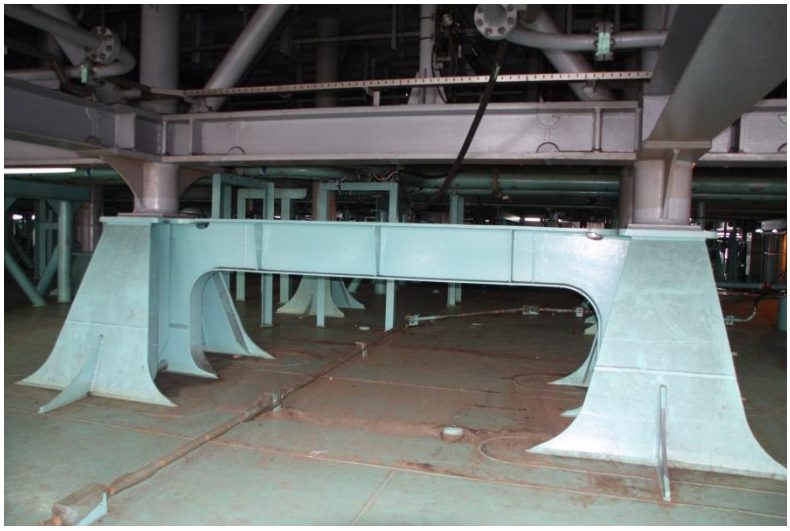

Figure 9 - Topsides connection with the deck

Moreover, during the design stage, the structure has been checked with respect to more than one design condition (installation, transportation, operation). In our case, we are only interested in the operation phase. Therefore we can neglect the data monitored during the transportation and installation phase. This will also improve further our reassessment procedure (that is: we will not only use some measured loads instead of design loads, but we are also using the measured loads relative to the only design condition we are interested in).

1.8 Failure criteria

It was decided to check the deck structures with respect to:

1) first yielding;
2) gross yielding;
3) buckling;
4) fracture.

A limit state function, with the capacity C expressed as a function of the thickness random variable, and the loads L as a function of the MONITAS monitored loads, has been set up for each of the above limit states in the form:

$$g = C - L \tag{1.1}$$

- C: capacity of the structure
- L: loads acting on the structure

To derive the limit state functions it was decided to use analytical models from literature (simple beam theory, large deflection analysis, linear fracture mechanics and other). Many of the equations have been taken from the ALPS/ULSAP theory (Analysis of Large Plated

Structures/Ultimate Limit State Assessment Program) developed by professor J. K. Paik ([7]), which allows to write down failure functions in a closed-form expression.

1.9 Reliability analysis

In general, there are four different levels of reliability analysis:

1) Level I (first-moment methods): characteristic values of the random variables are used, together with some safety factors covering the uncertainties.
2) Level II (second-moment method): the various random variables are presented by their mean value and standard deviation.
3) Level III (full probabilistic): these procedures utilize the complete probability distribution functions of all random variables, which are then combined into an overall probability of failure.
4) Level IV: these procedures are similar to level III but they combine both even probability of failure and the associated benefits and costs.

A full probabilistic (level III) method has chosen. In particular, for the case study, a Monte Carlo simulation method was used. The first order reliability method (FORM) and the second order reliability method (SORM) were not considered due to the complexity of the limit state functions (some of which are not even differentiable).

1.10 Summary of main assumptions

It has been chosen to sum up in the following lists all the main assumptions which have been introduced and justified in this first chapter:

1) pitting - and other form of corrosion different from the uniform corrosion - will not be considered;
2) we will only consider the corroded thickness as it is now, with no corrosion prediction;
3) the reassessment will only focus on the analyzed structure during inspections;
4) no global hull-girder reassessment;
5) only operational condition (no transportation, no installation) will be considered.

1.11 Structure of this report

Chapter 2 will describe the way the thickness measurements coming from the inspection of a real FPSO have been processed in order to derive their statistical properties.

In chapter 3 a general methodology to derive loads for our structural reliability analysis starting from the MONITAS monitored parameter are given. In this chapter the way to model uncertainties is also explained.

In chapter 4 the limit state functions for all the identified failure criteria will be derived. It is important to underline the general character of chapters 3 and 4, as they will not only focus on the specific deck case.

In chapter 5 and 6 the theory described in chapter 3 and 4 will be applied to the specific FPSO deck situation. A case study is also introduced in chapter 6.

In chapter 7 the results on the case study are given.

Finally, chapter 8 presents some conclusions and recommendations for future developments.

References

[1] http://www.offshore-mag.com/content/dam/offshore/print-articles/Volume%2072/aug/2012FPSO-072512Ads.pdf

[2] M. L. Kaminski, MARIN, "Sensing and Understanding Fatigue Lifetime of New and Converted FPSOs", Offshore Technology Conference, 2007

[3] R. E. Melchers, University of Newcastle, "Probabilistic models of corrosion for reliability assessment and maintenance planning", International Conference on Offshore Mechanics and Arctic Engineering, 2001

[4] J. K. Paik, R. E. Melchers, "Condition assessment of aged structures", Woodhead publishing in mechanical engineering, 2008

[5] N. Yamamoto, ClassNK Research Institute, "Reliability based criteria for measures to corrosion", International Conference on Offshore Mechanics and Arctic Engineering, 1998

[6] R. Hageman, P. Aalberts, M. Shaik, H. van den Boom, "Development of an Advisory Hull Fatigue Monitoring System"

[7] J. K. Paik, A. K. Thayamballi, "Ultimate Limit State Design of Steel-Plated Structures", Wiley, 2003

[8] D. Beghin, "Reliability-Based Structural Design", Ship Structural Analysis and Design (chapter 5), SNAME, 2010

2

Thickness measurements processing

A real inspection report, with thickness measurements, of a generic FPSO has been analyzed. The structure inspected is an oil storage tank. The vessel was built almost 30 years before as a tanker, and it has been installed as an FPSO 9 years earlier the inspection. This thickness measurements analysis is divided in two parts.

The first one is more generic: its goal is to gain some knowledge about the corrosion effects in FPSOs, trying to find an answer to the following questions:

1) For side shell and bulkheads, do we see a certain trend of the corroded thickness along the height?
2) Is the corroded thickness the same for the web, the flange and eventually also the plates, for a given structure?
3) Is the corroded thickness the same for those structure experiencing exactly the same corrosion environment on both sides (for example, the transverse web frames)?

We must point out that these answers have been derived analyzing only *one* inspection report, relatively to *one* tank of *one* FPSO in *one* specific year of its lifetime. This must never be forgotten when analyzing the results, which therefore have only a partial validity.

The second part is more specific: once all these questions have been answered, some probability density functions have been estimated for the deck plates and stiffeners . The results of this chapter will be one of the input for the reliability analysis introduced in chapter 6.

Between the first and the second part some statistical concepts which are needed to understand the way the probability distribution functions have been derived are introduced.

The analysis has been carried out using MATLAB as numerical tool.

No distinction is made between a one-side corroded plate and a two-sides corroded plate. In the estimation of the statistical properties of the thickness measurements, it was decided not to consider all measurements, but to disregard the measurements which gave a zero or negative corrosion (a negative corrosion is possible since any new steel plate has always some points with actual thickness higher than the nominal thickness). This choice was made as considering

all the measurements together could led to too optimistic results, since there may be some inter-stiffeners plating with an average corroded thickness higher than the average corroded thickness calculated over the whole panel (see also paragraph 8.2.1.).

2.1 Mean corroded thickness for the different structures

First of all, let us give a look at the following table, which contains a global summary of the mean corroded thickness in the whole tank. The tank is an oil cargo tank, located on the starboard side, storing processed oil. The ship has neither double bottom nor double side.

Table 1 - Mean values of the corroded thicknesses

	Plate	Stiffener web	Stiffener flange	Stiffener (web + flange)	Whole structure
	[mm]	*[mm]*	*[mm]*	*[mm]*	*[mm]*
Deck	0.36	0.11	-	0.11	(0.27)
Side shell	0.75	0.99	1.52	1.26	(1.00)
Longitudinal bulkhead	0.96	0.91	1.46	1.18	(1.07)
Transverse web frame number 1	1.31	-	-	-	(1.31)
Transverse bulkhead number 1	0.68	0.43	0.47	0.46	0.53
Transverse bulkhead number 2	0.83	0.95	0.74	0.82	0.82
Transverse web frame number 2	0.71	-	-	-	(0.70)
Bottom	0.52	0.34	0.49	0.72	(0.48)

In this table some values have been written in brackets as they are the average between structural elements which do not face the same environment (e.g. a deck longitudinal is in contact with oil on both side, while deck plate is in contact with oil only on one side) and thus they are not very meaningful.

As expected, we have quite a large variability of the mean corroded thickness in the whole tank. Each of the above value is the average among, at least, 50 thickness measurements. Therefore, it is unlikely that their differences are simply due to the randomness of the corroded thickness variable itself, but are clearly due to the different environment with whom each structure is in contact with.

The deck plates, the side shell plates, the bottom plates, the longitudinal bulkhead plates and the plates of the transverse bulkheads are experiencing different environments on the outer surface. Hence it is logic to expect – for any of them – a different value of the mean corroded thickness. And this is actually what we observe from the table above.

We also know that processed oil is less aggressive than seawater (this is not the case for fresh oil, which contains some considerable reactive elements). However, we see that the longitudinal bulkhead and the transverse bulkhead number 1 have both experienced a quite severe corrosion, more than the deck, the bottom, the side shell and the transverse bulkhead number 2. The reason for that is that the surfaces exposed to oil are not coated in the inspected FPSO, and both the longitudinal bulkhead and the transverse bulkhead number 1 have both sides in contact with oil. This is of course not true for the deck, the side, and the bottom but also for the transverse bulkhead number 2, which is between an oil tank and a ballast tank.

Webs and flanges of the stiffeners are all exposed - on both sides - to oil, therefore we would expect for all of them similar values of the mean corroded thickness. However, this is not always the case. Moreover it is surprising the difference in the mean corroded thickness between the web and the flange of the same stiffener, which sometimes is quite large. A possible explanation for this may be the accumulation of residual oil, dirty water or dust on the stiffeners (for example, on the top surface of a web of a side longitudinals or on top of a flange of a bottom stiffener), which therefore creates some microenvironment with different corrosion rate.

The big differences in the mean corroded thicknesses are suggesting us to consider each structure separately. Furthermore, for a more precise analysis, also the corroded thicknesses of the stiffeners and the attached plates must be treated separately. Analogously this need to be done for the web and flange of stiffeners.

2.2 Corrosion trend as a function of the position on the vertical axis

For the vertical panels (bulkheads, web frame and side shell) it is reasonable to expect different corrosion rate along the height. For example, a side shell plate would probably have an higher corrosion close to the waterline rather than at its lowest part (corrosion is generally more severe in the splash zone, [8]).

To investigate this effect let us plot the mean corroded thicknesses as a function of the position. In the figures from 2 to 5, each dot is the average between 8 or 10 different measurements made on a single unstiffened plate (each blue portion in figure 1). On the horizontal axis the location (from the lowest to the highest) of the unstiffened plate with respect to the structure height is plotted (each horizontal stiffener is numbered, from down to the top; the values on the horizontal axis are the numbers of the horizontal stiffener attached to lower side of the inspected unstiffened plate).

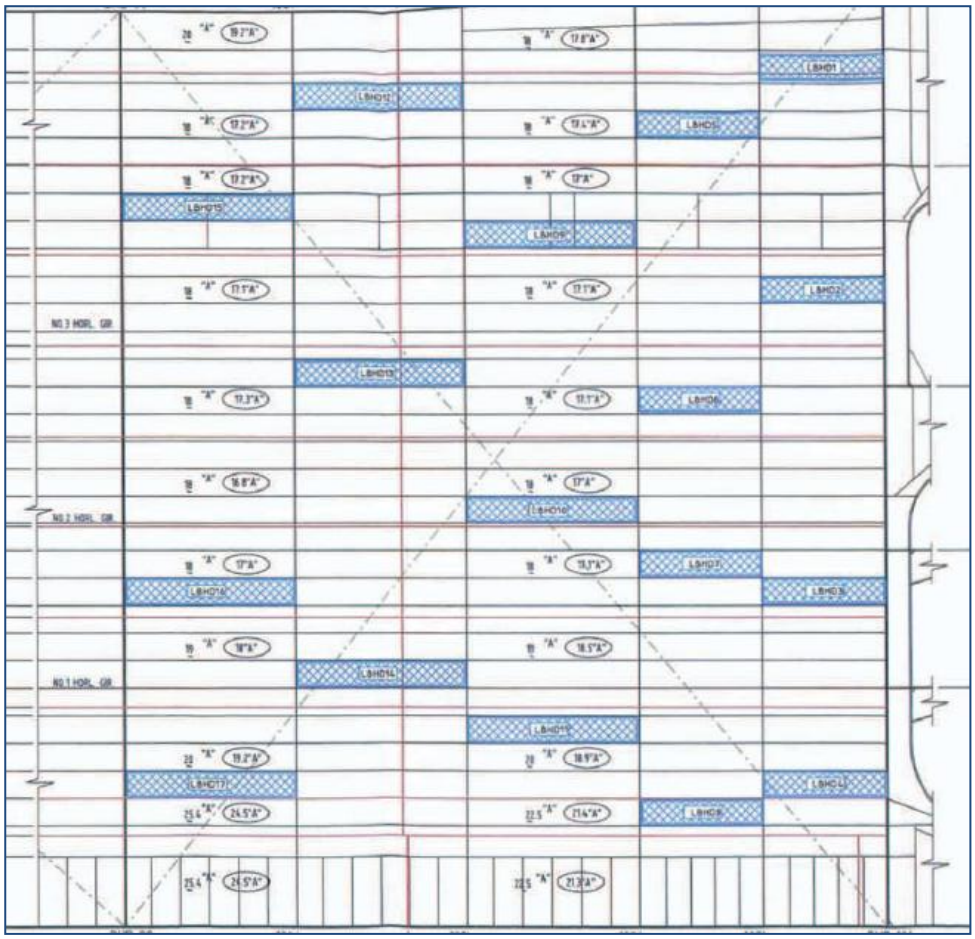

Figure 1 - Example of measurement location on a FPSO bulkhead

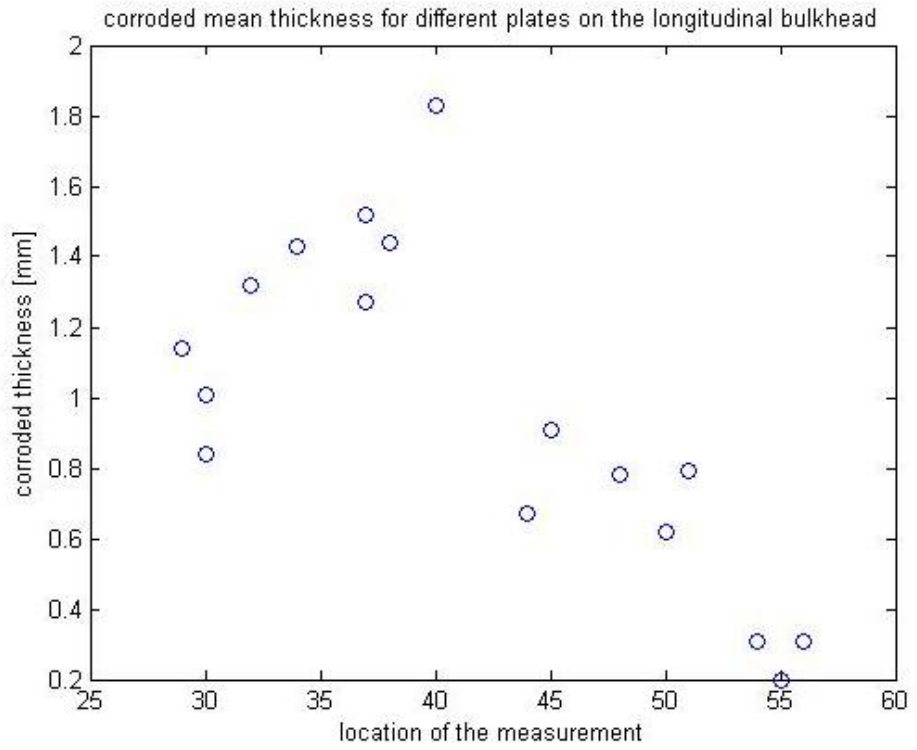

Figure 2 – Corroded thickness trend on the longitudinal bulkhead

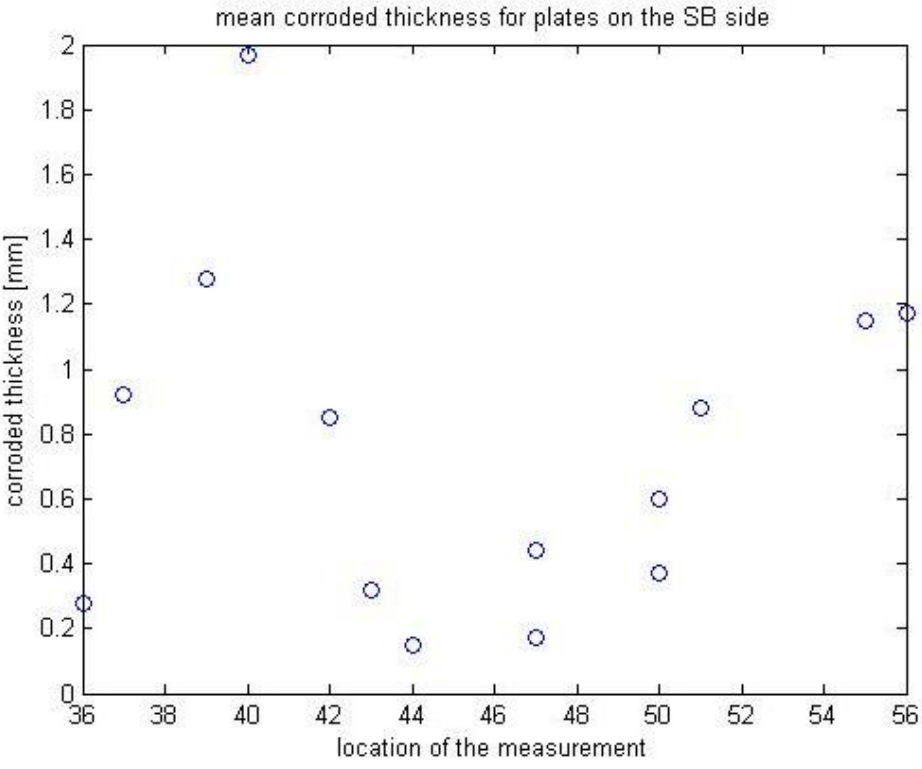

Figure 3 – Corroded thickness trend on the side shell

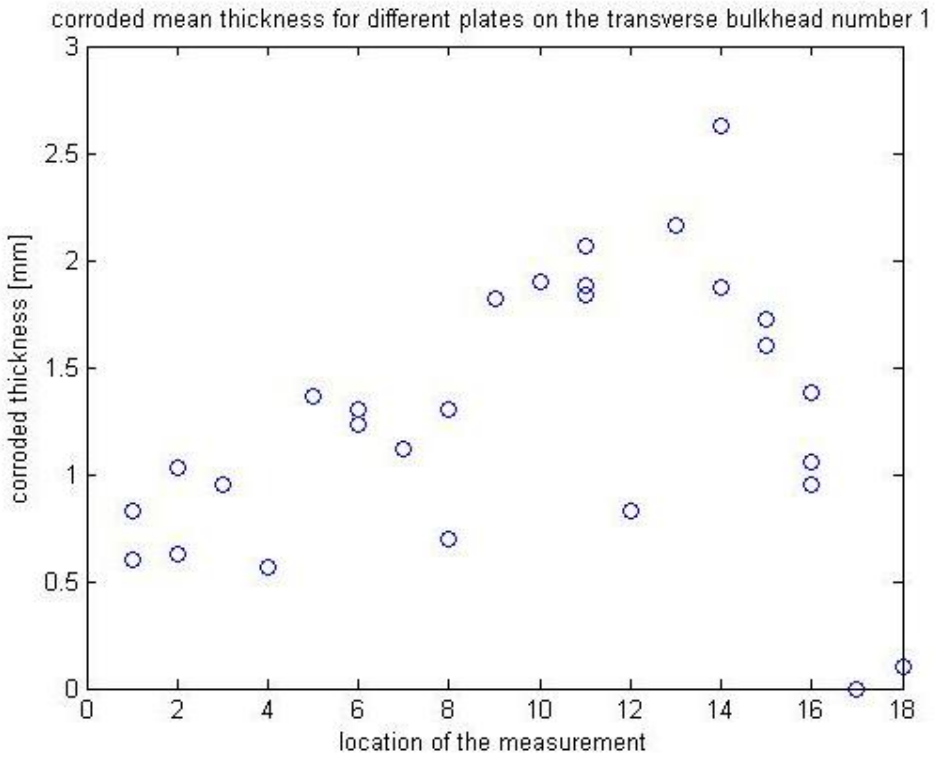

Figure 4 – Corroded thickness trend on the transverse bulkhead number 1

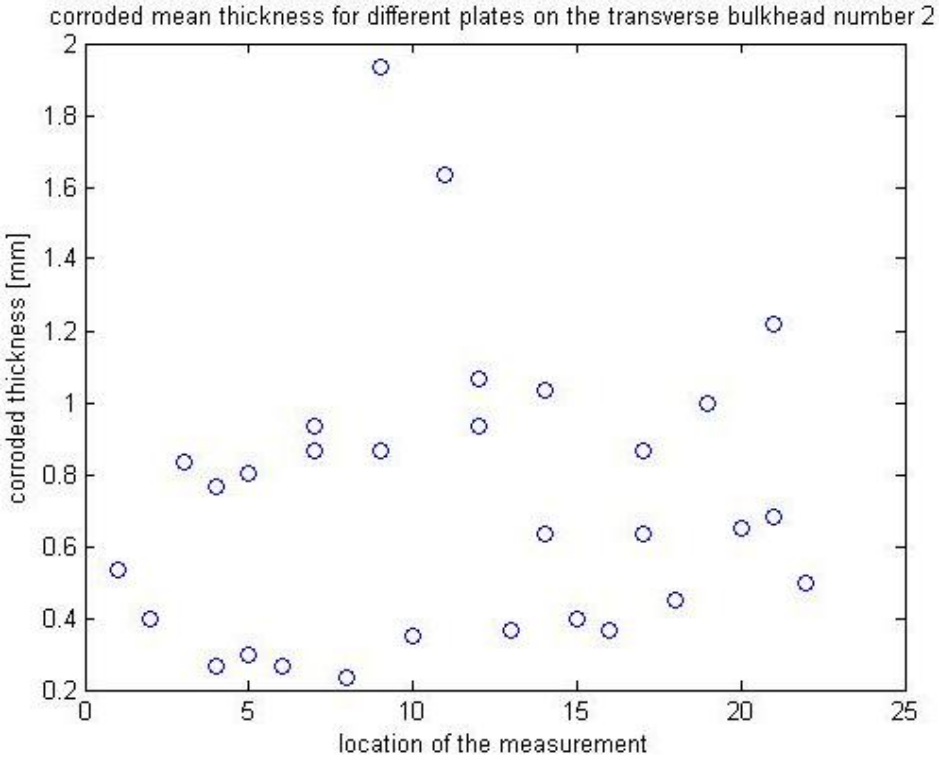

Figure 5 – Corroded thickness trend on the transverse bulkhead number 2

From the figures above we see that:

- for the longitudinal bulkheads the corrosion rate is higher at the bottom, and decreases going upwards;
- for the transverse bulkhead number 1 we see the opposite behavior;
- for the transverse bulkhead number 2 and the side shell we don't see any particular trend of the corrosion rates along the height of the structure.

Therefore it is quite hard to make any conclusion based on this results, as we do not see a common trend in all structures, and sometimes we even see opposite trends. If a (re)assessment of one of these vertical structure was needed, then the best choice – on the base of these observations – would be to group and process all the measurements relative to that structure together.

In order to make some definitive conclusions more inspection reports, possibly from more tanks, more units and more ocean areas must be analyzed. Since this analysis is focusing on the deck, this has not been done. For the deck case, it was chosen to group and process all the plate corroded thickness measurements together. However, in order to include a degree of conservativeness, only the measurements which actually showed some corrosion have been considered. This means that all measurements giving a zero corroded thickness have been disregarded.

This last hypothesis is also needed to take into account the fact that such a large structure like the deck may not have a corrosion rate equivalent all over its surface, and therefore "grouping all the measurements together" may led sometimes to too optimistic results. Hence, an extra degree of conservativeness is needed, and it was chosen to apply it for the considered case by neglecting the zero corroded thickness measurements.

2.3 Probability and statistics theoretical background

2.3.1 Truncated distribution

A *truncated distribution* is a conditional distribution that results from restricting the domain of some other probability distribution. We need to use truncated distributions for the corroded thickness as of course we cannot generate corroded thicknesses higher than the initial gross thickness. Furthermore, since all measurements which gave a zero (or negative) corroded thickness have not been considered, a lower truncation is also needed. This lower truncation does not occur at $t_{corr} = 0.00\ mm$ but, due to "rounding up" reason, at $t_{corr} = 0.05\ mm$.

The table 2 is giving the truncations for the corroded thickness distribution functions used in the case study which will be introduced in chapter 5. t_p, t_w and t_f are the gross thicknesses of the plate, the stiffener's web and stiffener's flange, respectively.

Table 2 - Truncations in the corroded thickness distribution functions used in the case study

	Lower truncation	Higher truncation
	[mm]	*[mm]*
Plate	0.05	t_p
Web	0.05	t_w
Flange	0.05	t_f

A truncated probability distribution function is defined as:

$$f_{tr}(x) = f(x|a < x \leq b) = \frac{g(x)}{F_X(b) - F_X(a)} \tag{2.1}$$

Where:

$$g(x) = \begin{cases} f(x) & if\ a < x \leq b \\ 0 & elsewhere \end{cases} \tag{2.2}$$

and $F_X(x)$ is the corresponding Cumulative Distribution Function (CDF) of the non-truncated distribution. Note that the truncated distribution has been created by not only "cutting" the original non-truncated pdf, but also scaling it, so to keep the value of the integral $\int_a^b f_{tr}\,(x)dx$ equal to 1.

The CDF of the truncated distribution can be found through integration:

$$F_{tr}(x) = \int_{-\infty}^{x} \frac{g(x)}{F_X(b) - F_X(a)}\,dx = \frac{1}{F_X(b) - F_X(a)} \int_{-\infty}^{x} g(x)\,dx = \frac{1}{F_X(b) - F_X(a)} \int_{a}^{x} g(x)\,dx$$
$$= \frac{1}{F_X(b) - F_X(a)} \int_{a}^{x} f(x)\,dx = \frac{F_X(x) - F_X(a)}{F_X(b) - F_X(a)}, \qquad x \leq b \tag{2.3}$$

It is important to underline that a truncated distribution is defined by two more parameters, besides the usual scale and shape factor (or, in some cases, the standard deviation and the mean, with the exception of the exponential distribution which is defined by only one parameter). These two parameters are the truncations a and b. A 4 parameters dependent distribution is a more flexible distribution than a 2 parameters distribution, and therefore should fits better to the empirical one.

2.3.2 Methods for estimating parameters and distributions

There are different methods to estimate the parameters of a distribution. In our case we will use two of them:

1. the method of moments;
2. the maximum likelihood estimation (MLE).

The *method of moments* assumes that the parameters of the assumed distributions are the same than the parameters of the empirical distribution. The mean value and standard deviations of the observations are first calculated, and then converted to the desired parameters of the theoretical distributions. Sometimes (e.g. for the normal distribution) the parameters of the distribution are the mean and the standard deviation themselves, and thus no conversion is needed. This is the easiest method, but not always the more efficient.

The *maximum likelihood estimation* calculates the parameters by maximizing a so-called *likelihood function* $L(p|\vec{X})$. The likelihood function expresses the *likelihood* of a set of parameters, p, given the observed outcomes $\vec{X}$, which is equal to the *probability* of those observed outcomes, given those parameters values p. That is:

$$L(p|\vec{X}) = f_X(\vec{X}|p) = \prod_{i=1}^{n} f_X(X_i|p)$$

Often, the log-likelihood function $\log[L(p|\vec{X})]$ is used rather than the simple likelihood function, as the obtained analytical expression of the log-likelihood function is usually simpler. Very often the estimator computed with the MLE are more efficient than the one derived using the method of moments.

In our analysis, we will check the quality of fitting (with the methods explained in paragraphs from 2.3.5 to 2.3.8) of the following assumed theoretical distributions:

1) truncated exponential distribution;
2) truncated lognormal distribution;
3) truncated gamma distribution;
4) truncated normal distribution;
5) truncated Gumbel distribution.

2.3.3 Method of moments for the considered distribution type

With this method, at first the mean $\bar{x}$ and standard deviation s of the observed material are calculated:

$$\bar{x} = \frac{\sum_{i=1}^{n} x_i}{n} \tag{2.4}$$

$$s = \left[\frac{1}{n-1}\sum_{i=1}^{n}(x_i - \bar{x})^2\right]^{\frac{1}{2}} \tag{2.5}$$

Then, starting from the above, the parameters of the assumed distribution (which here are also called *estimators*) are calculated.

The truncated exponential distributions is a 3 dependent parameter distribution. The first two (lower truncation and higher truncation) have been already determined. The last one is the rate parameter λ:

$$\lambda = \frac{1}{\bar{x}} \tag{2.6}$$

The truncated lognormal distribution is a 4 dependent parameter distributions. The last two unknown parameters are the mean value and standard deviation of the associated normal distribution:

$$\mu = \log\left(\frac{\bar{x}^2}{\sqrt{s^2 + \bar{x}^2}}\right) \tag{2.7}$$

$$\sigma = \sqrt{\log\left[\left(\frac{s}{\bar{x}}\right)^2 + 1\right]} \tag{2.8}$$

The truncated gamma distribution is a 4 dependent parameter distributions. The last two unknown parameters are the shape parameter k and the scale parameter θ of the associated normal distribution:

$$k = \frac{\bar{x}^2}{s^2} \tag{2.9}$$

$$\theta = \frac{s^2}{\bar{x}} \tag{2.10}$$

The truncated normal distribution is the simplest case, since its last two unknown parameters are exactly the mean and standard deviation:

$$\mu = \bar{x} \tag{2.11}$$

$$\sigma = s \tag{2.12}$$

Finally, for the Gumbel distribution, we have that the last two unknown parameters are the scale parameter b_{Gumbel} and the location parameter a_{Gumbel}:

$$a_{Gumbel} = \bar{x} - \frac{s\sqrt{6}}{pi}\gamma \tag{2.13}$$

$$b_{Gumbel} = \frac{s\sqrt{6}}{pi} \tag{2.14}$$

Where γ is the Euler-Mascheroni constant:

$\gamma \cong 0.57721$

2.3.4 *Method of the maximum likelihood for the considered distribution type*

A likelihood function (or a log-likelihood function) need to be written for any of the 5 truncated distributions listed in paragraph 2.3.2.

The exponential truncated distribution is given by the following:

$$f(x;\lambda,a,b)=\begin{cases}\dfrac{\lambda e^{-\lambda x}}{e^{-a\lambda}-e^{-b\lambda}} & if\ a<x\le b\\ 0 & elsewhere\end{cases} \tag{2.15}$$

For the exponential truncated distributions, the maximum likelihood estimator exists if ([3]):

$$0<\bar{x}<\frac{a+b}{2}$$

Then, if (2.15) is true, the MLE estimator of an exponential truncated distribution is the root of the equation ([3]):

$$\frac{1}{\lambda}-\left(be^{-b\lambda}-ae^{-a\lambda}\right)\left(e^{-a\lambda}-e^{-b\lambda}\right)^{-1}-\bar{x}=0$$

The above nonlinear equation has been solved numerical by MATLAB using the command "fsolve". The algorithm used is the trust-region dogleg algorithm. This is a variant of the Powell dogleg method described in [4].

The truncated lognormal distribution is:

$$f(x;\mu,\sigma,a,b)=\begin{cases}\dfrac{\frac{1}{x\sqrt{2\pi}\sigma}\exp\left(-\frac{(\log(x)-\mu)^2}{2\sigma^2}\right)}{\frac{1}{2}\operatorname{erf}\left[\frac{\log(b)-\mu}{\sqrt{2}\sigma}\right]-\frac{1}{2}\operatorname{erf}\left[\frac{\log(a)-\mu}{\sqrt{2}\sigma}\right]} & if\ a<x\le b\\ 0 & elsewhere\end{cases} \tag{2.16}$$

The log-likelihood function of the truncated lognormal distribution is:

$$L(\mu,\sigma)=\prod_{i=1}^{n}\frac{\frac{1}{x_i\sqrt{2\pi}\sigma}\exp\left(-\frac{(\log(x_i)-\mu)^2}{2\sigma^2}\right)}{\frac{1}{2}\operatorname{erf}\left[\frac{\log(b)-\mu}{\sqrt{2}\sigma}\right]-\frac{1}{2}\operatorname{erf}\left[\frac{\log(a)-\mu}{\sqrt{2}\sigma}\right]}$$

$$L(\mu,\sigma)=\left\{\frac{1}{2}\operatorname{erf}\left[\frac{\log(b)-\mu}{\sqrt{2}\sigma}\right]-\frac{1}{2}\operatorname{erf}\left[\frac{\log(a)-\mu}{\sqrt{2}\sigma}\right]\right\}^{-n}\left\{\frac{1}{\sqrt{2\pi}\sigma}\right\}^{n}\prod_{i=1}^{n}\left(\frac{1}{x_i}\right)\exp\left(-\sum_{i=1}^{n}\frac{(\log(x_i)-\mu)^2}{2\sigma^2}\right)$$

$$\log[L(\mu,\sigma)] = log\left\{\frac{1}{2}\text{erf}\left[\frac{\log(b)-\mu}{\sqrt{2}\sigma}\right]-\frac{1}{2}\text{erf}\left[\frac{\log(a)-\mu}{\sqrt{2}\sigma}\right]\right\}^{-n} + log\left\{\frac{1}{\sqrt{2\pi}\sigma}\right\}^{n} + ln\left\{\prod_{i=1}^{n}\left(\frac{1}{x_i}\right)\exp\left(-\sum_{i=1}^{n}\frac{(\log(x_i)-\mu)^2}{2\sigma^2}\right)\right\}$$

$$\log[L(\mu,\sigma)] = -n * log\left\{\frac{1}{2}\text{erf}\left[\frac{\log(b)-\mu}{\sqrt{2}\sigma}\right]-\frac{1}{2}\text{erf}\left[\frac{\log(a)-\mu}{\sqrt{2}\sigma}\right]\right\} + n * log\left\{\frac{1}{\sqrt{2\pi}\sigma}\right\} + log\left\{\prod_{i=1}^{n}\left(\frac{1}{x_i}\right)\right\} - \sum_{i=1}^{n}\frac{(\log(x_i)-\mu)^2}{2\sigma^2}$$

$$\frac{\log[L(\mu,\sigma)]}{n} = -log\left\{\frac{1}{2}\text{erf}\left[\frac{\log(b)-\mu}{\sqrt{2}\sigma}\right]-\frac{1}{2}\text{erf}\left[\frac{\log(a)-\mu}{\sqrt{2}\sigma}\right]\right\} + log\left\{\frac{1}{\sqrt{2\pi}\sigma}\right\} + \frac{1}{n}\sum_{i=1}^{n} log\left(\frac{1}{x_i}\right) - \frac{1}{n}\sum_{i=1}^{n}\frac{(\log(x_i)-\mu)^2}{2\sigma^2} \quad (2.17)$$

The truncated gamma distribution is:

$$f(x;k,\theta,a,b) = \begin{cases} \dfrac{\frac{1}{\Gamma(k)\theta^k}x^{k-1}\exp\left(-\frac{x}{\theta}\right)}{\frac{1}{\Gamma(k)}\gamma\left(k,\frac{b}{\theta}\right)-\frac{1}{\Gamma(k)}\gamma\left(k,\frac{a}{\theta}\right)} & if\ a < x \le b \\ 0 & elsewhere \end{cases} \quad (2.18)$$

The log-likelihood function of the truncated gamma distribution is:

$$L(k,\theta) = \prod_{i=1}^{n}\frac{\frac{1}{\Gamma(k)\theta^k}x_i^{k-1}\exp\left(-\frac{x_i}{\theta}\right)}{\frac{1}{\Gamma(k)}\gamma\left(k,\frac{b}{\theta}\right)-\frac{1}{\Gamma(k)}\gamma\left(k,\frac{a}{\theta}\right)}$$

$$L(k,\theta) = \left[\frac{1}{\Gamma(k)\theta^k}\right]^n\left[\frac{1}{\Gamma(k)}\gamma\left(k,\frac{b}{\theta}\right)-\frac{1}{\Gamma(k)}\gamma\left(k,\frac{a}{\theta}\right)\right]^{-n}\prod_{i=1}^{n}\left(x_i^{k-1}\right)\exp\left(-\frac{\sum_{i=1}^{n}x_i}{\theta}\right)$$

$$\log[L(k,\theta)] = log\left\{\left[\frac{1}{\Gamma(k)\theta^k}\right]^n\right\} + log\left\{\left[\frac{1}{\Gamma(k)}\gamma\left(k,\frac{b}{\theta}\right)-\frac{1}{\Gamma(k)}\gamma\left(k,\frac{a}{\theta}\right)\right]^{-n}\right\} + log\left\{\left(\prod_{i=1}^{n}x_i\right)^{k-1}\right\} + log\left\{\exp\left(-\frac{\sum_{i=1}^{n}x_i}{\theta}\right)\right\}$$

$$\log[L(k,\theta)] = n * \left\{k * log\left[\frac{1}{\theta}\right] - log[\Gamma(k)]\right\} - n * log\left[\frac{1}{\Gamma(k)}\gamma\left(k,\frac{Bb}{\theta}\right)-\frac{1}{\Gamma(k)}\gamma\left(k,\frac{a}{\theta}\right)\right] + (k-1)\sum_{i=1}^{n} log(x_i) - \frac{\sum_{i=1}^{n}x_i}{\theta}$$

$$\frac{\log[L(k,\theta)]}{n} = k * log\left[\frac{1}{\theta}\right] - log[\Gamma(k)] - log\left[\frac{1}{\Gamma(k)}\gamma\left(k,\frac{b}{\theta}\right) - \frac{1}{\Gamma(k)}\gamma\left(k,\frac{a}{\theta}\right)\right] + \frac{(k-1)}{n}\sum_{i=1}^{n} log(x_i) - \frac{\overline{x_i}}{\theta} \quad (2.19)$$

The truncated normal distribution is:

$$f(x;\mu,\sigma,a,b) = \begin{cases} \dfrac{\frac{1}{\sqrt{2\pi}\sigma}\exp\left(-\frac{(x-\mu)^2}{2\sigma^2}\right)}{\frac{1}{2}\mathrm{erf}\left(\frac{b-\mu}{\sigma\sqrt{2}}\right) - \frac{1}{2}\mathrm{erf}\left(\frac{a-\mu}{\sigma\sqrt{2}}\right)} & if\ a < x \le b \\ 0 & elsewhere \end{cases} \quad (2.20)$$

The log-likelihood function of the truncated normal distribution is:

$$L(\mu,\sigma) = \prod_{i=1}^{n} \frac{\frac{1}{\sqrt{2\pi}\sigma}\exp\left(-\frac{(x_i-\mu)^2}{2\sigma^2}\right)}{\frac{1}{2}\mathrm{erf}\left(\frac{b-\mu}{\sigma\sqrt{2}}\right) - \frac{1}{2}\mathrm{erf}\left(\frac{a-\mu}{\sigma\sqrt{2}}\right)}$$

$$L(\mu,\sigma) = \left\{\frac{1}{2}\mathrm{erf}\left(\frac{b-\mu}{\sigma\sqrt{2}}\right) - \frac{1}{2}\mathrm{erf}\left(\frac{a-\mu}{\sigma\sqrt{2}}\right)\right\}^{-n}\left\{\frac{1}{\sqrt{2\pi}\sigma}\right\}^{n}\exp\left(-\sum_{i=1}^{n}\frac{(x_i-\mu)^2}{2\sigma^2}\right)$$

$$\log[L(\mu,\sigma)] = log\left\{\frac{1}{2}\mathrm{erf}\left(\frac{b-\mu}{\sigma\sqrt{2}}\right) - \frac{1}{2}\mathrm{erf}\left(\frac{a-\mu}{\sigma\sqrt{2}}\right)\right\}^{-n} + log\left\{\frac{1}{\sqrt{2\pi}\sigma}\right\}^{n} + log\left\{\exp\left(-\sum_{i=1}^{n}\frac{(x_i-\mu)^2}{2\sigma^2}\right)\right\}$$

$$\frac{\log[L(\mu,\sigma)]}{n} = -log\left\{\frac{1}{2}\mathrm{erf}\left(\frac{b-\mu}{\sigma\sqrt{2}}\right) - \frac{1}{2}\mathrm{erf}\left(\frac{a-\mu}{\sigma\sqrt{2}}\right)\right\} + log\left\{\frac{1}{\sqrt{2\pi}\sigma}\right\} - \frac{1}{n}\sum_{i=1}^{n}\frac{(x_i-\mu)^2}{2\sigma^2} \quad (2.21)$$

The truncated Gumbel distribution is:

$$f(x;a_{Gumbel},b_{Gumbel},a,b) = \begin{cases} \dfrac{\frac{1}{\beta}\exp\left\{-\left[\frac{x-a_{Gumbel}}{\beta} + \exp\left(-\frac{x-a_{Gumbel}}{\beta}\right)\right]\right\}}{\exp\left\{-\left[\exp\left(-\frac{b-a_{Gumbel}}{\beta}\right)\right]\right\} - \exp\left\{-\left[\exp\left(-\frac{a-a_{Gumbel}}{\beta}\right)\right]\right\}} & if\ a < x \le b \\ 0 & elsewhere \end{cases} \quad (2.22)$$

The log-likelihood function of the truncated Gumbel distribution is:

$$L(a_{Gumbel},b_{Gumbel}) = \prod_{i=1}^{n} \frac{\frac{1}{\beta}\exp\left\{-\left[\frac{x_i-a_{Gumbel}}{b_{Gumbel}} + \exp\left(-\frac{x_i-a_{Gumbel}}{b_{Gumbel}}\right)\right]\right\}}{\exp\left\{-\left[\exp\left(-\frac{b-a_{Gumbel}}{b_{Gumbel}}\right)\right]\right\} - \exp\left\{-\left[\exp\left(-\frac{a-a_{Gumbel}}{b_{Gumbel}}\right)\right]\right\}}$$

$$L(a_{Gumbel}, b_{Gumbel})$$
$$= \left(\exp\left\{-\left[\exp\left(-\frac{b - a_{Gumbel}}{b_{Gumbel}}\right)\right]\right\} - \exp\left\{-\left[\exp\left(-\frac{a - a_{Gumbel}}{b_{Gumbel}}\right)\right]\right\}\right)^{-n}$$
$$* \frac{1}{{b_{Gumbel}}^{n}} * \prod_{i=1}^{n} \exp\left\{-\left[\frac{x_i - a_{Gumbel}}{b_{Gumbel}} + \exp\left(-\frac{x_i - a_{Gumbel}}{b_{Gumbel}}\right)\right]\right\}$$

$$L(a_{Gumbel}, b_{Gumbel})$$
$$= \left(\exp\left\{-\left[\exp\left(-\frac{b - a_{Gumbel}}{b_{Gumbel}}\right)\right]\right\} - \exp\left\{-\left[\exp\left(-\frac{a - a_{Gumbel}}{b_{Gumbel}}\right)\right]\right\}\right)^{-n}$$
$$* \frac{1}{{b_{Gumbel}}^{n}} * \exp\left\{-\sum_{i=1}^{n}\left[\frac{x_i - a_{Gumbel}}{b_{Gumbel}} + \exp\left(-\frac{x_i - a_{Gumbel}}{b_{Gumbel}}\right)\right]\right\}$$

$$\log[L(a_{Gumbel}, b_{Gumbel})]$$
$$= log\left\{\left(\exp\left\{-\left[\exp\left(-\frac{b - a_{Gumbel}}{b_{Gumbel}}\right)\right]\right\} - \exp\left\{-\left[\exp\left(-\frac{a - a_{Gumbel}}{b_{Gumbel}}\right)\right]\right\}\right)^{-n}\right.$$
$$\left. * \frac{1}{{b_{Gumbel}}^{n}} * \exp\left\{-\sum_{i=1}^{n}\left[\frac{x_i - a_{Gumbel}}{b_{Gumbel}} + \exp\left(-\frac{x_i - a_{Gumbel}}{b_{Gumbel}}\right)\right]\right\}\right\}$$

$$\log[L(a_{Gumbel}, b_{Gumbel})]$$
$$= -n$$
$$* log\left(\exp\left\{-\left[\exp\left(-\frac{b - a_{Gumbel}}{b_{Gumbel}}\right)\right]\right\} - \exp\left\{-\left[\exp\left(-\frac{a - a_{Gumbel}}{b_{Gumbel}}\right)\right]\right\}\right) + n$$
$$* log\left(\frac{1}{b_{Gumbel}}\right) + log\left(\exp\left\{-\sum_{i=1}^{n}\left[\frac{x_i - a_{Gumbel}}{b_{Gumbel}} + \exp\left(-\frac{x_i - a_{Gumbel}}{b_{Gumbel}}\right)\right]\right\}\right)$$

$$\frac{\log[L(a_{Gumbel}, b_{Gumbel})]}{n}$$
$$= -log\left(\exp\left\{-\left[\exp\left(-\frac{b - a_{Gumbel}}{b_{Gumbel}}\right)\right]\right\} - \exp\left\{-\left[\exp\left(-\frac{a - a_{Gumbel}}{b_{Gumbel}}\right)\right]\right\}\right)$$
$$+ log\left(\frac{1}{b_{Gumbel}}\right) - \frac{1}{n}\sum_{i=1}^{n}\left[\frac{x_i - a_{Gumbel}}{b_{Gumbel}} + \exp\left(-\frac{x_i - a_{Gumbel}}{b_{Gumbel}}\right)\right] \qquad (2.23)$$

The log-likelihood functions (2.18), (2.20), (2.22) and (2.24) have been maximized by means of the MATLAB command "fminsearch". The algorithm used is the Nedler-Mead simple algorithm ([5]).

2.3.5 Kolmogorov-Smirnov test

The *Kolmogorov-Smirnov test* (KV test) is a way to check the goodness of fitting an empirical distribution with a theoretical assumed distribution. First of all, the following test quantity has to be calculated:

$$y_{KS} = \max\left(\left|\frac{i}{n} - F_X(x_i)\right|\right) \tag{2.24}$$

- i: index of the observations, after that all of them have been properly sorted, from lowest to highest value
- n: total number of observations
- $F_X(x)$: theoretical assumed distribution

It is good to note that (2.25) is actually giving an indication of the maximum difference between the assumed distribution and the empirical one.

This quantity has to be lower than a threshold value, otherwise the assumed distribution must be dismissed. If the parameters of the distribution $F_X(x)$ have been estimated from the same statistical material with which the distribution is compared (which is the case here), and if $n \geq 35$, then:

$$y_{threshold} = \frac{\alpha}{\sqrt{n-r}} \tag{2.25}$$

- r: number of parameters
- α: parameter function of n and the significance level p

In a intuitive way, although not very rigorous, the *significance level* can be defined as the probability that the experimental results have been caused by purely statistical accident. In our case a significance level of 5% has been chosen.

In annex A the table for the $y_{threshold}$ as a function of n and p is given.

2.3.6 Least squares method

First of all, an empirical distribution need to be calculated. The literature proposes different way to calculate the CDF of an empirical set of data, namely:

$$F_X(x) = \frac{i}{n} \tag{2.26}$$

$$F_X(x) = \frac{i}{n+1} \tag{2.27}$$

$$F_X(x) = \frac{i-0.5}{n} \tag{2.28}$$

i is the index of the observed value, after that they all have been properly sorted from the lowest to the highest, n is the total number of empirical values.

The empirical CDF estimated with (2.27) has showed to have better statistical properties than the other two ([2], p. 270) and therefore this is the formula which has been chosen.

Then, the sum of squares error (SS) is calculated:

$$sum\ of\ squares\ error = \sum_{i=1}^{n} \left[\widehat{F_X}(x_i) - F_X(x_i)\right]^2 \tag{2.29}$$

- $\widehat{F_X}(x)$: empirical distribution
- $F_X(x)$: assumed theoretical distribution

Of course the distribution giving the least squares error is, according to this method, giving the best fit.

Often, it was decided to use a weighed sum of squares errors, in order to give more importance to the tails of the distributions, which is of course the parts in which we are more interested in:

$$sum\ of\ squares\ error = \sum_{i=1}^{n} x_i * \left[\widehat{F_X}(x_i) - F_X(x_i)\right]^2 \tag{2.30}$$

2.3.7 Linearization of the cumulative distribution function

In order to visualize graphically the efficiency of the estimator, sometimes it may be convenient to linearize the CDF. To do that, a relationship like (2.31) has to be found.

$$Y(x) = \frac{x - a}{b}, \quad b > 0 \tag{2.31}$$

a and b are two parameters (first one is a "location parameter", the second a "scale parameter). In this way the linearized empirical CDF $\hat{Y}(x)$ – as it will be clear in the following examples – can be expressed as a function of the empirical original distribution, $\widehat{F_X}(x)$.

For the truncated exponential distribution:

$$F_X(x) = \frac{1 - e^{-\lambda x} - F_X(a)}{F_X(b) - F_X(a)} \tag{2.32}$$

$$Y(x) = \log\left[1 - F_X(a) - F_X(x)[F_X(b) - F_X(a)]\right]^{-1} = \lambda x \tag{2.33}$$

$$\hat{Y}(x_i) = \log\left[1 - F_X(a) - \widehat{F_X}(x)[F_X(b) - F_X(a)]\right]^{-1} \tag{2.34}$$

For the truncated lognormal distribution:

$$F_X(x) = \frac{\frac{1}{2} + \frac{1}{2}\,\mathrm{erf}\left[\frac{log(x) - \mu}{\sqrt{2}\sigma}\right] - F_X(a)}{F_X(b) - F_X(a)} \tag{2.35}$$

$$Y(x) = erfinv[2 * \{F_X(x)[F_X(b) - F_X(a)] + F_X(a)\} - 1] = \frac{log(x) - \mu}{\sqrt{2}\sigma} \tag{2.36}$$

$$\hat{Y}(x_i) = erfinv\left[2 * \left\{\widehat{F_X}(x_i)[F_X(b) - F_X(a)] + F_X(a)\right\} - 1\right] \quad (2.37)$$

The (2.35) will look linear if we use a logarithmic scale on the horizontal axis.

For the truncated gamma distribution:

$$F_X(x) = \frac{gammainc\left(\frac{x}{\theta}, k\right) - F_X(a)}{F_X(b) - F_X(a)} \quad (2.38)$$

$gammainc\left(\frac{x}{\theta}, k\right)$ is the lower gamma incomplete function. Sometimes there is some ambiguity about its definition. Hence here I will report the definition used in this report, which is the same used by the MATLAB software:

$$gammainc\left(\frac{x}{\theta}, k\right) = \frac{1}{\Gamma(k)} \int_0^{x/\theta} t^{k-1} e^{-t} dt \quad (2.39)$$

Where $\Gamma(k)$ is the gamma function.

Then:

$$Y(x) = F_X(x)[F_X(b) - F_X(a)] + F_X(a) = gammainc\left(\frac{x}{\theta}, k\right) \quad (2.40)$$

$$\hat{Y}(x_i) = \widehat{F_X}(x_i)[F_X(b) - F_X(a)] + F_X(a) \quad (2.41)$$

The (2.39) will look linear if we plot $Z = gammainc\left(\frac{x}{\theta}, k\right)$ on the horizontal axis.

For the truncated normal distribution:

$$F_X(x) = \frac{\frac{1}{2} + \frac{1}{2}\text{erf}\left[\frac{x-\mu}{\sqrt{2}\sigma}\right] - F_X(a)}{F_X(b) - F_X(a)} \quad (2.42)$$

$$Y(x) = erfinv[2 * \{F_X(x)[F_X(b) - F_X(a)] + F_X(a)\} - 1] = \frac{x-\mu}{\sqrt{2}\sigma} \quad (2.43)$$

$$\hat{Y}(x_i) = erfinv\left[2 * \left\{\widehat{F_X}(x_i)[F_X(b) - F_X(a)] + F_X(a)\right\} - 1\right] \quad (2.44)$$

For the truncated Gumbel distribution:

$$F_X(x) = \frac{\exp\left[-\exp\left(-\frac{x - a_{Gumbel}}{b_{Gumbel}}\right)\right] - F_X(a)}{F_X(b) - F_X(a)} \quad (2.45)$$

$$Y(x) = -\log(-log\{F_X(x)[F_X(b) - F_X(a)] + F_X(a)\}) = \frac{x - a_{Gumbel}}{b_{Gumbel}} \quad (2.46)$$

$$\hat{Y}(x_i) = -\log\left(-log\left\{\widehat{F_X}(x_i)[F_X(b) - F_X(a)] + F_X(a)\right\}\right) \quad (2.47)$$

As we will see in paragraph 2.4 the plots of the linearized versions of the empirical and assumed distributions can give some useful indications on the overall quality of fitting. It must be underlined the word "overall" as they cannot give any information on the local quality of fitting (e. g. in the tales of the distributions). This is due to the different scale on the vertical axis, that is, if we calculate two differences in the linearized CDF between the assumed distribution and the empirical one:

$$\Delta Y_1 = \left|\hat{Y}(x_1) - Y(x_1)\right|$$

$$\Delta Y_2 = \left|\hat{Y}(x_2) - Y(x_2)\right|$$

with: $\Delta Y_1 = \Delta Y_2$ and $x_1 \neq x_2$, then it does not automatically follow that:

$$\Delta F_1 = \left|\widehat{F_X}(x_1) - F_X(x_1)\right| = \Delta F_2 = \left|\widehat{F_X}(x_2) - F_X(x_2)\right|$$

Hence, attention must be used when reading this graphs (especially when comparing two different types of distributions; they work much better when comparing the same type of distribution – e.g. the lognormal – but with different estimators – i.e. the method of moments estimators and the maximum likelihood estimators).

2.3.8 Quantile-quantile plot

Another graphical method to evaluate how close an assumed distribution is to an empirical one are the quantile-quantile plots (q-q plot). These plots are also useful to compare two or more distributions.

Quantiles are values taken at regular intervals from the inverse of the cumulative distribution function of a random variable. A q-q plot is then a plot in which:

- the quantiles of the assumed theoretical distributions are plotted on the horizontal axis;
- the quantiles of the empirical distributions are plotted on the vertical axis.

Each dot of a q-q plot represents then a value of the CDF (e.g. 30%) whose x-coordinate is the inverse of it according to the assumed theoretical distributions (that is, the value with a probability of non-exceedance equal to 30% according to the assumed theoretical distributions), and the y-coordinate is the inverse of it according to the observed samples (that is, the value with a probability of non exceedance equal to 30% according to the empirical data). Obviously, the closer each dot will be to the bisector of the quadrant, the closer to the empirical distribution the assumed distribution is.

2.4 Results of the distribution estimation

In this paragraph, all the statistical concepts introduced in paragraph 2.3 (method of moments, MLE method, KS test, q-q plot, weighed and non weighed least squares error, linearized CDF)

will be used to evaluate which truncated distributions fits better to the data coming from the inspections. Much attention has been given to this part, as the results of a reliability analysis strongly depends on the quality of the assumed distributions for the input data.

This procedure has been repeated three times: for the deck plate, the web deck longitudinals and the flange deck longitudinals. Indeed, the FPSO used for the case study run as a part of this Master Thesis (see chapter 6) has L-profile stiffeners attached to the deck. However, since it was not possible to get thickness measurements from this monitored unit, for the case study it was chosen to use thickness measurements coming from another FPSO, and assume that they are the same also for the MONITAS monitored FPSO used in the case study.

The problem is that the inspected FPSO from which thickness measurements comes from has flat bar stiffeners on the deck (thus with no flange). Hence, it was assumed that the corroded thickness data for the web longitudinals are valid also for the flange longitudinals. This does not mean that the corroded thickness distributions for the web and the flange will be the same, as the truncation values a and b are different (since the gross thicknesses for the flange and the web are not equal)!

2.4.1 Deck plate

The first two parameters of the distributions are the two truncation values a and b, which are already known:

$a = 0.05\ mm$

$b = t_p = 17\ mm$

We will start with giving the results of the KS test (table 3) and the least squares method (table 4).

Table 3 - Kolmogorov-Smirnov test for the deck plate corroded thicknesses

	Method of moments		MLE	
	y	*y threshold*	*y*	*y threshold*
Exponential truncated distribution	0.095	0.178	0.106	0.178
Lognormal truncated distribution	0.170	0.179	0.109	0.179
Gamma truncated distribution	0.112	0.179	0.098	0.179
Normal truncated distribution	0.210	0.179	0.156	0.179
Gumbel truncated distribution	0.145	0.179	0.096	0.179

Table 4 - Least squares method for deck plate corroded thicknesses

	Method of moments	MLE
	SS	*SS*
Exponential truncated distribution	0.042	0.033
Lognormal truncated distribution	0.063	0.043
Gamma truncated distribution	0.038	0.032
Normal truncated distribution	0.241	0.112
Gumbel truncated distribution	0.081	0.031

The MLE is almost always giving better approximation than the method of moments (and this one will be a constant throughout this report, as expected).

The KS test is giving particularly good results for the gamma truncated distribution and the Gumbel truncated distribution (provided that the parameters are estimated with the MLE method). The sum of squares method is also giving very good results for these two distributions, but it is also giving analogous good results for the exponential truncated distribution (still with MLE parameter).

The weighed sum of squares method has been implemented using (2.48), and the results of this method are listed in table 5.

$$SS_{weighed} = \sum_{i=1}^{n} \left[t_{corr,i} * \left(CDF_{empirical}(t_{corr,i}) - CDF_{theoretical}(t_{corr,i}) \right)^2 \right] \qquad (2.48)$$

Table 5 – Weighed least squares method for deck plate corroded thicknesses

	Method of moments	MLE
	Weighed SS	*Weighed SS*
Exponential truncated distribution	0.037	0.023
Lognormal truncated distribution	0.020	0.020
Gamma truncated distribution	0.018	0.016
Normal truncated distribution	0.149	0.070
Gumbel truncated distribution	0.041	0.016

One more time, the gamma and the Gumbel truncated distributions (with MLE parameters) are giving the best results (although the differences between all the considered distributions are generally small, with the only exception of the normal truncated distributions which is very far from the empirical one). The lognormal and the exponential distribution are also giving quite precise approximations.

The results gained so far are also confirmed by the following figures. In figures 6 to 10 the linearized empirical and assumed distributions are plotted. We don't see very large disagreement

between the two, with the only exceptions of the normal distribution, as expected. For all of them we can see the better performance of the maximum likelihood estimators compared to the method of moments estimator.

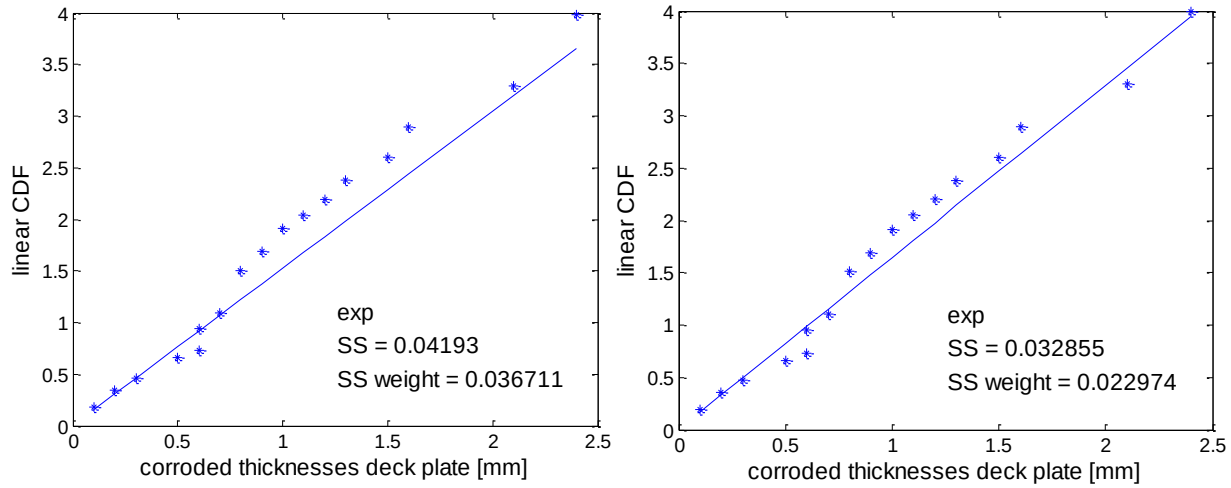

Figure 6 – Linearized exponential CDF for the deck plate corroded thickness: method of moments (left) and MLE (right)

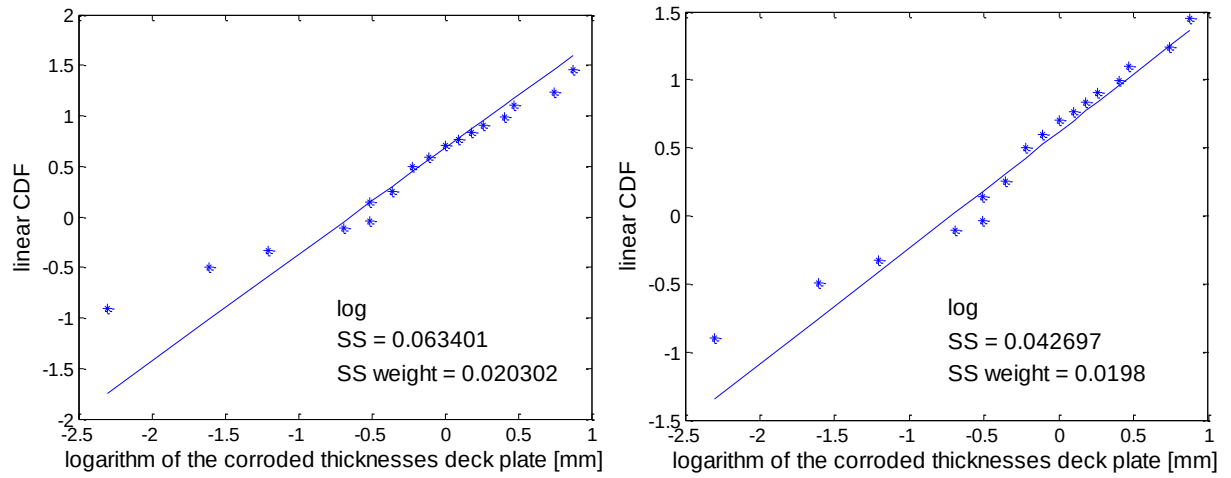

Figure 7 - Linearized lognormal CDF (MLE) for the deck plate corroded thickness: method of moments (left) and MLE (right)

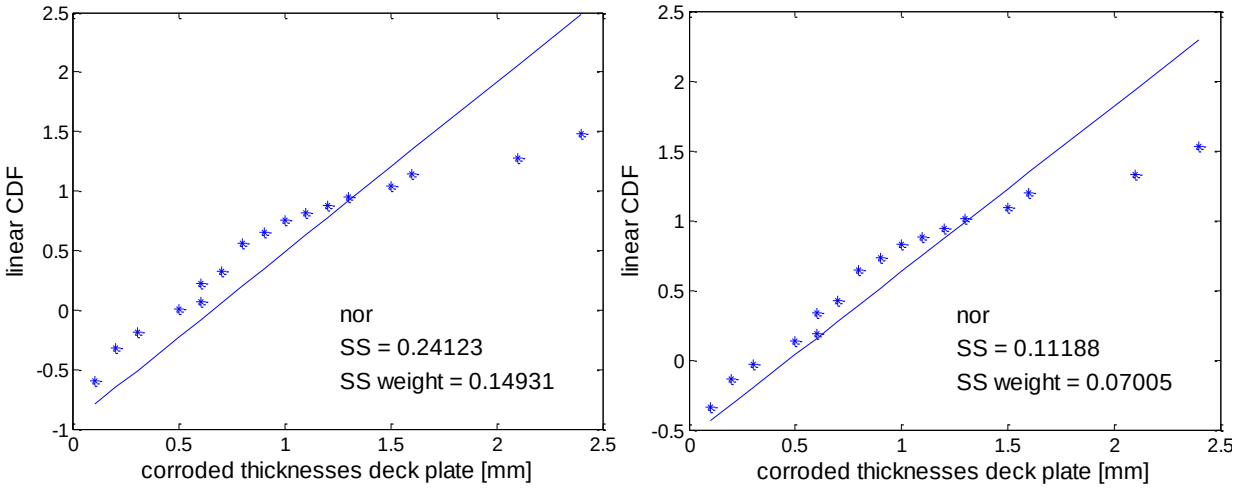

Figure 8 - Linearized normal CDF (MLE) for the deck plate corroded thickness: method of moments (left) and MLE (right)

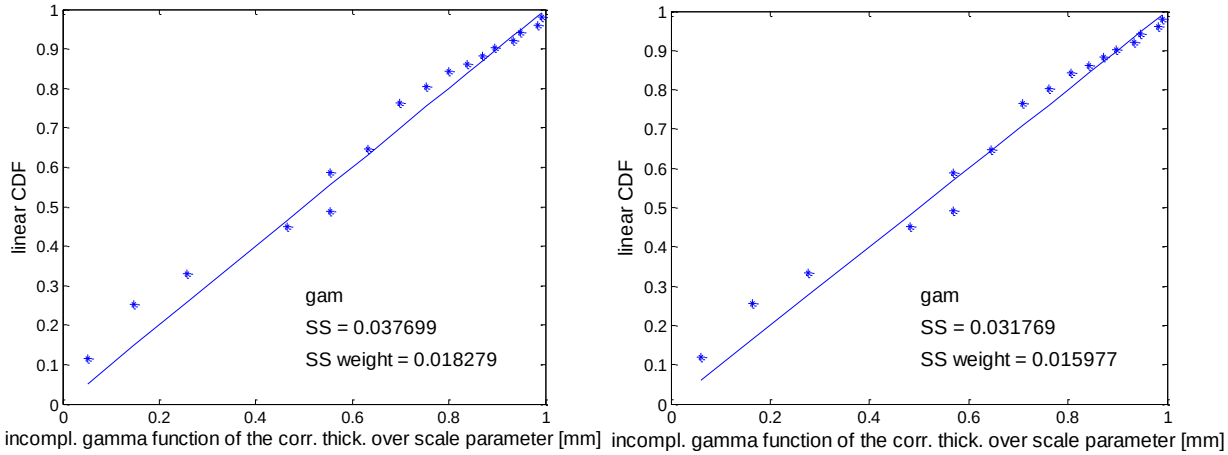

Figure 7 - Linearized gamma CDF (MLE) for the deck plate corroded thickness: method of moments (left) and MLE (right)

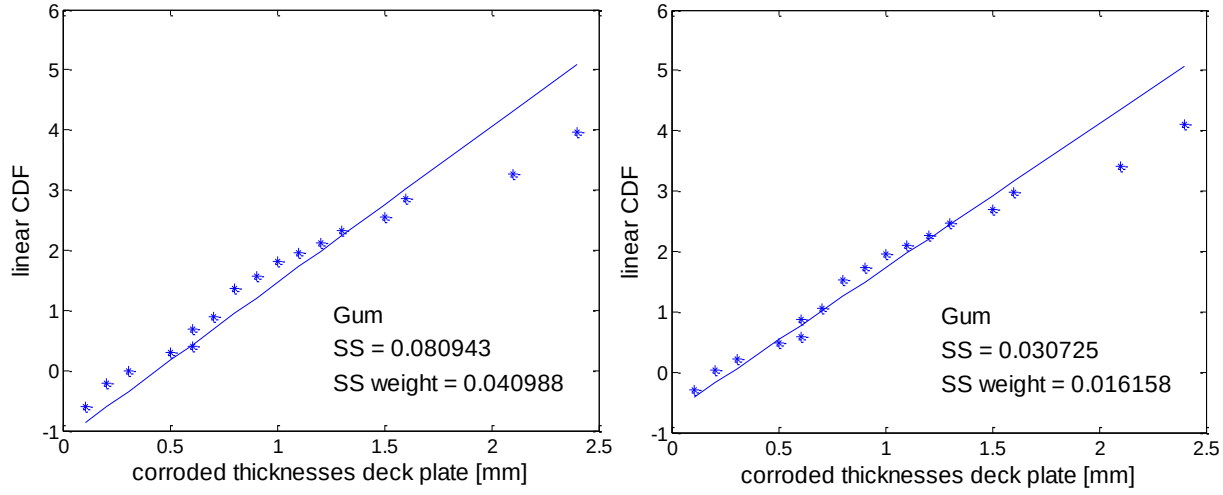

Figure 8 - Linearized Gumbel CDF (MLE) for the deck plate corroded thickness: method of moments (left) and MLE (right)

Since more than one distributions is giving a satisfactory approximation (and this was possible thanks to the high number of samples; for the web and the flange we will see that this will be no longer the case), it was decided to choose the one which is giving the best results in the very extreme tail of the distributions (since our strength reassessment is an ultimate state analysis, thus we are more concerned with the extreme events). We can clearly see from figure 11 that the lognormal and exponential distributions are very close to the empirical distributions.

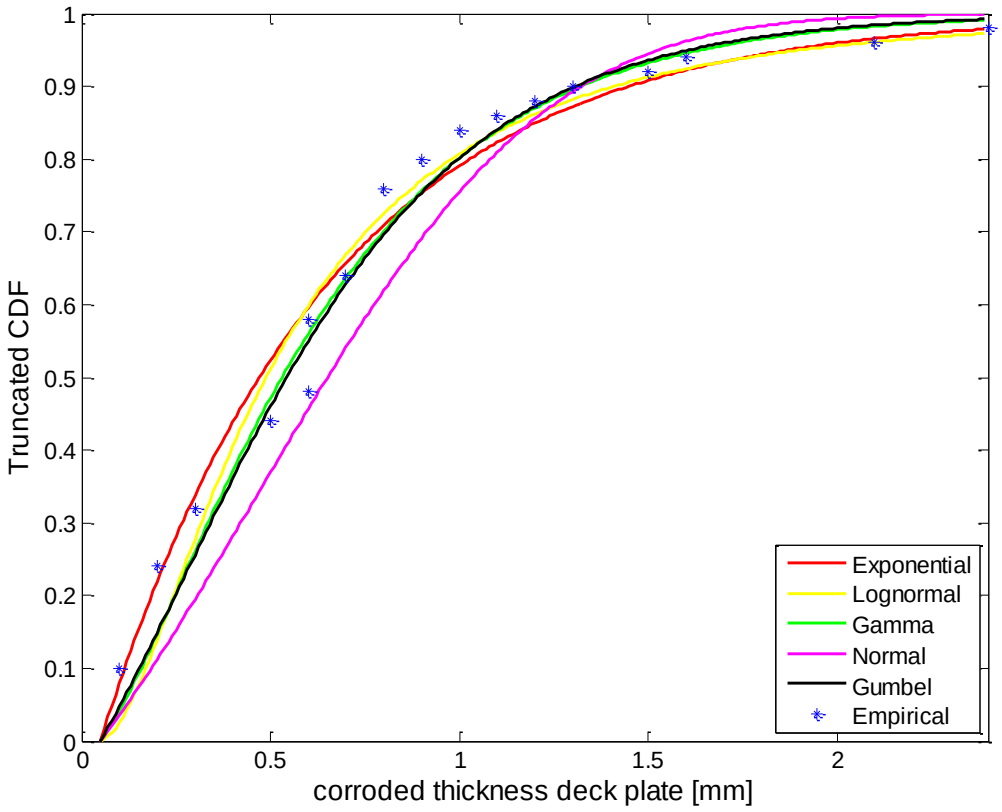

Figure 9 - Comparisons of the empirical CDF with the assumed ones for the deck plate corroded thicknesses

Finally, the q-q plot is showing extremely good results in the very extreme tail of the empirical distribution for the exponential distribution (and, to a less extent, for the lognormal distribution).

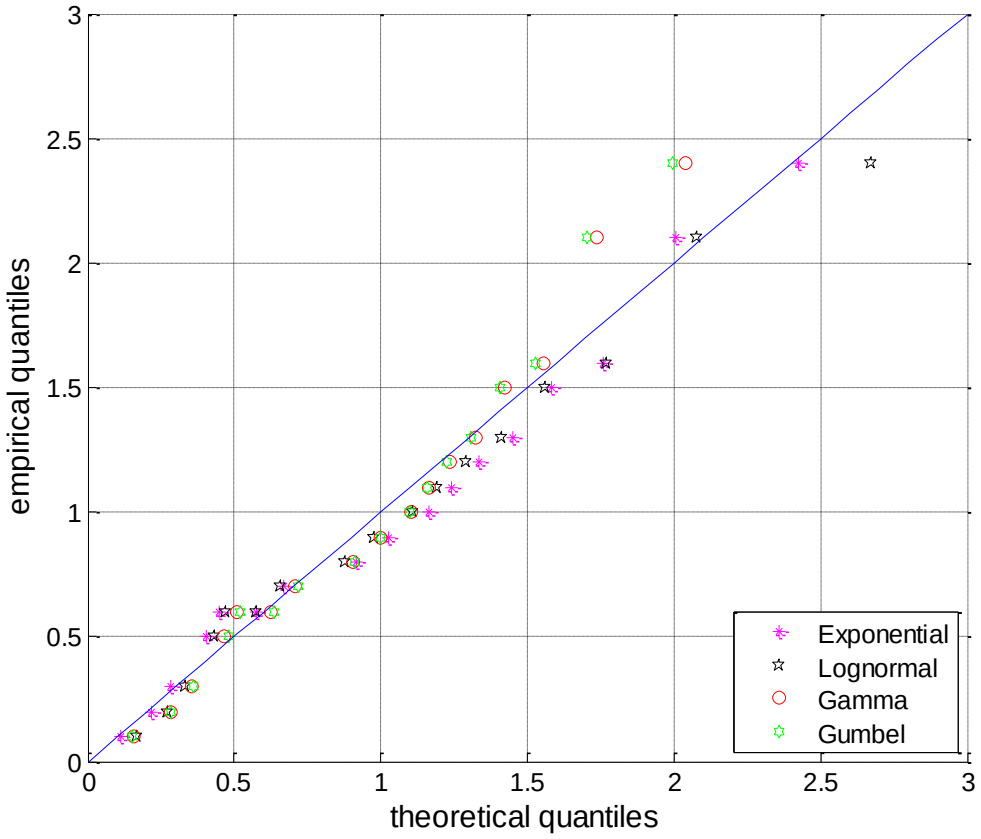

Figure 10 – q-q plot for the deck plate corroded thicknesses

To sum up:

- the KS test is suggesting us to use the **gamma** and **Gumbel** distributions;
- the SS method is giving the same good results for the **gamma**, the **Gumbel** and the **exponential** distribution;
- the weighed method is giving very good results for the **gamma** and the **Gumbel**, and good results for the **lognormal** and the **exponential**;
- comparison of the different assumed CDFs with the empirical one is telling us that the **exponential** and the **lognormal** distribution are the closest to the empirical distribution in the extreme upper tail of the empirical distribution;
- the q-q plot is confirming what it has been seen with the comparison of the different assumed CDFs in figure 11, but it is also underlining that the **exponential** distribution has a slightly better performance than the lognormal distribution in the extreme tail of the distribution.

Finally, the exponential distribution (with MLE estimator) was chosen (figure 13), with the following parameter:

$\lambda = 1.647$ ($\mu = 0.607\ mm$)

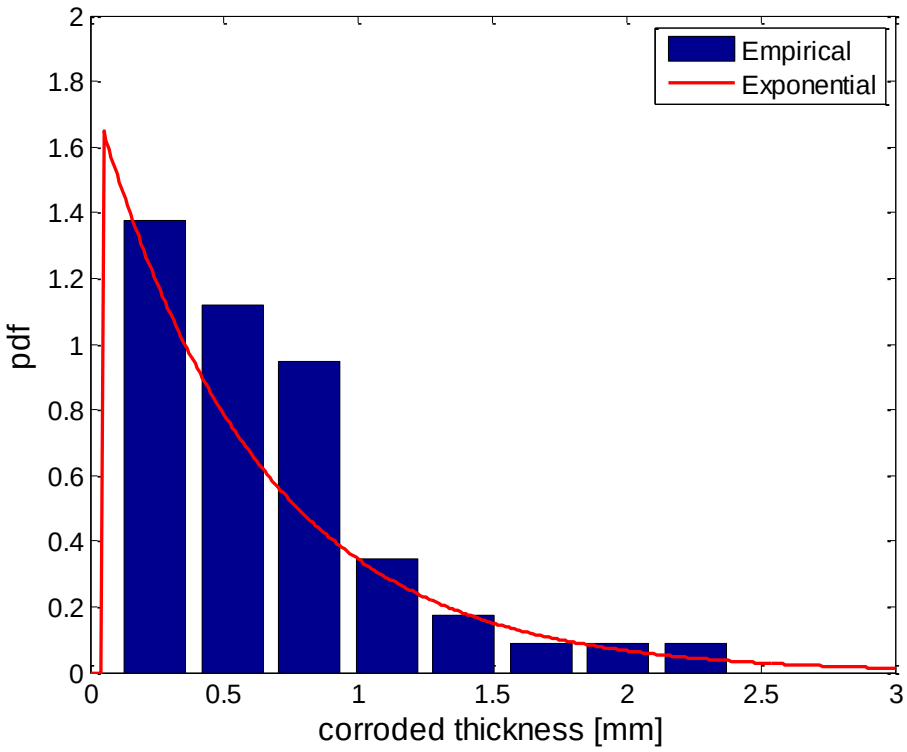

Figure 11 - Exponential truncated probability distribution function for the deck plate corroded thickness

2.4.2 Web deck longitudinals

The first two parameters of the distributions are the two truncation values a and b, which are already known:

$a = 0.05\ mm$

$b = t_w = 10\ mm$

In tables 6 and 7 there are the results of the KS test and SS method respectively, for the web deck longitudinals.

Table 6 - Kolmogorov-Smirnov test for the web deck longitudinals corroded thicknesses

	Method of moments		MLE	
	y	*y threshold*	*Y*	*y threshold*
Exponential truncated distribution	0.242	0.225	0.144	0.225
Lognormal truncated distribution	0.290	0.228	0.287	0.228
Gamma truncated distribution	0.285	0.228	0.270	0.228
Normal truncated distribution	0.339	0.228	0.285	0.228
Gumbel truncated distribution	0.301	0.228	0.276	0.228

Table 7 - Least squares method for the web deck longitudinals corroded thicknesses

	Method of moments	MLE
	SS	*SS*
Exponential truncated distribution	0.134	0.037
Lognormal truncated distribution	0.101	0.095
Gamma truncated distribution	0.110	0.095
Normal truncated distribution	0.183	0.124
Gumbel truncated distribution	0.119	0.095

According to the KS test, all the distributions but one must be disregarded. The only good one is the truncated exponential distribution with the MLE estimator. The SS method is giving consistent results with the KS test.

If we look at the comparison between the different CDFs (figure 14) we clearly see the better performance of the exponential truncated distribution compared to the other.

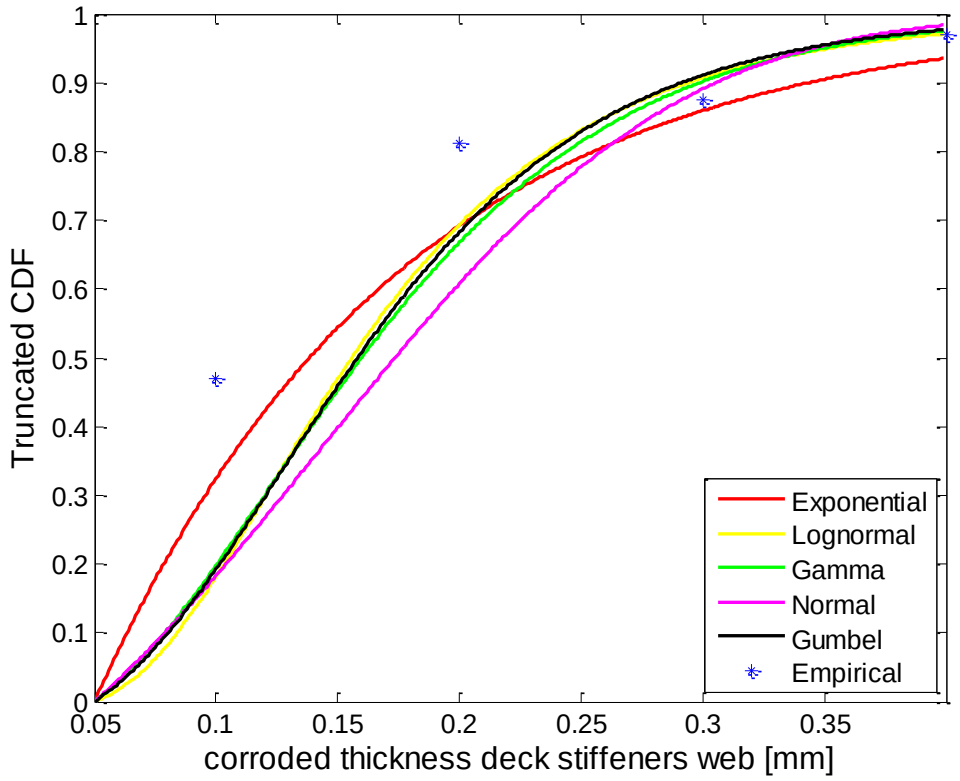

Figure 12 - Comparisons of the empirical CDF with the assumed ones for the web deck longitudinals corroded thicknesses

However, it may seem that the exponential distribution in the very upper extreme of the distribution is not the best approximation (as it is confirmed by the q-q plot, fig. 15).

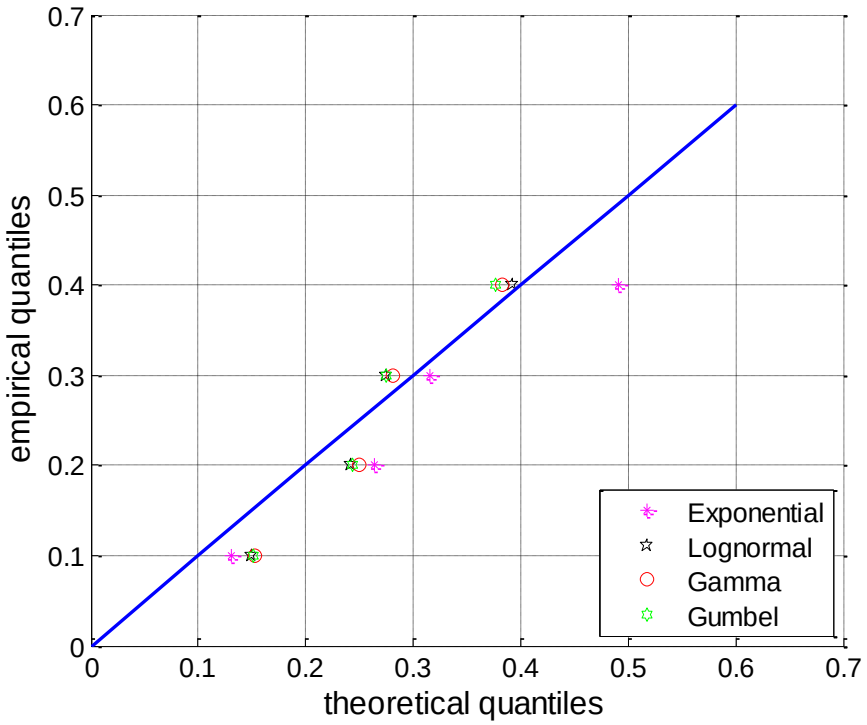

Figure 13 - q-q plot for the web deck longitudinals corroded thicknesses

The q-q plot may seems inconsistent with the weighed sum of squares method (tab. 8), which is – one more time – giving the lower error in the case of a truncated exponential distribution with MLE. This is only an apparent inconsistency, since the weighed SS method is still influenced by the very bad behavior of the non-exponential distribution in the lower and middle part of the distribution.

Table 8 – Weighed least squares method for the web deck longitudinals corroded thicknesses

	Method of moments	MLE
	Weighed SS	*Weighed SS*
Exponential truncated distribution	0.026	0.006
Lognormal truncated distribution	0.012	0.011
Gamma truncated distribution	0.014	0.012
Normal truncated distribution	0.025	0.017
Gumbel truncated distribution	0.015	0.011

Finally the truncated exponential distribution with the following MLE estimator was chosen:

$\lambda = 7.848$ ($\mu = 0.127\ mm$)

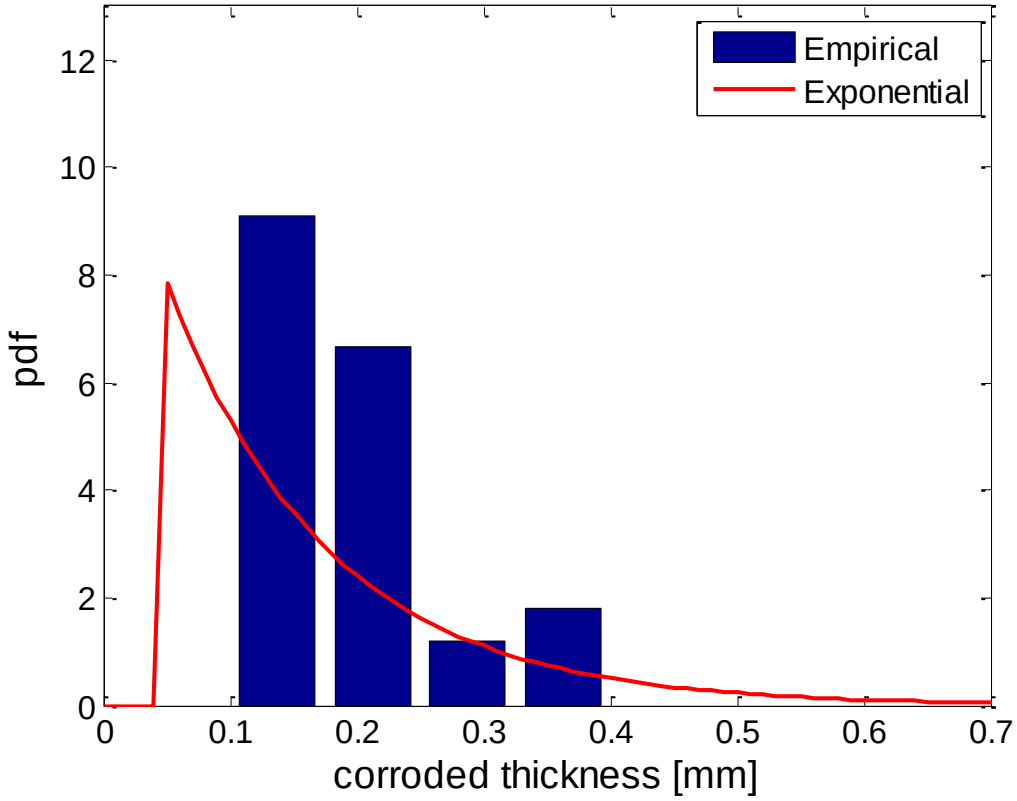

Figure 14 - Exponential truncated probability distribution function for the web deck longitudinals corroded thicknesses

2.4.3 Flange deck longitudinals

The first two parameters of the distributions are the two truncation values a and b, which are already known:

$a = 0.05\ mm$

$b = t_f = 16\ mm$

As already said before, the thickness measurements for the flange are not available. Hence, the corroded thicknesses for the web have been used, assuming they would be the same. The results for the flange will not be shown, as they are exactly the same than the one for the web. This conclusion may seem extremely obvious: on one hand this is right, but on the other we should underline that the parameter b is not the same for the web and the flange. This might have led to some small differences in the results between the web and the flange, but it did not.

2.4.3 Summary of the results

In conclusion, the following random variables will be used as input data for the case study.

Table 9 – Results of the corroded thickness processing

Variable	Distribution type
Corroded thickness of the deck plate	$Exp(\lambda = 1.647)$
Corroded thickness of the deck longitudinal's web	$Exp(\lambda = 7.848)$
Corroded thickness of the deck longitudinal's flange	$Exp(\lambda = 7.848)$

References

[1] H. K. T. Kuijper et al., "Probability in Civil Engineering, part 1: the theory of probability design", TU Delft, 1997

[2] P. Erto, "Probabilita' e statistica per le scienze e l'ingegneria", McGraw-Hill, 2008 (in italian)

[3] G. Lominashvili, M. Patsatsia, "On the estimation of a maximum likelihood truncated exponential distributions", Bulletin of the Georgian national academy of sciences, 2013

[4] M. J. D. Powell, "A Fortran subroutine for solving systems of nonlinear algebraic equations", Numerical methods for nonlinear algebraic equations, 1970

[5] J. C. Lagarias, J. A. Reeds, M.H. Wright, P. E. Wright, "Convergence properties of the Nedler-Mead simplex method in low dimentions", SIAM Journal of Optimization (vol. 9, no. 1), 1998

[7] Bruno Vasconcelos de Farias, Theodor Antoun Netto, "FPSO hull structural integrity evaluation via Bayesian updating of inspection data", Ocean engineering, 2012

[8] R. E. Melchers, "Probabilistic models of corrosion for reliability assessment and maintenance planning", 20th International Conference on Offshore Mechanics and Arctic Engineering, 2001

3

Modelling load variables

In this chapter, the general methodology to determine the loads to use in our structural reliability reassessment, and the way to model uncertainties (both load uncertainties and strength uncertainties), are introduced.

For the monitored loads it was possible to model the statistical uncertainties starting from the measurements. For the non-monitored loads, some literature research has been done.

Actually, a lot of material has been found in the literature about the quantification of the statistical characteristics of the random variables involved in ship design. Indeed, this is a hot topic in the marine/offshore engineering, as the description of the statistical properties of the random variables significantly affects the result of a reliability-based structural analysis.

However, not many material exists for FPSOs and ship-shaped offshore structures, and therefore many times it has been assumed that the validity of the probabilistic properties of the random variables for traditional ships still holds for FPSOs.

Finally, some methods to combine loads and stresses are explained.

It is important to underline the *general* validity of the content of this chapter, which – together with chapter 4 – is giving all the methodology behind the structural reassessment of corroded FPSOs. The application to a specific case study of the things described in these two chapters will be treated in chapters 5 and 6.

In annex B there is a summary of all the random variables, and the way to model them, which will be used in the FPSO strength reassessment.

3.1 MONITAS monitored data

First of all, let's summarize all the monitored data which are available from a ship endowed with the advisory hull monitoring system, in order to have an overview of the available monitored data.

1. Load conditions: draft and ullage of all tanks (cargo tanks, ballast tanks, etc.);

2. Waves: any 6 hours the significant wave height and peak period, for both windsea and swell, are recorded in two different scatter diagrams (one for wave and one for swell). Moreover, also the main direction (for both swell and sea) and the probability of occurrence of swell and swell together with sea are recorded. The peak period, the significant wave height and main direction will allow the calculation of a wave spectra (which is also recorded);
3. 6 DOF motions of the vessel (in particular first order wave-induced accelerations; the second order wave drift force's contribution to inertia force is negligible);
4. FPSO orientation;
5. Relative wave height;
6. Stresses (in location free of stress concentration and caused by one dominant mechanism), measured by two different type of sensors (normal strain gauges and long base strain gauges);
7. Wind speed and direction;
8. Current.

3.2 Long term distribution for wave induced loads

In general, we can distinguish two different ways to derive a long term distribution from a numerical samples of measured data.

The first one is to consider all the numerical measured values together, and to process them by finding a suitable pdf which best describes their distribution. This is the easiest way: it requires a direct monitoring of the parameters of interest, and not also of the sea states.

The second method is what it is usually considered during the design of a new vessel, that is: for each sea state (wave spectra), get at first a response spectra, then a short term probability distribution. Finally the long term distribution is obtained by a "weighed sum" of the short term distributions, considering the probability of occurrence of each sea state and of each wave direction. This process requires the monitoring of the sea states and the wave main direction. Eventually, the response spectra can also be obtained by considering the measured response spectra (for example, in the case of stresses).

In both cases a sufficiently long monitoring period (at least one year to take into account the seasonal variation) has to be considered.

The first approach will be used in the current thesis. It is assumed that after a "sufficiently long" monitored period, the updated statistical properties of the loads derived from the monitored data will stabilize themselves.

3.3 Modelling uncertainties for traditional cargo ships

According to Nikolaidis and Kaplan ([2]) , the uncertainties of any generic random variables can be divided into:

1) statistical uncertainties, that arise simply from the randomness of the variable itself;
2) modelling uncertainties, that arise from all the assumptions, simplifications, approximations necessarily involved in any engineering process.

Hence, any random variable can be expressed as:

$$X = B_I B_{II} X_0 = B_{II} X \tag{3.1}$$

Where:

- X_0 is the design value of the variable;
- B_I accounts for the statistical uncertainties;
- B_{II} accounts for the modelling uncertainties;

B_I and B_{II} are random variables as well.

This uncertainties classification has been used throughout the current project.

3.3.1 Statistical uncertainties

In our case, B_I:

- for the monitored parameters, it is already incorporated in the random variables X we will consider, since we will start directly from the measurements of a random variables rather than from its design value.
- for the non-monitored parameters, it is a distinct random variables which multiplies the assumed deterministic value.

A quick overview of the way statistical uncertainties are currently modelled during the structural reliability analysis of a traditional vessels is now given here:

- Several studies have showed the stochastic nature of the SWBM. It has also been demonstrated that the coefficient of variation c.o.v. for the SWBM is usually higher for tankers (and hence FPSOs) rather than for containerships ([10]). In particular, from the results of studies carried out by Guedes Soares ([3]) and Guedes Soares and Dias ([4]), it can be concluded that the still-water bending moment can be approximated by a normal distribution for traditional cargo ships.
- Static sea pressure can be considered a deterministic value, since the draught is usually a well monitored parameter, as it cannot exceed the freeboard draught ([1]).
- Errors in the level of filling of tanks are generally small, and thus also them are considered deterministic values ([1]).
- In the same way, stiffeners' lengths and stiffeners' spacing (and, in general, all constructional parameters) can be taken as deterministic value ([1]).
- The static cargo pressure is usually assumed to be normal distributed for commercial vessel, with a coefficient of variance of 0,05 for liquid cargoes, which is the case for a FPSO.

- The extreme wave-induced loads (wave sea pressure, wave cargo pressure and wave induced bending moments) are best fitted by a Gumbel distribution, as proposed by Faulkner ([5]).
- The material properties (yield stress, Young's modulus and others) are also usually taken as normal or lognormal distributed, but with a c.o.v. quite small (between 0,06 and 0,1) ([12]).

Table 1 – Usual way to model statistical uncertainties for traditional vessels

Variable	Probability density function
Vertical static bending moment	Normal distribution
Vertical wave bending moment	Gumbel distribution
Horizontal wave bending moment	Gumbel distribution
Load cargo dynamic pressure	Gumbel distribution
Load cargo static pressure	Normal distribution
Sea water dynamic pressure	Gumbel distribution
Sea water static pressure	Normal distribution
Material properties (yield stress, fracture toughness, Young modulus)	Normal or lognormal distribution
Level of filling of tanks	Deterministic value
Geometric dimension (stiffener length/spacing, main hull dimensions, design thickness)	Deterministic value

3.3.2 Modelling uncertainties

Some of the uncertainties which B_{II} has to take into account are:

- approximations made in the fitting of the empirical distribution with a continuous probability distributions function, especially in the tales (i.e. at the extremes) of the pdf, where there is obviously a lack of data since we are dealing with rare events;
- application of the simple beam theory for stiffeners;
- applications of the different plate theories for plates;
- approximations in modelling of the failure mechanism;
- approximations due to the structural idealization (beam model, plate model, boundary conditions);
- human error;
- fabrication tolerances;
- differences resulting from use of different reliability analysis methods.

Analogously to what has been done before for the statistical uncertainties, the following presents a short summary of the way modelling uncertainties are currently usually modelled.

- Modelling errors for the static loads (SWBM, static cargo loads and static pressure) are generally neglected ([1]).

- For both the VWBM and wave-induced local loads, an average value equal to unity and a c.o.v. between 0,1 and 0,15 can be assumed for the coefficient B_{II}, which will be taken as normally distributed ([1]). The same coefficients will be also used for the HWBM.
- The load combination factors introduce new statistical uncertainties, which are usually taken as normally distributed ([1]).

We should underline one more time that this way of modelling the modelling uncertainties refers to traditional commercial vessel, and therefore the extension of the validity of these coefficients to our FPSO reassessment procedure must be discussed and eventually justified.

Table 2 – Usual way to model modelling uncertainties for traditional vessels

Modelling errors' variables	Mean value	c.o.v.	Probability density function
Vertical static bending moment	-	-	-
Vertical wave bending moment	1	0.1-0.15	Normal
Horizontal wave bending moment	1	0.1-0.15	Normal
Load cargo dynamic pressure	1	0.1-0.15	Normal
Load cargo static pressure	-	-	-
Sea water static pressure	-	-	-
Sea water wave pressure	1	0.1-0.15	Normal
Loads combination factors local static pressure and wave induced pressure	1	0.15	Normal
Loads combination factors SWBM and VWBM	1	0.15	Normal
Loads combination factors HWBM and VWBM	0.9	0.15	Normal
Loads combination factors local load induced stress and hull girder induced stress	1	0.15	Normal

However, an important consideration needs to be done for the monitored loads. All these modelling uncertainties coefficients are valid for the design phase. They have all been estimated to "correct" all the mistakes which are made by assuming a certain deterministic design value. However, the reason we monitor loads is actually to reduce the modelling uncertainties. Therefore, it is a non-sense to use the modelling uncertainties coefficients, which are supposed to be used for the design of a new vessel, also to multiply the monitored random variables. In other words, we have now some knowledge which during the design of the unit we did not have, and if we use the modelling uncertainties coefficients that are intended for the design of a new vessel, we "throw away" a portion of the extra knowledge gained.

On the other hand, we still cannot set to zero the modelling uncertainties. Therefore it was chosen to keep using the same modelling coefficients, but it must be pointed out the paradox in using these coefficients.

Finally, there are also some modelling uncertainties related to the methods adopted to derive the failure functions. In chapter 4 a large number of models (simple beam theory, classical plate theory, large deflection analysis, and others) have been used to write down the limit state functions. However, these models are not the only one. For each failure modes, different equivalent methods, either analytical or empirical or numerical, which can give similar but different results, exist. In the present work these uncertainties have not been modelled. However, in chapter 4 the validity of the analytical methods used for the computation of the ultimate strengths is shown through a comparison with a non-linear finite element model.

3.4 Loads combination

In any ship structural assessment there are some loads which need to be combined. In our case, the loads to combine are:

1. SWBM and VWBM (and the corresponding induced stress);
2. HWBM and VWBM (and the corresponding induced stress);
3. The local static pressure and local wave induced pressure (and the corresponding induced stress);
4. The local load induced stress and the hull girder induced stress.

It must be pointed out a fundamental difference between the distribution of static loads and wave induced loads: in a reliability analysis the distributions for wave induced loads are extreme value distributions, while the distributions for the static loads are not. It is evident then the extremes values of wave induced loads may not occur at the same time. Hence, we should consider a way to combine these wave induced loads, in order not to make our assessment too conservative.

To combine the a static load and a wave-induced load two different methods have been used and compared in this thesis.

The first one is the Square Root of Sum of Squares (SRSS) method. If $X(t) = \sum_i X_i(t)$ is a linear combination of independent loads, then the maximum combined loads using the SRSS method is:

$$X_{max} = \sqrt{\sum_i X_{i,max}^2(t)} \tag{3.2}$$

The second one is the Turkstra's rule. If $X(t) = X_1(t) + X_2(t)$ is a linear combination of independent loads, then the maximum combined loads using this method is:

$$X_{max} = max\{X_{1,max} + \mu_{X_2}, \mu_{X_1} + X_{2,max}\} \tag{3.3}$$

For the static loads and wave induced loads it is more likely that the maximum loads will occur simultaneously, thus a more conservative combination method will be used, which is the peak coincidence method:

$$X_{max} = \sum_i X_{i,max}(t) \tag{3.4}$$

This method can also be used to combine a local load induced stress with an hull-girder induced stress.

Both the peak coincidence method and the SRSS method are deterministic methods. However, in literature it is also possible to find stochastic methods to combine the SWBM and HWBM (Ferry Borges and Castenheta, [7] and Moan and Jiao, [8]). In 1984 Guedes Soares ([9]) demonstrated that stochastic methods provide exact solutions for combining still-water and wave-induced bending moments. However, they have not been used in the current master thesis, but it is important to point it out for eventual further improvements of the FPSO reassessment procedure

3.5 Loads identification for FPSOs endowed with AHMS

On the base of all the considerations made before, let us see the way each load can be derived and modeled for the specific FPSO case. In annex B it is possible to find a summary of this paragraph.

3.5.1 Still water bending moment

The vertical static bending moment can be written as:

$$X_{M_{SW}} = B_I B_{II} M_{SW,0} = B_I M_{SW,0} \tag{3.5}$$

B_{II}, the modelling uncertainties, have been neglected, analogously to the usual practice for traditional vessels. The statistical uncertainties will be modeled by processing all the SWBM values recorded by the on-board computer.

The statistical nature of the still water bending moment is due to the different load conditions in which an FPSO may be during its lifetime. This variability is further increased by the utilization of on-board computer load programmes, which give more freedom to the operator during the loading procedure. These software can calculate the SWBM distribution for any load condition, and - as long as the maximum load is within the specified allowable limit – the operator is free to load the ship in any way he prefers.

As already said before, B_I for traditional commercial vessels has usually been modelled as a normal distributed random variable. However, in 1988 - based on 453 actual still water load condition recorded during the first two operational years of an FPSO (with typical duration of each load condition varying from several hours to one day), Moan and Jiao ([11]) found that the

SWBM was best fitted by a Rayleigh distribution in sagging and exponential distribution in hogging.

An important distinction between the time domain representations of the SWBMs for commercial oil tanker and FPSO must be pointed out. For a tanker the SWBM time history looks more like a rectangular pulse process:

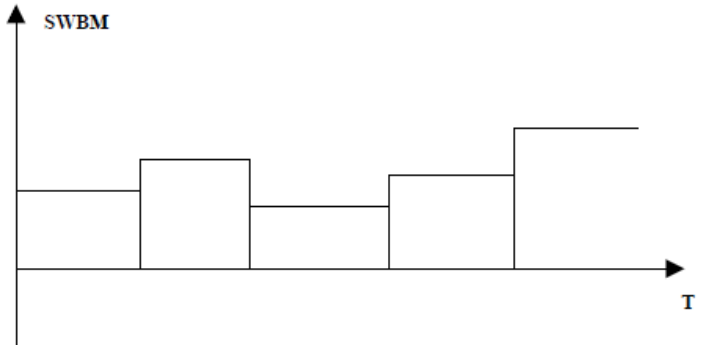

Figure 1 – SWBM time trace in a traditional tanker

The probability distribution function is then estimated by considering each load condition independently, without looking at the duration of each load condition (which is also a random variable).

For FPSO the SWBM time history will look more like a saw tooth wave (every two/three weeks the FPSO is offloaded, and offloading operation will take about one/two days).

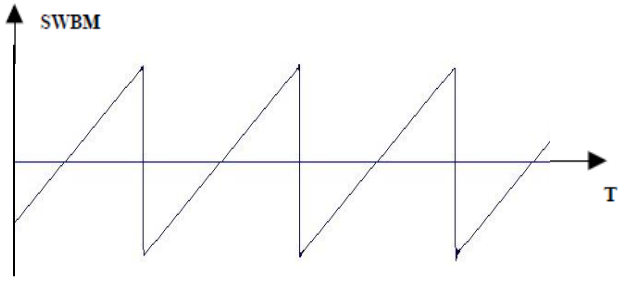

Figure 2 – SWBM time trace in an FPSO

Hence, in this case a uniform distribution is expected.

3.5.2 Vertical wave bending moment

On the deck of a ship endowed with the MONITAS system, there are 4 long base strain gauges (usually located on two different cross section), which are used to measure the wave bending moments induced strains (and thus stresses). If we know the section modulus of the FPSO, it is possible to compute the VWBM from the strain measurement. Then, we can fit the extremes distribution, to find its probability distribution (usually this is a Gumbel distribution).

However, we will have the results for just two sections. We can extend the determination of the VWBM to the whole hull girder length by considering the design VWBM distribution over the hull girder length (for different heading angles, if the FPSO is a spread moored FPSO), and scaling it by a factor which was obtained by comparing the design VWBM and the measured VWBM in the two cross section with gauges (one different factor for any heading angle). We assume then that the ratio between measured VWBM and design-predicted VWBM is the same along the whole hull girder length. The scaling factors have to be calculated comparing the measured VWBM and the design VWBM with an equal probability of occurrence. Generally the characteristic value computed during the design (with a strip theory or diffraction code) or the characteristic value used in a rule-based design have a probability of occurrence in the whole ship lifetime of 10^{-8}.

A sufficiently long monitoring period needs to be taken, for sure no less than one year (typically in one year we have $3 * 10^6$ load cycles) to take into account the seasonal variations.

The modelling uncertainties in the current tanker design practice are modelled with a normal distribution with average value equal to 1 and c.o.v. between 0,1 and 0,15. In our case it was chosen to use the less conservative of these two values (thus c.o.v. equal to 0,1), since – as we are using some monitored stress on the deck – it is reasonable to expect a less uncertain VWBM.

3.5.3 Horizontal wave bending moment

The long base strain gauge can be used also for the determination of the HWBM, by a comparison of the PS and SB gauges. This is possible under the assumption that the vertical neutral axis will lie in the central plane of the unit. This hypothesis is absolutely valid for turret moored FPSO, but may not be valid for unit with a lot of risers attached to one of its sides.

The modelling uncertainties will be modeled in the same way as it was done for the VWBM (normal distribution with mean 1 and c.o.v. 0,1).

3.5.4 Static sea pressure

If we know the draft, then the hydrostatic sea pressure can be calculated without adding extra uncertainties. Therefore the hydrostatic sea pressure will be a random variable, whose distribution will be the same of the draft.

3.5.5 Dynamic sea pressure on the side

In the MONITAS system there are no pressure sensors on the sides of the vessel. However the wave pressure on the sides of the vessel can be indirectly measured from the relative wave elevation. The pressure above the wave is zero. The pressure beneath the wave trough is calculated according to the linear wave theory:

$$p = \rho * g * \zeta_{RWA} * e^{k(z-z_{swl})} \qquad z < z_{swl} - \zeta_{RWA} \tag{3.6}$$

- ρ is the density of water
- ζ_{RWA} is the (monitored) relative wave amplitude

- z is the vertical position
- z_{swl} is the still water line vertical position
- k is the wave number

The modelling uncertainties will be modeled – according to table 2 – with a normal distribution with an average 1 and a c.o.v. of 0,1.

3.5.6 Cargo/ballast static pressure

There is no modelling uncertainty related to the static cargo/ballast pressure. There is, however, a statistical uncertainty related, for example, to a density variation of the liquid cargo/ballast or to tank ullage variation. This can be modeled with a coefficient with a normal distribution, an average value equal to 1, and a c.o.v. of 0,05 ([1]). The nominal value of the cargo/ballast static pressure is, of course, the design value.

3.5.7 Cargo/ballast dynamic pressure

Moreover, we need to model the cargo and ballast dynamic pressure. This includes:

- the inertia pressure;
- the sloshing impact pressure.

Due to its complexity, the sloshing impact pressure will be assumed to be a deterministic (design) value.

The inertia pressure can be expressed as a function of the monitored accelerations.

Indeed, the inertia pressure is a function of the liquid density too, which is also a random variable. If we assume that the cargo/ballast static pressure uncertainties are only due to the density variations, then we can model the statistical uncertainties of the density in the same way as the cargo/ballast static pressure, that is with a normal distribution with a c.o.v. of 0,05.

Since the cargo/ballast inertia loads are still wave-induced loads, the modelling uncertainties will be modeled in the same way as for the wave sea pressure on the side.

3.5.8 Load combination factor

As already said, three different load combination methods will be used. The peak coincidence method is assuming that the peaks of the two loads occur simultaneously; the SSRS method is assuming that the peak coincidence method of the two loads occur with a phase shift of 90 degrees; the Turkstra's rule is combining the mean value of a load component with the extreme value of the other load component. Each of these three load combination methods introduces new modelling uncertainties.

Reference [17] is giving some modelling uncertainties (table 3) for different load combination methods. They have been derived for the particular case of the combination of the VWBM with the slamming-induced vertical bending moment. There is a shortage of data related to this topic, therefore we will assume that they are still valid for all the types of load combination (and, in

particular, for the load combination between the VWBM and the HWBM, which is the only one needed in the case study – see chapter 6).

Table 3 – Modelling uncertainties for load combination methods

Modelling uncertainties	Bias	c.o.v.
Peak coincidence	0.72	0.11
SRSS	1.01	0.12
Turkstra	1.17	0.11

3.5.9 Material properties and constructional parameters

The material properties we are interested in, are:

- Yield stress;
- Fracture toughness;
- Young modulus;
- Poisson's ratio;

The source of statistical uncertainties for these values is the material non-homogeneity, the presence of defects, etc.. The modelling uncertainties are due, for example, to the different conditions (for example of temperature) in which the measurement tests have been made, or to measurement error.

The constructional (geometric) parameters we are interested in are:

- Main hull dimensions;
- Stiffener length;
- Stiffener spacing;
- Thickness (design gross thickness, thus no corroded yet).

The continuous improvement of the methods of construction and implementation of quality control procedure in shipyards and steel works has made uncertainties in the main dimensions of the hull and thicknesses more and more negligible. Therefore uncertainties for constructional parameters can be assumed to be zero.

With regards to the statistical uncertainties of the mechanical properties, more detailed study revealed that:

- The Poisson ratio is generally considered to be a deterministic value;
- With regards to the yielding strength, Mansour et al. ([13]) in 1984 conducted several tests on different steels. They recommended the lognormal distribution for both ordinary and higher strength steels. Hess et al. ([12]), on the basis of the same data used by Mansour in 1984, suggested to use an average bias of 1,11 and average c.o.v. of 0,068 for ordinary steel, and an average bias of 1,22 and average c.o.v. of 0,089 for high strength

steel. Moreover more recent tests have showed that a Weibull distribution or a Gumbel distribution are all equally valid choice for describing the yield strength of steel. However, we will use the lognormal distribution. We should keep in mind that also the steel thickness (besides the steel type) has an influence on the yield strength distribution; however this influence, which Hess ([12]) proved to be small, has been neglected.

- Hess et al. ([12]), on the basis of several studies, concluded that a either normal or lognormal distribution can be used for the Elastic Modulus distribution. For both ordinary steel and high strength steel they recommended to use a mean bias of 1,024 and a c.o.v. of 0,0179.
- Limited studies related to the ultimate strength of steels are available. Hess et al. ([12]), on the basis of the few studies available, suggested to use a normal distribution with a bias of 1,046 and a c.o.v. of 0,0477.
- With regards to the stress intensity factor, if the linear fracture mechanics is used, and if only the mode I for crack propagation is considered, the SCF is $K = \sigma\sqrt{a\pi}$, where σ (remote stress) is the sum of the applied stress and the residual stress, and it is a random variable. a is the half-length of the crack. The applied stress can be calculated directly from the load measurements (SWBM, VWBM, HWBM and lateral pressures), and the residual stress can be assumed to be half of the yielding stress (thus it is also a random variable). The crack length is also a random variable, but due to the lack of literature it will be considered a deterministic value. In particular, according to DNV ([16]) the value of 6.67 mm has been used. This represent the zero probability in the probability crack detection curve, that is smaller cracks cannot be detected.
- Analogously to what has been done for the crack length, the critical fracture toughness K_C will be considered as a deterministic value as well. It is a property of the material, and it is possible to compute it using specific tables once the steel grade is known.

As already said before, Nikolaidis and Kaplan (1991, [2]), on the basis of some FEM calculations they performed, concluded that a normal distribution with an average value of 1 and a c.o.v. between 0,1 and 0,15 can be used to model the modelling uncertainties of the strength capability. A c.o.v. value of 0,125 will be considered here.

3.5.10 Corroded thickness

The corroded thickness distribution will be estimated in each situation, based on the thickness measurements.

Besides the statistical uncertainties, in the corroded thickness random variable there are also some modelling uncertainties, in particular due to errors in fitting the histograms with a continuous probability distribution, or error measurements. However, since in chapter 2 the thickness measurements processing was made in a conservative way, by not considering the zero corroded thicknesses, these uncertainties have not been modelled.

References

[1] Dominique Beghin, Bureau Veritas, “Reliability-based structural design”, Ship structural analysis and design (Chapter 5), SNAME 2010

[2] E. Nikolaidis, P. Kaplan, “Uncertainties in stress analysis of marine structures”, SNAME structural Inspection, maintenance and monitoring symposium (SSC Report-363), 1991

[3] C. Guedes Soares, “Stochastic modelling of maximum still water load effects in ship structures”, Journal of ship research (Vol. 3), 1990

[4] C. Guedes Soares, S. Dias, “Probabilistic models of still water load effects in container ships”, Marine Structures (Vol. 9), 1996

[5] D. Faulkner, “Semi-probabilistic approach to the design of marine structures”, International symposium on the extreme load response, Trans. SNAME, 1981

[6] A. E. Mansour, “Extreme loads and load combinations”, Journal of ship research (vol. 39), 1995

[7] J. Ferry-Borges, M. Castenheta, “Structural safety”, Lisbon: laboratoria nacional de engenhera civil, 1971

[8] T. Moan, G. Jiao, “Characteristic still water load effect for production ships”, Report MK/R 104/88, Trondheim: the Norwegian institute of technology, 1988

[9] C. Guedes Soares, “Probabilistic models for load effects in ship structures”, Report UR-84-38, Trondheim: department of marine technology, Norwegian institute of technology, 1984

[10] M. Kaplan, M. Benatar, J. Bentson, T. A. Achtarides, “Analysis and assessment of major uncertainties associated with ship hull ultimate failure”, Ship structure committee (SSC Report-322), 1984

[11] T. Moan, G. Jiao, “Characteristic still-water load effects for production ships”, The Norwegian institute of technology (Report MK/R 104/88), 1988

[12] P. E. Hess, D. Bruchmann, I. A. Assakkag, B. M. Ayyub, “Uncertainties in material strength, geometric and load variables”, 2008

[13] A. E. Mansour, H. Y. Jan, C. I. Zigelman, Y. N. Chen, S. J. Harding, “Implementation of Reliability methods to marine structures”, Trans. SNAME (Vol. 92), 1984

[14] Henk van den Boom, Max Krekel, Pieter Aalberts, “FPSO Integrity; structural monitoring of Glas Dowr”, Offshore Technology conference, 2000

[15] R. B. Hageman, “Improved load calculation for risk based inspection”, MARIN report, 2014

[16] “Structural reliability analysis of marine structures”, DNV classification notes (No. 30.6), 1992

[17] A. Mansour, A. Thayamballi, “Probability based ship design; loads and load combinations”, SSC Report-373, 1994

4

Limit state functions

In this chapter, some failure modes and failure criteria are introduced. For any of them a failure function (or limit state function, LSF) is given.

4.1 Introduction

Any limit state functions has been written as:

$$g(x) = Capacity\ C - Demand\ D \tag{4.1}$$

The above equation is actually only valid if the capacity *C* and the demand *D* are independent random variables, but this is indeed the case for any of the examined cases.

The structural elements in ships can be categorized as follows:

1. hull girder;
2. primary structure (transverse web frames, longitudinals girders, etc.);
3. stiffened panels;
4. unstiffened plate;
5. structural details.

In this master thesis, attention is given to stiffened panels and unstiffened plates. For any of these two structural elements, some limit states (i.e. some failure modes) have been identified. They have been further divided into two categories:

- Serviceability limit state (SLS), involving deterioration of less vital functions under normal service loads;
- Ultimate limit state (ULS), leading under extreme loads to the collapse of the structure.

Both the stiffened panels and the unstiffened plate will be considered as single independent components.

All the initial deflections and residual stresses will be neglected.

4.1.1 *Sign convention and reference system*

The vessel has the horizontal longitudinal x-axis pointed forward, the vertical z-axis pointed upwards, the transverse y-axis pointed to the portside (right turning axis system).

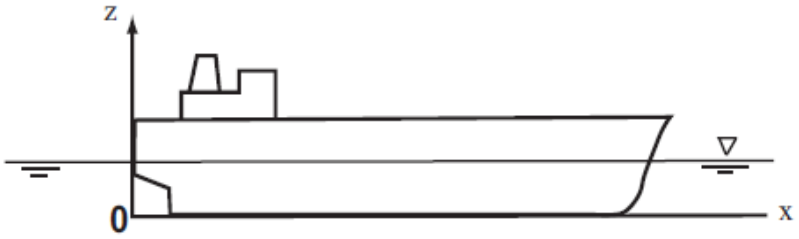

Figure 1 – Reference system

The hogging bending moment is taken as positive, and the sagging bending moment as negative. The positive vertical shear is the upwards shear on the forward surface of a hull girder chunk.

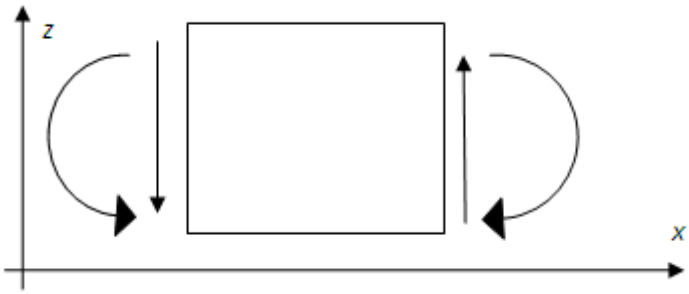

Figure 2 – Sign convention for vertical bending moment and vertical shear

Analogously, the positive horizontal bending moment and positive horizontal shear are:

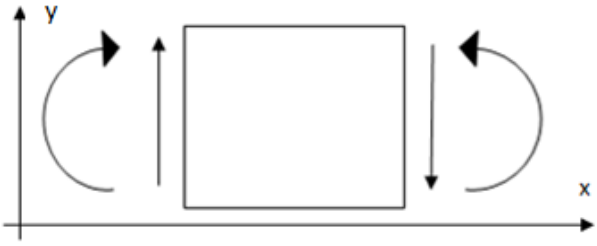

Figure 3 – Sign convention for horizontal bending moment and horizontal shear

The compressive normal stress are assumed to be negative, the tensile normal stress positive.

4.2 Effective width and effective breadth

Even though sometimes the expressions “effective width” and “effective breadth” are used as synonyms, they do not mean the same thing.

- We talk of "effective breadth" when lateral pressure is the dominant load components causing lateral deflection. Thus we are still in the elastic regime (no buckling caused by the axial components). Here the reduction of the plate breadth is due to the need to take into account the effect of the shear lag (and so the fact that the plating is not taking the same magnitude of normal stress along its breadth).
- We talk of "effective width" when the plate deflections is mainly due to the axial compressive loads (thus, we are in the post buckling regime). Here the necessity to reduce the plate width is due to the lower ability of a buckled plate to absorb loads. There are actually more than one method to deal with a buckled plate, and the effective width is only one of them. In the effective width method, the buckled plate is modelled as a flat plate, but with a reduced plate breadth and eventually also a reduced effective length.

It would be convenient to use the same effective breadth formulae which have been used for the original design of the FPSO. If they are not available, a Class Society formula may be used. A very simple design rules, used by ABS and other Class Societies, is to use an effective width which is the minimum between the stiffener spacing or the 1/3 of the stiffener span:

$$b_{eff} = min\left\{b, \frac{1}{3}L\right\} \tag{4.2}$$

- b: stiffeners spacing
- L: panel length

In 1975 Faulkner ([3]) has proposed a formula to calculate the effective width of a plate subjected to axial compressive loads in the x direction. The formula is:

$$b_{eff} = \begin{cases} 1 & for\ \beta < C_3 \\ \frac{C_1}{\beta} - \frac{C_2}{\beta^2} & for\ \beta \geq C_3 \end{cases} \tag{4.3}$$

Where:

- $C_1 = 2, C_2 = 1$ and $C_3 = 1$ for simply supported plates
- $C_1 = 2.25, C_2 = 1.25$ and $C_3 = 1.25$ for clamped plates
- $\beta = \frac{b}{t_P}\sqrt{\frac{\sigma_Y}{E}}$ is the plate slenderness coefficient

4.3 Unstiffened plate limit state functions

The limit state functions of unstiffened plates refer to the failure of the plating between longitudinals, under the assumption that the strength of the secondary stiffeners (e. g. longitudinals) is sufficient to prevent their collapse prior to that of the unstiffened plate.

The limit states identified are:

- Serviceability limit states:

    - First yielding of the panel
    - Formation of plastic hinges
- Ultimate limit states:
    - Elasto-plastic buckling
    - Fracture

In order to help the reader, table 1 is giving a summary of all these failure modes, together with the analytical theory used for the derivation of the LSFs and the reference paragraph.

Table 1 – Failure modes for unstiffened plates

Failure mode	Model	Paragraph
First yielding	Classical plate theory	4.3.1
Formation of plastic hinges	Classic plate theory and elasto-perfectly plastic material	4.3.2
Elasto-plastic buckling	Analytical method (Large deflection analysis combined with the membrane stress-based method)/Empirical method (Johnson Ostenfeld formula method)	4.3.3
Fracture	Linear fracture mechanics	4.5

Actually the elasto-plastic buckling is not a real "ultimate failure", since ultimate failure of the plating almost never occurs (unless we have a fatigue or brittle fracture) because the stiffeners usually have a much lower load capacity than the plating. When the plate deflections became very large, there does arise some restraints against pull-in, and hence the plate gradually becomes a fully plastic membrane, for which the rupture load is enormous ([18]).

For the serviceability limit state analysis of the panel, the small-delflection theory has been used, since in FPSO usually we are dealing with sturdy plates, that is plate with a small b/t ratio (slenderness coefficient $\beta = {}^{b}/_{t}\sqrt{{}^{\sigma_Y}/_{E}} < 2.4$). For this kind of plate the relative deflection w/t (w is the lateral deflection of the plate) will be generally small ([18]). This is the same reason why elastic buckling has not been taken into account.

For the yielding limit state the classical plate theory has been used (see 4.3.1), for the formation of hinges the elasto-plastic theory (see 4.3.2), for the elasto-plastic buckling the large deflection analysis combined with the membrane stress-based method (see 4.3.3) and finally for the fracture limit state the linear fracture mechanics (see 4.5) .

Furthermore, in the small deflections elasto-plastic theory it is possible to base the failure criteria both on stress/bending moment (formation of one or more plastic hinges) and on deflections (formation of a permanent set). It was chosen the first criteria, since, as we said, deflections are usually small for sturdy plates and do not represent a problem.

4.3.1 Yielding of unstiffened plates

Four different load conditions will be considered here:

1. laterally loaded panel;
2. laterally loaded panel with axial (compressive or tensile) load in the longer direction;
3. laterally loaded panel with axial (compressive or tensile) load in the shorter direction;
4. laterally loaded panel with axial (compressive or tensile) loads in both directions.

Let's consider an infinitely long plates with lateral uniform load. The edges parallel to the y axis are the longer ones. The classical plate theory will be used. The behaviour of this unstiffened plates loaded laterally can be described by:

$$D\frac{d^4w}{dx^4} = q \tag{4.4}$$

Where:

- $D = \frac{Et_P^3}{12(1-\nu^2)}$ is the flexural rigidity
- ν is the Poisson's ratio, $\nu = 0.3$
- E is the Young's modulus
- t_P is the plate thickness

An infinitely long plate is usually a good approximation for ship unstiffened plates, which often have one of the edges much longer than the other one. For plates with aspect ratio lower than 3, a different governing equation (to take into account the bending stresses in both directions), and thus a different solution, need to be used.

The maximum bending moment, per unit length, occurring on the longer sides (and thus inducing the highest bending stress in the *x* direction) is given by:

- Clamped edges:
  $$M_{max} = \frac{qb^2}{12} \tag{4.5}$$
- Simply supported edges:
  $$M_{max} = \frac{qb^2}{8} \tag{4.6}$$

The maximum bending stress is:

$$\sigma_x = \frac{6M_{max}}{t_P^2} \tag{4.7}$$

The last formula is valid for both clamped plates and simply supported plate, but the location where the highest stress occurs is different (for a simply supported plate it is in the centre, for a clamped plate is at the edges).

Differently from beams, if we have a bending stress σ_x, we have in this case also a transverse stress $\sigma_y = \nu\sigma_x$ (fig. 4).

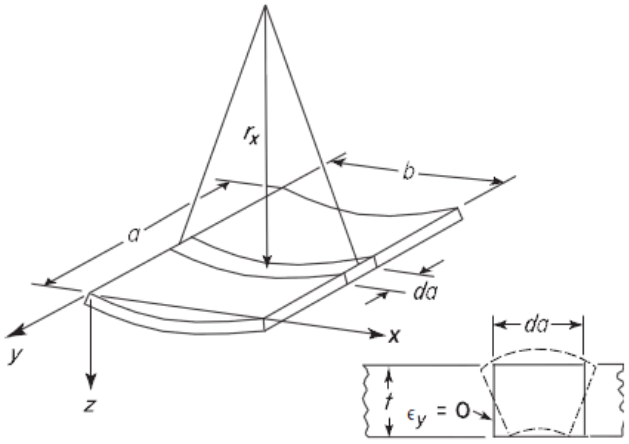

Figure 4 - Infinitely long plate in bending

For a laterally loaded panel, the limit state function is simply (we are using the Von Mises criterion):

$$g(x) = \sigma_Y - \sigma_{eq} \tag{4.8}$$

The equivalent stress, if we neglect the shear stress, is:

$$\sigma_{eq}^2 = \frac{1}{2}\left[\left(2\sigma_x^2 + 2\sigma_y^2 - 2\sigma_x\sigma_y\right) + 6\tau_{xy}^2\right] = \frac{1}{2}(2\sigma_x^2 + 2\nu^2\sigma_x^2 - 2\nu\sigma_x^2) = \sigma_x^2(1 + \nu^2 - \nu) \tag{4.9}$$

Hence:

$$g(x) = \sigma_Y - \sigma_{eq} = \sigma_Y - \frac{6M_{max}}{t_P^2}\sqrt{1 + \nu^2 - \nu} \tag{4.10}$$

(Please, note the difference between σ_y – stress in the y direction – and σ_Y – yielding stress!)

If, besides the lateral load, we have also an axial load N_y, then the governing equation is:

$$D\frac{d^4w}{dx^4} + N_y\frac{d^2w}{dx^2} = q \tag{4.11}$$

We can apply the superposition principle (and we can since we are still in the linear elastic regimes):

$$\sigma_{eq}^2 = \left(\sigma_x^2 + \sigma_y^2 - \sigma_x\sigma_y\right) = \left[\left(\frac{6M_x}{t_P^2}\right)^2 + \left(\nu\frac{6M_x}{t_P^2} + \frac{N_y}{bt_P}\right)^2 - \left(\frac{6M_x}{t_P^2}\right)\left(\nu\frac{6M_x}{t_P^2} + \frac{N_y}{bt_P}\right)\right] \tag{4.12}$$

$$g(x) = \sigma_Y - \sigma_{eq} = \sigma_Y - \sqrt{\left(\frac{6M_x}{t_P^2}\right)^2 + \left(\nu\frac{6M_x}{t_P^2} + \frac{N_y}{bt_P}\right)^2 - \left(\frac{6M_x}{t_P^2}\right)\left(\nu\frac{6M_x}{t_P^2} + \frac{N_y}{bt_P}\right)} \tag{4.13}$$

Analogously a similar limit state function can be derived if the axial load is in the *x* direction or in the *x* and *y* direction simultaneously. In the *x* direction:

$$g(x) = \sigma_Y - \sigma_{eq} = \sigma_Y - \sqrt{\left(\frac{6M_x}{t_P^2} + \frac{N_x}{bt_P}\right)^2 + \left(\nu\frac{6M_x}{t_P^2}\right)^2 - \left(\frac{6M_x}{t_P^2} + \frac{N_x}{bt_P}\right)\left(\nu\frac{6M_x}{t_P^2}\right)} \qquad (4.14)$$

In both directions:

$$g(x) = \sigma_Y - \sigma_{eq}$$
$$= \sigma_Y - \sqrt{\left(\frac{6M_x}{t_P^2} + \frac{N_x}{bt_P}\right)^2 + \left(\nu\frac{6M_x}{t_P^2} + \frac{N_y}{bt_P}\right)^2 - \left(\frac{6M_x}{t_P^2} + \frac{N_x}{bt_P}\right)\left(\nu\frac{6M_x}{t_P^2} + \frac{N_y}{bt_P}\right)} \qquad (4.15)$$

It must be pointed out that an implicit assumption behind this limit state functions is that we are in the small deformation regime. This means that the maximum deflection is lower than the thickness of the plate. This is of course no more valid if the axial load, in combination with the lateral load, will cause the plate to buckle. This situation will be treated in paragraph 4.3.3, with the help of the large deformation theory.

Furthermore, if $q \neq 0$, the stiffener spacing b need to be replaced by the effective breadth b_{eff}.

4.3.2 Plastic hinges formation in unstiffened plates

Eight different load conditions will be considered here:

1. simply supported laterally loaded panel;
2. simply supported laterally loaded panel with axial (compressive or tensile) load in the longer direction;
3. simply supported laterally loaded panel with axial (compressive or tensile) load in the shorter direction;
4. simply supported laterally loaded panel with axial (compressive or tensile) loads in both directions;
5. clamped laterally loaded panel;
6. clamped laterally loaded panel with axial (compressive or tensile) load in the longer direction;
7. clamped laterally loaded panel with axial (compressive or tensile) load in the shorter direction;
8. clamped laterally loaded panel with axial (compressive or tensile) loads in both directions.

If yielding starts to occur, the panel has still some residual capacity to absorb loads before the formation of one plastic hinge (for a simply supported panel) or of three plastic hinges (for a clamped panel) will terminate. However, as we are assuming that the failure of an unstiffened plate is always prior to that one of the surrounding stiffeners, the formation of plastic hinges in

the unstiffened plate is to consider a serviceability limit states, as it just affect the efficiency of structural elements, but it will not cause the overall failure of the structure.

The theory applied is based on an idealized "elastic-perfectly plastic" stress-strain curve (fig. 5). This means that we have a definite yield point above which we have the switch from the elastic to the plastic deformation (which is usually the case for steel) and we are ignoring the strain-hardening of the material (thus our model is a conservative one).

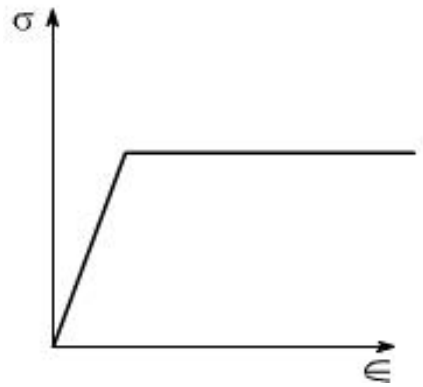

Figure 5 – Elasto-perfecty plastic material

For a infinitely long panels with simply supported edges, with a lateral uniform pressure, the maximum bending moment (per unit length) is given by:

$$M_{max} = \frac{qb^2}{8} \tag{4.16}$$

The limit state function is then:

$$g(x) = \sigma_{perm} Z_{pm} - \frac{qb^2}{8} \tag{4.17}$$

Where:

- $Z_{pm} = \frac{t_P^2}{4}$ is the plastic section modulus in the middle of the panel
- σ_{perm} is given by the Von Mises criteria:

$$\sigma_Y^2 = \frac{1}{2}\left[\left(2\sigma_{perm}^2 + 2\sigma_y^2 - 2\sigma_{perm}\sigma_y\right) + 6\tau_{xy}^2\right] = \left(\sigma_{perm}^2 + \nu^2\sigma_{perm}^2 - \nu\sigma_{perm}^2\right)$$
$$= \sigma_{perm}^2(1 + \nu^2 - \nu)$$

In (4.18) we decided to neglect the shear stress.

Hence:

$$\sigma_{perm} = \frac{\sigma_Y}{\sqrt{(1 + \nu^2 - \nu)}} \tag{4.18}$$

If we have also an axial load in the longer direction, then the limit state function is still the (4.17), but the allowable stress is different:

$$g(x) = \sigma_{perm} Z_{pm} - \frac{qb^2}{8} \tag{4.19}$$

Where:

- $Z_{pm} = \frac{t_P^2}{4}$ is the plastic section modulus in the middle of the panel
- σ_{perm} is given by the Von Mises criteria (neglecting the shear stress):

$$\begin{aligned}\sigma_Y^2 &= \left[\sigma_{perm}^2 - \sigma_{perm}(\nu\sigma_{perm} + \sigma_n) + \left(\nu\sigma_{perm} + \sigma_n\right)^2\right] \\ &= \left[\sigma_{perm}^2 - \nu\sigma_{perm}^2 - \sigma_{perm}\sigma_n + \nu^2\sigma_{perm}^2 + \sigma_n^2 + 2\nu\sigma_{perm}\sigma_n\right] \\ &= \left[\sigma_{perm}^2 - \nu\sigma_{perm}^2 + \nu^2\sigma_{perm}^2 - \sigma_{perm}\sigma_n + 2\nu\sigma_{perm}\sigma_n + \sigma_n^2\right] \\ &= \left[\sigma_{perm}^2(1 - \nu + \nu^2) + \sigma_{perm}(2\nu\sigma_n - \sigma_n) + \sigma_n^2\right]\end{aligned}$$

- σ_n is the stress induced by the axial load in the longer direction

Hence:

$$\sigma_{perm}^2(1 - \nu + \nu^2) + \sigma_{perm}(\sigma_n + 2\nu\sigma_n) + \sigma_n^2 - \sigma_Y^2 = 0$$

$$\sigma_{perm} = \frac{-(\sigma_n + 2\nu\sigma_n) \pm \sqrt{(2\nu\sigma_n - \sigma_n)^2 - 4(\sigma_n^2 - \sigma_Y^2)(1 - \nu + \nu^2)}}{2(1 - \nu + \nu^2)}$$

$$= \frac{-(\sigma_n + 2\nu\sigma_n) \pm \sqrt{\sigma_n^2 + 4\nu^2\sigma_n^2 - 4\nu\sigma_n^2 - 4\sigma_n^2 + 4\sigma_n^2\nu - 4\sigma_n^2\nu^2 + 4\sigma_Y^2 - 4\sigma_Y^2\nu + 4\sigma_Y^2\nu^2}}{2(1 - \nu + \nu^2)}$$

$$= \frac{-(\sigma_n + 2\nu\sigma_n) \pm \sqrt{-3\sigma_n^2 + 4\sigma_Y^2(1 - \nu + \nu^2)}}{2(1 - \nu + \nu^2)}$$

Thus:

$$\sigma_{perm} = min\left\{\left|\frac{-(\sigma_n + 2\nu\sigma_n) + \sqrt{-3\sigma_n^2 + 4\sigma_Y^2(1 - \nu + \nu^2)}}{2(1 - \nu + \nu^2)}\right| \right\} \tag{4.20}$$
$$\left\{\left|\frac{-(\sigma_n + 2\nu\sigma_n) - \sqrt{-3\sigma_n^2 + 4\sigma_Y^2(1 - \nu + \nu^2)}}{2(1 - \nu + \nu^2)}\right|\right\}$$

If the argument of the square root is lower than 0, this means that:

$$\sigma_n^2 > \frac{4}{3}\sigma_Y^2(1 - \nu + \nu^2) \approx 1.05\sigma_Y^2 \tag{4.21}$$

If the axial load is acting in the *x* direction (shorter one), then:

$$g(x) = M_{pm} - \frac{qb^2}{8} \tag{4.22}$$

The plastic bending moment M_{pm} is computed in this way (see fig. 6):

- At first, the axial load is assumed to be carried by a central portion (whose width is d_N) of the cross section of the plate, such that:
  $N_x = \sigma_{perm} * d_N$
- The plastic bending moment is then given by the two extreme portions of the stress distribution:
  $$M_{pm} = \frac{(t_P - d_{N_x})}{2} * \sigma_{perm} * \left[d_{N_x} + \frac{t_P - d_{N_x}}{2} \right]$$
  Hence:
  $$M_{pm} = \frac{\left(t_P - \frac{N_x}{\sigma_{perm}}\right)}{2} * \sigma_{perm} * \left[\frac{N_x}{\sigma_{perm}} + \frac{t_P - \frac{N_x}{\sigma_{perm}}}{2} \right] \quad (4.23)$$

Finally:

$$g(x) = \frac{\left(t_P - \frac{N_x}{\sigma_{perm}}\right)}{2} * \left[\frac{N_x}{\sigma_{perm}} + \frac{t_P - \frac{N_x}{\sigma_{perm}}}{2} \right] * \sigma_{perm} - \frac{qb^2}{8} \quad (4.24)$$

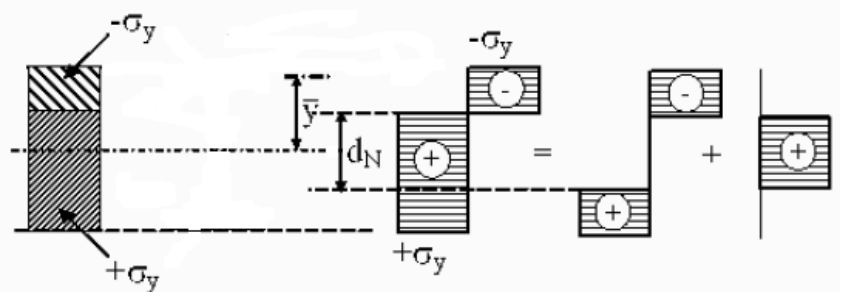

Figure 6 – Computation of the plastic bending moment

Where σ_{perm} is (4.18) if we have only the lateral load and axial load in the *x* direction, and (4.20) if besides the lateral load and axial load in the *x* direction we have also the axial load in the *y* direction.

For a clamped panel laterally loaded (with no axial loads), we have at first the formation of two plastic hinges at the ends (i.e. on the longer sides of the panel) when the applied pressure is such that the bending moment at the ends equals the plastic bending moment:

$$\frac{qb^2}{12} = \sigma_{perm} Z_{pe}$$

Then, if the pressure increase further, we can have the formation of a plastic hinge in the centre of the plate. The bending moment (per unit length) in the centre of a clamped plate is:

$$M_{centre} = M_{end} + \frac{qb^2}{8}$$

- $M_{end} = -\sigma_{perm} Z_{pe}$ is the reaction moment at the ends of the plate (i.e. on the long edge)

Hence:

$$g(x) = \sigma_{perm} Z_{pm} - M_{centre} = \sigma_{perm} Z_{pm} + \sigma_{perm} Z_{pe} - \frac{qb^2}{8}$$
$$= (Z_{pm} + Z_{pe})\sigma_{perm} - \frac{qb^2}{8} \quad (4.25)$$

If we have a clamped beam with only lateral loads:

- $Z_{pe} = Z_{pm} = \frac{t_P^2}{4}$ (4.26)
- $\sigma_{perm} = \frac{\sigma_Y}{\sqrt{(1+\nu^2-\nu)}}$ (4.27)

If, we have a clamped beam with axial load in the transverse direction:

- $Z_{pe} = Z_{pm} = \frac{\left(t_P - \frac{N_x}{\sigma_{perm}}\right)}{2} * \left[\frac{N_x}{\sigma_{perm}} + \frac{t_P - \frac{N_x}{\sigma_{perm}}}{2}\right]$ (4.28)
- $\sigma_{perm} = \frac{\sigma_Y}{\sqrt{(1+\nu^2-\nu)}}$ (4.29)

If we have a clamped beam with an axial load in the longitudinal direction:

- $Z_{pe} = Z_{pm} = \frac{t_P^2}{4}$ (4.30)
- $\sigma_{perm} =$
$$min\left\{\left|\frac{-(\sigma_n+2\nu\sigma_n)+\sqrt{-3\sigma_n^2+4\sigma_Y^2(1-\nu+\nu^2)}}{2(1-\nu+\nu^2)}\right|, \left|\frac{-(\sigma_n+2\nu\sigma_n)-\sqrt{-3\sigma_n^2+4\sigma_Y^2(1-\nu+\nu^2)}}{2(1-\nu+\nu^2)}\right|\right\} \quad (4.31)$$

If we have a clamped beam with an axial load in both directions:

- $Z_{pe} = Z_{pm} = \frac{\left(t_P - \frac{N_x}{\sigma_{perm}}\right)}{2} * \left[\frac{N_x}{\sigma_{perm}} + \frac{t_P - \frac{N_x}{\sigma_{perm}}}{2}\right]$ (4.32)
- $\sigma_{perm} =$
$$min\left\{\left|\frac{-(\sigma_n+2\nu\sigma_n)+\sqrt{-3\sigma_n^2+4\sigma_Y^2(1-\nu+\nu^2)}}{2(1-\nu+\nu^2)}\right|, \left|\frac{-(\sigma_n+2\nu\sigma_n)-\sqrt{-3\sigma_n^2+4\sigma_Y^2(1-\nu+\nu^2)}}{2(1-\nu+\nu^2)}\right|\right\} \quad (4.33)$$

4.3.3 Ultimate collapse of unstiffened plates

The ultimate collapse of an unstiffened plate will occur when we have elasto-plastic buckling. There are several analytical models proposed to calculate the ultimate strength of plates:

- the Johnson-Ostenfeld formula method;
- the rigid-plastic theory method;
- the elastic large deflection analysis combined with the membrane stress-based method.

The first and the third methods will be used. The first one is an empirical method, acting on the conservative side. The third one is an analytical method.

Large deflection analysis combined with the membrane stress-based method

In this method it is assumed that the plate at first buckles in the elastic regimes , and then it keeps to carry some loads before it reaches plasticity at some critical locations. The two events (elastic buckling and yielding) are here – for modelling purposes - considered separately as if one follows the other. In the reality, for FPSO unstiffened plates, it is not possible to distinguish the two events, as the buckling of an unstiffened plates often happens directly in the plastic regimes (stocky plate).

a is the length of the plate in the x (not necessarily the longer/shorter one) direction and b is the length of the plate in the y direction. The residual stresses and the initial imperfections are neglected.

In general, the steps to perform an elastic-large deflection analysis are the followings (Paik, [13]) :

1) at first, assume a deflection of the plate with unknown amplitude;
2) then, substitute it into the compatibility equations in order to get the stress function F:
$$\frac{\partial^4 F}{\partial x^4} + 2\frac{\partial^4 F}{\partial x^2 \partial y^2} + \frac{\partial^4 F}{\partial y^4} - E\left[\left(\frac{\partial^2 w}{\partial x \partial y}\right)^2 - \frac{\partial^2 w}{\partial x^2}\frac{\partial^2 w}{\partial y^2}\right] = 0 \qquad (4.34)$$
3) substitute F into the equilibrium equation:
$$D\left(\frac{\partial^4 w}{\partial x^4} + 2\frac{\partial^4 w}{\partial x^2 \partial y^2} + \frac{\partial^4 w}{\partial y^4}\right) - t_P\left[\frac{\partial^2 F}{\partial y^2}\frac{\partial^2 w}{\partial x^2} - 2\frac{\partial^2 F}{\partial x \partial y}\frac{\partial^2 w}{\partial x \partial y} + \frac{\partial^2 F}{\partial x^2}\frac{\partial^2 w}{\partial y^2} + \frac{q}{t_P}\right] = 0 \qquad (4.35)$$
4) apply the Galerkin method to solve the equilibrium equation. At the end of the integration we will get a third-order equation with regard to the unknown amplitude:
$$C_1 A^3 + C_2 A^2 + C_3 A + C_4 = 0 \qquad (4.36)$$
5) once the deflection has been determined, the membrane stresses inside the plate at the mid-thickness can be obtained from equations:
$$\sigma_x = \frac{\partial^2 F}{\partial y^2} - \frac{Ez}{1-\nu^2}\left[\frac{\partial^2 w}{\partial x^2} + \nu\frac{\partial^2 w}{\partial y^2}\right] \qquad (4.37)$$
$$\sigma_y = \frac{\partial^2 F}{\partial x^2} - \frac{Ez}{1-\nu^2}\left[\frac{\partial^2 w}{\partial y^2} + \nu\frac{\partial^2 w}{\partial x^2}\right] \qquad (4.38)$$

$$\tau = \tau_{xy} = -\frac{\partial^2 F}{\partial x \partial y} - \frac{Ez}{2(1+\nu)}\frac{\partial^2 w}{\partial x \partial y} \tag{4.39}$$

6) finally, to find the ultimate strength, the so called membrane stress-based method will be applied.

The membrane stress-based method assumes that ultimate collapse will occur when the most stressed boundary locations yield because the plate can no longer keep the boundaries straight, thus resulting in a rapid increase in lateral deflection.

There are three possible locations for initial yield. For any location, a different equivalent Von Mises stress can be computed. The ultimate strength will be then the lowest of the three equivalent stresses:

1) Plasticity at the corners:

$$\sigma_{eq1} = \sqrt{\sigma_{xmax}^2 - \sigma_{xmax}\sigma_{ymax} + \sigma_{ymax}^2 + 3\tau^2} \tag{4.40}$$

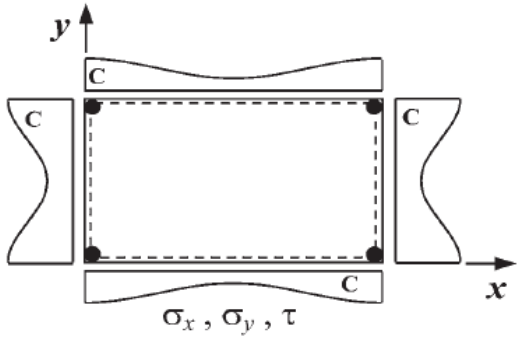

Figure 7 – Membrane stress-based method: plasticity at the corners

2) Plasticity at the longitudinal midedges:

$$\sigma_{eq2} = \sqrt{\sigma_{xmax}^2 - \sigma_{xmax}\sigma_{ymin} + \sigma_{ymin}^2 + 3\tau^2} \tag{4.41}$$

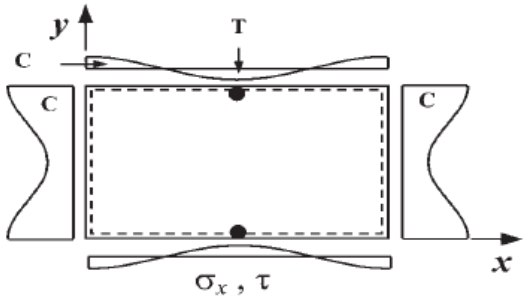

Figure 8 - Membrane stress-based method: plasticity at the longitudinal midedges

3) Plasticity at the transverse midedges:

$$\sigma_{eq3} = \sqrt{\sigma_{xmin}^2 - \sigma_{xmin}\sigma_{ymax} + \sigma_{ymax}^2 + 3\tau^2} \tag{4.42}$$

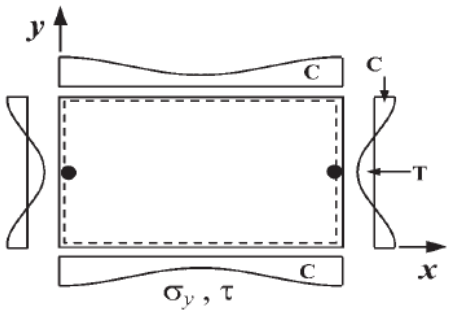

Figure 9 - Membrane stress-based method: plasticity at the transverse midedges

Thus:

$$\beta = \min\{\beta_1, \beta_2, \beta_3\} \tag{4.43}$$

Where:

$$g_1(x) = \sigma_Y - \sigma_{eq1} \tag{4.44}$$

$$g_2(x) = \sigma_Y - \sigma_{eq2} \tag{4.45}$$

$$g_3(x) = \sigma_Y - \sigma_{eq3} \tag{4.46}$$

The unstiffened plate will be modeled as a simply supported panel. Indeed an unstiffened panel is neither clamped nor simply supported, as it is actually a simple supported plate with partially rotation-restrained edges. For the sake of simplicity we will not consider now the effects of the rotational restraints, thus acting in the more conservative way.

As usual, we will consider different load cases: lateral pressure loads, combined biaxial loads and lateral pressure with combined biaxial loads.

Let's start with the case of an unstiffened plate with lateral pressure loads. In this case the lateral deflection can be approximated as follows (one half-wave in both directions):

$$w = A \sin\left(\frac{\pi x}{a}\right) \sin\left(\frac{\pi x}{b}\right) \tag{4.47}$$

Following the steps described above, we get to the following:

$$C_1 A^3 + C_2 A^2 + C_3 A + C_4 = 0$$

Where:

$$C_1 = \frac{\pi^2 E}{16}\left(\frac{b}{a^3} + \frac{a}{b^3}\right) \tag{4.48}$$

$$C_2 = 0 \tag{4.49}$$

$$C_3 = \frac{\pi^2 D}{t_P} * \frac{1}{ab}\left(\frac{b}{a} + \frac{a}{b}\right)^2 \tag{4.50}$$

$$C_4 = -\frac{16ab}{\pi^4 t_P} q \tag{4.51}$$

Once the third-order equation has been solved, and the unknown amplitude A has been found, we can calculate the membrane stresses using the (4.37), (4.38) and (4.39). Results are:

$$\sigma_{xmax} = -\frac{E\pi^2 A^2}{8a^2} \tag{4.52}$$

$$\sigma_{xmin} = \frac{E\pi^2 A^2}{8a^2} \tag{4.53}$$

$$\sigma_{ymax} = -\frac{E\pi^2 A^2}{8b^2} \tag{4.54}$$

$$\sigma_{ymin} = \frac{E\pi^2 A^2}{8b^2} \tag{4.55}$$

Shear stresses have been neglected.

For the combined biaxial loads case, the assumed deflection is:

$$w = A_{mn} \sin\left(\frac{m\pi x}{a}\right) \sin\left(\frac{n\pi y}{b}\right) \tag{4.56}$$

m and n are the buckling half-wave numbers in the x and y direction, respectively. In the shorter direction, the buckling half-wave number must be taken as 1. In the longer direction, assuming $a/b \geq 1$, then $n = 1$ and m must be taken such that ([12]):

1) when σ_{xav} and σ_{yav} are both non-zero compressive (negative):

$$\frac{\left(\frac{m^2}{a^2} + \frac{1}{b^2}\right)^2}{\frac{m^2}{a^2} + \frac{c}{b^2}} \leq \frac{\left[\frac{(m+1)^2}{a^2} + \frac{1}{b^2}\right]^2}{\frac{(m+1)^2}{a^2} + \frac{c}{b^2}} \tag{4.57}$$

$$c = \frac{\sigma_{yav}}{\sigma_{xav}}$$

2) When σ_{xav} is tensile (positive) or zero, no matter what value of σ_{yav}:

$$m = 1 \tag{4.58}$$

3) When σ_{xav} is compressive and σ_{yav} is tensile or zero:

$$\frac{a}{b} \leq \sqrt{m(m+1)} \tag{4.59}$$

Then:

$$C_1 A_{mn}^3 + C_2 A_{mn}^2 + C_3 A_{mn} + C_4 = 0$$

$$C_1 = \frac{\pi^2 E}{16}\left(\frac{m^4 b}{a^3} + \frac{n^4 a}{b^3}\right) \tag{4.60}$$

$$C_2 = 0 \tag{4.61}$$

$$C_3 = \frac{mb^2}{a}(\sigma_{xav}) + \frac{n^2 a}{b}(\sigma_{yav}) + \frac{\pi^2 D}{t_P} * \frac{m^2 n^2}{ab}\left(\frac{mb}{na} + \frac{na}{mb}\right)^2 \tag{4.62}$$

$$C_4 = 0 \tag{4.63}$$

It follows that:

$$A_{mn} = \sqrt{-\frac{C_3}{C_1}} \tag{4.64}$$

Note that C_1 in (4.64) is always positive. C_3 may be positive or negative, and thus (4.64) may return us a either real or imaginary number. If $C_3 < 0$, it follows from (4.62) that:

$$\frac{mb^2}{a}(\sigma_{xav}) + \frac{n^2 a}{b}(\sigma_{yav}) > -\frac{\pi^2 D}{t_P} * \frac{m^2 n^2}{ab}\left(\frac{mb}{na} + \frac{na}{mb}\right)^2 \tag{4.65}$$

However, (4.65) is the elastic buckling safety criteria for an unstiffened plate under biaxial loads ([14]). This means that, if $C_3 < 0$, the elastic buckling is not reached, and thus A_{mn} is 0. The ultimate failure of the plate is then reached when we have yielding in one of the locations of figures 7, 8 and 9. The (4.64) can then be modified as follows:

$$A_{mn} = Real\left(\sqrt{-\frac{C_3}{C_1}}\right) \tag{4.66}$$

Once A_{mn} has been found, the maximum and minimum membrane stresses inside the plates are:

$$\sigma_{xmax} = \sigma_{xav} - \frac{E\pi^2 m^2 A_{mn}^2}{8a^2} \tag{4.67}$$

$$\sigma_{xmin} = \sigma_{xav} + \frac{E\pi^2 m^2 A_{mn}^2}{8a^2} \tag{4.68}$$

$$\sigma_{ymax} = \sigma_{yav} - \frac{E\pi^2 n^2 A_{mn}^2}{8b^2} \tag{4.69}$$

$$\sigma_{ymin} = \sigma_{yav} + \frac{E\pi^2 n^2 A_{mn}^2}{8b^2} \tag{4.70}$$

Finally the most complicated case of biaxial loads and lateral pressure must be considered. In this case a great number of deflection components should be considered. For the sake of simplicity, the non linear membrane stresses inside the plate is approximated as the sum of the stresses arising from the two previous cases.

However, the amplitude A_{mn} of the deflection arising from the biaxial load must be computed using the following C_4 coefficient rather than $C_4 = 0$:

$$C_4 = -\frac{16ab}{\pi^4 t_P} q \tag{4.71}$$

Johnson-Ostenfeld formula method

The Johnson-Ostenfeld formula is an empirical formula often used in the maritime engineer practice. It gives a good indication of the ultimate strength, albeit somewhat on the conservative side ([1]). The ultimate strength is estimated as:

$$\sigma_u = \begin{cases} \sigma_E & for\ \sigma_E \leq 0.5\sigma_F \\ \sigma_F \left(1 - \frac{\sigma_F}{4\sigma_E}\right) & for\ \sigma_E > 0.5\sigma_F \end{cases} \tag{4.72}$$

- σ_E is the elastic buckling stress, calculated using the proper boundary conditions;
- σ_F is the reference yield stress; $\sigma_F = \sigma_Y$ for compressive stress and $\sigma_F = \tau_Y = \frac{\sigma_Y}{\sqrt{3}}$ for shear stress.

In using (4.72) the sign of the compressive stress is taken as positive.

The elastic buckling stress, for a simply supported plate under uniaxial compression in the x direction is:

$$\sigma_E = k \frac{\pi^2 E}{12(1-\nu^2)} \left(\frac{t}{b}\right)^2 \tag{4.73}$$

Where k is the buckling coefficient:

$$k = \left(\frac{mb}{a} + \frac{a}{mb}\right)^2 \tag{4.74}$$

m is the buckling half wave numbers in the loading direction. It is determined as the lowest integer satisfying the following:

$$\frac{a}{b} \leq \sqrt{m(m+1)} \tag{4.75}$$

While, under biaxial compression, if the loading ratio between σ_x and σ_y is kept constant, che buckling stress of the plate can be obtained as follows:

$$\sigma_{E,x} = \frac{\pi^2 D}{b^2 t} \frac{(1 + m^2 b^2/a^2)^2}{c + m^2 b^2/a^2} \tag{4.76}$$

Where $c = \sigma_y/\sigma_x$ and:

$$\sigma_{E,y} = c\sigma_{E,x} \tag{4.77}$$

m is the buckling half-wave numbers in the loading direction. It is determined as the lowest integer satisfying the following:

$$\frac{\left(\frac{m^2}{a^2} + \frac{1}{b^2}\right)^2}{\frac{m^2}{a^2} + \frac{c}{b^2}} \leq \frac{\left[\frac{(m+1)^2}{a^2} + \frac{1}{b^2}\right]^2}{\frac{(m+1)^2}{a^2} + \frac{c}{b^2}} \tag{4.78}$$

If we have also lateral pressure, then the elastic buckling strengths calculated with (4.73) and (4.76) need to be multiplied times a correction coefficient:

$$C_{qx} = 1 + \frac{1}{576}\left(\frac{qb^4}{Et_P^4}\right)^{1.6} \qquad for\ a/b \geq 2 \tag{4.79}$$

Analogously, the elastic buckling strength in the *y* direction (4.77) has to be augmented by the following correction factor:

$$C_{qx} = 1 + \frac{1}{160}\left(\frac{b}{a}\right)^{0.95}\left(\frac{qb^4}{Et_P^4}\right)^{175} \qquad for\ a/b \geq 2 \tag{4.80}$$

4.4 Stiffened panel limit state functions

The limit state functions of stiffened panels refer to the failure of secondary stiffeners (longitudinals) under the assumption that the strength of the primary supporting structure is sufficient to prevent its collapse prior to that of secondary stiffeners.

The limit states identified are ([15]):

- Serviceability limit states:
  - First yielding of stiffener (paragraph 4.4.1)
- Ultimate limit states (paragraph 4.4.3):
  - Formation of plastic hinges (paragraph 4.4.2)
  - Overall collapse of the plating and stiffeners as a unit, mode I (paragraph 4.4.4)
  - Yielding along the plate-stiffener intersection, mode II (paragraph 4.4.5)
  - Beam-column type collapse, mode III (paragraph 4.4.6)
  - Local buckling of the stiffener web, mode IV (paragraph 4.4.7)
  - Flexural-torsional buckling of the stiffeners, mode V(paragraph 4.4.8)
  - Fracture (paragraph 4.5)

In order to help the reader, table 2 is giving a summary of all these failure modes, together with the analytical theory used for the derivation of the LSFs and the reference paragraph.

Table 2 – Failure modes for stiffened panels

Failure mode	Model	Paragraph
First yielding	Simple beam theory	4.4.1
Formation of plastic hinges	Simple beam theory and elasto-perfectly plastic material	4.4.2
Mode I: overall collapse of the plating and stiffeners as a unit	Large deflection analysis combined with the membrane stress-based method, using the orthotropic plate model	4.4.4
Mode II: yielding along the plate-stiffener intersection	Large deflection analysis combined with the membrane stress-based method, using the isotropic plate model	4.4.5
Mode III: beam-column type collapse	Johnson Ostenfeld formula method	4.4.6
Mode IV: local buckling of the stiffener web	Analytical method (Large deflection analysis combined with the membrane stress-based method)/Empirical method (Johnson Ostenfeld formula method)	4.4.7
Mode V: flexural-torsional buckling of the stiffeners	Analytical method (Large deflection analysis combined with the membrane stress-based method)/Empirical method (Johnson Ostenfeld formula method)	4.4.8
Fracture	Linear fracture mechanics	4.5

4.4.1 First yielding of stiffeners

In an axially and laterally loaded stiffeners, we can distinguish:

- a normal stress induced by the bending of the stiffener;
- a normal stress induced by the axial load.

Hence the failure criteria is:

$\sigma_n + \sigma_{bending} > \sigma_Y$

Where:

- $\sigma_n = \frac{N}{A_S + bt_P}$
- N is the axial force
- A_S is the cross sectional area of the stiffener without the attached plate
- t_P is the plate thickness
- b is the stiffener spacing
- $\sigma_{bending} = \frac{M_{max}}{Z_s}$
- $M_{max} = \frac{qbl^2}{8}$ for a simply supported stiffener, $M_{max} = \frac{qbl^2}{12}$ for a fixed stiffener
- Z_s is the section modulus of the stiffener with attached plate
- q is the lateral pressure applied on the stiffener

- l is the stiffener span

Thus the limit state functions, for a simply supported and for a clamped stiffener, respectively are:

$$g(x) = \sigma_Y - \frac{qbl^2}{8Z_s} - \frac{N}{A_S + bt_P} \tag{4.81}$$

$$g(x) = \sigma_Y - \frac{qbl^2}{12Z_s} - \frac{N}{A_S + bt_P} \tag{4.82}$$

In the presence of shear stress, Von Mises criterion should be used:

$$\sqrt{\sigma_x^2 + 3\tau^2} \geq \sigma_Y$$

Hence:

$$\sigma_x^2 + 3\tau^2 \geq (\sigma_Y)^2$$

$$\sigma_x^2 \geq \sigma_Y^2 - 3\tau^2$$

$$\sigma_x \geq \sigma_Y \sqrt{1 - 3\left(\frac{\tau}{\sigma_Y}\right)^2} = \sigma_Y{}' \tag{4.83}$$

$\sigma_Y{}'$ is called equivalent yield stress. However, we are neglecting the shear stress, as we can reasonably assume that it is very close to zero in the plate or in the stiffener flange, which are the two locations where the maximum bending stress occurs.

If needed, in the calculation of the stiffener section modulus, the width of the attached plate can be replaced by the effective breadth (assuming it will be constant along the length of the stiffener).

4.4.2 Plastic hinge formation in stiffeners

Four different load conditions will be considered here:

1. Simply supported laterally loaded stiffener
2. Simply supported laterally loaded stiffener with axial (compressive or tensile) load
3. Clamped laterally loaded stiffener
4. Clamped laterally loaded stiffener with axial (compressive or tensile) load

The ultimate moment that the cross section of a beam in bending can take occurs when the entire cross section is yielded in compression or tension. This correspond to the formation of a plastic hinge. Analogously to what has been done for plates, the elasto-perfectly plastic material model will be used.

The ultimate collapse of a fixed stiffener under uniform lateral loads occurs when we have the formation of three plastic hinges, two at the ends and one at mid-span.

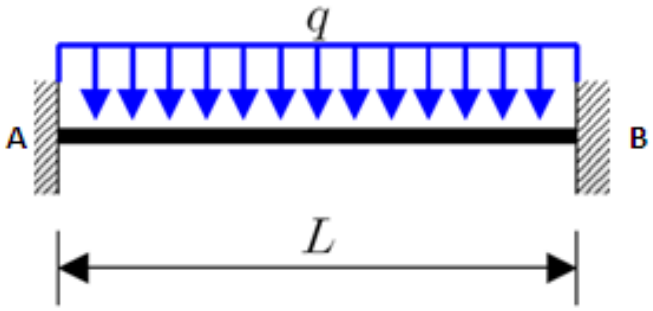

Figure 10 – Fixed beam with uniforn lateral pressur

For a uniformly and laterally loaded beam with fixed boundary conditions (fig. 10), the shear and moment bending moment are given by:

$$T(x) = \frac{M_B - M_A}{l} + \frac{dM(x)}{dx} \tag{4.84}$$

$$M(x) = M_A + T_A x - \frac{qbx^2}{2} \tag{4.85}$$

Where:

- T_A and T_B are the shear reaction forces
- M_A and M_B are the end bending moments

The bending moment at the mid length is:

$$M\left(\frac{l}{2}\right) = M_A + \frac{T_A l}{2} - \frac{qbl^2}{8}$$

Since $T_A = T_B = qbl/2$:

$$M\left(\frac{l}{2}\right) = M_A + \frac{qbl^2}{4} - \frac{qbl^2}{8} = M_A + \frac{qbl^2}{8} \tag{4.86}$$

The ultimate or plastic moment is:

$$M_{pm} = Z_{pm}\sigma_Y$$

Where:

- Z_{pm} is the plastic section modulus in the middle of the beam

Hence our limit state function is:

$$M\left(\frac{l}{2}\right) > M_{pm} = Z_{pm}\sigma_Y$$

And, because at the collapse the reaction moments is equal to the plastic moment (in a fixed-fixed beam, the formation of the plastic hinge at the tips is earlier than that one at mid-span), i.e. $M_A = M_B = -Z_{pe}\sigma_Y$:

$$M\left(\frac{l}{2}\right) = M_A + \frac{qbl^2}{8} = -Z_{pe}\sigma_Y + \frac{qbl^2}{8} > Z_{pm}\sigma_Y$$

Thus:

$$g(x) = \left(Z_{pe} + Z_{pm}\right)\sigma_Y - \frac{qbl^2}{8} \tag{4.87}$$

The plastic section moduli are calculated in this way:

- First, the plastic neutral axis is found. The plastic neutral axis is the axis that split the cross section such that the (absolute value of) the compression force from the area in compressions equals the (absolute value of) the tension force from the area in tension. In our case, since steel has the same yielding stress for both compression and tension, it is sufficient to find the axis that splits the cross section in two equal areas.
- Then, the plastic section modulus is given by the sum of the areas of the cross section on each side of the plastic neutral axis multiplied by the distance from the local centroids of the two areas of the plastic neutral axis.

Usually the plastic neutral axis falls inside the plate (fig. 11, where x is the coordinate of the plastic neutral axis and x_1 of the local centroid of area $bx + t_w h_w + b_f t_f$).

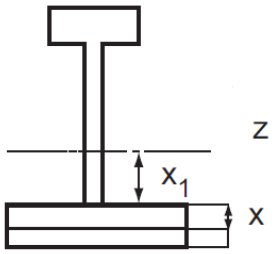

Figure 11 – Plastic neutral axis in a T-profile stiffener

$$b\left(t_p - x\right) = bx + t_w h_w + b_f t_f$$

$$x = \frac{bt_p - t_w h_w - b_f t_f}{2b}, \quad x > 0 \tag{4.88}$$

Hence:

$$Z_{pe} = Z_{pm} = b * (t_p - x) * \left(\frac{t_p - x}{2} + x + x_1\right) \tag{4.89}$$

x_1 is the centre of the cross section of area $bx + t_w h_w + b_f t_f$:

$$x_1 = \frac{bx * \left(t_p - \frac{x}{2}\right) + \frac{t_w h_w h_w}{2} + t_f b_f \left(t_p + h_w + \frac{t_f}{2}\right)}{bx + t_w h_w + b_f t_f} - t_p \tag{4.90}$$

Actually, at the ends we should take into account the shear stress as well, which will cause a "reduction" of the web area. Coherently with what we have done before, we neglected them.

For a simply supported beam we have ultimate collapse if the bending moment at the central moment reaches the plastic moment, i.e.:

$$g(x) = Z_{pe}\sigma_Y - \frac{qbl^2}{8} \tag{4.91}$$

Where the plastic section modulus is given by (4.89).

For laterally and axially loaded stiffeners, the derivation of the ultimate limit state function gets a little bit more complicated. The ultimate collapse (for a clamped beam) occurs still when we have the formation of three elastic hinges (two at the ends and one at mid-span). However, in this case part of the cross section must be given over to carry the axial load and so it is not available to carry the moment. Then the plastic neutral axis will not divide the cross section into two equal areas.

Analogously to what has been done before, the limit state function can be written, for a simply supported beam, with lateral load and axial compression, as:

$$g(x) = Z_{pe}\sigma_Y — \frac{qbl^2}{8} \tag{4.92}$$

And, for a clamped beam:

$$g(x) = 2(Z_{pe} + Z_{pm})\sigma_Y — \frac{qbl^2}{8} \tag{4.93}$$

In so doing we are neglecting the shear stresses.

Furthermore, for the laterally loaded stiffener with axial compressive load, the effective breadth has to be used. This "effective breadth" in this case is neither the "effective breadth" due to the shear lag effect (as we are no more in the elastic proportional regimes), neither the "effective width" (4.3) proposed by Faulkner in 1975 (as we are not yet in the post buckling regimes). Indeed, the effective width to be used in this case is to take into account the plastic deformation of the interframe unstiffened plate, which is likely to have occurred prior to the ultimate failure

of the surrounding stiffeners. In 1993 Godo and Guedes Soares ([5]) extended the validity of the Faulkner formula by defining a generalized slenderness of plating:

$$\beta_e = \frac{b}{t_P}\sqrt{\frac{(\sigma_e)_x}{E}} \tag{4.94}$$

Where:

- $b_{eff} = \begin{cases} 1 & for\ \beta < C_3 \\ \frac{C_1}{\beta_e} - \frac{C_2}{\beta_e^2} & for\ \beta \geq C_3 \end{cases}$ (4.95)
- $C_1 = 2, C_2 = 1$ and $C_3 = 1$ for simply supported plates
- $C_1 = 2.25, C_2 = 1.25$ and $C_3 = 1.25$ for clamped plates
- $(\sigma_e)_x = \frac{A_s + bt_P}{A_s + b_e t_P}\sigma_n$

Hence, if we manipulate the last equations, we get:

$$(\sigma_e)_x = \left\{\frac{-C_1 t_P^2\sqrt{E} + \sqrt{\left(C_1 t_P^2\sqrt{E}\right)^2 + 4A_s\left[(A_s + bt_P)\sigma_n + C_2\left(\frac{t_P}{s}\right)t_p^2 E\right]}}{2A_s}\right\}^2 \tag{4.96}$$

Once we know $(\sigma_e)_x$ we can calculate consequently β_e and b_e with (4.94) and (4.95).

For a simply supported or clamped stiffener with lateral and axial load the plastic section modulus is:

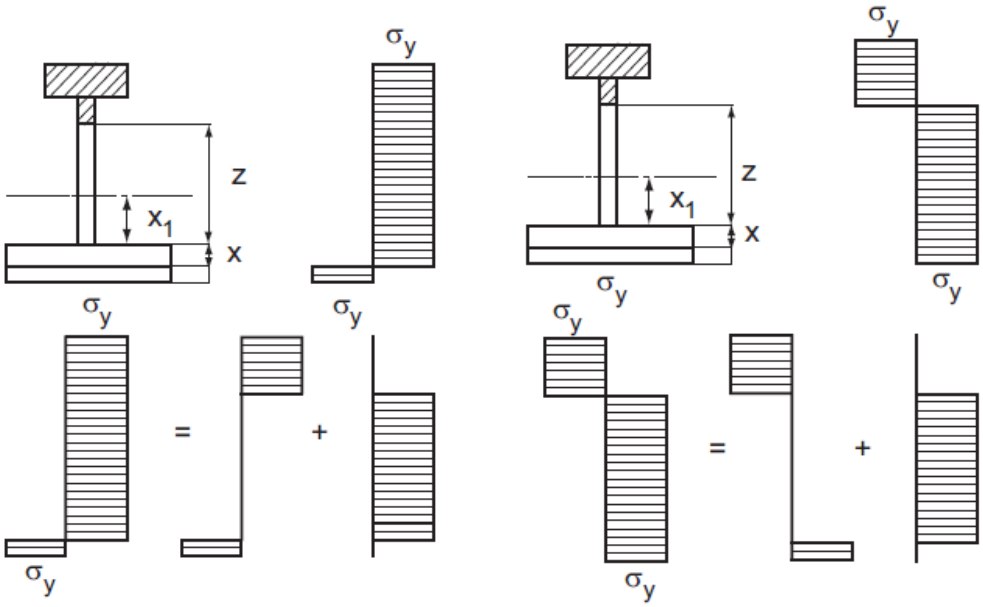

Figure 12 – Computation of the plastic section modulus

$$Z_p = b_{eff}(t_p - x) * \left(x_1 + \frac{(t_p + x)}{2}\right) + t_f b_f * \left(\frac{t_f}{2} + h_w - x_1\right) + t_w(h_w - z) * \left(\frac{h_w + z}{2} - x_1\right) \quad (4.97)$$

Where x, x_1 and z are the solutions to the following system:

$$\sigma_Y(b_{eff}x + t_w z) = N_x \quad (4.98)$$

$$b_{eff}(t_P - x) = b_f t_f + t_w(h_w - z) \qquad z < h_w \quad and\ x < t_P \quad (4.99)$$

$$x_1 = \frac{b_{eff}x\left(-\frac{x}{2}\right) + \frac{z}{2}(t_w z)}{b_{eff}x + t_w z} \quad (4.100)$$

4.4.3 Elasto-plastic buckling of stiffened panels

According to Paik and Thayamballi ([12]), there are six different ultimate collapse modes for a stiffened panel. The ultimate strength of a stiffened panel is then the smallest value among the computed ultimate strengths for each of the collapse mode. Collapse mode VI is gross yielding, which has already been considered in 4.4.2.

The other 5 collapse modes are:

1. Collapse mode I: overall collapse of the plating and stiffeners as a unit. Overall buckling often occurs under an elastic regime. This collapse mode typically occurs when the stiffeners are relatively weak compared with the plating.

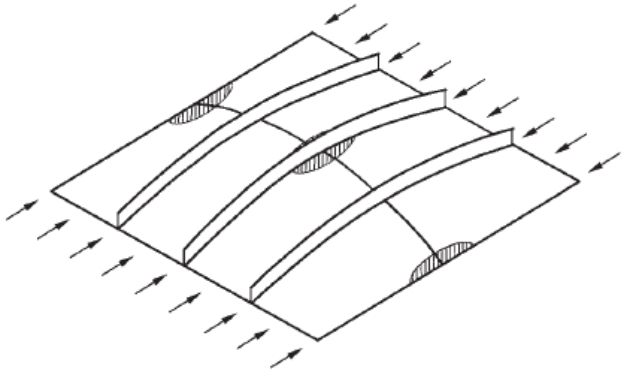

Figure 13 – Collapse mode I

2. Collapse mode II: yielding along the plate-stiffener intersection. This modes assumes that the plating collapses first. It typically occurs under biaxial compressive loads.

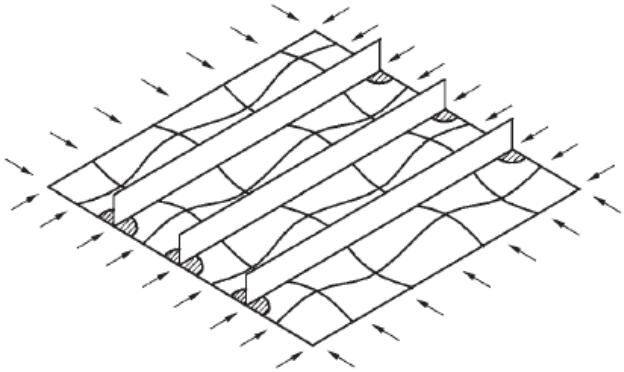

Figure 14 – Collapse mode II

3. Collapse mode III: beam-column type collapse. This collapse modes typically occurs when the stiffeners are neither too strong nor too weak compared to the plating.

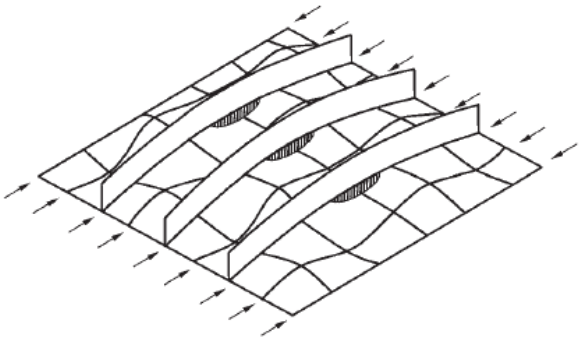

Figure 15 – Collapse mode III

4. Collapse mode IV: local buckling of the stiffener web. This collapse mode occurs when the height to thickness ratio of the stiffener web is large.

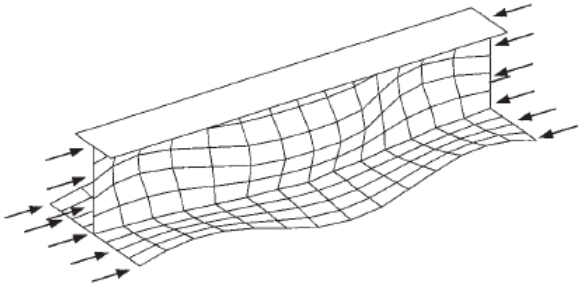

Figure 56 – Collapse mode IV

5. Collapse mode V: flexural-torsional buckling of the stiffeners. This collapse mode occurs when the stiffener flange is of a type that is unable to remain straight. This flexural-torsional buckling phenomenon is also called tripping.

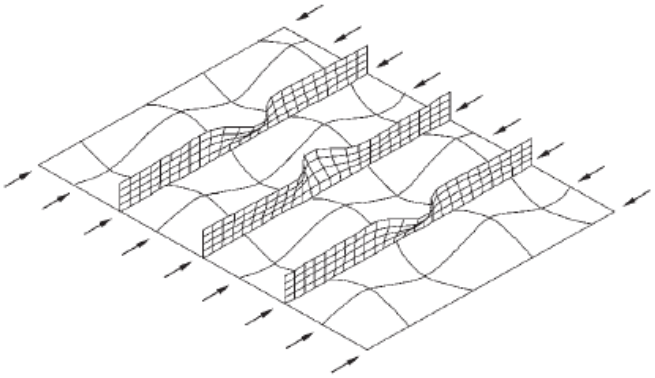

Figure 67 – Collapse mode V

In the following, we will always consider x as the longitudinal direction, which is also parallel to the stiffeners.

4.4.4 Collapse mode I for a stiffened panels: overall collapse of the plating and stiffeners as a unit

When a stiffened panel reaches its ultimate strength by mode I, it can be reasonably modelled as an orthotropic plate. We will neglect the initial imperfections and residual stresses (actually residual stresses in a panel with numerous stiffeners effectively cancel each other). We will model the stiffened panel as a simply supported one, and apply the large deflection analysis in a similar way to what has been done for an unstiffened panel in paragraph 4.3.3. The only difference is that now we are dealing with an orthotropic plate rather than an isotropic one.

The equilibrium and compatibility equation for an orthotropic plate with lateral pressure are the followings:

$$D_x \frac{\partial^4 w}{\partial x^4} + 2H \frac{\partial^4 w}{\partial x^2 \partial y^2} + D_y \frac{\partial^4 w}{\partial y^4} - t_P \left[\frac{\partial^2 F}{\partial y^2} \frac{\partial^2 w}{\partial x^2} - 2 \frac{\partial^2 F}{\partial x \partial y} \frac{\partial^2 w}{\partial x \partial y} + \frac{\partial^2 F}{\partial x^2} \frac{\partial^2 w}{\partial y^2} + \frac{q}{t_P} \right] = 0 \qquad (4.101)$$

$$\frac{1}{E_y} \frac{\partial^4 F}{\partial x^4} + \left(\frac{1}{G_{xy}} - \frac{2\nu_x}{E_x} \right) \frac{\partial^4 F}{\partial x^2 \partial y^2} + \frac{1}{E_x} \frac{\partial^4 F}{\partial y^4} - \left[\left(\frac{\partial^2 w}{\partial x \partial y} \right)^2 - \frac{\partial^2 w}{\partial x^2} \frac{\partial^2 w}{\partial y^2} \right] = 0 \qquad (4.102)$$

Where:

- F is the stress function
- $E_x = E\left(1 + \frac{n_S A_S}{B t_P}\right)$ is the elastic modulus of the orthotropic plate in the x direction
- $E_y = E$ is the elastic modulus of the orthotropic plate in the y direction
- B is the width of the plate
- t_P is the initial thickness of the plate (eventually, this is an average thickness if the plate has a variable thickness)
- n_S is the number of stiffeners
- $A_S = h_w t_w + b_f t_f$

- $D_x = \frac{Et_P^3}{12(1-\nu_x\nu_y)} + \frac{Etz_0^2}{1-\nu_x\nu_y} + \frac{EI}{b}$ is the flexural rigidity of the orthotropic plate in the x direction
- $D_y = \frac{Et^3}{12(1-\nu_x\nu_y)}$ is the flexural rigidity of the orthotropic plate in the y direction
- $H = \frac{1}{2}\left(\nu_y D_x + \nu_x D_y + \frac{G_{xy}t_P^3}{3}\right)$ is the effective torsional rigidity of the orthotropic plate
- $G_{xy} \cong \frac{\sqrt{E_x E_y}}{2(1+\sqrt{\nu_x\nu_y})}$ is the elastic shear modulus of the orthotropic plate
- $I = \frac{t_w h_w^3}{12} + t_w h_w \left(\frac{h_w}{2} + \frac{t_P}{2} - z_0\right)^2 + \frac{b_f t_f^3}{12} + b_f t_f \left(\frac{t_f}{2} + h_w + \frac{t_P}{2} - z_0\right)^2$
- $z_0 = \frac{0.5h_w t_w(h_w+t_P)+b_f t_f(0.5t_f+h_w+0.5t_P)}{bt_P+h_w t_w+b_f t_f}$
- b is the stiffeners spacing
- $\nu_x = c\left[\frac{\frac{Et_P^3}{12}+Etz_0^2+\frac{EI}{b}}{\frac{EI}{b}\left(\frac{E_y}{E_x}\right)}\right]^{0.5}$ is the Poisson's ratio of the orthotropic plate in the x direction
- $\nu_y = \frac{D_y}{D_x}\nu_x$ is the Poisson's ratio of the orthotropic plate in the y direction
- c is a correction that can approximately taken as $c = \frac{\nu}{0.86}$ where ν is the Poisson's ratio for an isotropic plate

Once we have the deflections and the stress function, the membrane stresses can be determined:

$$\sigma_x = \frac{\partial^2 F}{\partial y^2} - \frac{E_x z}{1-\nu_x\nu_y}\left(\frac{\partial^2 w}{\partial x^2} + \nu_y \frac{\partial^2 w}{\partial y^2}\right) \tag{4.103}$$

$$\sigma_x = \frac{\partial^2 F}{\partial x^2} - \frac{E_y z}{1-\nu_x\nu_y}\left(\frac{\partial^2 w}{\partial y^2} + \nu_x \frac{\partial^2 w}{\partial x^2}\right) \tag{4.104}$$

z is the axis in the plate thickness direction, and $z = 0$ is the mid-thickness coordinate.

Using this formulae, it is possible to calculate the ultimate strength in a way very similar as it was done for an unstiffened plate. That is:

1) presume a deflection;
2) substitute it into the compatibility equation to find the stress function (4.102);
3) substitute the stress function into the equilibrium equation(4.101) and apply the Galerkin method;
4) solve the third order equation to find the amplitude of the deflection;
5) find the membrane stresses;
6) apply the membrane stress-based method and the Von Mises criteria in order to find the ultimate strength.

It must be pointed out that the plates and the stiffeners may be made of different steel, thus they may have different yielding stress. In this case, we should define an equivalent yield stress, as follows:

$$\sigma_{Yeq} = \frac{Bt_P\sigma_{Yp} + n_s(h_w t_w + b_f t_f)\sigma_{YS}}{Bt_P + n_s(h_w t_w + b_f t_f)} \tag{4.105}$$

Five different load conditions will be analysed:

1. axial compressive load in stiffener direction;
2. axial load in stiffener direction and lateral pressure;
3. axial compressive load perpendicular to stiffener direction;
4. axial load perpendicular to stiffener direction and lateral pressure
5. only lateral pressure.

For a plate subjected to only axial longitudinal compressive load, the amplitude of the deflection can be determined by solving the following third order equation:

$$C_1 A^3 + C_3 A = 0$$

$$C_1 = \frac{\pi^2}{16}\left(\frac{E_x m^4 B}{a^3} + \frac{E_y a}{B^3}\right) \tag{4.106}$$

$$C_3 = \frac{m^2 B}{a}\sigma_{xav} + \frac{\pi^2}{t_P}\left(\frac{D_x m^4 B}{a^3} + \frac{2Hm^2}{aB} + \frac{D_y a}{B^3}\right) \tag{4.107}$$

Where m (buckling half-wave numbers) must be the minimum integer that satisfies the following condition:

$$\frac{a}{B} \leq \sqrt[4]{\frac{D_x}{D_Y} m^2 (m+1)^2} \tag{4.108}$$

a is the length of the plate in the x direction. The average stresses, for the collapse mode I, are (see fig. 18):

$$\sigma_{xav} = \frac{\sigma_{x1} + \sigma_{x2}}{2} \tag{4.109}$$

$$\sigma_{yav} = \frac{\sigma_{y1} + \sigma_{y2}}{2} \tag{4.110}$$

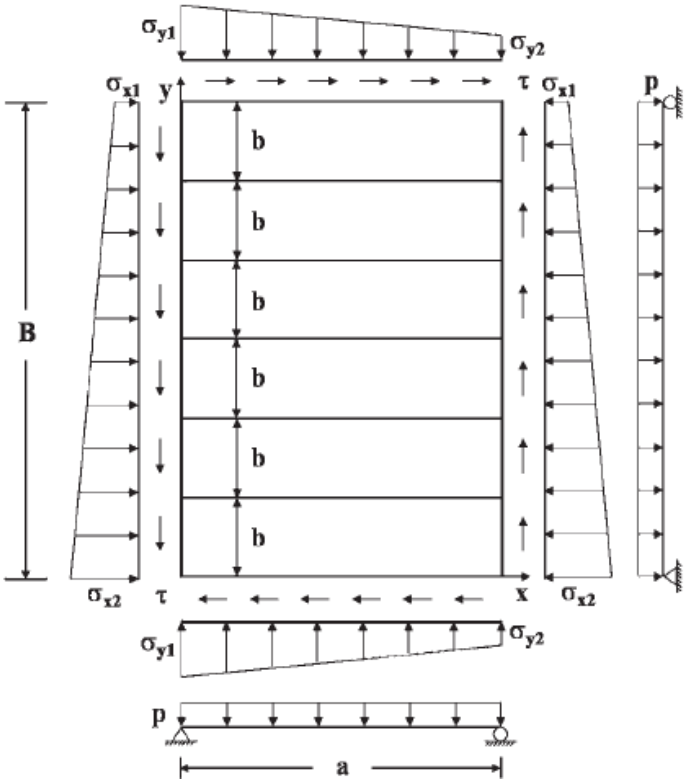

Figure 78 – Orthotropic plate

Once we know A, we can find the membrane stresses as follows:

$$\sigma_{xmax} = \sigma_{xav} - \frac{m^2\pi^2 E_x A^2}{8a^2} \tag{4.111}$$

$$\sigma_{xmin} = \sigma_{xav} + \frac{m^2\pi^2 E_x A^2}{8a^2} \tag{4.112}$$

$$\sigma_{ymax} = -\frac{\pi^2 E_y A^2}{8B^2} \tag{4.113}$$

$$\sigma_{ymin} = +\frac{\pi^2 E_y A^2}{8B^2} \tag{4.114}$$

The panel will collapse when anyone of the following three failure functions is negative:

$$g_1(x) = \sigma_{Yeq} - \sqrt{\sigma_{xmax}^2 - \sigma_{xmax}\sigma_{ymin} + \sigma_{ymax}^2 + 3\tau^2} \tag{4.115}$$

$$g_2(x) = \sigma_{Yeq} - \sqrt{\sigma_{xmax}^2 - \sigma_{xmax}\sigma_{ymin} + \sigma_{ymax}^2 + 3\tau^2} \tag{4.116}$$

$$g_3(x) = \sigma_{Yeq} - \sqrt{\sigma_{xmin}^2 - \sigma_{xmin}\sigma_{ymax} + \sigma_{ymax}^2 + 3\tau^2} \tag{4.117}$$

For a plate with combined axial load (either compressive or tensile) and lateral pressure, the third order equation looks like:

$$C_1 A^3 + C_2 A^2 + C_3 A + C_4 = 0$$

$$C_1 = \frac{\pi^2}{16}\left(\frac{E_x m^4 B}{a^3} + \frac{E_y a}{B^3}\right) \tag{4.118}$$

$$C_2 = 0 \tag{4.119}$$

$$C_3 = \frac{m^2 B}{a}\sigma_{xav} + \frac{\pi^2}{t_P}\left(\frac{D_x m^4 B}{a^3} + \frac{2Hm^2}{aB} + \frac{D_y a}{B^3}\right) \tag{4.120}$$

$$C_4 = -\frac{16aB}{\pi^2 t_P} q \tag{4.121}$$

The half-wave number m is the same as before for compressive axial load, and is equal to 1 for tensile axial load. The maximum and minimum membrane stresses are still the same as for the case with no lateral pressure (from (4.111) to (4.114)).

Let's consider now the case for transverse compressive load. Here the third order equation is:

$$C_1 A^3 + C_3 A = 0$$

$$C_1 = \frac{\pi^2}{16}\left(\frac{E_x B}{a^3} + \frac{E_y n^4 a}{B^3}\right) \tag{4.122}$$

$$C_3 = \frac{n^2 a}{B}\sigma_{yav} + \frac{\pi^2}{t_P}\left(\frac{D_x B}{a^3} + \frac{2Hn^2}{aB} + \frac{D_y n^4 a}{B^3}\right) \tag{4.123}$$

The maximum and minimum membrane stresses are:

$$\sigma_{xmax} = -\frac{\pi^2 E_x A^2}{8a^2} \tag{4.124}$$

$$\sigma_{xmin} = \frac{\pi^2 E_x A^2}{8a^2} \tag{4.125}$$

$$\sigma_{ymax} = \sigma_{yav} - \frac{n^2 \pi^2 E_y A^2}{8B^2} \tag{4.126}$$

$$\sigma_{ymin} = \sigma_{yav} + \frac{n^2 \pi^2 E_y A^2}{8B^2} \tag{4.127}$$

And the buckling half-wave number n is the minimum integer that satisfies the following condition:

$$\frac{B}{a} \leq \sqrt[4]{\frac{D_y}{D_x} n^2 (n+1)^2} \tag{4.128}$$

If, besides the transverse axial load, we have also the lateral pressure, then:

$$C_1 A^3 + C_2 A^2 + C_3 A + C_4 = 0$$

$$C_1 = \frac{\pi^2}{16}\left(\frac{E_x B}{a^3} + \frac{E_y n^4 a}{B^3}\right) \tag{4.129}$$

$$C_2 = 0 \tag{4.130}$$

$$C_3 = \frac{n^2 a}{B}\sigma_{yav} + \frac{\pi^2}{t_p}\left(\frac{D_x B}{a^3} + \frac{2Hn^2}{aB} + \frac{D_y n^4 a}{B^3}\right) \tag{4.131}$$

$$C_4 = -\frac{16aB}{\pi^4 t_P} q \tag{4.132}$$

Finally, if we have a stiffened panel with only lateral pressure, then:

$$m = n = 1 \tag{4.133}$$

$$\sigma_{xav} = \sigma_{yav} = 0 \tag{4.134}$$

And:

$$\sigma_{xmax} = -\frac{\pi^2 E_x A^2}{8a^2} \tag{4.135}$$

$$\sigma_{xmin} = \frac{\pi^2 E_x A^2}{8a^2} \tag{4.136}$$

$$\sigma_{ymax} = -\frac{\pi^2 E_y A^2}{8B^2} \tag{4.137}$$

$$\sigma_{ymin} = \frac{\pi^2 E_y A^2}{8B^2} \tag{4.138}$$

$$C_1 A^3 + C_2 A^2 + C_3 A + C_4 = 0$$

$$C_1 = \frac{\pi^2}{16}\left(\frac{E_x B}{a^3} + \frac{E_y a}{B^3}\right) \tag{4.139}$$

$$C_2 = 0 \tag{4.140}$$

$$C_3 = \frac{\pi^2}{t_P}\left(\frac{D_x B}{a^3} + \frac{2H}{aB} + \frac{D_y a}{B^3}\right) \tag{4.141}$$

$$C_4 = -\frac{16aB}{\pi^4 t_P} q \tag{4.142}$$

4.4.5 Collapse mode II for stiffened panels: yielding along the plate-stiffener intersection

Collapse mode II is solely associated with the plating between the stiffeners, and specifically with the most highly stressed plating. Then, we do not need to consider the equivalent yield stress, but the plate yield stress. We will neglect the initial imperfections and residual stresses and we will model the stiffened panel as a simply supported one.

A stiffened panel reaches ultimate strength by collapse mode II if the most highly stressed plating between the stiffeners has plasticity at the corners. Indeed, this is a sub-case of the ultimate limite state for unstiffened panel (paragraph 4.3.3). In that occasion, three different equivalent stress have been considered (plasticity at the corners, plasticity at the short mid-edges and plasticity at the long mid-edgese).

In our case the equivalent stress is given only by (4.40) (plasticity at the corners) and thus the limit state function is:

$$g(x) = \sigma_{Yp} - \sqrt{\sigma_{xmax}^2 - \sigma_{xmax}\sigma_{ymax} + \sigma_{ymax}^2} \tag{4.143}$$

4.4.6 Collapse mode III for stiffened panels: beam-column type collapse

Collapse mode III occurs when the most highly stressed stiffener, together with the attached plating, collapses as a beam-column. There are three methods to calculate the ultimate strength of stiffened panel under axial compression:

1. the Johnson-Ostenfeld formula method;
2. the Perry-Robertson formula method;
3. the Paik-Thayamballi empirical formula method.

The Johnson-Ostenfeld formula method will be used. For a beam under axial compression the ultimate strength is then given by:

$$\sigma_u = \begin{cases} \sigma_E & for\ \sigma_E \le 0.5\sigma_{Yeq} \\ \sigma_{Yeq}\left(1 - \frac{\sigma_{Yeq}}{4\sigma_E}\right) & for\ \sigma_E > 0.5\sigma_{Yeq} \end{cases} \tag{4.144}$$

- σ_E is the elastic buckling stress;

In using (4.72) the sign of the compressive stress is taken as positive.

The elastic buckling stress, for a simply supported plate under uniaxial compression in the x direction is:

$$\sigma_E = \frac{\pi^2 E I_{eff}}{a^2(A_s + bt_P)} \tag{4.145}$$

Where:

$$I_{eff} = \frac{b_{eff}t_P^3}{12} + b_{eff}t_P\left(z_0 - \frac{t_P}{2}\right)^2 + \frac{h_w^3 t_w}{12} + h_w t_w\left(z_0 - t_p - \frac{h_w}{2}\right)^2 + \frac{b_f t_f^3}{12} + b_f t_f\left(t_p + h_w + \frac{t_f}{2} - z_0\right)^2 \tag{4.146}$$

$$z_0 = \frac{0.5b_{eff}t_P^2 + h_w t_w(t_P + 0.5h_w) + b_f t_f\left(t_P + h_w + 0.5t_f\right)}{b_{eff}t_P + h_w t_w + b_f t_f} \tag{4.147}$$

I_{eff} is the mass moment of inertia of the beam-plate cross section calculated using the effective width b_{eff} given by (4.3).

4.4.7 Collapse mode IV for stiffened panels: local buckling of the stiffener web

The stiffened panel reaches ultimate strength by collapse mode IV if the most highly stressed stiffener together with its attached plate collapses by buckling of the stiffener web. As usual, we will consider the plate as a simply supported plate, and we will neglect the initial distortion and the residual stresses. The ultimate strength of the panel for collapse mode IV is computed as the sum of the ultimate plate strength and stiffener web buckling strength, as follows ([1]):

$$\sigma_{xu} = \frac{\sigma_{xu}^P bt_P + \sigma_u^W\left(h_w t_w + b_f t_f\right)}{bt_P + h_w t_w + b_f t_f} \tag{4.148}$$

- σ_{xu}^P is the ultimate strength of the plating between the stiffeners
- σ_u^W is the ultimate strength of the stiffener because of web buckling

Hence:

$$g(x) = \sigma_{xu} - \sigma_{xav} = \frac{\sigma_{xu}^P bt_p + \sigma_u^W\left(h_w t_w + b_f t_f\right)}{bt_p + h_w t_w + b_f t_f} - \sigma_{xav} \tag{4.149}$$

The ultimate strength σ_{xu}^P can be computed using the elastic large deformation analysis and the membrane based stress method, with $n = 1$ and $\sigma_{yav} = 0$:

$$\sigma_{xmax} = \sigma_{xav} - \frac{E\pi^2 m^2 A^2}{8a^2} \tag{4.150}$$

$$\sigma_{xmin} = \sigma_{xav} + \frac{E\pi^2 m^2 A^2}{8a^2} \tag{4.151}$$

$$\sigma_{ymax} = -\frac{E\pi^2 A^2}{8b^2} \tag{4.152}$$

$$\sigma_{ymin} = \frac{E\pi^2 A^2}{8b^2} \tag{4.153}$$

$$\sigma_{xav} = \sigma_{x2} - \frac{b}{B}(\sigma_{x2} - \sigma_{x1}) \tag{4.154}$$

For the meaning of σ_{x2} and σ_{x1} see fig. 18.

Where:

$$\frac{a}{b} \leq \sqrt{m(m+1)} \tag{4.155}$$

The amplitude A of the deflection can be calculated by solving the third order equation:

$$C_1 A^3 + C_2 A^2 + C_3 A + C_4 = 0$$

$$C_1 = \frac{\pi^2 E}{16}\left(\frac{m^4 b}{a^3} + \frac{a}{b^3}\right) \tag{4.156}$$

$$C_2 = 0 \tag{4.157}$$

$$C_3 = \frac{m^2 b}{a}\sigma_{xav} + \frac{\pi^2 D}{t_P}\frac{m^2}{ab}\left(\frac{mb}{a} + \frac{a}{mb}\right)^2 \tag{4.158}$$

$$C_4 = -\frac{16ab}{\pi^4 t_P} q \tag{4.159}$$

Then:

$$\sigma_{xu}^P = \min\left\{\begin{matrix}\sqrt{\sigma_{xmax}^2 - \sigma_{xmax}\sigma_{ymax} + \sigma_{ymax}^2} \\ \sqrt{\sigma_{xmax}^2 - \sigma_{xmax}\sigma_{ymin} + \sigma_{ymin}^2}, \\ \sqrt{\sigma_{xmin}^2 - \sigma_{xmin}\sigma_{ymax} + \sigma_{ymax}^2}\end{matrix}\right\} \tag{4.160}$$

This case can also be generalized for the case with no lateral pressure, by imposing $q = 0$.

Alternatively, the Jonshon-Ostenfeld formula (4.72) can also be used for σ_{xu}^P.

The Johnson-Ostenfeld formula can be also used for the ultimate strength of the stiffener because of web buckling:

$$\sigma_u^W = \begin{cases}\sigma_E^W & for\ \sigma_E^W \leq 0.5\sigma_{Ys} \\ \sigma_{Ys}\left(1 - \frac{\sigma_{Ys}}{4\sigma_E^W}\right) & for\ \sigma_E^W > 0.5\sigma_{Ys}\end{cases} \tag{4.161}$$

The elastic buckling stress is:

$$\sigma_E^W = -k_W \frac{\pi^2 E}{12(1-\nu^2)}\left(\frac{t_w}{h_w}\right)^2 \tag{4.162}$$

Where, for T-section stiffeners ([12]):

- $k_w = \begin{cases} C_1\zeta_P + C_2 & for\ 0 \le \zeta_P \le \eta_W \\ C_3 - \frac{1}{C_4\zeta_P + C_5} & for\ \eta_w < \zeta_P \le 60 \\ C_3 - \frac{1}{60C_4 + C_5} & for\ 60 < \zeta_P \end{cases}$
- $\zeta_P = \frac{GJ_P}{h_w D_w}$
- $\zeta_f = \frac{GJ_f}{h_w D_w}$
- $J_P = \frac{b_{eff} t_P^3}{3}$ is the torsion constant of the attached effective plating
- $J_f = \frac{b_f t_f^3}{3}$ is the torsion constant of the stiffener flange
- $D_w = \frac{Et_w^3}{12(1-\nu^3)}$
- $G = \frac{E}{2(1+\nu^2)}$
- $\eta_w = 0.444\zeta_f^{\,2} + 3.333\zeta_f + 1.0$
- $b_{eff} = \begin{cases} b & if\ \beta < C_3^* \\ b\left(\frac{C_1^*}{\beta} - \frac{C_2^*}{\beta}\right) & if\ \beta \ge C_3^* \end{cases}$ is the effective width
- $\beta = \frac{b}{t_P}\sqrt{\frac{\sigma_Y}{E}}$
- $C_1^* = 2 \quad C_2^* = 1 \quad C_3^* = 1$ (only for simply supported plates)

And where:

$$C_1 = -0.001\zeta_f + 0.303$$

$$C_2 = 0.308\zeta_f + 0.4267$$

$$C_3 = \begin{cases} -4.350\zeta_f^2 + 3.965\zeta_f + 1.277 & for\ 0 \le \zeta_f \le 0.2 \\ -0.427\zeta_f^2 + 2.267\zeta_f + 1.460 & for\ 0.2 < \zeta_f \le 1.5 \\ -0.133\zeta_f^2 + 1.567\zeta_f + 1.850 & for\ 1.5 < \zeta_f \le 3.0 \\ 5.354 & for\ 3.0 < \zeta_f \end{cases}$$

$$C_4 = \begin{cases} -6.70\zeta_f^2 + 1.40 & for\ 0 \le \zeta_f \le 0.1 \\ \dfrac{1}{5.10\zeta_f + 0.860} & for\ 0.1 < \zeta_f \le 1.5 \\ \dfrac{1}{4.0\zeta_f + 1.814} & for\ 1.0 < \zeta_f \le 3.0 \\ 0.0724 & for\ 3.0 < \zeta_f \end{cases}$$

$$C_5 = \begin{cases} -1.135\zeta_f + 0.428 & for\ 0 \le \zeta_f \le 0.2 \\ -0.299\zeta_f^3 + 0.803\zeta_f^2 - 0.783\zeta_f + 0.328 & for\ 0.2 < \zeta_f \le 1.0 \\ -0.016\zeta_f^3 + 0.117\zeta_f^2 - 0.285\zeta_f + 0.235 & for\ 1.0 < \zeta_f \le 3.0 \\ 0.001 & for\ 3.0 < \zeta_f \end{cases}$$

For flat-bar stiffeners, k_w is calculated by taking $\zeta_f = 0$.

For the combined transverse axial load and lateral pressure, the reliability index is the same as for collapse mode III under the same loading conditions.

4.4.8 *Collapse mode V: flexural-torsional buckling of the stiffeners*

The stiffened panel reaches ultimate strength by collapse mode V if the most highly stressed stiffener together with its attached plate collapses by flexural-torsional buckling or tripping. As usual, we will consider the plate as a simply supported plate, and we will neglect the initial distortion and the residual stress. The ultimate strength of the panel σ_{xu} is calculated as the sum of the ultimate plate strength and stiffener flexural-torsional buckling strength ([1]):

$$\sigma_{xu} = \frac{\sigma_{xu}^P b t_P + \sigma_u^T \left(h_w t_w + b_f t_f\right)}{b t_P + h_w t_w + b_f t_f} \tag{4.163}$$

- σ_{xu}^P is the ultimate strength of the plating between the stiffeners
- σ_u^T is the ultimate strength of the stiffener because of lateral-torsional buckling or tripping

Hence:

$$g(x) = \sigma_{xu} - \sigma_{xav} = \frac{\sigma_{xu}^P b t_P + \sigma_u^T \left(h_w t_w + b_f t_f\right)}{b t_P + h_w t_w + b_f t_f} - \sigma_{xav} \tag{4.164}$$

Let's start to consider the case with combined longitudinal axial load and lateral pressure.

The ultimate strength σ_{xu}^P can be calculated in the same way as it has been done for the collapse mode IV.

The ultimate strength of the stiffener because of lateral-torsional buckling is calculated with the Johnson-Ostenfeld formula:

$$\sigma_u^T = \begin{cases} \sigma_E^T & for\ \sigma_E^T \le 0.5\sigma_{Ys} \\ \sigma_{Ys}\left(1 - \frac{\sigma_{Ys}}{4\sigma_E^T}\right) & for\ \sigma_E^T > 0.5\sigma_{Ys} \end{cases} \quad (4.165)$$

The elastic flexural buckling strength is a function of the types of stiffeners ([12]).

For a flat bar stiffeners, the elastic flexural buckling strength is equal to the elastic web stiffener buckling strength:

$$\sigma_E^T = \sigma_E^W \quad (4.166)$$

For symmetric T-stiffeners:

$$\sigma_E^T = -1 * \min_{m=1,2,3\ldots} \left| -\frac{a^2 G\left(J_w + J_f\right) + EI_f h_w^2 m^2 \pi^2}{I_p a^2} + \frac{qa^2}{12}\frac{S_4}{I_y I_p}\left(1 - \frac{3}{m^2\pi^2}\right) \right| \quad (4.167)$$

Where:

- $S_4 = -\left(z_p - h_w\right)t_f\left(h_w^2 b_f + \frac{b_f^3}{12}\right) - h_w^3 t_w\left[\frac{1}{3}z_p - \frac{h_w}{4}\right]$
- $I_p = \frac{t_w h_w^3}{3} + \frac{t_w^3 h_w}{12} + \frac{b_f t_f^3}{12} + \frac{b_f^3 t_f}{12} + b_f t_f h_w^2$
- $I_f = \frac{b_f^3 t_f}{12}$
- $I_y = \frac{b_e t_P^3}{12} + b_e t_P z_p^2 + \frac{t_w h_w^3}{12} + h_w t_w\left(z_p - \frac{t_P}{2} - \frac{h_w}{2}\right)^2 + \frac{b_f t_f^3}{12} + b_f t_f\left(z_p - \frac{t_P}{2} - h_w - \frac{t_f}{2}\right)^2$
- $z_p = \frac{0.5h_w t_w(t_P + h_w) + b_f t_f\left(0.5t_P + h_w + 0.5t_f\right)}{b_e t_P + h_w t_w + b_f t_f}$
- $b_e = \begin{cases} b & if\ \beta < C_3 \\ b\left(\frac{C_1}{\beta} - \frac{C_2}{\beta}\right) & if\ \beta \ge C_3 \end{cases}$ is the effective width
- $\beta = \frac{b}{t_p}\sqrt{\frac{\sigma_Y}{E}}$
- $C_1 = 2 \quad C_2 = 1 \quad C_3 = 1$ (only for simply supported plates)

For asymmetric stiffeners:

$$\sigma_E^T = -1 * \min_{i=1,2,3\ldots} \left| \frac{C_2 + \sqrt{C_2^2 - 4C_1 C_3}}{2C_1} \right| \quad (4.168)$$

Where:

- $C_1 = \left(b_e t_p + h_w t_w + b_f t_f\right)I_p - S_f^2$

- $C_2 = -I_p\left[EI\left(\frac{m\pi}{a}\right)^2 - \frac{q_l a^2}{12} * \frac{S_1}{I_y}\left(1 - \frac{3}{m^2\pi^2}\right)\right] - \left(b_e t_p + h_w t_w + b_f t_f\right)\left[G\left(Jw + J_f\right) + EIzhw2m\pi a2 - qla212 * S2Iy1 - 3m2\pi 2 + 2SfEIzyhwm\pi a2 - qla212 * S3Iy1 - 3m2\pi 2\right.$

- $C_3 = \left[EI_y\left(\frac{m\pi}{a}\right)^2 - \frac{q_l a^2}{12} * \frac{S_1}{I_y}\left(1 - \frac{3}{m^2\pi^2}\right)\right]\left[G\left(J_w + J_f\right) + EI_z h_w^2\left(\frac{m\pi}{a}\right)^2 - \frac{q_l a^2}{12} * S2Iy1 - 3m2\pi 2 - EIzyhwm\pi a2 - qla212 * S3Iy1 - 3m2\pi 22\right.$

- $S_f = -\frac{t_f b_f^2}{2}$
- $S_1 = -\left(z_p - h_w\right)t_f b_f - b_e t_p z_p - h_w t_w\left(z_p - \frac{h_w}{2}\right)$
- $S_2 = -\left(z_p - h_w\right)t_f\left(h_w^2 b_f + \frac{b_f^3}{3}\right) - h_w^3 t_w\left[\frac{1}{3}z_p - \frac{h_w}{4}\right]$
- $S_3 = \frac{\left(z_p - h_w\right)b_f^2 t_f}{2}$
- $I_y = \frac{b_e {t_p}^3}{12} + b_e t_p z_p^2 + \frac{t_w h_w^3}{12} + h_w t_w\left(z_p - \frac{t_p}{2} - \frac{h_w}{2}\right)^2 + \frac{b_f t_f^3}{12} + b_f t_f\left(z_p - \frac{t_p}{2} - h_w - \frac{t_f}{2}\right)^2$
- $I_z = b_e t_p y_0^2 + h_w t_w y_0^2 + b_f t_f\left(y_0^2 - b_f y_0 + \frac{b_f^2}{3}\right)$
- $I_{zy} = b_e t_p z_p y_0 + h_w t_w\left(z_p - \frac{t_p}{2} - \frac{h_w}{2}\right)y_0 + b_f t_f\left(z_p - \frac{t_p}{2} - h_w - \frac{t_f}{2}\right)\left(y_0 - \frac{b_f}{2}\right)$
- $I_p = \frac{t_w h_w^3}{3} + \frac{t_w^3 h_w}{3} + \frac{b_f^3 t_f}{3} + \frac{b_f t_f^3}{3} + b_f t_f h_w^2$
- $z_p = \frac{0.5 h_w t_w\left(t_p + h_w\right) + b_f t_f\left(0.5 t_p + h_w + 0.5 t_f\right)}{b_e t_p + h_w t_w + b_f t_f}$
- $y_0 = \frac{b_f^2 t_f}{2\left(b_e t_p + h_w t_w + b_f t_f\right)}$
- $J_w = \frac{1}{3}t_w^3 h_w\left(1 - \frac{192}{\pi^5}\frac{t_w}{h_w}\sum_{n=1,3,5}^{\infty}\frac{1}{n^5}\frac{tanhn\pi h_w}{2t_w}\right)$
- $J_f = \frac{1}{3}t_f^3 b_f\left(1 - \frac{192}{\pi^5}\frac{t_f}{b_f}\sum_{n=1,3,5}^{\infty}\frac{1}{n^5}\frac{tanhn\pi b_f}{2t_f}\right)$
- $q_l = q * b\ (equivalent\ line\ pressure)$
- $b_e = \begin{cases} b & if\ \beta < C_3^* \\ b\left(\frac{C_1^*}{\beta} - \frac{C_2^*}{\beta}\right) & if\ \beta \geq C_3^* \end{cases}$
- $\beta = \frac{b}{t_P}\sqrt{\frac{\sigma_Y}{E}}$
- $C_1^* = 2 \quad C_2^* = 1 \quad C_3^* = 1$ (only for simply supported plates)

For the combined transverse axial load and lateral pressure, the reliability index is the same as for collapse modes III and IV under the same loading conditions.

Since the ultimate strength for collapse mode IV and V is the same for a plate stiffened with flat bars under combined longitudinal axial load and lateral pressure, then collapse mode IV and V can be treated together under all load conditions if the stiffeners used are flat bars.

4.5 Fracture mechanics

Although unlikely, brittle fracture may also be an eventual failure ([17]). The model adopted to write down the failure function is the simplest one, i.e. the one following the linear fracture mechanics approach. This means that the applied stresses are low, so that the plastic zone is small compared to the size of the crack.

There are three different modes in which a crack in a solid is categorized:

- Mode I, opening mode: the displacement of the cracked surfaces are perpendicular to the plane of crack;
- Mode II, sliding mode: the displacement of the cracked surfaces is in the plane of the crack and perpendicular to the leading edge of the crack;
- Mode III, tearing mode: caused by out-of-plane shear.

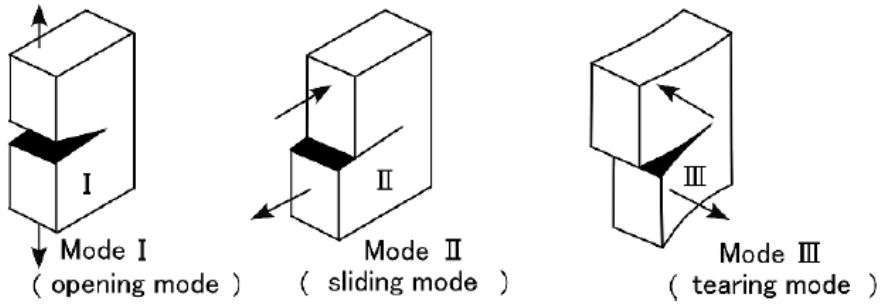

Figure 19 – Crack propagation modes

The mode I is usually the most important and hence only this one will be considered. For an infinite plate subjected to uniform tension, the in-plane crack tip stress is expressed as follows:

$$\sigma_{ij} = \frac{K}{\sqrt{2\pi r}} f_{ij}(\theta) \tag{4.169}$$

σ_{ij} is the stress acting on a plate element at a distance r from crack tip and at an angle θ from crack plane (see fig. 20).

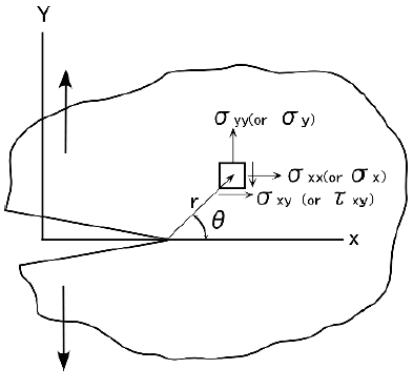

Figure 20 – Stresses close to a crack

K is the stress intensity factor, which for mode I is:

$$K_1 = \sigma \sqrt{a\pi} \tag{4.170}$$

σ is the remote stress and a is the half-length of the crack.

σ is given by the sum of the applied stress (which is a random variable) and the residual stress. If we assume the residual stress to be half of the yielding stress, then the residual stress is a random variable as well.

$$K = \sigma\sqrt{a\pi} = (\sigma_a + 0.5\sigma_Y)\sqrt{a\pi} \tag{4.171}$$

Brittle fracture will occur when the K value exceeds a certain critical value K_c, which is called critical fracture toughness, which is also a random variable. Hence:

$$g(\sigma_a, \sigma_Y, a, K_c) = K_c - (\sigma_a + 0.5\sigma_Y)\sqrt{a\pi} \tag{4.172}$$

There is a critical value of K_c for different materials, which corresponds to the energy balance criterion being met.

4.6 ALPS-ULSAP validation

All the methods (both empirical and analytical), used in this chapter for the calculation of the ultimate strength of stiffened and unstiffened plates, have been taken from the ALPS-ULPS theory, developed by professor Paik in 2003. The great advantage of this theory is the extremely short computational time, compared to the nonlinear finite element method. The formulae have been validated by Paik himself through a comparison with the nonlinear finite element method. A good agreement was found through a wide range of panel dimensions and different loading conditions ([16]).

In this paragraph not all the results of the validation study will be presented, but only the ones relevant for the case study which will be introduced in chapter 6. In particular, we are interested

in the ultimate strength of unstiffened plates and panels stiffened with L bars, under a longitudinal compressive load.

Figure 21 is showing the ultimate strength of an unstiffened plate with thickness $t_P = 16\ mm$ (in the case study, the plate is 17 mm thick) under biaxial load. If we look at the value corresponding to $\sigma_{yu} = 0$, we see that the ultimate strength σ_{xu} calculated with the ALPS-ULSAP theory is very close to the FEM solution.

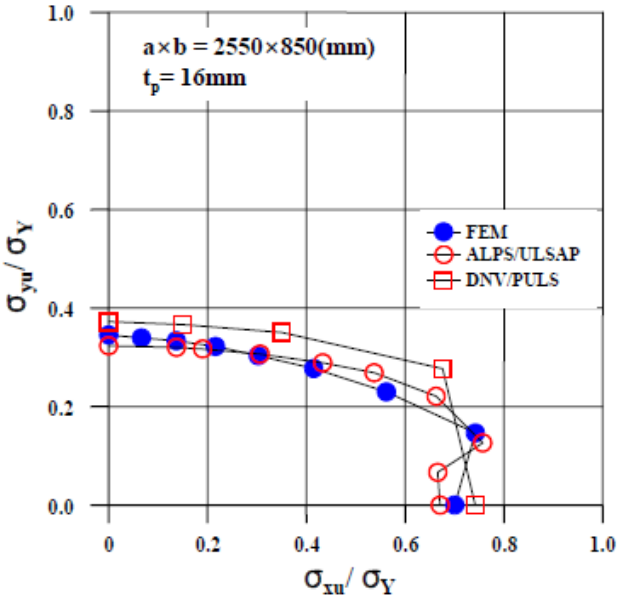

Figure 21 – Comparison ultimate strength of unstiffened plate between ALPS-ULSAP and nonlinear FEM

Figure 22 is showing the ultimate strength of a stiffened panel with L bars, as a function of the slenderness ration. The dimension of the stiffeners are *383x100x12/17 mm.* In the case study, the stiffener dimensions are *312x100x10/16 mm* and the slenderness ratio *1,7*. If we look at the results corresponding to this particular slendernees ratio, a very good agreement between ALPS-ULSAP and FEM is found.

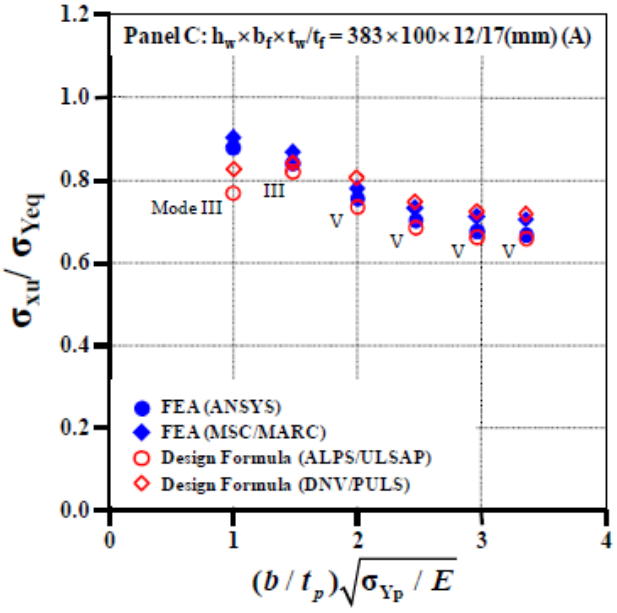

Figure 22 – Comparison ultimate strength of stiffened plate with L bars between ALPS-ULSAP and nonlinear FEM

4.7 Conclusion and recommendations

In this chapter, analytical equations for all the possible failure modes have been written down. This was a quite extensive operation, which required the utilization of different theories and models. Several simplifications were then necessary for the sake of simplicity.

Hence a compact list of the main assumptions is then provided here, in order to get a clear understanding of the validity and limitations of the limit state functions, and also to identify margins for eventual further improvements.

First of all, plate imperfections (residual stresses and initial distortion) have always been neglected when non-empirical formulae have been adopted. This may led to too optimistic results, and therefore it must be taken in mind when analyzing the result. The shear stresses have also been neglected, even if their non-inclusion may give less optimistic results than the non-inclusion of plate imperfections.

Another important aspect which has been not treated properly are the boundary conditions. Most of the time a simply supported plate has been assumed. However, this may consistently underestimate the ultimate strength, since the actual boundary conditions should be those ones of a simple support with rotational restraint. The consequences of such an hypothesis must be considered when reading the results.

References

[1] Dominique Beghin, Bureau Veritas, “Reliability-based structural design”, Ship structural analysis and design (chapter 5), SNAME 2010

[2] E. Nikolaidis, P. Kaplan, “Uncertainties in stress analysis of marine structures”, SNAME structural Inspection, maintenance and monitoring symposium (SSC Report-35), 1991

[3] D. Faulkner, “A review of effective plating for use in the analysis of stiffened plating in bending and compression”, Journal of ship research (Vol. 19), 1975

[4] P. H. Miller, J.W. Stettler, “Ship structures, notes for an undergraduate course”, Naval architecture program, US Naval Academy, Annapolis, 2009

[5] J. M. Gordo, C. Guedes Soares, “Approximate load shortening curves for stiffened plates under uni-axial compression”, Conference on integrity of offshore structures, Glasgow, 1993

[6] A. E. Mansour, A. K. Thayamballi, “Probability based ship design; loads and load combinations”, Ship structure committee (Report SSC-373), Washington DC, 1994

[7] J. Ferry-Borges, M. Castenheta, “Structural safety”, Lisbon: laboratoria nacional de engenhera civil, 1971

[8] T. Moan, G. Jiao, “Characteristic still water load effect for production ships”, Report MK/R 104/88, Trondheim: the Norwegian institute of technology, 1988

[9] C. Guedes Soares, “Probabilistic models for load effects in ship structures”, Report UR-84-38, Trondheim: department of marine technology, Norwegian institute of technology, 1984

[10] A. E. Mansour, “Extreme loads and load combinations”, Journal of ship research (vol. 39), 1995

[11] Y. Okumoto, Y. Takeda, M. Mano, T. Okada, “Design of ship hull structures, A practical guide for engineers”, Springer, 2009

[12] J. K. Paik, A. K. Thayamballi, “Ultimate limit state design of steel-plated structures”, 2003

[13] J. K. Paik, “Large deflection behaviour and ultimate strength of plates”, Ship structural analysis and design (chapter 13), SNAME 2010

[14] J. K. Paik, “Elastic buckling of plates”, Ship structural analysis and design (chapter 12), SNAME 2010

[15] J. K. Paik, “Large deflection behaviour and ultimate strength of stiffened panels”, Ship structural analysis and design (chapter 15), SNAME 2010

[16] J. Paik, “Ultimate Strength of Plates and Stiffened Panels”, Presentation given at the LRET Research Collegium, Southampton, 11 July – 2 September 2011

[17] O. Huges, H. G. Payer, “Loads, Structural Response, Limit States and Optimization”, Ship Structural Analysis and Design (chapter 2), SNAME, 2010

[18] O. Huges., J. B. Caldwell, “Plate bending”, Ship structural analysis and design (chapter 9), SNAME 2010

5

Monitored data processing

In this chapter, with a procedure similar to that one explained in chapter 2 for thicknesses, the loads data from MONITAS are processed in order to find which probability distribution function fits better the observations.

In paragraph 5.2 some probability and statistics formulae which are needed in the following paragraphs are derived. Results are presented and explained in parapgraph from 5.3 to 5.5. In paragraph 5.6 the correlation between load variables is studied.

5.1 The loads

Since the lateral pressure, for the deck, has been neglected, all the loads acting on the structure are the hull girder bending moments, that is: SWBM, VWBM and HWBM.

For the SWBM, 868 daily measurements have been recorded by the load master, and properly processed.

The HWBM and VWBM have been obtained by means of two long base strain gauges (LBSG) located on the deck, symmetrically with respect to the central plane of the unit. A LBSG is a gauge whose 2 meters length overcomes the effects of local stress conditions. In this way we monitor only the longitudinal and horizontal bending moment induced stresses.

Figure 1 - A long base strain gauge

Furthermore the sampling rate is 10 Hz, which means that all frequency lower than $f = 5\ Hz$ are filtered out. Since for FPSO the local vibration modes (like the vibration of the deck plating between two stiffeners) are typically in the range between 10 Hz and 50 Hz, and the primary vibration modes (like bottom vibrations between two transverse bulkheads) are typicallu in the range between 5 Hz and 20 Hz, this gives a further reason why local induced stresses are not included in the LBSG measurements.

The strength reassessment has been conducted over an ordinary section of the monitored FPSO, assumed to be located at the same cross section of the two LBSGs.

5.2 Probability and statistics theoretical background

The loads have been processed using the same procedure as the one applied to thickness measurements in chapter 2. The distributions considered here are non truncated, hence different sets of formulae for the maximum likelihood estimators and the linearized CDF are needed. This paragraph explains how these formulae have been derived.

5.2.1 Maximum likelihood estimation

For the SWBM the normal, the uniform and the Gumbel distributions have been considered. For the wave induced bending moments the exponential, the lognormal, the gamma, the normal, the Gumbel and the Weibull have been selected as assumed theoretical distribution. For any of these distributions, the maximum likelihood estimator have been found as follows.

The exponential distribution is a 1-parameter dependent distribution:

$$f(x) = \lambda \exp(-\lambda x) \tag{5.1}$$

The likelihood function is:

$$L(\lambda) = \prod_{i=1}^{n} \lambda \exp(-\lambda x_i) = \lambda^n \prod_{i=1}^{n} \exp(-\lambda x_i) = \lambda^n \exp\left(-\lambda \sum_{i=1}^{n} x_i\right) = \lambda^n \exp(-\lambda \bar{x} n) \qquad (5.2)$$

Its derivative is:

$$\frac{dL(\lambda)}{d\lambda} = n\lambda^{n-1} \exp(-\lambda \bar{x} n) - \bar{x} n \lambda^n \exp(-\lambda \bar{x} n) = \lambda^n n \exp(-\lambda \bar{x} n)\left(\frac{1}{\lambda} - \bar{x}\right)$$

Then:

$$\frac{dL(\lambda)}{d\lambda} \begin{cases} > 0 & if\ \lambda < \frac{1}{\bar{x}} \\ = 0 & if\ \lambda = \frac{1}{\bar{x}} \\ < 0 & if\ \lambda > \frac{1}{\bar{x}} \end{cases}$$

Then the maximum likelihood estimator for the exponential distribution is:

$$\lambda = \frac{1}{\bar{x}} \qquad (5.3)$$

which is exactly the same as the method of moments estimator.

The uniform distribution is a two-parameters dependent function:

$$f(x) = \begin{cases} \frac{1}{b-a} & for\ a \le x \le b \\ 0 & otherwise \end{cases} \qquad (5.4)$$

The likelihood function is:

$$L(a,b) = \prod_{i=1}^{n} \frac{1}{b-a} = \left(\frac{1}{b-a}\right)^n \qquad a \le x_i \le b \qquad (5.5)$$

The likelihood function is maximized when $(b-a)^n$ is minimized, keeping that $a \le x_i \le b, \forall x_i$. Then:

$$a = \min(x_i) \qquad (5.6)$$

$$b = \max(x_i) \qquad (5.7)$$

The Gumbel distribution is a 2-parameters dependent distribution:

$$f(x) = \frac{1}{b_{Gumbel}} \exp\left\{-\left[\frac{x - a_{Gumbel}}{b_{Gumbel}} + \exp\left(-\frac{x - a_{Gumbel}}{b_{Gumbel}}\right)\right]\right\} \qquad (5.8)$$

The maximum likelihood estimators for the Gumbel distribution are found by finding the numerical solution of the following equations ([1]):

$$b_{Gumbel} = a_{Gumbel}\left\{\log n - \log \sum_{i=1}^{n} \exp\left[-\left(\frac{x_i}{a_{Gumbel}}\right)\right]\right\} \tag{5.9}$$

$$\bar{x} = a_{Gumbel} + \frac{\sum_{i=1}^{n} x_i \exp\left[-\left(\frac{x_i}{a_{Gumbel}}\right)\right]}{\sum_{i=1}^{n} \exp\left[-\left(\frac{x_i}{a_{Gumbel}}\right)\right]} \tag{5.10}$$

The normal distribution is a two parameters-dependent distribution.

$$f(x) = \frac{1}{\sigma\sqrt{2\pi}} \exp\left[-\frac{(x-\mu)^2}{2\sigma^2}\right] \tag{5.11}$$

The maxim likelihood estimators of the mean and the variance are [2]:

$$\mu = \bar{x} \tag{5.12}$$

$$\sigma = \sqrt{\frac{1}{n}\sum_{i=1}^{n}(x_i - \mu)^2} \tag{5.13}$$

Note that (5.13) does not mean that $\sigma = s$ as the standard deviation of the samples has been calculated using the (5.14), slightly different from the (5.13):

$$s = \sqrt{\frac{1}{n-1}\sum_{i=1}^{n}(x_i - \bar{x})^2} \tag{5.14}$$

The gamma distribution is also characterized by a shape parameter and a scale parameter:

$$f(x) = \frac{1}{\Gamma(k)\theta^k} x^{k-1} \exp\left(-\frac{x}{\theta}\right) \tag{5.15}$$

To find them, an iterative procedure, as the one proposed in [3] has been used. The log-likelihood function for the gamma distribution is:

$$\log[L(k,\theta)] = n(k-1)\,\overline{\log x} - n * \log\Gamma(k) - nk * \log\bar{x} + nk * \log k - nk \tag{5.16}$$

The maximum of (5.16) is found by the following iterative procedure:

$$\frac{\Gamma'(k_{new})}{\Gamma(k_{new})} = \overline{\log x} - \log\bar{x} + a * \log k \tag{5.17}$$

$$\theta_{new} = \frac{\bar{x}}{k_{new}} \tag{5.18}$$

As initial value the method of moments estimators have been used. The function $\Gamma'(k_{new})/\Gamma(k_{new})$ is called "digamma function" and it is often indicated with the letter $\Psi(k_{new})$.

For the lognormal distribution (5.19) the maximum likelihood estimation of the two parameters μ and σ ([4]) is similar as for the normal distribution:

$$f(x) = \frac{1}{\sigma\sqrt{2\pi}} \exp\left[-\frac{(\log x - \mu)^2}{2\sigma^2}\right] \tag{5.19}$$

$$\mu = \frac{\sum_{i=1}^{n} \log x_i}{n} \tag{5.20}$$

$$\sigma = \sqrt{\frac{1}{n}\sum_{i=1}^{n} (\log x_i - \mu)^2} \tag{5.21}$$

Finally, the Weibull distribution is also a 2-parameters dependent distribution:

$$f(x) = \frac{a_{Weibull}}{b_{Weibull}} \left(\frac{x}{b_{Weibull}}\right)^{a_{Weibull}-1} \exp\left[-\left(\frac{x}{b_{Weibull}}\right)^{a_{Weibull}}\right] \tag{5.22}$$

Its two parameters are found solving numerically the followings [5]:

$$\frac{\sum_{i=1}^{n} x_i^{a_{Weibull}} \log x_i}{\sum_{i=1}^{n} x_i^{a_{Weibull}}} - \frac{1}{a_{Weibull}} - \frac{1}{n}\sum_{i=1}^{n} \log x_i = 0 \tag{5.23}$$

$$b_{Weibull} = \left(\frac{\sum_{i=1}^{n} x_i^{a_{Weibull}}}{n}\right)^{\frac{1}{a_{Weibull}}} \tag{5.24}$$

5.2.2 Linearization of the cumulative distribution function

Sometimes the linearization of the cumulative distribution function may be useful to compare graphically the efficiency of the estimators (see par. 2.3.7).

For the exponential distribution the linearization has been done as follows:

$$F_X(x) = 1 - e^{-\lambda x} \tag{5.25}$$

$$Y(x) = \log[1 - F_X(x)]^{-1} = \lambda x \tag{5.26}$$

$$\hat{Y}(x_i) = \log\left[1 - \widehat{F_X}(x)\right]^{-1} \tag{5.27}$$

For the uniform distribution:

$$F_X(x) = \frac{x-a}{b-a} \tag{5.28}$$

$$Y(x) = \frac{x-a}{b-a} \tag{5.29}$$

$$\hat{Y}(x_i) = \widehat{F_X}(x) \tag{5.30}$$

For the Gumbel distribution:

$$F_X(x) = \exp\left[-\exp\left(-\frac{x-a_{Gumbel}}{b_{Gumbel}}\right)\right] \tag{5.31}$$

$$Y(x) = -\log[-log\, F_X(x)] = \frac{x-a_{Gumbel}}{b_{Gumbel}} \tag{5.32}$$

$$\hat{Y}(x_i) = -\log\left[-log\, \widehat{F_X}(x_i)\right] \tag{5.33}$$

For the normal distribution:

$$F_X(x) = \frac{1}{2} + \frac{1}{2}\text{erf}\left[\frac{x-\mu}{\sqrt{2}\sigma}\right] \tag{5.34}$$

$$Y(x) = erfinv(2 * F_X(x) - 1) = \frac{x-\mu}{\sqrt{2}\sigma} \tag{5.35}$$

$$\hat{Y}(x_i) = erfinv\left(2 * \widehat{F_X}(x_i) - 1\right) \tag{5.36}$$

For the gamma distributions:

$$F_X(x) = gammainc\left(\frac{x}{\theta}, k\right) \tag{5.37}$$

$$Y(x) = gammainc\left(\frac{x}{\theta}, k\right) \tag{5.38}$$

$$\hat{Y}(x_i) = \widehat{F_X}(x_i) \tag{5.39}$$

The (5.38) will look linear if we plot $Z = gammainc\left(\frac{x}{\theta}, k\right)$ on the horizontal axis.

For the lognormal distributions:

$$F_X(x) = \frac{1}{2} + \frac{1}{2}\text{erf}\left[\frac{log(x)-\mu}{\sqrt{2}\sigma}\right] \tag{5.40}$$

$$Y(x) = erfinv(2 * F_X(x) - 1) = \frac{log(x)-\mu}{\sqrt{2}\sigma} \tag{5.41}$$

$$\hat{Y}(x_i) = erfinv\left(2 * \widehat{F_X}(x_i) - 1\right) \tag{5.42}$$

For the Weibull distributions:

$$F_X(x) = 1 - \exp\left[-\left(\frac{x}{b_{Weibull}}\right)^{a_{Weibull}}\right] \tag{5.43}$$

$$Y(x) = -\log\left(1 - F_X(x)\right)^{\frac{1}{a_{Weibull}}} = \frac{x}{b_{Weibull}} \tag{5.44}$$

$$\hat{Y}(x_i) = -\log\left(1 - \widehat{F_X}(x_i)\right)^{\frac{1}{a_{Weibull}}} \tag{5.45}$$

5.3 The SWBM

In figures 2, 3 and 4 the SWBM daily values have been plotted, together with the draft and the trim. The time trace of the SWBM has been divided into three figures for the only purpose to make the graphs more readable. The positive moments are the hogging moments.

First of all, we notice that the SWBM is not actually having a regular "saw-tooth" path, which is what we expected to see from an FPSO. At a quick look, the SWBM time trace looks very irregular and with no apparent logic behind.

However, if we look it more carefully, we see that the draft is actually having a "saw-tooth" path and that at each drop of the draft a rapid increase of the SWBM is occurring. We also see that, at each loading-offloading cycle, the trend of the SWBM is – although irregular – decreasing. The irregular behavior of the trim is giving us the explanation why the SWBM trend is irregular as well.

The flat curve at the beginning is due to the fact that at that time the FPSO was not operative yet.

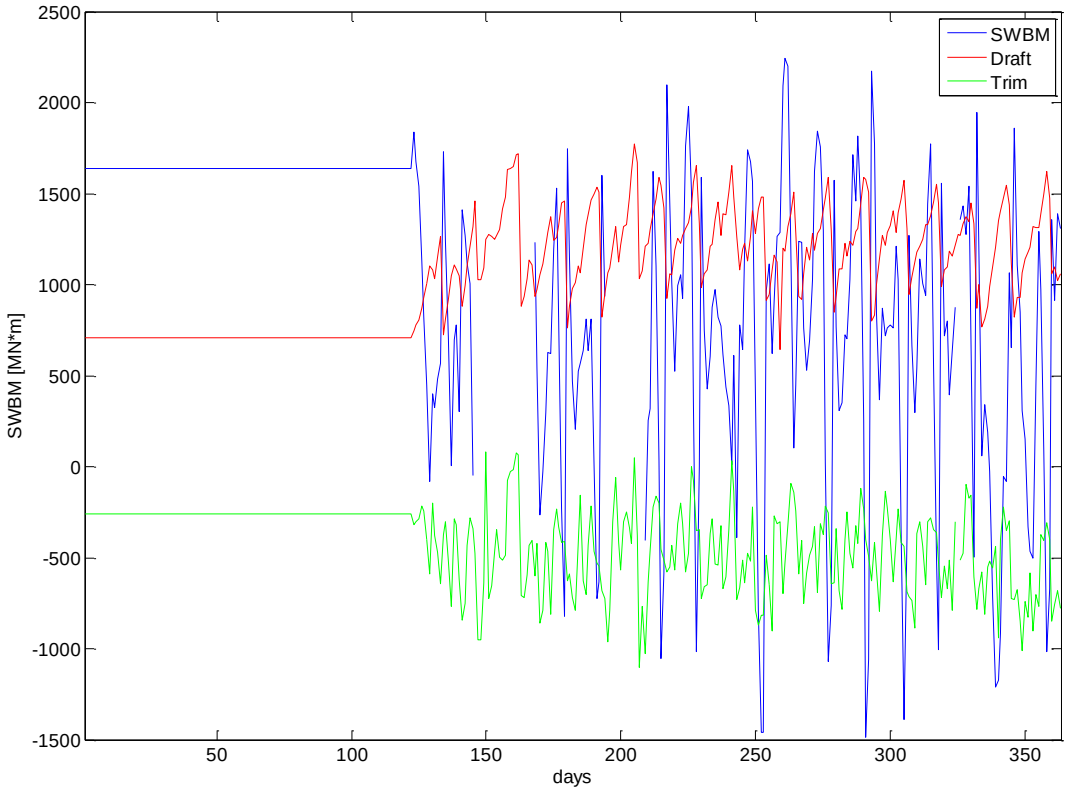

Figure 215 – SWBM part 1

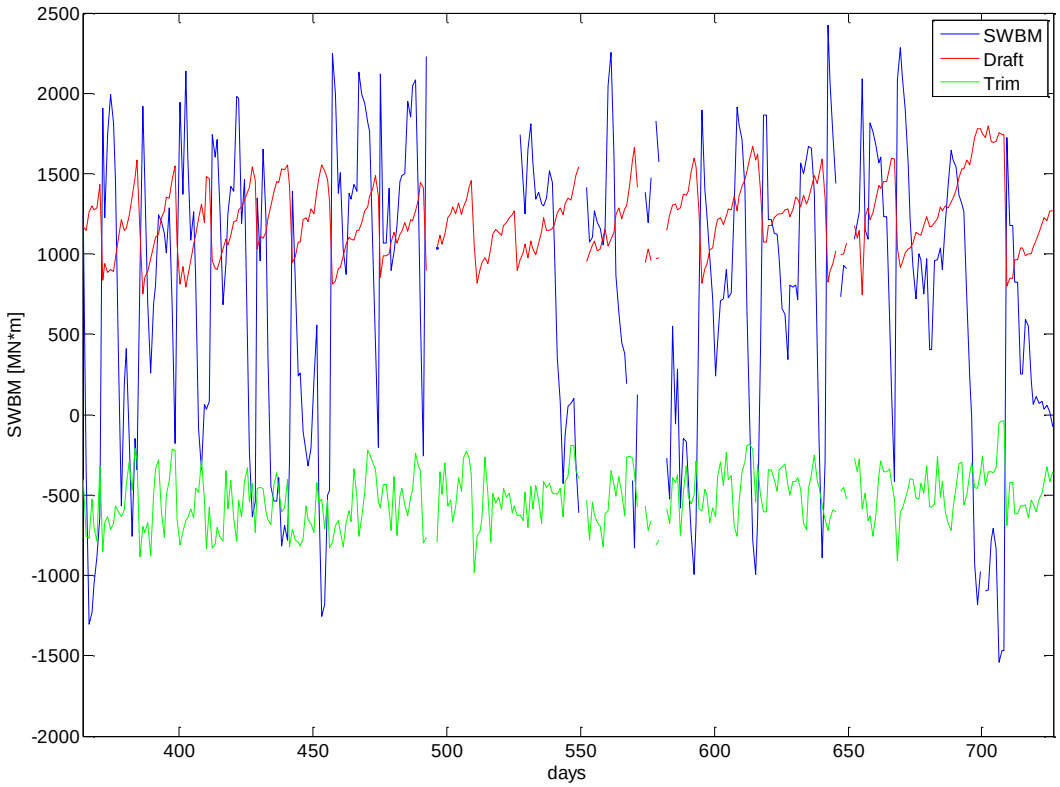

Figure 3 – SWBM part 2

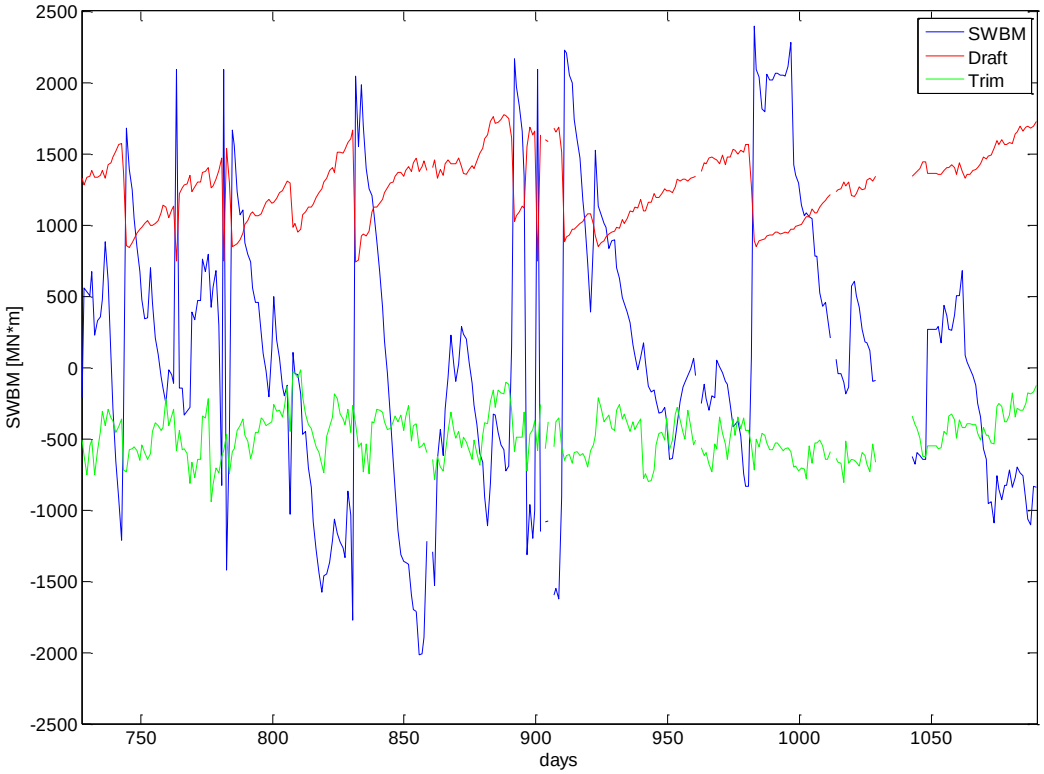

Figure 4 – SWBM part 3

All these data have been then properly processed.

First of all, only the operational condition has been considered (thus the measurements in the first days giving us a constant SWBM have been disregarded).

Then, all the statistical concept introduced in chapter 2 and paragraph 5.3 for the estimation of a continuous distribution starting from some observed values are then applied here in an analogous way to what has already been done for thicknesses.

The assumed probability distribution functions are:

1. The normal distribution
2. The uniform distribution
3. The Gumbel distribution

The normal distribution has been selected since it is usually the way the SWBM is modeled for commercial vessel. The uniform distribution has been selected because this is what we would expect to see from a regular "saw-tooth" time trace path of the SWBM, as it is often the case for FPSOs. The Gumbel distribution is the usual way the VWBM is modeled in commercial vessels.

All the SWBM values have been considered together, with no distinction between hogging and sagging.

Table 1 and table 2 are giving the results of the Kolmogorv-Smirnov test and the sum of squares method.

Table 1 – Kolmogorov-Smirnov test for the SWBM

	Method of moments		MLE	
	y	*y threshold*	*y*	*y threshold*
Normal distribution	0.0430	0.0418	0.0431	0.0418
Uniform distribution	0.0484	0.0418	0.1651	0.0418
Gumbel distribution	0.1005	0.0418	0.0798	0.0418

Table 2 – Least squares method for the SWBM

	Method of moments	MLE
	SS	*SS*
Normal distribution	0.408	0.411
Uniform distribution	0.492	8.271
Gumbel distribution	2.982	1.640

Both methods are saying that the normal distribution with the method of moments estimator is the best distribution.

Due to the high number of samples, it is more likely here that the method of moments estimators perform better than the maximum likelihood estimators. This is particularly true for the uniform distribution (fig. 6).

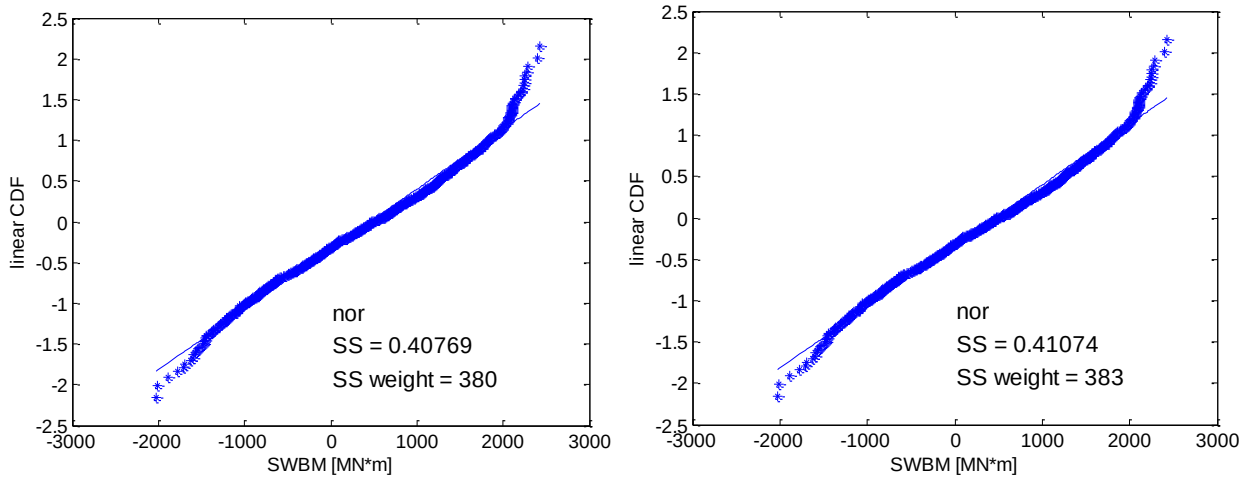

Figure 5 – Linearized normal CDF for the SWBM: method of moments estimator (left) and MLE estimators (right)

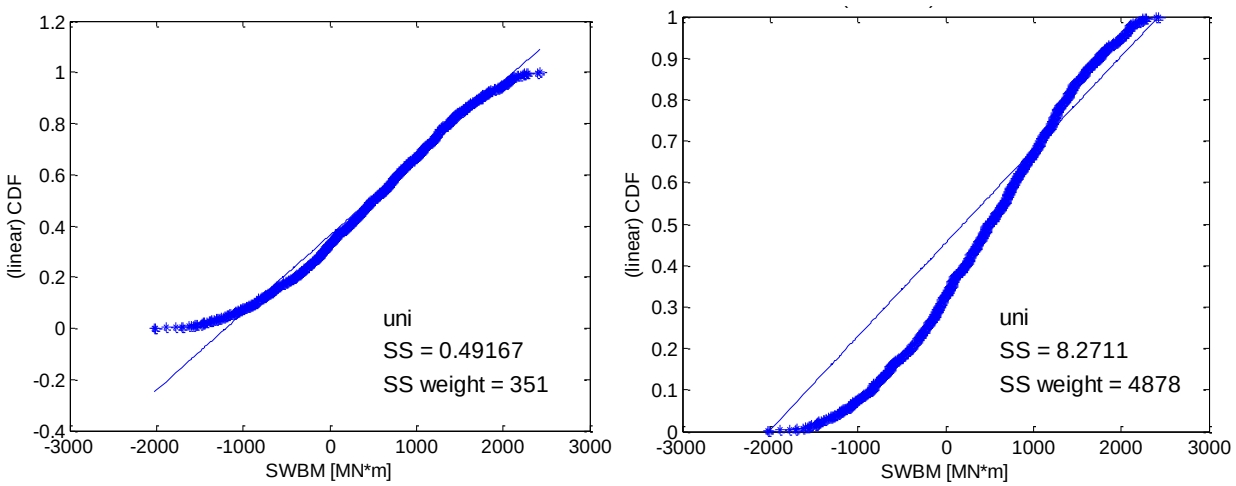

Figure 616 – Linearized uniform CDF for the SWBM: method of moments estimator (left) and MLE estimators (right)

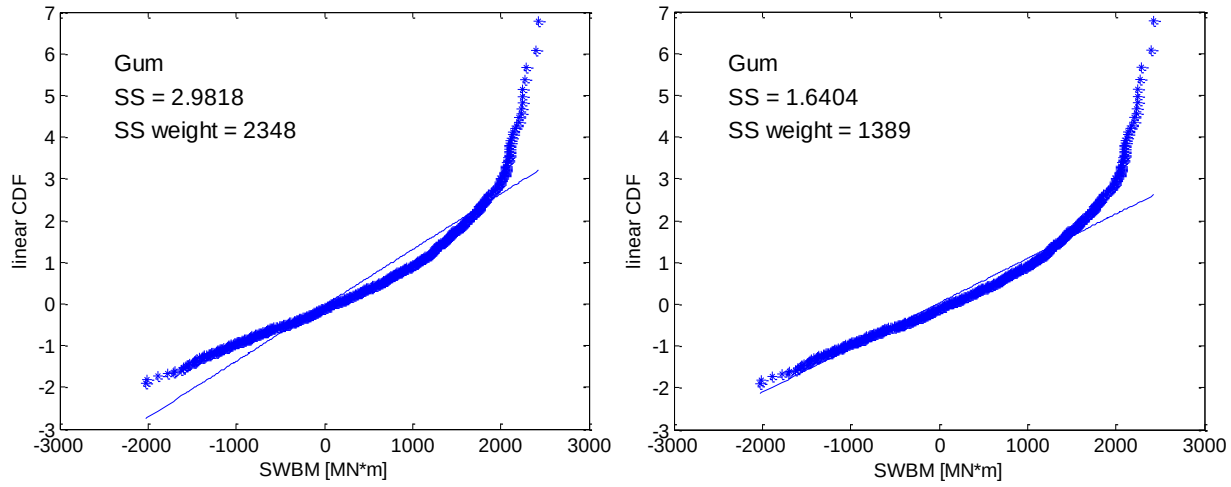

Figure 717 – Linearized Gumbel CDF for the SWBM: method of moments estimator (left) and MLE estimators (right)

The weighed SS method (tab. 3) is giving a slightly better result for the uniform distribution (with method of moments estimators) rather than for the normal distribution.

Table 3 – Weighed least squares method for the SWBM

	Method of moments	MLE
	SS	*SS*
Normal distribution	380	382
Uniform distribution	351	4 878
Gumbel distribution	2 349	1 389

Figures 8 is comparing some of the assumed distributions. Figure 9 is doing the same but in a q-q plot. In figure 9 it may seem that the uniform distribution and the normal distribution perform very similarly. However, if we look at fig. 8, we see that the uniform distribution is giving a zero probability for all values of the SWBM between -2000 MN*m and -1200 MN*m (which are

extreme moments, i.e. the values in which we are more interested in!). This is also true (but to a less extent) for the extreme positive SWBM. Thus opting for the uniform distribution would return us too optimistic results. This is the reason why it was chosen to use the normal distribution.

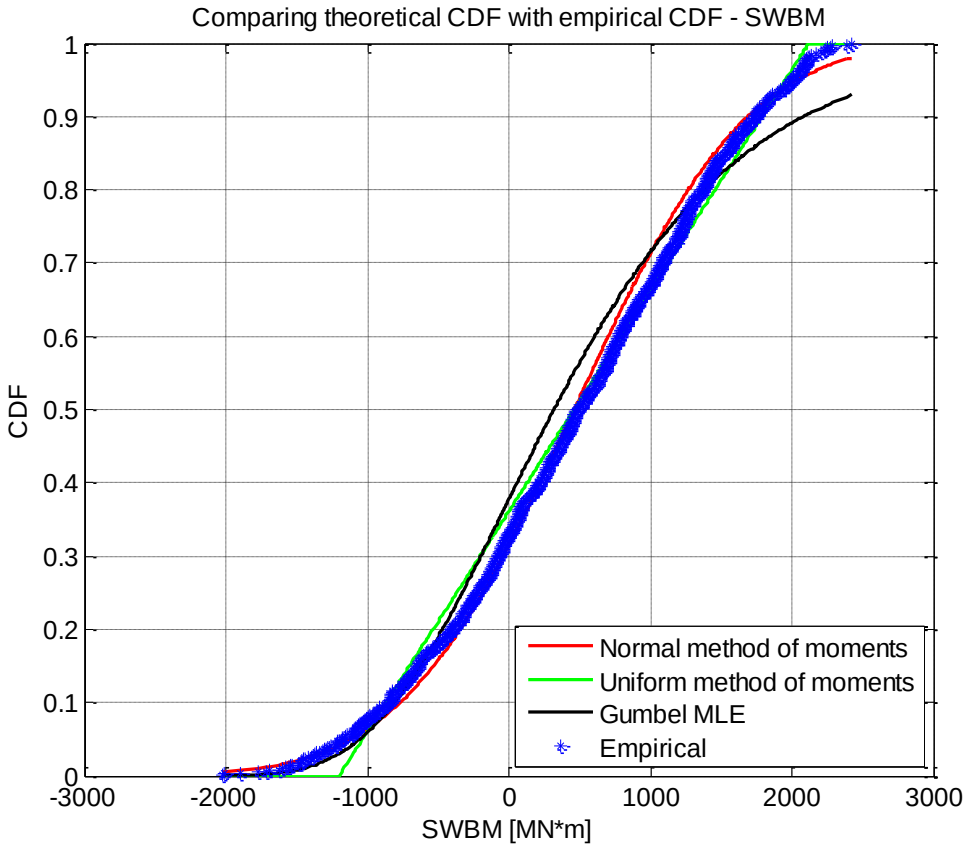

Figure 818 – Comparison between empirical CDF and assumed CDFs

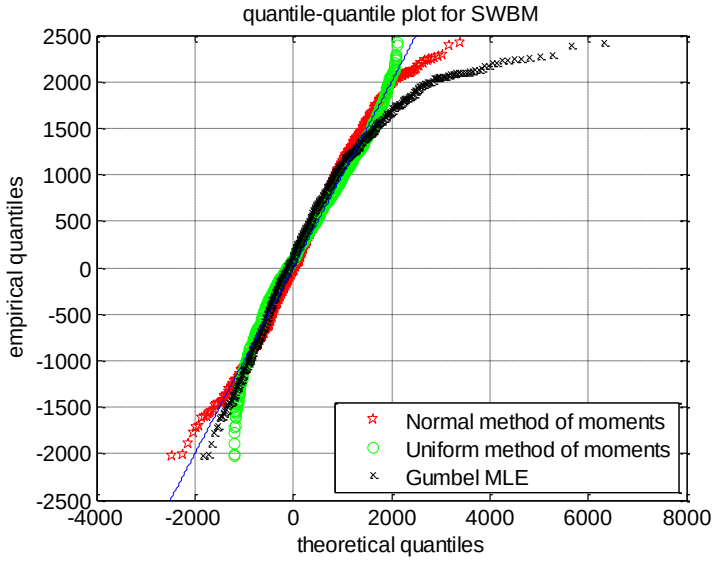

Figure 9 - q-q plot for the SWBM

Finally, the normal distribution with the following parameters (method of moments estimators) has been chosen:

$\mu = 461\ MN * m$

$\sigma = 959\ MN * m$

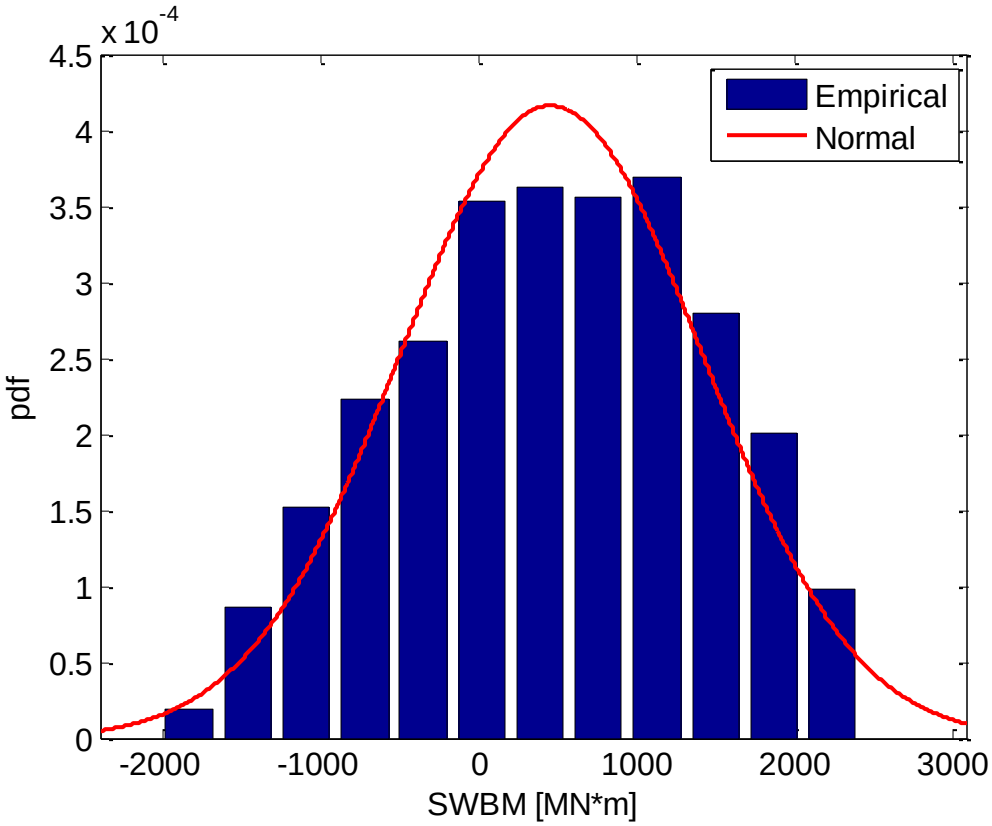

Figure 10 - Probability distribution function for the SWBM

5.4 The VWBM

For both the VWBM and the HWBM, 12 months of measurements have been considered (in order not to be influenced by the seasonal variation).

The VWBM time record has been obtained from the strain measurements on the deck carried out by the LBSGs, using the following:

$VWBM(t) = strain(t) * E * w$

- E: elasticity modulus
- w: section modulus

With a LBSG it is actually only possible to measure the stress ranges (thus they are quite suitable for a fatigue assessment). We are not able to read the absolute values of stresses, as we should know the strain on the deck at the moment of the installation of the LBSGs.

In our case it was decided to shift the time history of the VWBM so to have a mean value equal to 0. Generally this hypothesis is acceptable for unit with a large block coefficient. Our monitored FPSO has a block coefficient of $C_B = 0.82$.

For the VWBM hogging and sagging have been considered separately. However, due to the hypothesis of zero mean value, they are symmetric to each other. Thus we will here present the processing procedure only for the hogging case. The obtained results are also valid for the (absolute value of) the sagging VWBM.

First of all the local extreme value have been found with MATLAB (see figure 8).

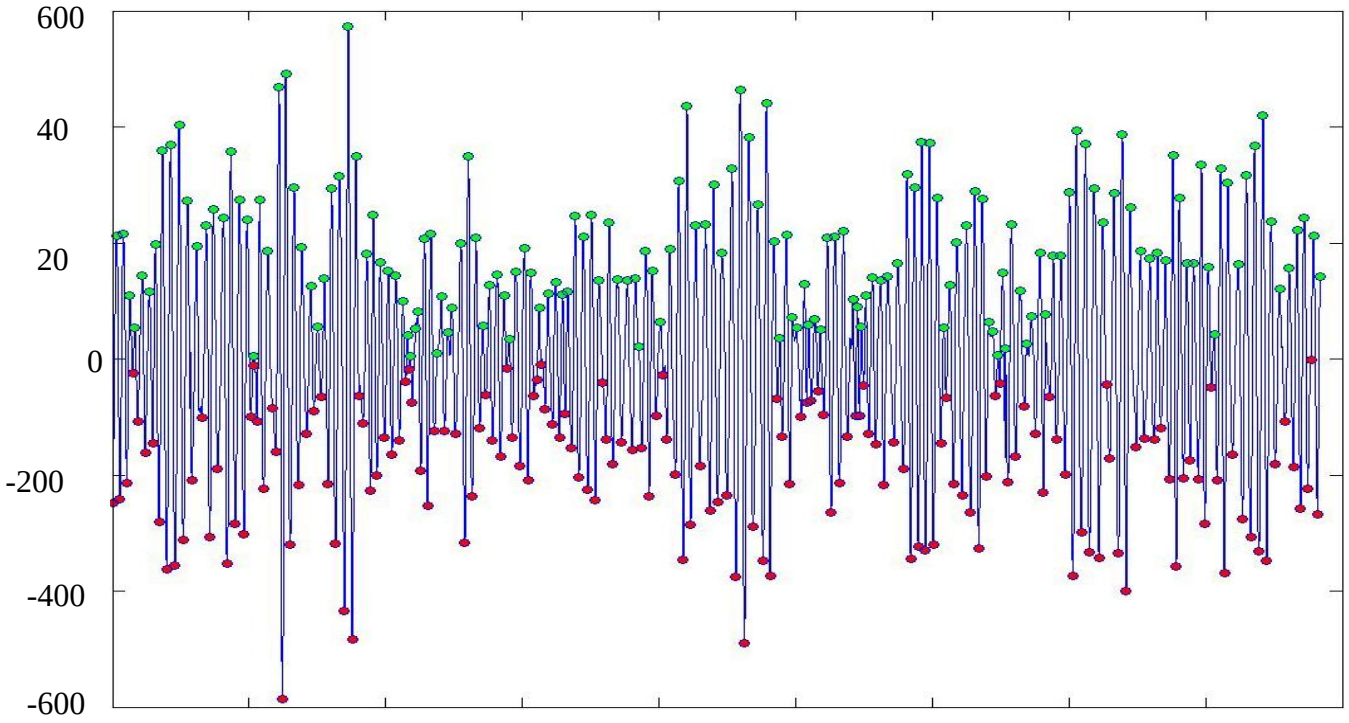

Figure 11 – VWBM time trace [MN*m]

Table 4 and 5 are giving the results for the KV test and the least squares method.

Table 4 – Kolmogorov-Smirnov test for the VWBM

	Method of moments		MLE	
	y	*y threshold*	*y*	*y threshold*
Exponential distribution	0.108	0.000784	0.108	0.000784
Lognormal distribution	0.0596	0.000784	0.0716	0.000784
Gamma distribution	0.0340	0.000784	0.0370	0.000784
Normal distribution	0.124	0.000784	0.124	0.000784
Gumbel distribution	0.0743	0.000784	0.049	0.000784
Weibull distribution	0.0448	0.000784	0.0293	0.000784

Table 5 - Least squares method for the VWBM

	Method of moments	MLE
	SS	*SS*
Exponential distribution	11 542	11 542
Lognormal distribution	2 149	5 650
Gamma distribution	1 057	1 236
Normal distribution	1 917	1 917
Gumbel distribution	4 586	2 842
Weibull distribution	1 898	1 127

In this case it is more common to have cases where the method of moments is giving better estimators than the MLE. This is due to the very high number of samples (for the VWBM we have more than 3 millions value), which is also the reason why the threshold y value is very low.

Anyway, both method agrees on the gamma distribution (with method of moments estimator). This may be surprising, as we would have expected a Gumbel or Weibull distribution, which is usually the way VWBM is modeled for commercial vessel.

If we plot the linearized CDFs (figures 12 to 17) it may seem that, besides the gamma distribution (which fits quite good to the empirical distribution), also the exponential distribution is apparently giving good results. However this is not confirmed by the Kolmogorov-Smirnov and the sum of squares methods. We should not forget that this is due to the fact that linearized CDF graphs must be read carefully, as the scale on the vertical axis is not constant (see par. 2.3.7). This is particularly true for the exponential distribution, where the actual $\Delta F = \left|\widehat{F_X}(x) - F_X(x)\right|$ (that is, the actual difference between empirical CDF and theoretical assumed CDF) corresponding to a constant $\Delta Y = \left|\hat{Y}(x) - Y(x)\right|$ (that is, the difference between linearized empirical CDF and linearized theoretical assumed CDF) is growing exponentially with x.

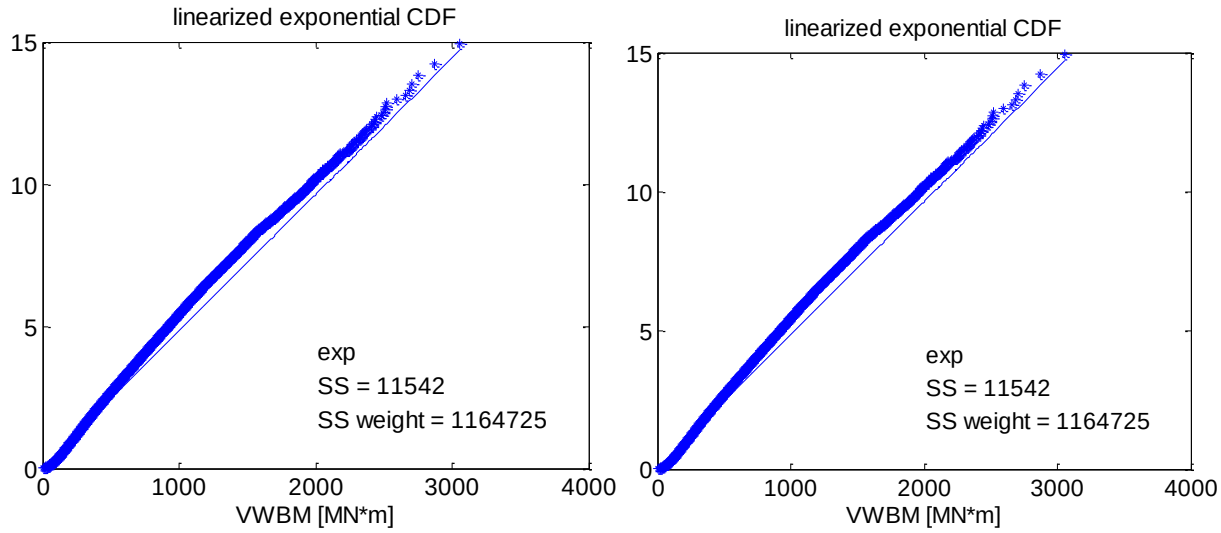

Figure 12 – Linearized exponential CDFs for the VWBM: with method of moments estimator (left) and MLE estimators (right)

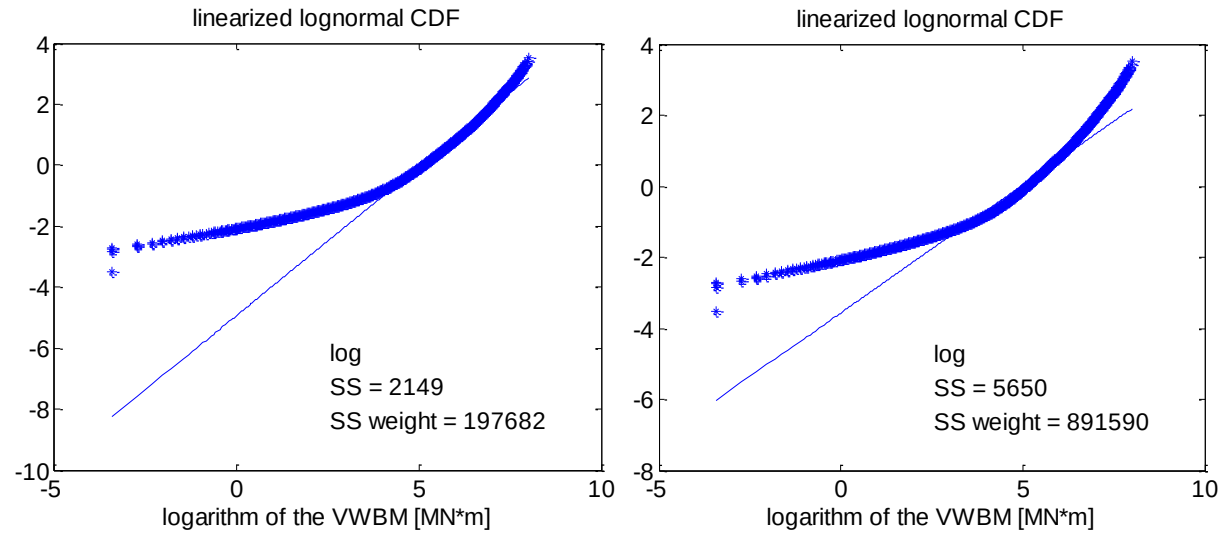

Figure 13 – Linearized lognormal CDFs for the VWBM: with method of moments estimator (left) and MLE estimators (right)

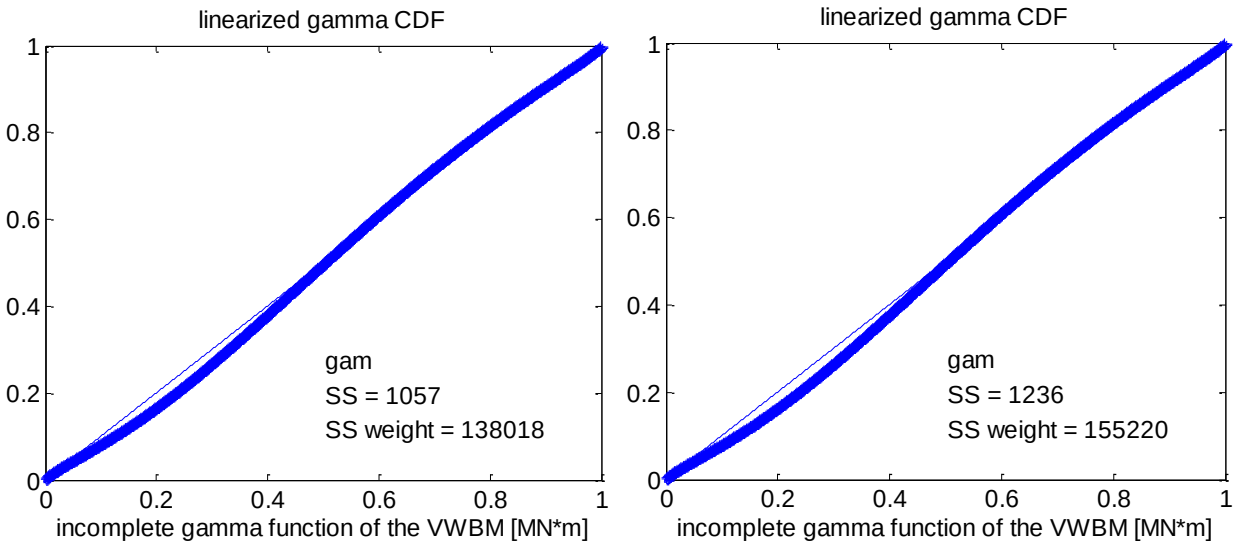

Figure 14 – Linearized gamma CDFs for the VWBM: with method of moments estimator (left) and MLE estimators (right)

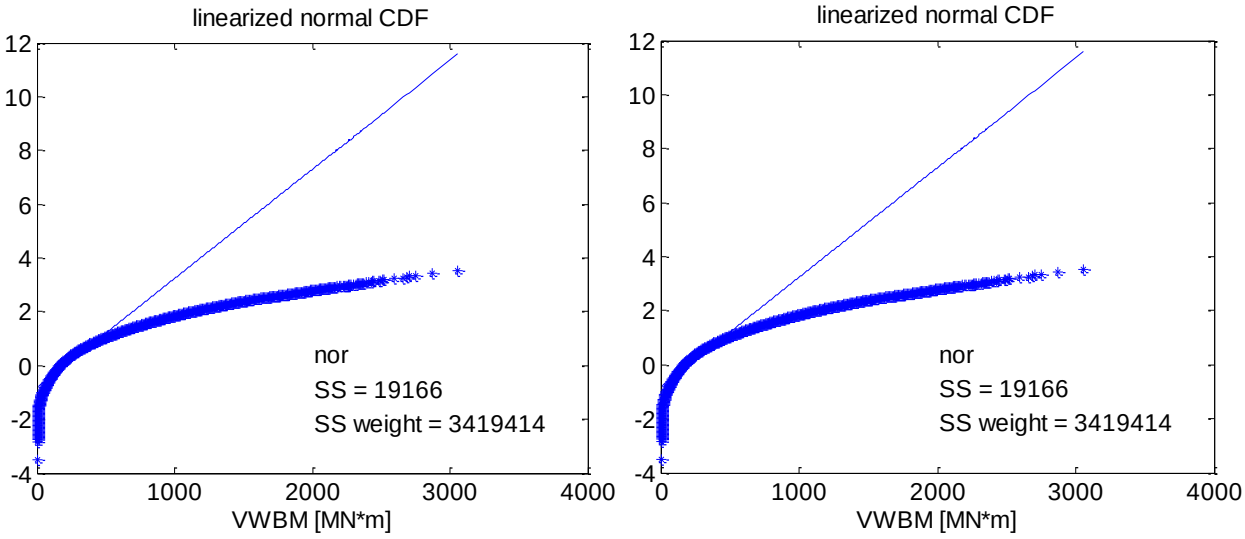

Figure 15 – Linearized normal CDFs for the VWBM: with method of moments estimator (left) and MLE estimators (right)

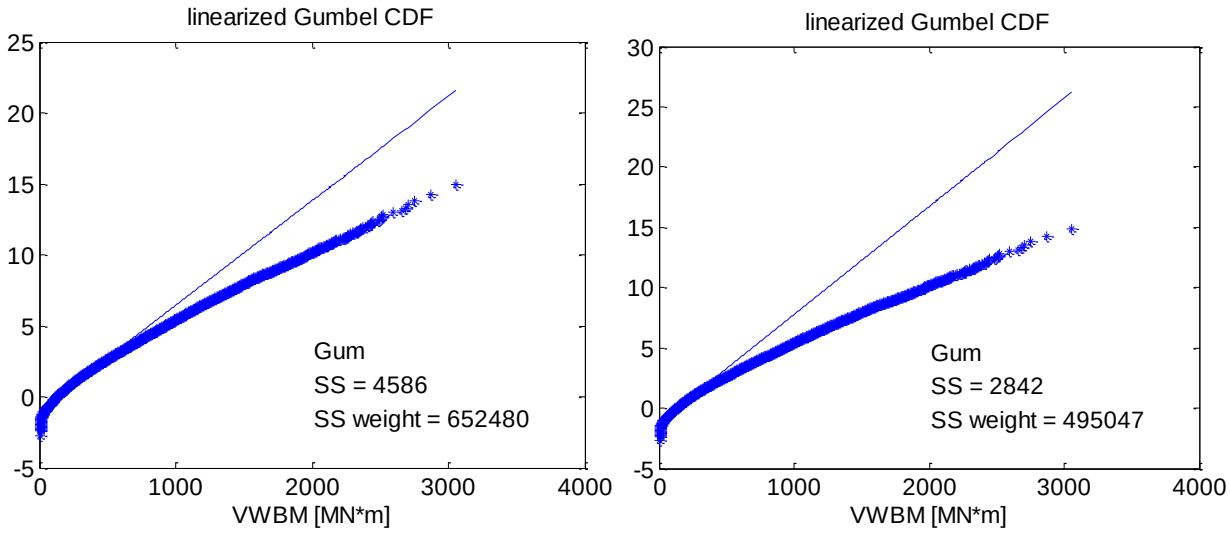

Figure 16 – Linearized Gumbel CDFs for the VWBM: with method of moments estimator (left) and MLE estimators (right)

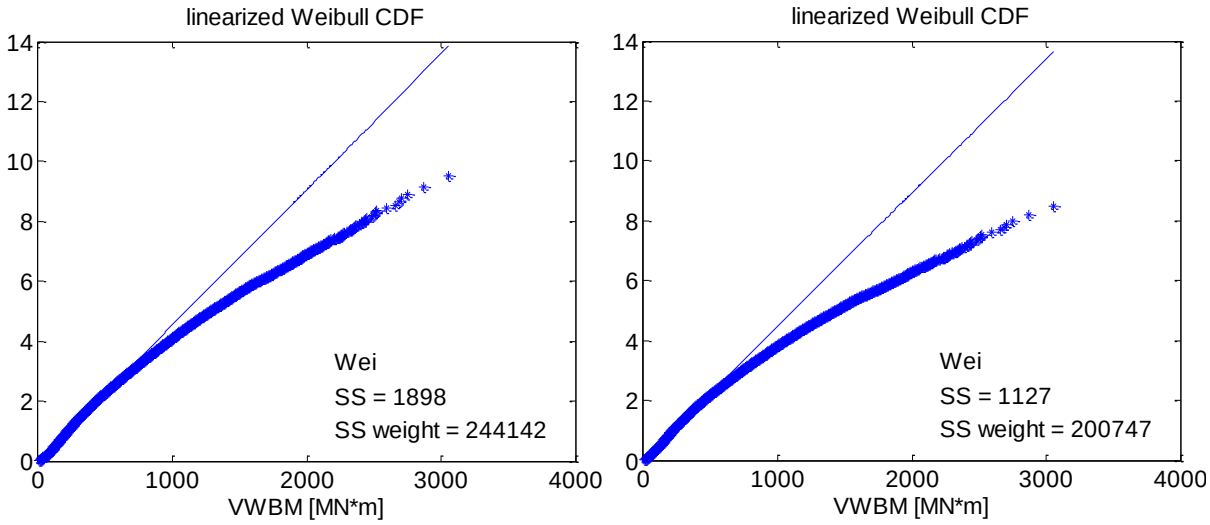

Figure 17 – Linearized Weibull CDFs for the VWBM: with method of moments estimator (left) and MLE estimators (right)

Table 6 is giving the weighed SS method. One more time, the gamma distribution with the method of moments estimator is the best fit.

Table 6 – Weighed least squares method for the VWBM

	Method of moments	MLE
	SS	*SS*
Exponential distribution	1 165 *10^3	1 165*10^3
Lognormal distribution	197*10^3	892*10^3
Gamma distribution	138*10^3	155*10^3
Normal distribution	3 419*10^3	3419*10^3
Gumbel distribution	652*10^3	495*10^3
Weibull distribution	244*10^3	201*10^3

Finally, figure 18 is giving the q-q plot for some of the assumed distributions. In reading this graph we should take into account that 99.6% of the considered value are below 1000 MN*m, and thus the (weighed and non weighed) least squares method is strongly influenced by the values in the region $x < 1000\ MN * m$. We can clearly see that the gamma distribution is the one which stays closer to the empirical in the range $x < 1000\ MN * m$.

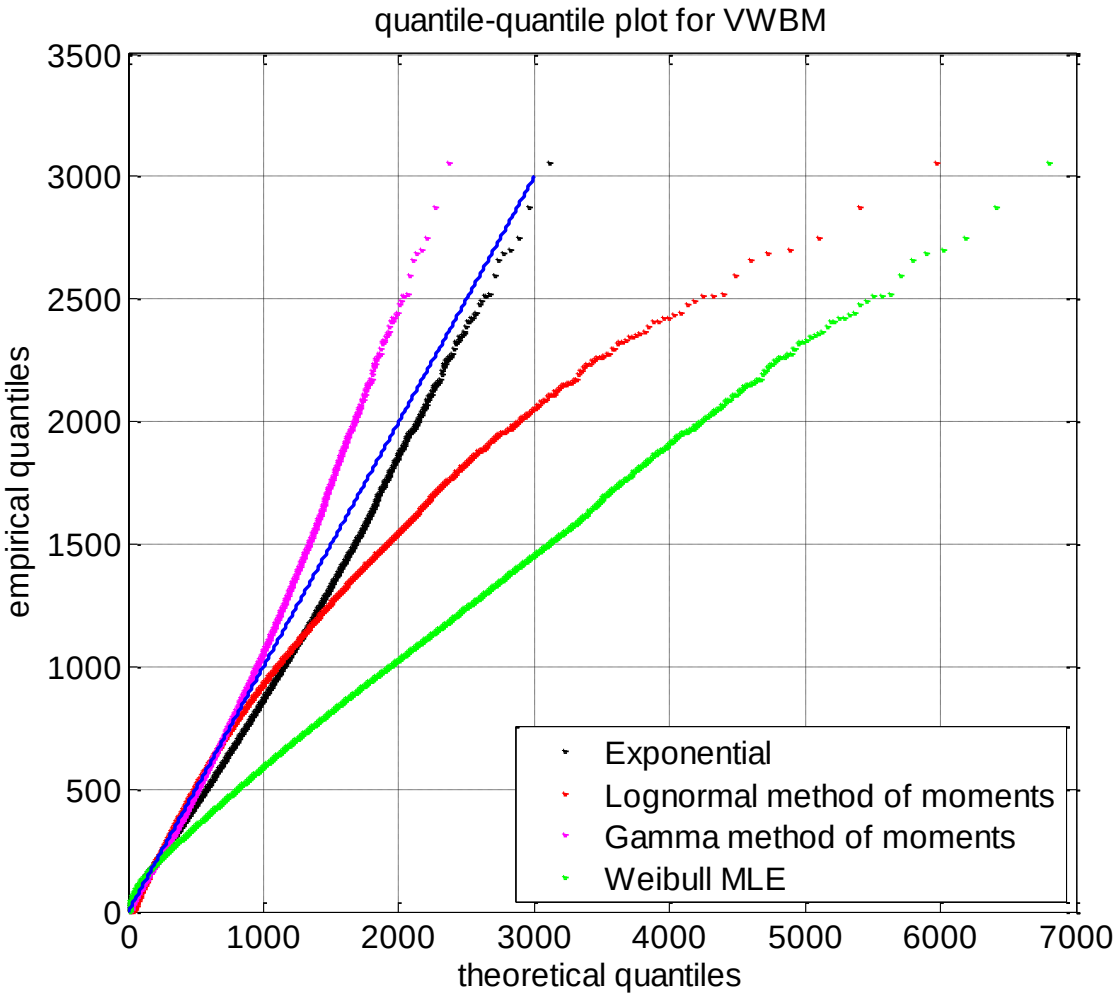

Figure 198 – q-q plot for the VWBM

In the end, the gamma distribution with the method of moments estimator was chosen:

$k = 1.43$

$\theta = 145.5$

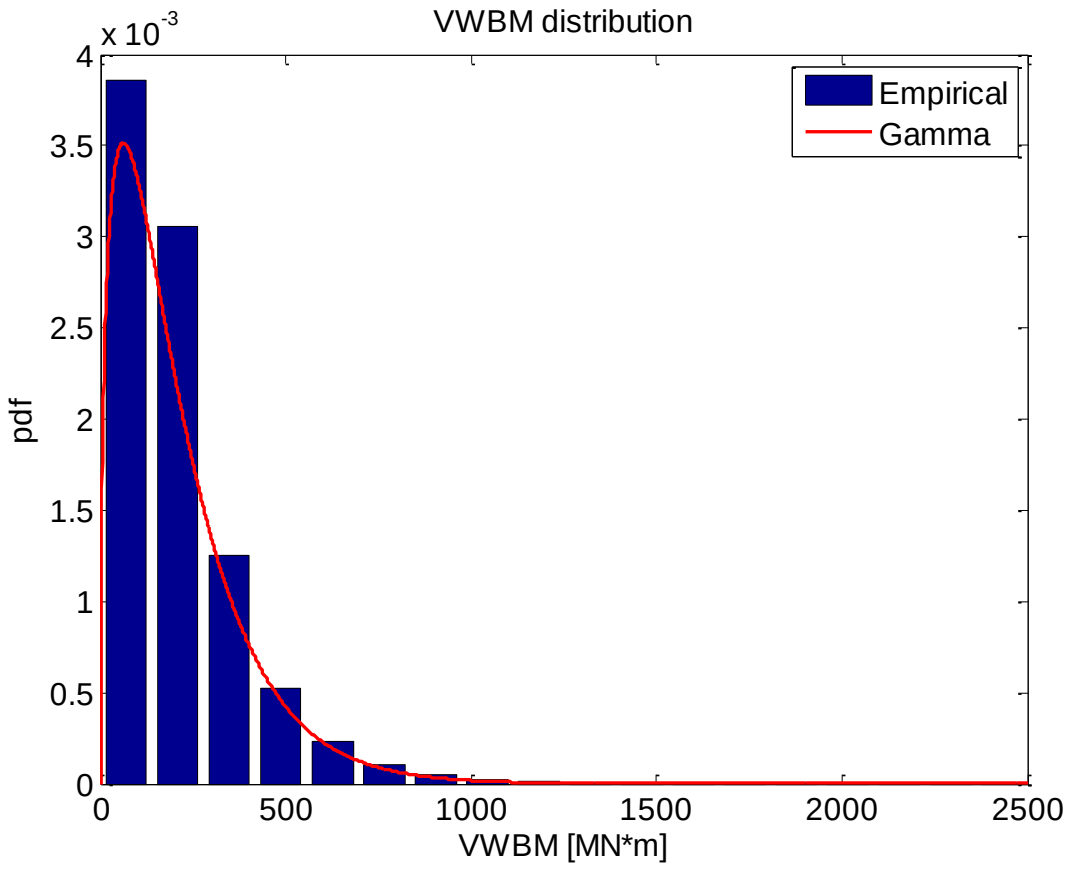

Figure 19 - Probability distribution function for the VWBM

5.5 The HWBM

Tables 7 and 8 summarize the results for the Kolmogorov-Smirnov test and the sum of squares test.

Table 7 – Kolmogorov-Smirnov test for the HWBM

	Method of moments		MLE	
	y	*y threshold*	*y*	*y threshold*
Exponential distribution	0.146	0.000657	0.146	0.000657
Lognormal distribution	0.0734	0.000657	0.0964	0.000657
Gamma distribution	0.0231	0.000657	0.0510	0.000657
Normal distribution	0.0859	0.000657	0.0859	0.000657
Gumbel distribution	0.0317	0.000657	0.0208	0.000657
Weibull distribution	0.0255	0.000657	0.0261	0.000657

Table 8 – Least squares method for the HWBM

	Method of moments	MLE
	SS	*SS*
Exponential distribution	26 965	26 965
Lognormal distribution	4 481	12 214
Gamma distribution	513	2 986
Normal distribution	10 521	10 521
Gumbel distribution	397	454
Weibull distribution	746	758

Similarly to the VWBM case, also here the method of moments estimators often perform better than the maximum likelihood estimators, as it is also confirmed in figures 20 to 25.

In particular, both the KS test and the sum of squares method suggested us to use one of the followings: gamma distribution (with method of moments estimators), Gumbel distribution (with either method of moments or maximum likelihood estimators) and Weibull distribution (with either method of moments or maximum likelihood estimators).

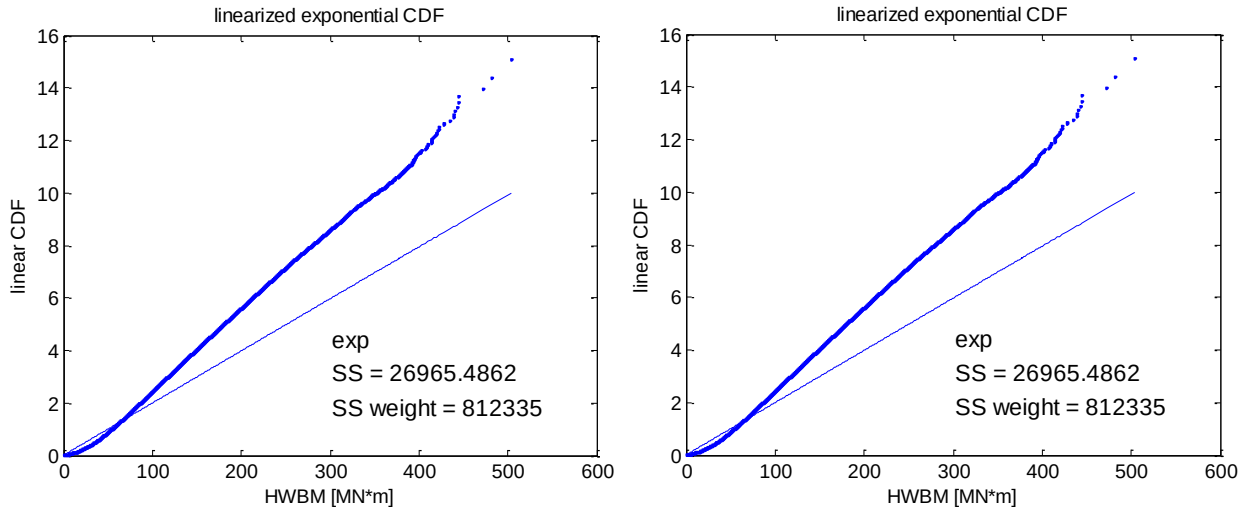

Figure 20 – Linearized exponential CDFs for the HWBM: with method of moments estimator (left) and MLE estimators (right)

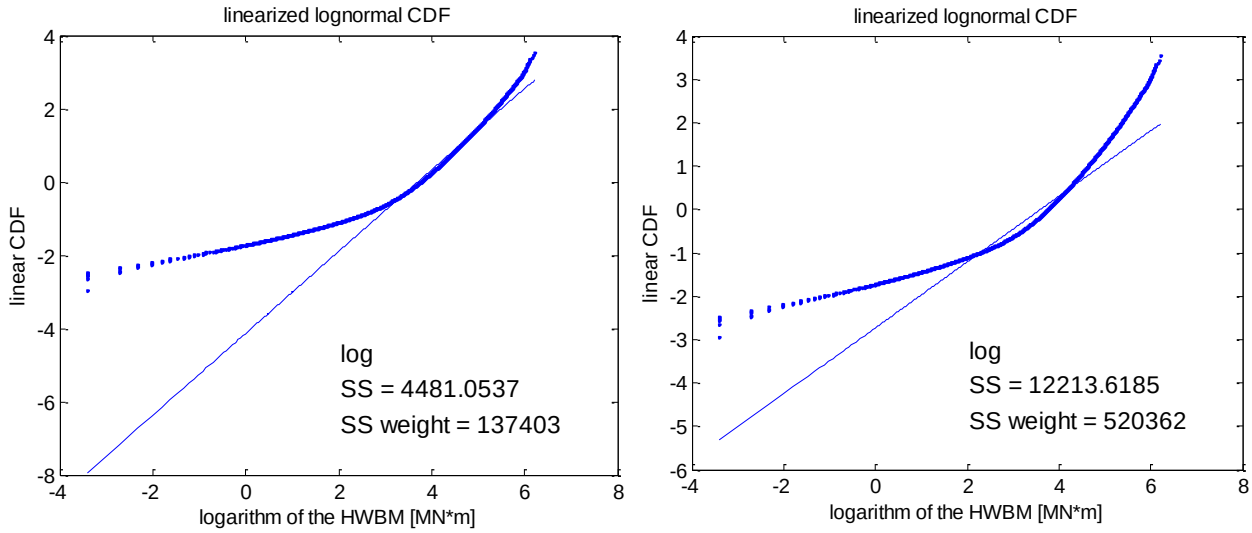

Figure 21 – Linearized lognormal CDFs for the HWBM: with method of moments estimator (left) and MLE estimators (right)

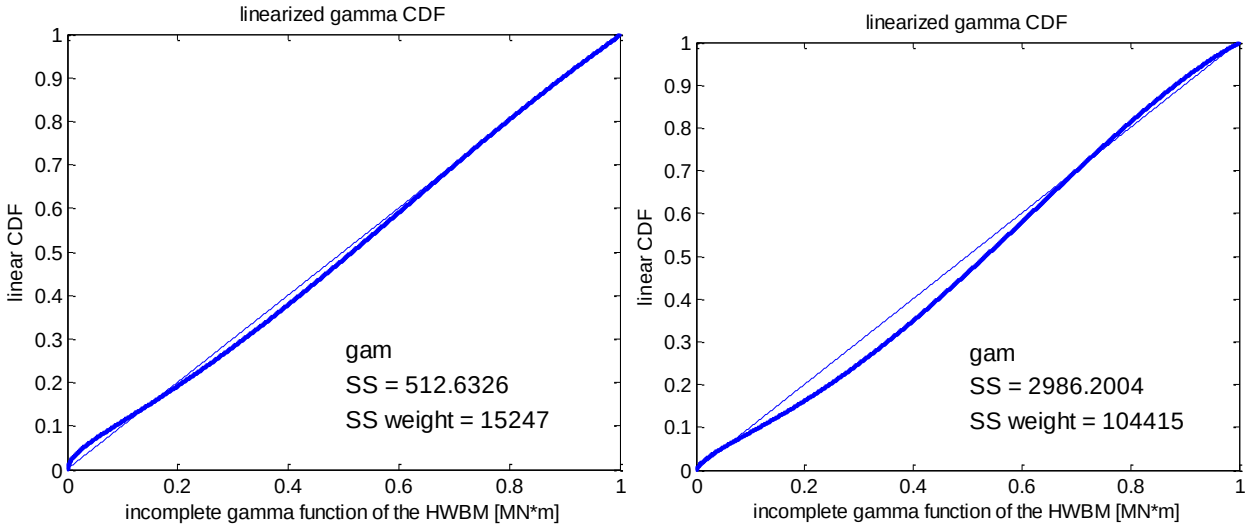

Figure 22 – Linearized gamma CDFs for the HWBM: with method of moments estimator (left) and MLE estimators (right)

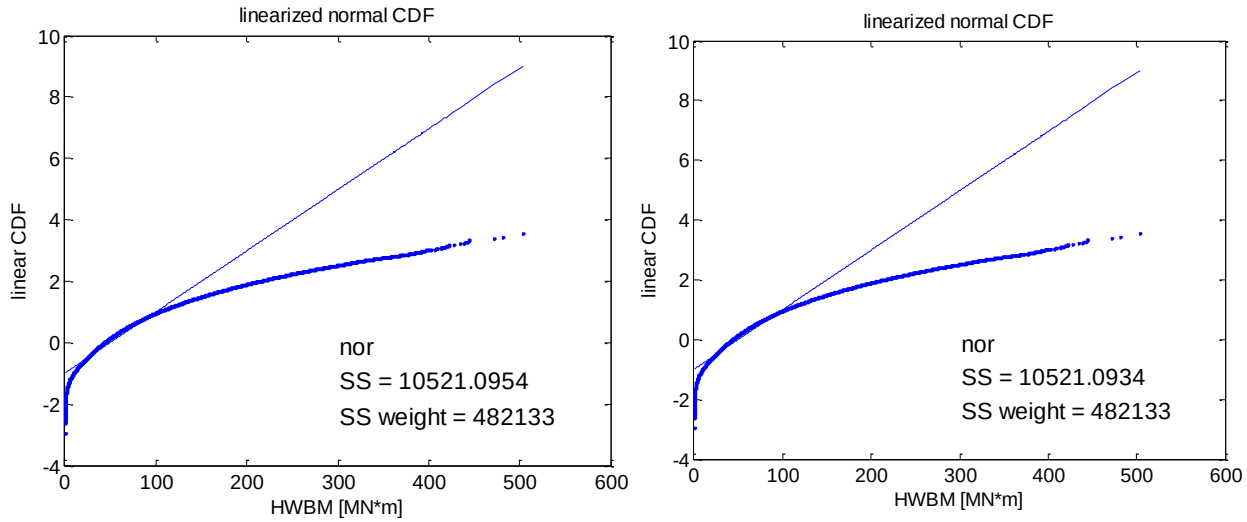

Figure 23 – Linearized normal CDFs for the HWBM: with method of moments estimator (left) and MLE estimators (right)

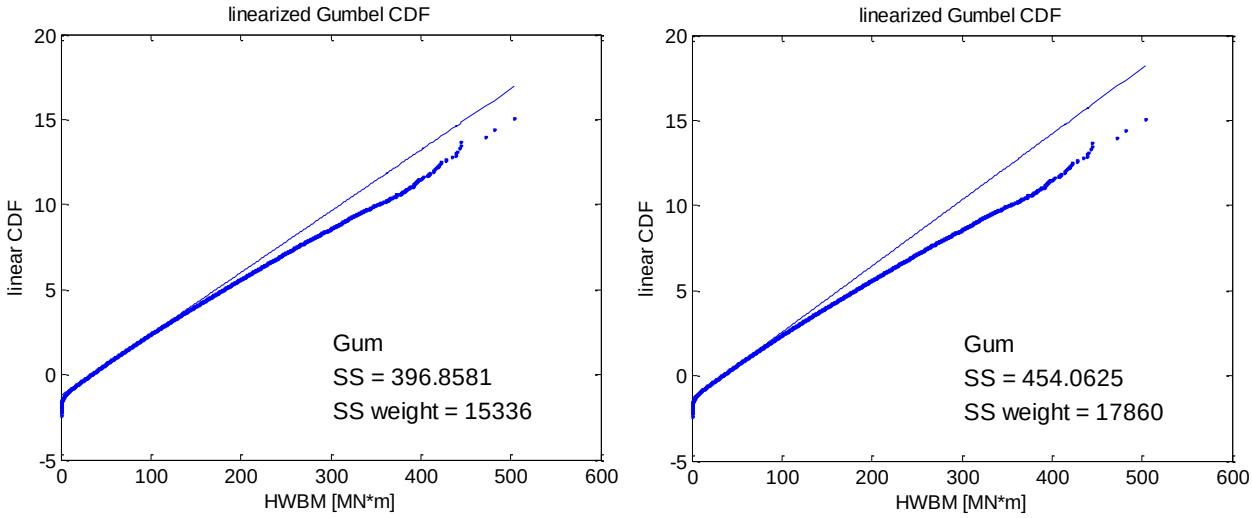

Figure 24 – Linearized Gumbel CDFs for the HWBM: with method of moments estimator (left) and MLE estimators (right)

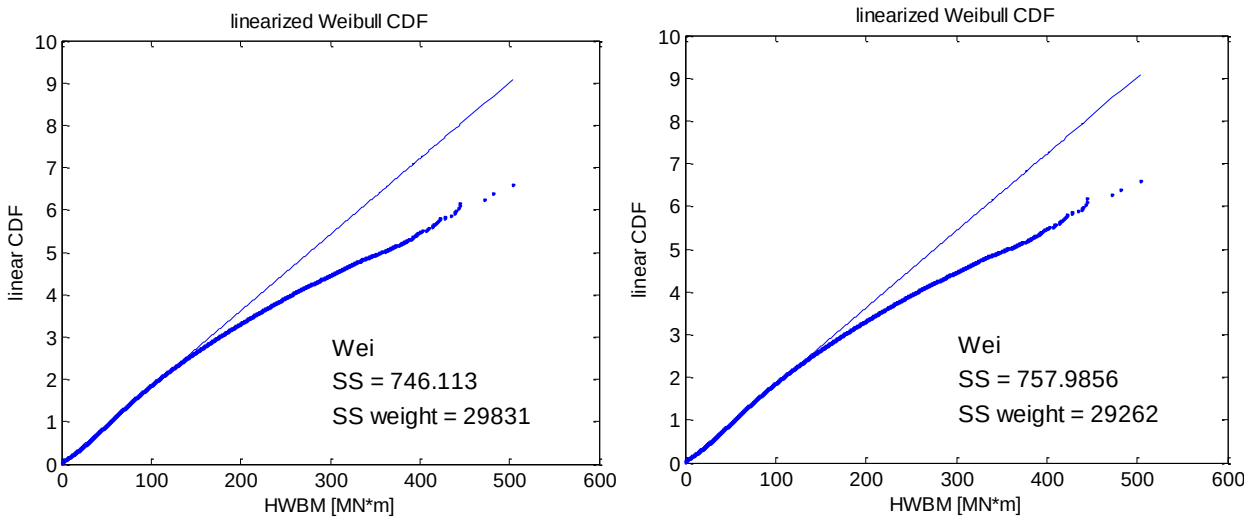

Figure 25 – Linearized Weibull CDFs for the HWBM: with method of moments estimator (left) and MLE estimators (right)

The weighed sum of squares test (tab. 9) is giving one more time analogous results: the gamma (with method of moments estimators), the Gumbel (with method of moments estimator) and the Weibull (with maximum likelihood estimators) distributions are the distributions which seems the closest to the empirical distribution, especially in the tale of the distribution. Hence, let us plot these three distributions together in a q-q plot (fig. 26) to compare them.

Table 9 – Weighed least squares method for the HWBM

	Method of moments	MLE
	SS	*SS*
Exponential distribution	$812*10^3$	$812*10^3$
Lognormal distribution	$137*10^3$	$520*10^3$
Gamma distribution	$15*10^3$	$104*10^3$
Normal distribution	$482*10^3$	$482*10^3$
Gumbel distribution	$15*10^3$	$18*10^3$
Weibull distribution	$30*10^3$	$29*10^3$

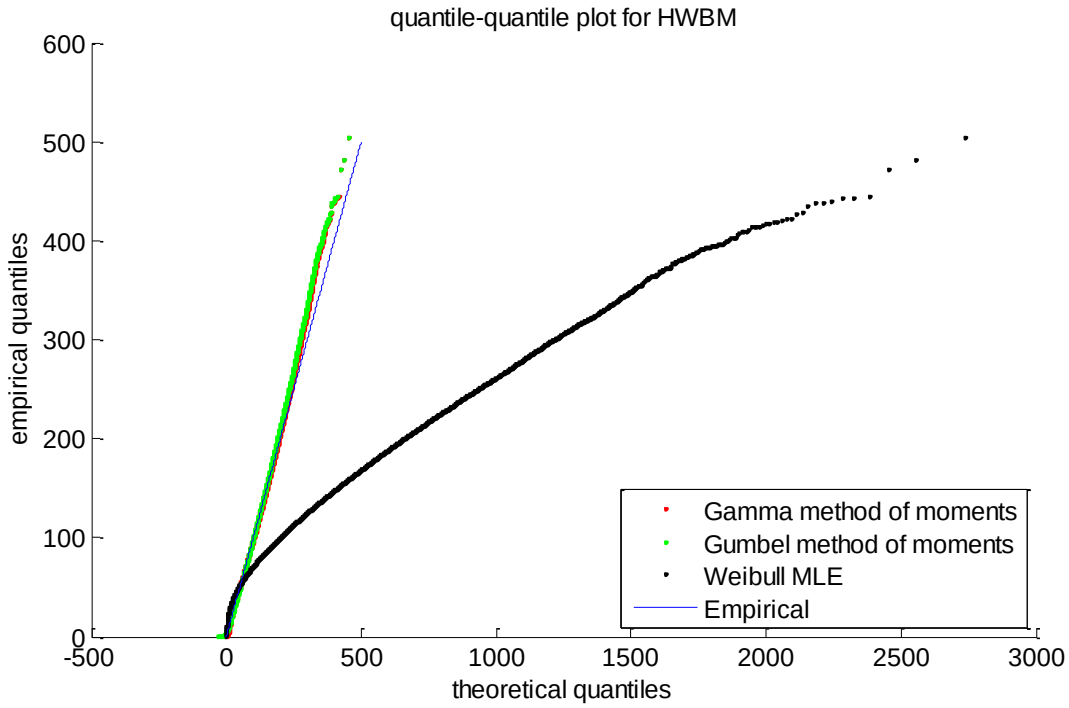

Figure 26 – q-q plot for the HWBM

Finally, the gamma distribution with method of moments estimator was chosen, as it is clearly the one which is closer to the empirical distribution in the tale of the distribution, as we can see in fig. 26.

$k = 2.0$

$\theta = 25.1$

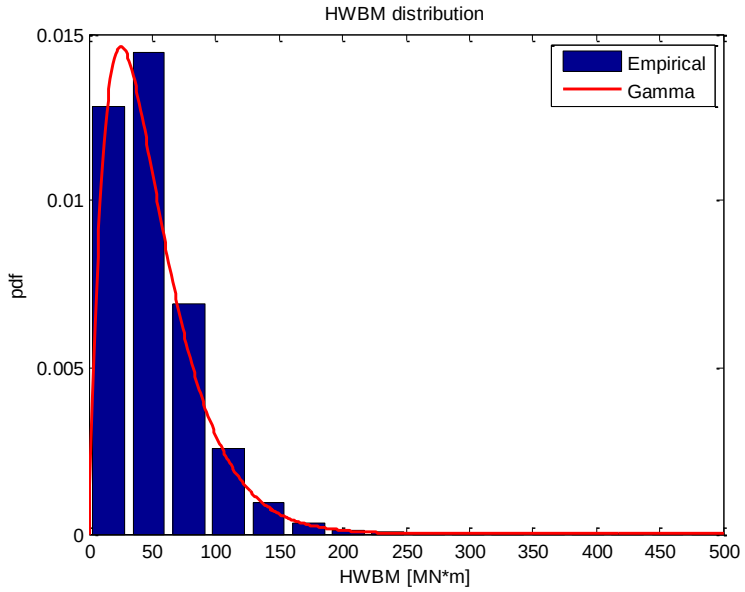

Figure 26 – Probability density function for the HWBM

5.6 Correlation between loads

In this last paragraph the correlation between the loads random variable is analyzed. In particular, the following types of correlation need to be studied:

- correlation between SWBM and VBWM;
- correlation between VWBM and HWBM.

SWBM is due to the hydrostatic pressure and gravity loads. VWBM is a wave induced bending moment. Thus they are due to two completely different applied loads. However, they both are related to some common parameters, like the mass distribution and the draft. Still, the combination between these two load effects seems to be negligible ([6]).

The VWBM and HWBM are both wave induced ending moments, thus we would expect for them a strict positive correlation. In fig. 27 the VWBM and HWBM values occurring at the same instant have been plotted. Four different period of the year have been considered. Apparently there is no correlation between the two.

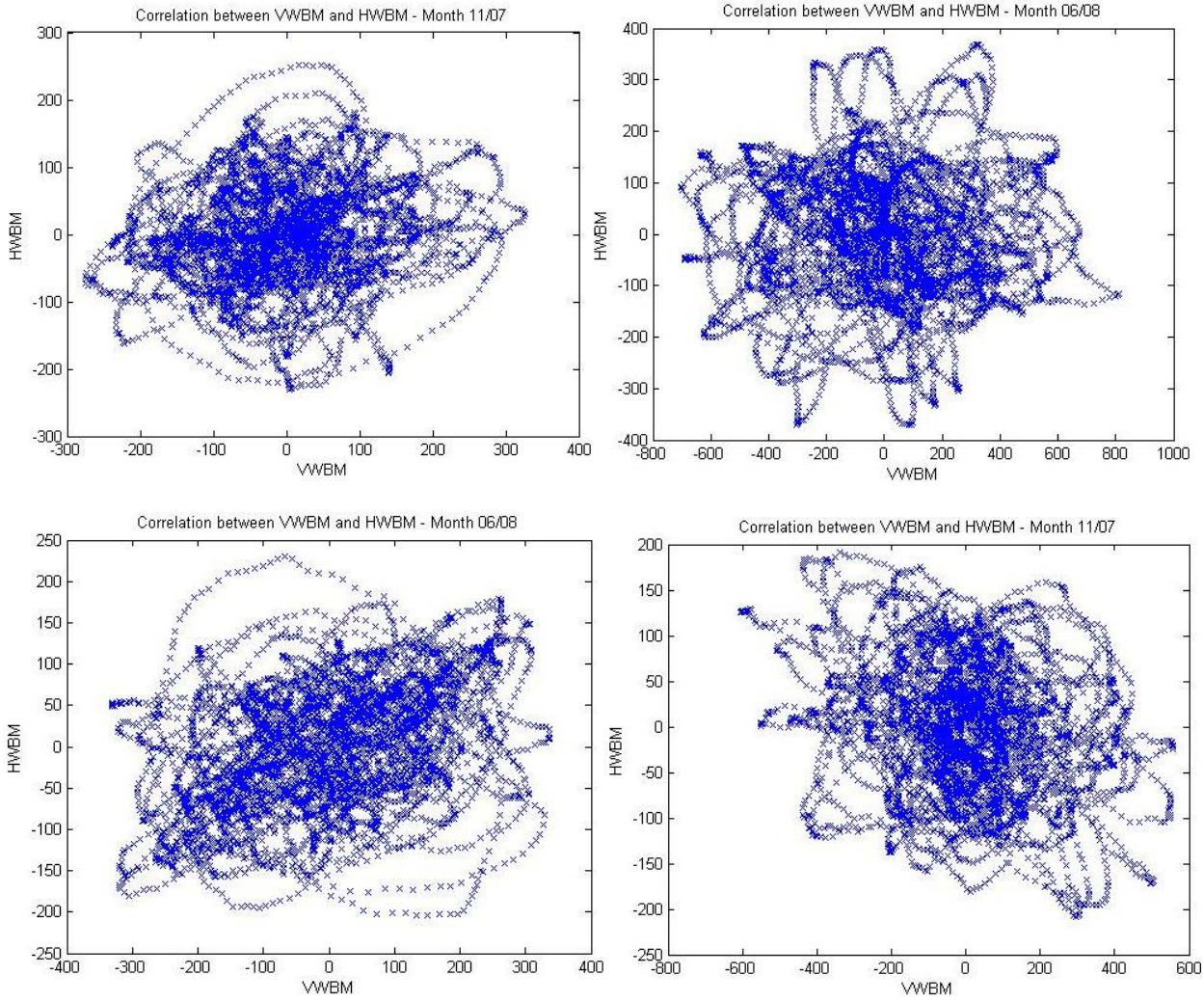

Figure 27 – Correlation between HWBM and VWBM

Furthermore, the correlation coefficient has been calculated for two months (June '08 and November '07). In both cases we have an almost zero correlation coefficient:

$\rho_{June} = -0.005$

$\rho_{November} = 0.01$

One of the reason for this is that there is a phase shift between the VWBM and HWBM, thus it is unlikely that their peaks occur simultaneously in time.

Moreover, it was decided to analyze also the extreme events correlation, since we are interested in the occurrence of the extreme events. To do that, it was decided to proceed as follows:

1) the absolute values (around 25 millions measurements) of the VWBM have been sorted from the lowest to the highest;
2) the HWBM values have also been sorted in such a way that $VWBM(i)$ and $HWBM(i)$ are the values which have been recorded at the same instant in time;
3) the correlation coefficient have been calculated; then, the first million of measurements is deleted, and the correlation coefficient calculated again. This procedure is repeated until all the measurements have been deleted.

The results are plotted in fig. 28. On the horizontal axis the "cut-off VWBM" has been plotted. This is because deleting the lowest million of measurements means to delete all the values of the VWBM (and the corresponding HWBM values occurring at the same instant in time) below a certain value.

What we observe in fig 28 is the following:

1) at first, the more extreme events we have, the more the correlation coefficient becomes negative. This is because the FPSO tends to align in the main wave direction. Thus we have a VWBM which is wave-induced, and an HWBM which is swell-induced.
2) when we have very extreme events, the correlation coefficient becomes "less negative". A possible reason for that may be the fact that here the sea is very rough, thus we may have high waves coming from more than one direction. Thus both load effects, VWBM and HWBM, are here wave-induced.

However we should underline that:

- in all cases the correlation coefficient is very small;
- in all cases the correlation coefficient is negative: a negative correlation coefficient between loads is actually a positive things.

Thus we decided to disregard the correlation between HWBM and VWBM, because it is very small and because in so doing we are acting on the conservative side.

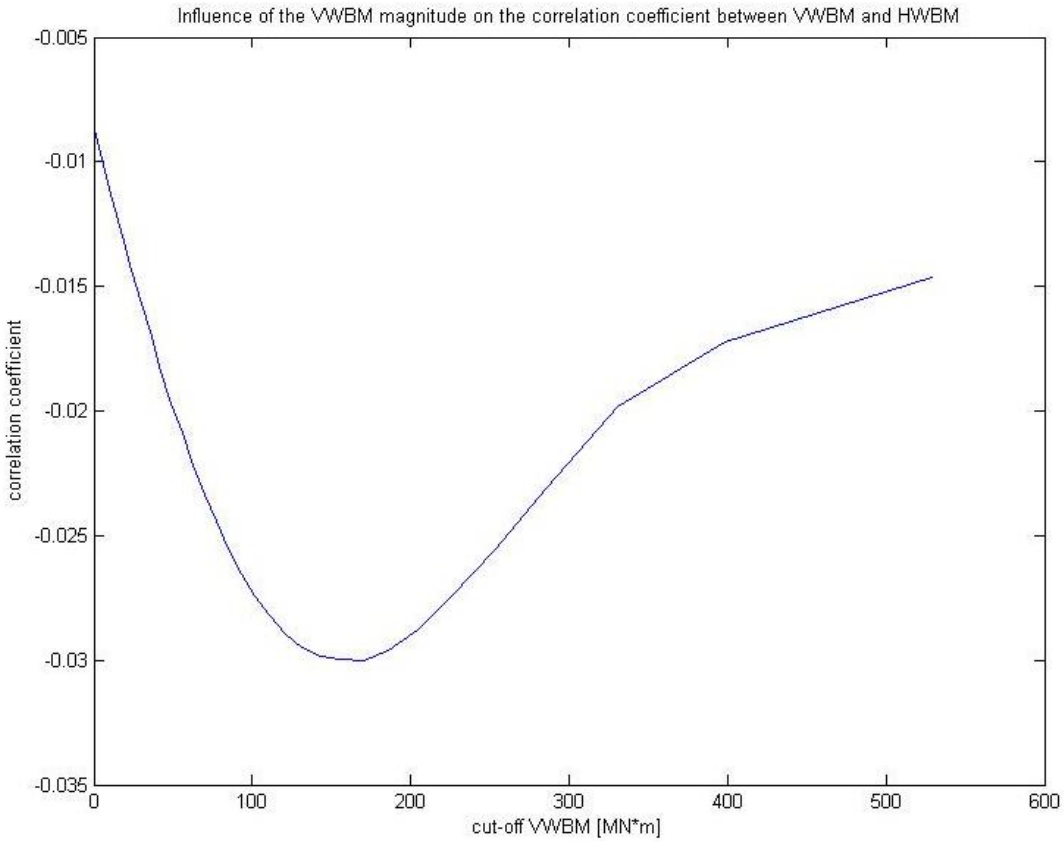

Figure 28 – Correlation coefficient between VWBM and HWBM as a function of the extreme events

5.7 Summary of the results

In conclusion, the following random variables will be used as input data for the case study.

Table 10 – Results of the loads processing

Variable	Distribution type
SWBM	$Nor(\mu = 461\ MN*m, \sigma = 959\ MN*m)$
VWBM hogging	$Gam(k = 1.43, \theta = 145.5)$
VWBM sagging (absolute value)	$Gam(k = 1.43, \theta = 145.5)$
HWBM	$Gam(k = 2.0, \theta = 25.1)$

The VWBM and HWBM distributions have been obtained processing one year of monitored data. The SWBM has been obtained considering 868 daily measurements. No correlation between loads variable will be modeled.

References

[1] S. Mahdi, M. Cenac, "Estimating parameters of Gumbel distribution using the method of moments, probability weighted moments and maximum likelihood", Revista de Matematica: teorria y aplicaciones, 2005

[2] www.statlect.com/normal_distribution_maximum_likelihood.htm

[3] T. P. Minka, “Estimating a Gamma distributuion”, 2002

[4] www.itl.nist.gov/div898/handbook/eda/section3/eda3669.htm

[5] M. A. Al-Fawzan, “Methods for Estimating the Parameters of the Weibull Distribution”, 2000

[6] X. Wang, T. Moan, “Stochastic and deterministic combinations of still water and wave bending moments in ship”, Marine structures, The Norwegian Institute of Technology, 1995

6

Reliability analysis

In chapter 2 it has been shown how to get a continuous probability distribution function from a set of thickness measurements. In a similar way, in chapter 5 some FPSO monitored parameters have been processed in order to get the statistical properties of some loads (SWBM, VWBM and HWBM) acting on the FPSO. In chapter 4 different failure modes have been identified and "converted" into closed-form equations.

In this chapter, all pieces are collected together. A case study is introduced, and all the findings of chapters 2, 4 and 5 are applied in order to run a full-probabilistic structural analysis.

6.1 The vessels

For this case study, two different FPSOs have been used.

The first one is a unit of which we know the thickness measurements for one tank. The unit was built almost 30 years before the inspection as a tanker, and it has been converted to a FPSO after 21 years of sailing.

The second FPSO is a unit which has been monitored for 3 years in the Sable field, off the coasts of South Africa. This is a relatively harsh environment, and thus interesting for extreme loads.

In order to avoid confusion, in this chapter we will call the first FPSO "inspected FPSO" and the second unit "monitored FPSO". Therefore we will reassess an "imaginary FPSO" with monitored data from the monitored FPSO and corroded thickness from the inspected FPSO. The geometry and initial thicknesses have been taken from the monitored FPSO, and are listed in table 1.

Table 1 – Geometrical and construcional parameters of the monitored FPSO

Parameter	Value
Length	230 m
Breadth moulded	42 m
Displacement	120 000 tons
Block coefficient	0.82
Stiffener spacing	840 mm
Web spacing	4800 mm
Deck plate thickness	17 mm
Stiffener web height	312 mm
Stiffener web thickness	10 mm
Stiffener flange width	125 mm
Stiffener flange thickness	16 mm

The thickness measurements processed in chapter 2 have been taken from the inspected FPSO, while the loads analyzed in chapter 5 comes from the monitored FPSO.

All the input data for the MCS, coming from the previous chaptes, are summarized in table 2.

Table 2 – Results of the thicknesses and loads processing

Variable	Distribution type
Corroded thickness of the deck plate	$Truncated\ Exp(\lambda = 1.647)$
Corroded thickness of the deck longitudinal's web	$Truncated\ Exp(\lambda = 7.848)$
Corroded thickness of the deck longitudinal's flange	$Truncated\ Exp(\lambda = 7.848)$
SWBM	$Nor(\mu = 461\ MN*m, \sigma = 959\ MN*m)$
VWBM hogging	$Gam(k = 1.43, \theta = 145.5)$
VWBM sagging (absolute value)	$Gam(k = 1.43, \theta = 145.5)$
HWBM	$Gam(k = 2.0, \theta = 25.1)$

However, the monitored FPSO has some L-section deck longitudinals, while the inspected FPSO has flat bars attached to the deck. So the results in table 2 for the flange have been obtained assuming that the measurements samples for the web is still valid for the flange. This is usually not true, as we have seen in table 1 from chapter 2. We cannot say if this is an optimistic or conservative hypothesis. On one hand table 1 from chapter 2 is showing that most of the time the flange corroded thickness is higher than the web corroded thickness (which may led us to think it is an optimistic assumption). On the other hand, the orientation of stiffeners for the bulkheads and side shell is different: residual oil, dust or dirty water may tend to accumulate on the web of the bulkheads/side shell stiffeners and on the flange of deck/bottom stiffeners. This will influence the corrosion rate, and thus we cannot easily apply the findings for the side shell/bulkheads stiffeners to deck longitudinals.

6.2 Monte-Carlo simulation

Due to the complexity of many failure functions (some of which are not even differentiable), the Monte Carlo simulation is the most suitable method to perform a reliability analysis, thanks to its simplicity. The numerical software used to run the MCS is MATLAB.

The principle behind MCS is the following: several sets of input variables $\boldsymbol{X}_i$ are generated, taking into account the type of probability distribution and the statistical properties of each input variable. Then the values of the LSF $g(\boldsymbol{x_i})$ are calculated. The probability of failure is then:

$$P_f = \frac{n_F}{n_S} \tag{6.1}$$

where:

- n_F is the number of failures, that is the number of $g(\boldsymbol{x_i})$ which fall in the failure area $(g(\boldsymbol{x}) < 0)$;
- n_S is the total number of samples.

However, since the wave loads have been monitored over a period of just one year, with this procedure we are able to get only the 1 year probability of failure. For the probability of failure in N years ([2]):

$$P_{f_N} = 1 - \left(1 - P_f\right)^N \tag{6.2}$$

The (6.2) is assuming that the probability of failure is the same every year, that is:

- the SWBM distribution is the same for every year: this hypothesis may be acceptable, even if there are some cases where the operator may decide to significantly increase/decrease the production;
- the VWBM and HWBM is the same for every year, which is also a reasonable assumption;
- the corroded thickness is the same every year, which is clearly not true. This last simplification can only be adjusted if a corrosion prediction model is available.

If a corrosion prediction model is available (see paragraph 6.5), then the (6.2) turns to the (6.3).

$$P_{f_N} = 1 - \prod_{i=1}^{N}\left[1 - P_{f,i}\left(t_{corr,i}\right)\right] \tag{6.3}$$

where N is the number of years and $P_{f,i}$ is the yearly probability of failure, which is function of the corroded thickness $t_{corr,i}$ measured (or predicted) at the i-th year.

According to DNV ([1]), the required number of simulations should be of an order of magnitude $100/P_f$ in order to estimate the failure probability P_f with good confidence. This means that for a $P_f = 10^{-6}$ at least 10^8 samples are needed (and thus very long computational time).

6.2.1 Generation of random variable for the Monte-Carlo simulation

The MATLAB version used in this work is not endowed with the Statistics Toolbox. This means that it is not possible to automatically generate, for example, a normal or lognormal distributed variable. It is only possible to generate uniform distributed uncorrelated random variables, and then it is required to transform them to the desired ones.

If the desired variable has a cumulative distribution function $F_X(x)$, and if V are the uniform generated random variables, then we can have the desired sample of X applying the transformation (6.4) ([2]).

$$X = F_X^{-1}(V) \tag{6.4}$$

On the other hand, if variables are correlated, then we need at first to transform them to uncorrelated standard normal variables, using (6.5) ([2]):

$$U = \Phi^{-1}(V) \tag{6.5}$$

Then, for the transformation of U into correlated random variables X, the so-called Gaussian copula model is used. Tre transformation to apply is the (6.6) ([2]):

$$X = F_X^{-1}[\Phi(L_U, U)\ ] \tag{6.6}$$

Where L_U is the results of the lower Cholesky decomposition of the correlation matrix R_{UU}:

$$L_U = chol(R_{UU}) \tag{6.7}$$

Note that the correlation coefficients between random variables U are different (although not very different, [2]) from the correlation coefficient between random variables X. Therefore it is also required to transform the (known) matrix R_{XX} to R_{UU}. Reference [3] explains how to do that.

Annex C is giving in detail all the equations adopted for the generation of the random variable used in the Monte Carlo simulation, and thus the application of (6.4), (6.5) and (6.6) to the specific case study.

Figure 1 is summarizing all the steps to get the desired sample of random variables starting from a sample of uniform uncorrelated variables.

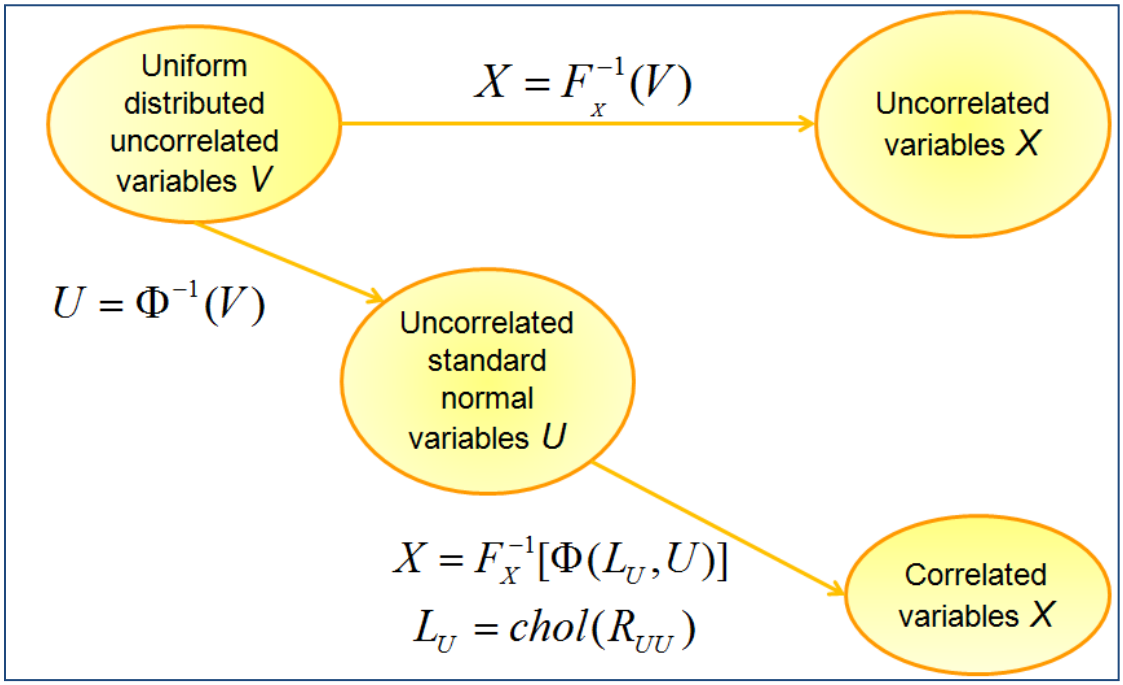

Figure 1 – Generation of random variables

6.3 Correlation between random variables

In general, we can distinguish the following kinds of correlation:

- between yielding stress of stiffeners and yielding stress of plates;
- between the corroded thicknesses of the plate and the stiffeners;
- between the HWBM and the VWBM;
- between the SWBM and the VWBM.

Often, the steel used for stiffeners and the one used for plates come from two different steel mills. Thus it was decided not to include this type of correlation in the analysis.

On the other hand, it is reasonable to expect an high positive correlation between the corroded thicknesses of the plate, the stiffener web and the stiffener flange. For example, if the environment is aggressive, then it is aggressive for all these three structural elements. Therefore, it has conservatively assumed a full correlation ($\rho_{ij} = 1$) between each pairs of these three random variables.

Finally, it was decided not to include the correlation between loads (SWBM-VWBM and VWBM-HWBM), for the motivations already given in paragraph 5.6.

6.4 Load cases

In the case study a reassessment of a FPSO deck structure under global-hull girder induced loads is made. Conservatively, the boundary conditions assumed throughout the whole analysis are simply supports.

3 different load combination methods have been used (peak coincidence method, SRSS method and Turkstra rule), and two different loading case (hogging and sagging), for a total number of 6 load cases.

Since we have no lateral pressure, the stress distribution over the cross section of the (stiffened or unstiffened) plate is constant (in the prebuckling phase). This means that the first yielding and gross yielding limit states are indeed the same failure mode. Thus the failure mode due to gross yielding (or "plastic hinges formations") will not be considered.

We expect to have a minimum probability of failure in the order of 10^{-6}. This means that, according to DNV, 10^{8} iterations are needed. The computational time for such an high number of iterations may be very long (approximately 10 hours). This is a significant problem, especially for the sensitivity analysis. Therefore, only for the sensitivity analysis, it was chosen to increase the loads, so to have higher probability of failures, and hence a lower number of necessary iterations. In particular, the wave loads (VWBM and HWBM) have been increased by a factor of 3 (both the mean value and the standard deviation), so to use "only" 10^{7} iterations.

Then, the MCS has also been run once with the real input loads of table 2.

6.5 Corrosion prediction model

In literature, there exist several corrosion prediction models for ships, even though their validity is limited. They can be essentially categorized in two groups: some of them are fully empirical, which means they are constructed trying to fit a certain set of empirical measurements, while others use selected first principles and then apply them to the data ([6]).

The problem of the first group is that – due to the high number of variables affecting the corrosion rate – their validity is limited to a very specific situation (e.g. a specific ocean area, a specific vessel, a specific location of the vessel, and so on). The problem of the second group is that they need to be calibrated for the specific situation, as they all have some parameters which must be tuned when some empirical data are collected.

The second approach is to be preferred, however – for our case study – we do not have enough empirical data relative to inspections to the same structure in different periods in time. This is the reason why, as it has already been said in chapter 1, no corrosion prediction model is included in this work.

However, it has been found in the literature a paper ([5]) where a theoretical corrosion prediction model has been adjusted to a specific FPSO situation. Just to show the methodology, this model

has been assumed to be valid also for our case study, and a time-dependent reliability analysis has been run (results are listed in chapter 7).

The corrosion prediction model is the non-linear one proposed in 1999 by Soares and Garbatov ([4], fig. 2):

$$t_{corr}(t) = \begin{cases} 0 & t \le \tau_c \\ d_\infty \left[1 - \exp\left(-\frac{t-\tau_c}{\tau_t}\right)\right] & t \le \tau_c \end{cases} \quad (6.8)$$

- t:time [years]
- t_{corr}: corroded thickness
- τ_c: lifetime of the coating
- d_∞: thickness loss for long term corrosion
- $\tau_t = \frac{d_\infty}{tg\alpha}$: transition time
- α: angle defined by OA and OB in fig. 2

In fig. 2 we can distinguish three stages. In the first stage (whose duration is τ_c) the metallic surface protection works effectively and there is no corrosion. The second stage begins when the protection or coating is damaged and corrosion starts reducing the plating thickness. The third stage corresponds to a stop of corrosion process when the corrosion rate tends to zero. The oxidized material produced does not allow contact between surface plating and corrosive environment anymore.

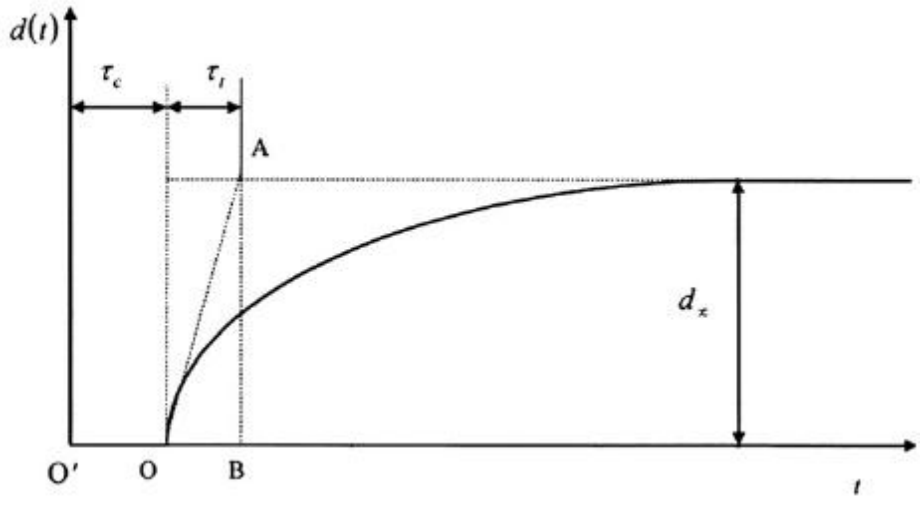

Figure 2 – Non-linear corrosion prediction model ([4])

Fig. 3 presents the thickness of a bottom plate in a cargo tank of a real FPSO ([5]). These data have been obtained through combining the Soares and Garbatov non-linear model with the empirical Bayesian inference.

$d_\infty = 2.5\ mm$

$\tau_c = 7\ years$

$\tau_t = \frac{2.5}{tg(55^\circ)} = 1.75\ years$

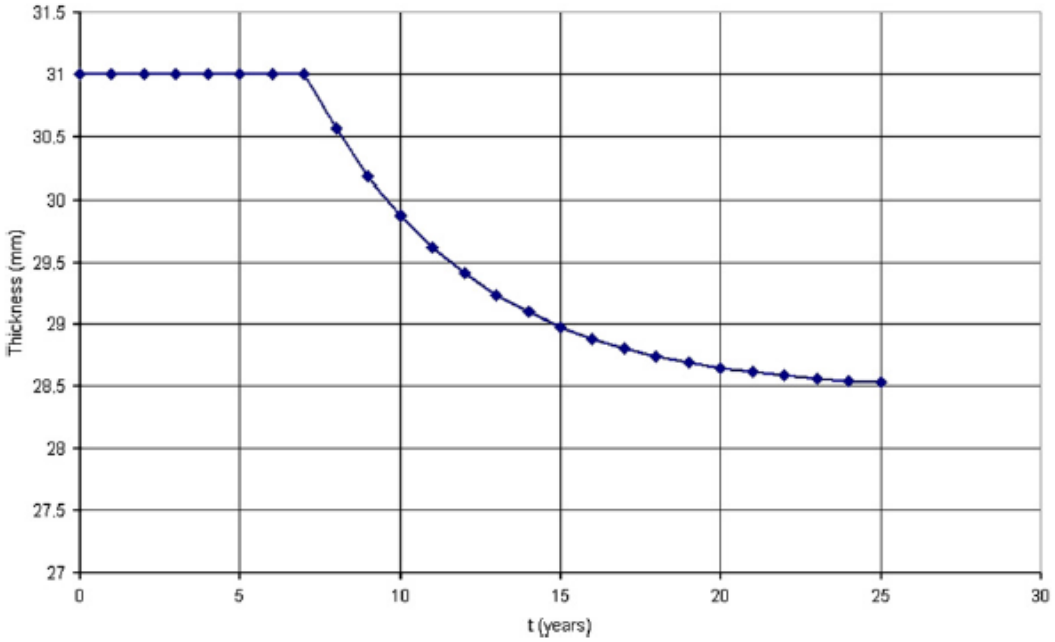

Figure 3 – Results of the corrosion model ([5])

The data refers to only one side of the plate. $d_\infty = 2.5\ mm$ is then quite a large corroded thickness (if we assume that on the other side of the plate the surface is experiencing the same corrosion, then we would have $5\ mm$ loss of thicknessin 25 years!). However, it must be underlined that the bottom panel analyzed in [5] has been intentionally selected as the one which has experienced the greatest corrosion.

In the time-dependent reliability analysis, the corrosion prediction model from figure 25 will be assumed valid also for the deck plate of the monitored FPSO. For the stiffeners, it will be scaled down by a certain factor, so to keep the ratios between the corrosion of the stiffener web/flange and the corrosion of the plating the same as they were found for the inspected FPSO in chapter 2.

In chapter 5, loads measurements from a whole year have been processed in order to derive the statistical properties of the wave loads. In the time-dependent reliability analysis, we are assuming that these statistical properties are the same every year. If the reassessment tool is going to be implemented on a real FPSO, this assumption cannot be considered valid: a longer

monitoring period is needed, so that the statistical properties of the wave loads would stabilize themselves.

References

[1] “Structural reliability analysis of marine structures”, DNV classification notes (No. 30.6), 1992

[2] D. Straub, “Lecture notes in structural reliability”, TU Munchen, 2012

[3] O. Ditlevsen, H. O. Madsen, “Structural reliability methods”, Technical university of Denmark, 2007

[4] C. G. Soares, Y. Garbatov, “Reliability of maintained, corrosion protected plates subjected to non linear corrosion and compressive loads”, Marine structures 12, 1999

[5] Bruno Vasconcelos de Farias, Theodor Antoun Netto, “FPSO hull structural integrity evaluation via Bayesian updating of inspection data”, Ocean engineering, 2012

[6] R. E. Melchers, “Probabilistic models of corrosion for reliability assessment and maintenance planning”, OMAE 2001

7

Results and sensitivity analysis

This chapter presents the results of the Monte Carlo simulations.

It is split in two parts: at first the influence of many parameters on the probability of failure is studied (paragraph 7.1). As anticipated in chapter 6, for the trend analysis the wave loads, both mean value and standard deviation, have been increased by a factor of 3, in order to have higher probabilities of failure (and so lower iterations, hence lower computational time).

Then, the MCS has been run also once using the real loads (paragraph 7.2) and a comparison of these results with some target reliability indices is made.

All the probabilities of failure are yearly probability of failures. In the sensitivity analysis it was chosen – with only one excpetion – to plot the probabilities of failure rather than the reliability indices β as – from an engineering point of view – they are easier to comprehend. On the other hand, the reliability index is preferred when a comparison with some target reliabilities is made, since rules generally recommend a target reliability index rather than a target probability of failure.

In order to make this chapter more readable, in the sensitivity analysis only the graphs are plotted, and all the tables with the numerical values have been moved to annex D, unless they are really necessary to understand the results. All graphs – unless otherwise specified – have the logarithmic scale on the vertical axis.

7.1 Sensitivity analysis

7.1.1 Analytical method vs. Jonshon-Ostenfeld formula

In chapter 4 two different models have been described for the ultimate limit strength calculation of both stiffened and unstiffened plates: an analytical method (large deflection analysis combined with the membrane stress-based method) and the Jonshon-Ostenfeld formula method. The latter is an empirical method which works good although sometimes it may be too conservative. The first one is a more “sophisticated” method which tries to solve the compatibility and equilibrium equations for (stiffened or unstiffened) plates.

The problem of the large deflection analysis is that many simplifications have been made in order to make the problem easier. In particular, all the initial imperfections (residual stress and initial deformations) have been disregarded. This may led to too optimistic results.

In order to compare these two methods, the probability of failure of an unstiffened plate under longitudinal compressive load has been calculated as a function of the initial plate thickness t_P. Results are plotted in figure 1, together with the probability of failure using the elastic buckling strength.

In this paragraph the peak coincidence method has been used to combine wave loads, and the correlation coefficients between the corroded thicknesses of the plate, the stiffener web and the stiffener flange have all been set equal to 1. The number of samples in the MCS is 10^7.

From figure 1 we notice that the elastic buckling strength and the Johnson-Ostenfeld formula are giving the same results for thin plate (as expected), but they are diverging for stockier plate. For thick plate the elastic buckling strength is giving totally unreliable results.

We also notice that the large deflection analysis curve looks like the Jonshon-Ostenfeld formula curve "shifted down" by a certain factor. This is in agreement with what was expected. However, it is possible to note that actually the influence of the initial imperfections on the ultimate strength is quite big, as the two curves are indeed very distant between each other. This means that, whenever is possible, the Johnson Ostenfeld formula need to be used for the ultimate strength computation, as the non-inclusion of the initial imperfections in the analytical method is an extremely optimistic assumptions.

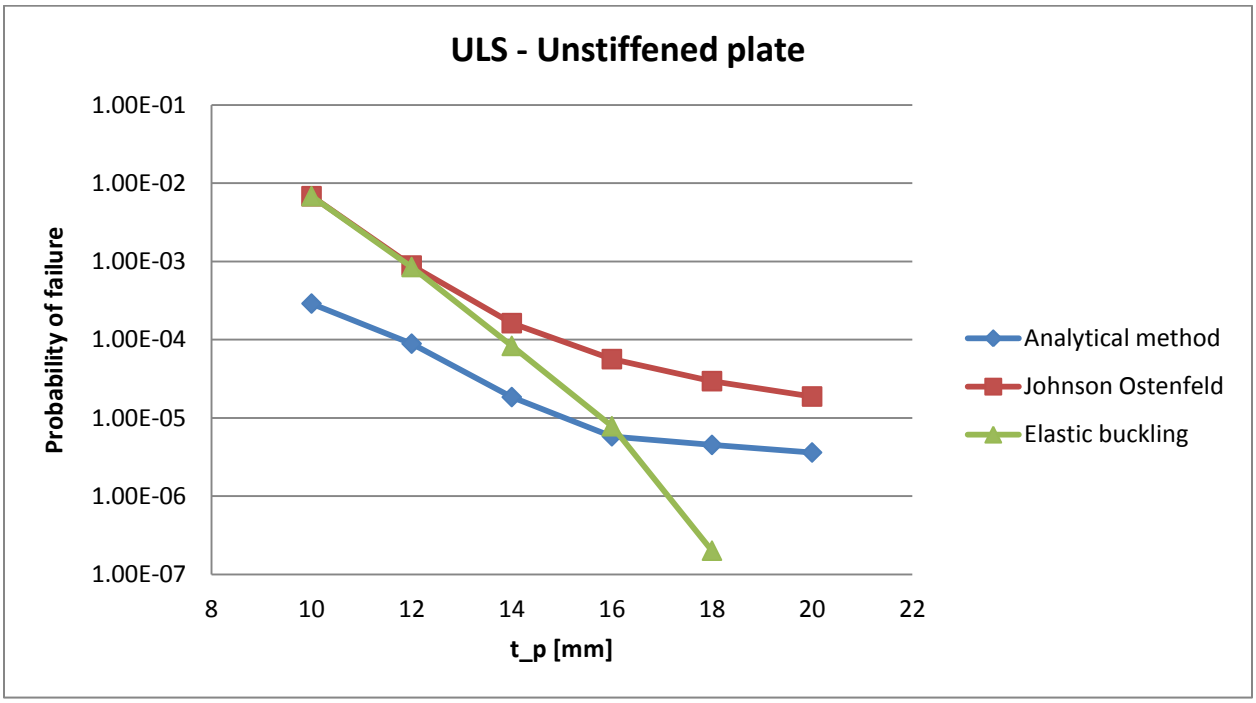

Figure 1 – Ultimate probability of failure of an unstiffened plate as a function of the initial gross plate thickness

The conclusions drawn here for an unstiffened plate can also be extended to the five failure modes of a stiffened panel. For istance, the ultimate strength of a stiffened panel due to failure mode I is calculated in the same way as that one of an unstiffened plate, with the only difference that the isotropic plate model is replaced by an orthotropic plate model. Analogously the ultimate strength due to failure mode IV is a combination of the ultimate strength of the unstiffened plate between longitudinals and the ultimate strength of the stiffener web. Similar considerations can also be made for the other failure modes.

7.1.2 Effects of the initial corroded thickness on the structural reliability

In this sensitivity analysis, the mean values of the corroded thicknesses have been all multiplied times a factor f:

$$\mu_{t_{corr,plate}} = f * \ 0.607\ mm$$

$$\mu_{t_{corr,web}} = f * \ 0.127\ mm$$

$$\mu_{t_{corr,flange}} = f * \ 0.127\ mm$$

Then, the probabilities of failure have been calculated as a function of this factor f in order to see the effects of the initial corroded thickness on the reliability. Only the failure modes which are actually function of the thickness are considered here (i.e. the ULS of stiffened panel and unstiffened plate; no yielding and no fracture).

In this paragraph the results using the Turkstra's rule to combine loads are shown. In annex D the results are also given for the other load combination methods. The correlation coefficients between the corroded thicknesses of plate, stiffener web and stiffener flange have all been set equal to 1. The number of samples in the MCS is 10^7.

Results are plotted in figures 2 and 3, for stiffened panel and unstiffened plate, respectively.

Figures 2 is giving the probability of failure for both the analytical method and the Johnson Ostenfeld formula. It is interesting to see that the probabilityof failure is actually constant for low value of f, before starting growing. This is because for low value of the corroded thickness the corrosion allowance is being consumed. The corrosion allowance is added during the design of the unit as a margin with respect to corrosion, thus it is not intended to increase the ultimate strength of the panel.

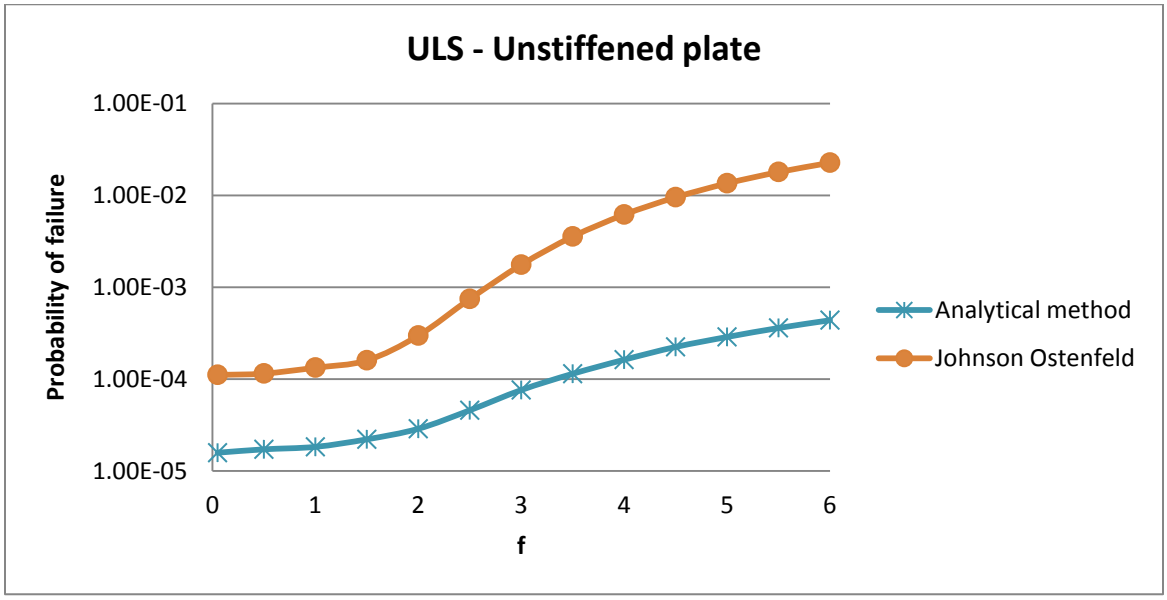

Figure 2 - Ultimate probability of failure of an unstiffened plate as a function of the initial corroded thickness

Figure 3 is giving the results for the stiffened panel. All failure modes for a stiffened panel are plotted together. The models adopted to calculate the ultimate strengths of each failure mode are:

- Mode I, overall collapse: analytical method
- Mode II, yielding along the plate-stiffener intersection: analytical method
- Mode III, beam-column type collapse: Johnson-Ostenfeld formula
- Mode IV, local buckling of the stiffener web: Johnson-Ostenfeld formula
- Mode V, flexural-torsional buckling of the stiffeners: Johnson-Ostenfeld formula

For mode I and mode II it was not possible to use a Johnson-Ostenfeld formula (or an equivalent empirical formula) as it does not exist. It may be not very consistent to plot together failure probabilities calculated with different models. However, it must be pointed that:

- Failure mode 1 is the typical collapse pattern when the stiffeners are relatively weak compared to the plate; in this case, they buckle together with plating, and the overall buckling remains elastic ([1]). This is not expected to be our case, as (see table 1) the stiffeners are not that weak compared to the plating (e.g. stiffener's flange is 16 mm, deck plate thickness 17 mm). Furthermore, an elastic buckling collapse is something which is also not expected in a FPSO, whose structural elements are in general all quite stocky.
- Failure mode 2 occurs when the panel is predominantly subjected to biaxial compressive loads ([1]), which is also not our case.

Table 1 – Initial dimensions of stiffeners and attached plate

Parameter	Value
Stiffener spacing	840 mm
Deck plate thickness	17 mm
Stiffener web height	312 mm
Stiffener web thickness	10 mm
Stiffener flange width	125 mm
Stiffener flange thickness	16 mm

In fig. 3 we see that failure modes IV is the most critical one. Failure mode IV typically arise when the ratio of stiffener web height to stiffener web thickness is too large. In this case study, the stiffener web dimensions are $312\ mm\ x\ 10\ mm$, and thus we are not surprised by this result.

We also notice that the blue line – the one giving the lowest probabilities of failure – is also the least smooth curve. This is due to the relatively low number of samples (10^7), which – for that particular curve – should have been higher to have even more reliable results.

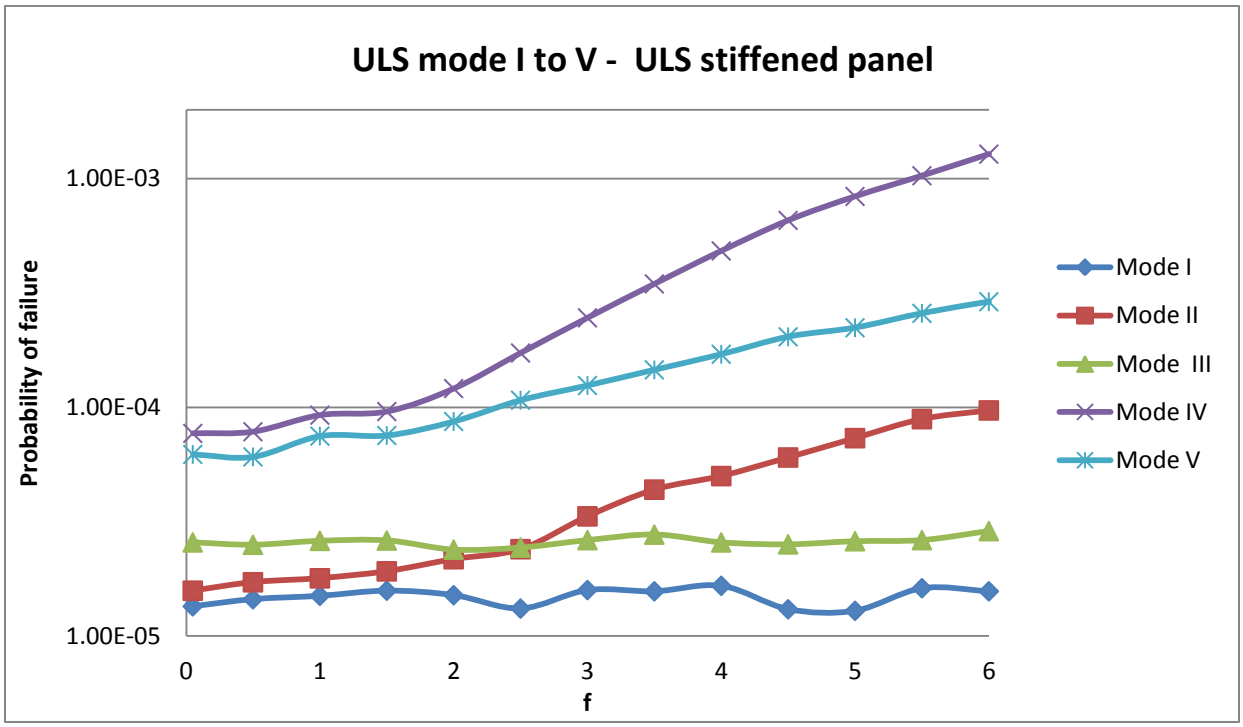

Figure 3 - Ultimate probability of failure of a stiffened panel as a function of the initial corroded thickness

Again, we see a constant trend of the probabilities of failure for small losses of thicknesses (which correspond to the corrosion allowance consumption). However, we note that mode I and mode III are always constant. Failure mode III is the beam-column type collapse; its ultimate strength is proportional to the elastic buckling strength, which is given by (4.145).

$$\sigma_E = \frac{\pi^2 E I_{eff}}{a^2(A_s + bt_P)} \tag{4.145}$$

From (4.145) we see that the elastic buckling strength is proportional to the ratio between the moment of inertia of the cross section (with attached plate) about the neutral axis and the area of the whole cross section.

$$\sigma_E \propto \frac{I_{eff}}{A_s + bt_P} \tag{7.1}$$

If t_{corr} is increasing, then both the numerator and the denominator of (7.1) are going down, but they are going down with a similar speed (see tab. 2). The reason for that is due to the large web height, which makes the moment of inertia less sensitive to the thickness.

Table 2 – Moment of inertia and cross sectional area of the stiffened panel as a function of f

f	I_{eff}	A_s+b*t_p	Ratio
	[mm^4]	*[mm^2]*	*[mm^2]*
0	2.44E+08	1.94E+04	1.26E+04
0.5	2.42E+08	1.91E+04	1.27E+04
1	2.42E+08	1.88E+04	1.28E+04
1.5	2.37E+08	1.86E+04	1.28E+04
2	2.34E+08	1.83E+04	1.28E+04
2.5	2.30E+08	1.80E+04	1.28E+04
3	2.27E+08	1.77E+04	1.28E+04
3.5	2.22E+08	1.74E+04	1.28E+04
4	2.21E+08	1.71E+04	1.29E+04
4.5	2.18E+08	1.69E+04	1.30E+04
5	2.15E+08	1.66E+04	1.30E+04
5.5	2.13E+08	1.63E+04	1.31E+04
6	2.09E+08	1.60E+04	1.31E+04

Failure mode I is the overall buckling of the stiffened panel. Like mode III, the ultimate strength for this failure mode is particularly influenced by the geometry of the cross section (in particular the stiffener web height) rather than by the thicknesses.

As a matter of fact, in figure 4 the probability of failure due to mode I and III is calculated as a function of the web height. These probability of failures are compared with the probability of failure due to mode IV (local buckling of the stiffener web) and V (flexural-torsional buckling of the stiffeners). Mode II (yielding along the plate-stiffener intersection) is not relevant as it is only related to the plating between longitudinals.

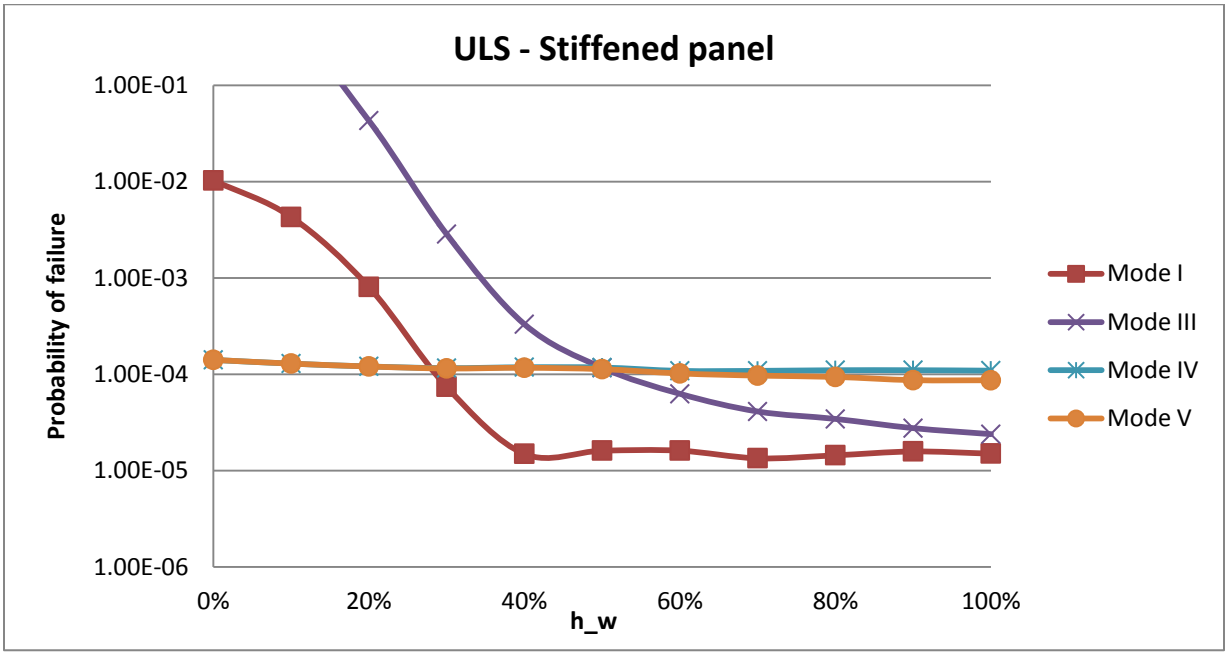

Figure 4 - Ultimate probability of failure of a stiffened panel as a function of the stiffener web height

We clearly see that Mode I and Mode III are much more sensitive to the stiffener web height than mode IV and V. This statement explains why in figure 3 the probabilities of failure due to mode I and mode III were constant.

On the other hand, we may actually be surprised by the fact that mode IV and mode V are very little influenced by the stiffener web height.

The reason for that is to be found in the formulae used for the calculations of the ultimate strengths: the (4.148) for mode IV and (4.163) for mode V.

$$\sigma_{xu}^{IV} = \frac{\sigma_{xu}^{P} b t_P + \sigma_u^W \left(h_w t_w + b_f t_f\right)}{b t_P + h_w t_w + b_f t_f} \tag{4.148}$$

$$\sigma_{xu}^{V} = \frac{\sigma_{xu}^{P} b t_P + \sigma_u^T \left(h_w t_w + b_f t_f\right)}{b t_P + h_w t_w + b_f t_f} \tag{4.163}$$

σ_{xu}^{IV} is calculated as a combination of the ultimate strength of the plating between the stiffeners σ_{xu}^{P} and the ultimate strength of the stiffener because of web buckling σ_u^W. However, we see that the first quantity is multiplied times the cross sectional area of the plating bt_P, while the second times the cross sectional area of the stiffener $h_w t_w + b_f t_f$. Since the cross sectional area of the plating is much larger than that one of the stiffener, the ultimate strength due to mode IV is much close to σ_u^W than σ_{xu}^{P}.

The same consideration is valid also for mode V, where – in this case – we have a combination between σ_{xu}^{P} and he ultimate strength of the stiffener because of lateral-torsional buckling σ_u^T.

7.1.3 *Effects of the load combinations method on the structural reliability*

In this paragraph the effects on the reliability of each of the three load combination methods, used to combine the VWBM and the HWBM, is studied. Table 3 is summarizing the results. It was chosen to use the reliability index rather than the probability of failure, just to make the table more readable.

Table 3 – Effects of the load combination method on the structural reliability

	Peak coincidence	SRSS	Turkstra
	β	β	β
Yielding hogging unst. plate	4.48	4.02	3.76
Yielding hogging stiff. panel	4.54	4.05	3.78
Yielding sagging unst. plate	4.99	4.49	4.14
Yielding sagging stiff. panel	5.07	4.51	4.16
Fracture	3.84	3.47	3.23
ULS unst. plate	4.65	3.97	3.64
ULS stiff. plate mode I	5.20	4.45	4.17
ULS stiff. plate mode II	5.15	4.44	4.13
ULS stiff. plate mode III	5.08	4.36	4.05
ULS stiff. plate mode IV	4.46	4.02	3.71
ULS stiff. plate mode V	4.58	4.10	3.79

Results may seem surprising, since in table 3 the peak coincidence method (i.e. the most conservative one) is giving the highest reliability. The reason for that is due to the modelling uncertainties (table 4) which have been used for each load combination method (see chapter 3).

Table 4 – Modelling uncertainties for load combination methods

Modelling uncertainties	Bias	c.o.v.
Peak coincidence	0.72	0.11
SRSS	1.01	0.12
Turkstra	1.17	0.11

Table 4 shows that the bias for the peak coincidence method is lower than 1, which means that the conservativity of this load combination method has already been considered, and this is the reason why table 3 is giving those apparently weird results.

Furthermore, we should not forget that the modelling uncertainties from table 4 have been derived for the load combination between the VWBM and the slamming-induced vertical bending moment. The assumption that they are still valid for the load combination of the VWBM and the HWBM has not been verified. Looking at the results from table 3, this assumption seems not to be valid, as we would have expected a lower differences between the reliability indices calculated with different load combination methods.

The reliability index has also been calculated once (only for the hogging case) without including the modelling uncertainties. Results are given in table 5.

Table 5 – Effects of the load combination method on the structural reliability

	Peak coincidence	SRSS	Turkstra
	β	β	β
Yielding hogging unst. plate	4.03	4.06	4.03
Yielding hogging stiff. panel	4.05	4.09	4.06
Fracture	3.46	3.49	3.45

Table 5 is showing that – without modelling uncertainties – the influence of the load combination method on the results is very limited. This is actually not surprising, because we are combining two loads (VWBM and HWBM) with very different magnitudes (VWBM is much larger than HWBM; the FPSO is a turret moored FPSO). Therefore we can conclude that actually all the differences in table 3 between the reliability indices calculated with different load combination methods are mainly due by the different modelling uncertainties, rather than by the load combination method itself.

More investigations on this topic are needed. So far we are only able to conclude that a strong influence on the results is given by the way the modelling uncertainties are modelled for each of the three load combination methods considered in this work.

7.1.4 Corrosion of the plate vs. Corrosion of the stiffeners

Paragraph 7.1.2 showed the effects of the initial corroded thickness on the reliability. There, the mean value of the corroded thickness of the plate, the stiffener web and the stiffener flange have all been multiplied times a factor f, which was varied from 0 to 6.

In this paragraph, the factor f has been varied once only for the plating and once only for the stiffener. In this way we are able to see the effects on the reliability of the corrosion of each single structural element.

Figure 5 is giving the results for the corrosion of the plate (the Turkstra's rule to combine loads has been used; the correlation coefficients between the corroded thicknesses of plate, the stiffener web and the stiffener flange have all been set equal to 1; the number of samples generated was 10^7). This figure is very similar to figure 3 (where no difference was made between the corrosion of the plate and the corrosion of the stiffeners).

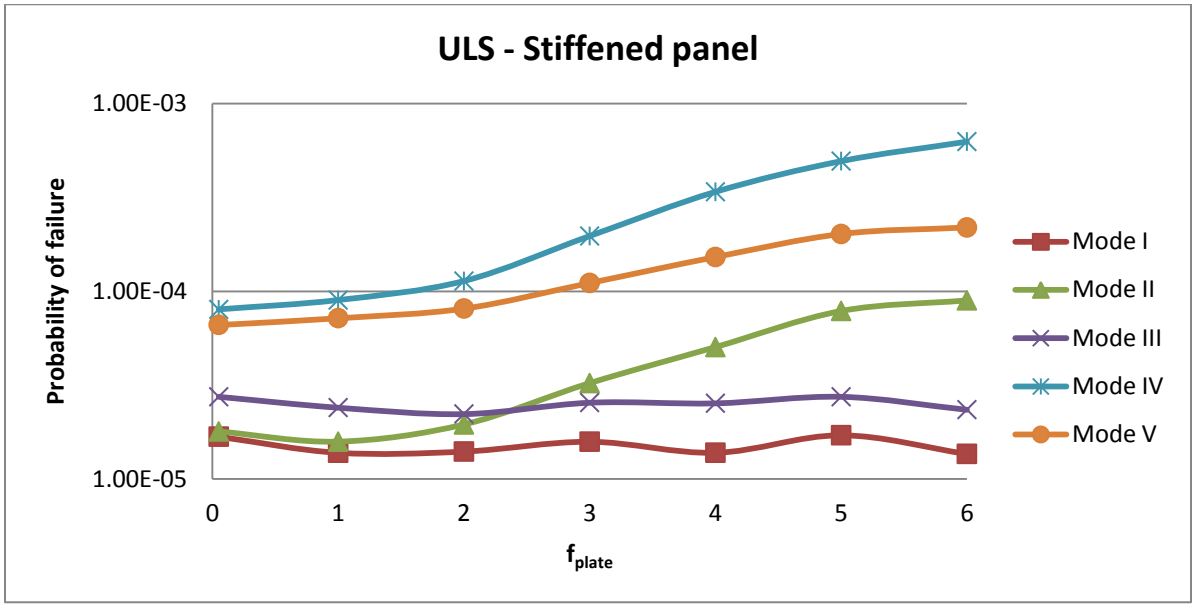

Figure 5 - Ultimate probability of failure of a stiffened panel as a function of the corrosion of the plate

Figure 6 is giving the results for the corrosion of the stiffeners. This time we see that the probabilities of failure of all limit states are almost constant with f.

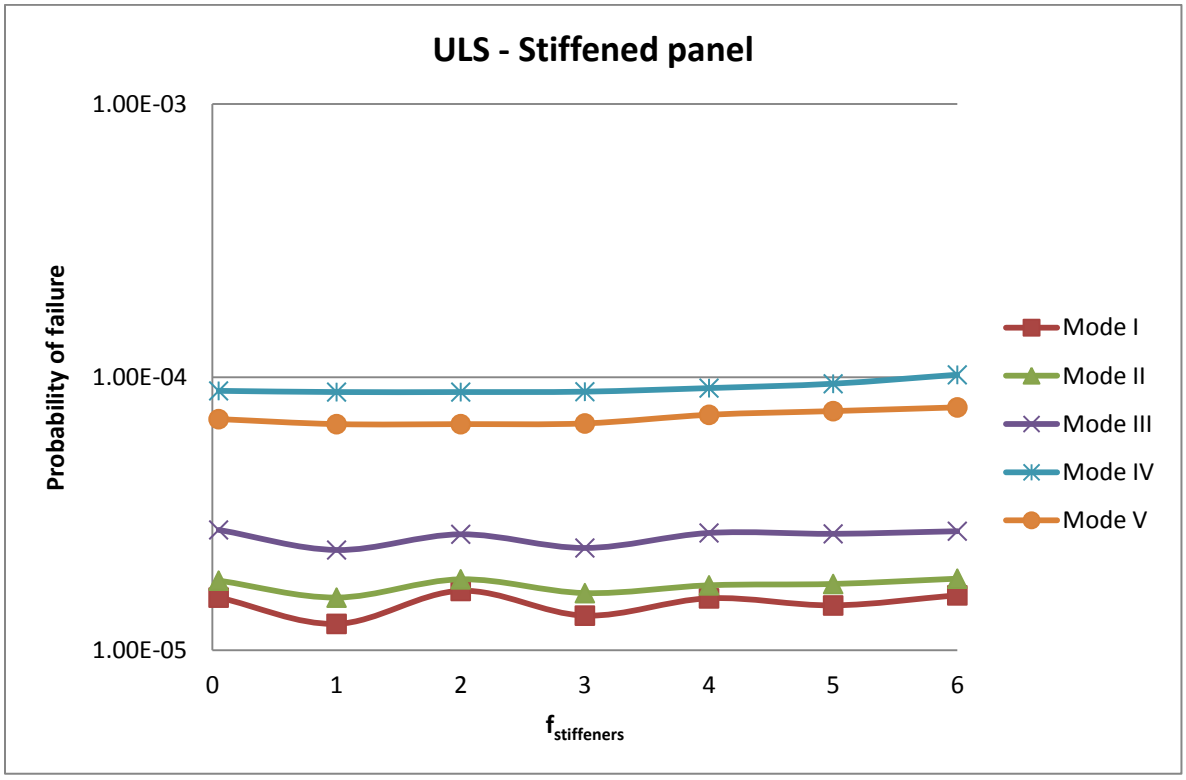

Figure 6 - Ultimate probability of failure of a stiffened panel as a function of the corrosion of the stiffeners

The reasons for these results are the following:

1. Mode I (overall collapse) and mode III (beam-column type collapse) are not influenced by the corrosion at all, as already explained (the ultimate strength for these failure modes is mainly a function of the geometry of the stiffener);
2. Mode II (yielding along the plate-stiffener intersection) is, by definition, only related to the plating between stiffeners;
3. Mode IV (local buckling of the stiffener web) and mode V (flexural-torsional buckling of the stiffeners) are influenced by the corrosion of the stiffener, but to a very little extent (in paragraph 7.1.2 it was shown that the ultimate strength for these failure modes is mainly a function of the ultimate strength of the plating between the stiffeners).

Furthermore, we should underline that no lateral pressure is applied to the assessed deck. It is likely to expect an higher influence of the corrosion of the stiffeners on the reliability if a lateral pressure is acting on one side of the stiffened panel.

7.1.5 Effects of the correlation coefficients on the structural reliability

In paragraph 6.3 the correlation between the corroded thicknesses (of the plate, of the stiffener web and of the stiffener flange) was discussed. There it was decided to assume a full correlation ($\rho = 1$). Since this assumption may be too conservative, here the effect of the correlation coefficients on the results is studied. The correlation coefficients have been varied from 0 to 1 (it has been assumed that the three correlation coefficients $\rho_{plate,web}$, $\rho_{plate,flange}$ and $\rho_{flange,web}$ have always the same value).

Results are given in figure 7 (the Turkstra's rule to combine loads was used; the number of samples generated was 10^7).

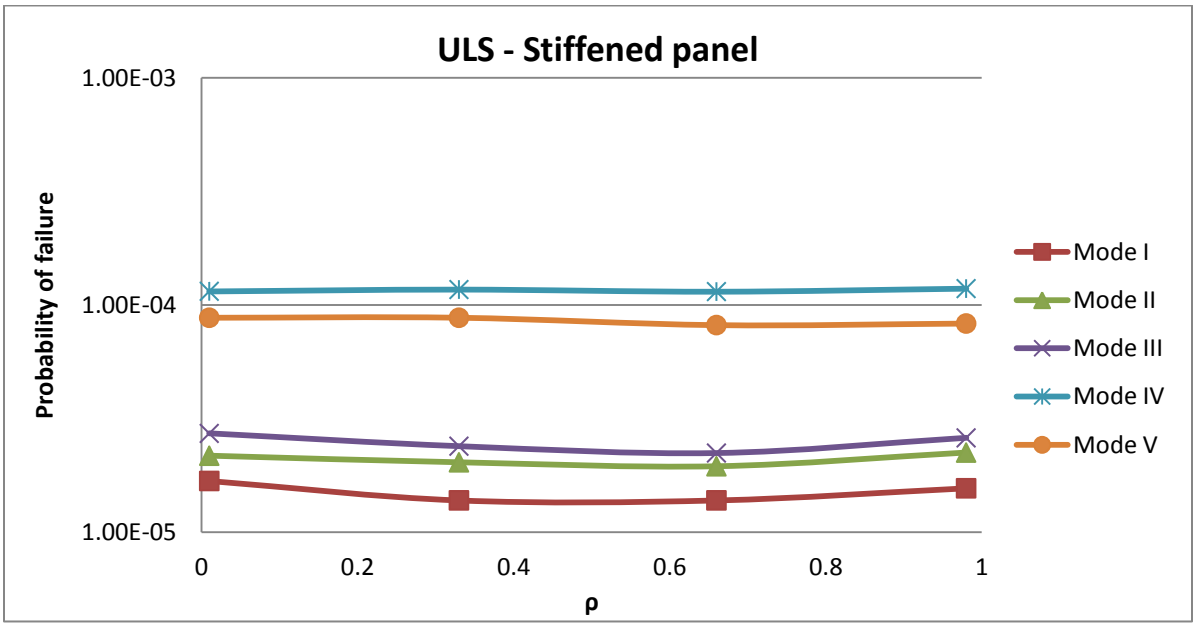

Figure 7 - Ultimate probability of failure of a stiffened panel as a function of the correlation coefficient

We can conclude that the correlation coefficients between corroded thicknesses have no effect at all on the results. The explanation for this has already been given in the previous paragraph: the probability of failure, for all ultimate failure modes, is basically sensitive only to either the corrosion of the plating or the geometry of the cross-section.

In this sensitivity analysis it has been assumed always a positive correlation ($0 \leq \rho \leq 1$). Since the structural elements are all – at least on one surface – in contact with the same environment, this seems to be the most logic assumption. However, a negative correlation may still be possible. For example, the web and the flange of the longitudinals have a different orientation: one is vertical, one is horizontal. This means that it is likely to have accumulation of dust or residual oil on one of the two elements (in our case – deck reassessment – on the flange), while the other one (the web) will obviously be more clean. This may have some effects on the corrosion of the two elements (e.g. the residual oil may act as a coating for the flange).

Anyway, since it has been showed that all failure modes are mainly sensitive to either the plating thickness or the geometry of the cross-section, it does not make sens to continue the sensitivity analysis also for negative values of the correlation coefficients (since we expect that we will get a constant trend).

7.1.6 Time-dependent reliability analysis

In chapter 6 a corrosion prediction model for the bottom plate of an FPSO oil cargo tank has been taken from the literature. If we assume that this corrosion prediction model is still valid for the deck of the monitored FPSO which has been used for our case study, we can use it to run a time-dependent reliability analysis. The results are shown here. The goal of this paragraph is only for illustration purposes,: it only shows the potentiality of the tool which has been developed, since the assumption on the validity of the corrosion prediction model is not confirmed.

The time-dependent reliability analysis has been performed running indipendent MCSs, one per each time step. The mean values of the corroded thicknesses have been calculated every year using the (6.8). Actually also the standard deviation of the corroded thicknesses should be changed, since we know that it tends to increase with the passage of time ([2]). However, this will come automatically, since the distributions adopted for the corroded thicknesses are the truncated exponential distributions (that is, the same adopted for the corroded thicknesses of the inspected FPSO of the case study) which, by definition, have the standard deviation equal to the mean value (and it has been assumed that the corroded thicknesses are exponentially distributed at any time step).

Results are given in figure 8. On the same figure it has been reported also:

- the time where – according to the corrosion prediction model – the corrosion allowance of 2 mm will be all consumed. The real value of the corrosion allowance for the monitored FPSO is actually unknown. The reported value of 2 mm has been taken from the DNV ([3]; values for the “tank region” and “within 1.5 m below weather deck”);

- two target probabilities of failure for stiffened and unstiffened plate. These target probability of failure are based on the review of proposals made by various regulatory bodies and analysis of results of reliability analysis performed for the last 30 years ([4]).

Looking at figure 8, the advantages of using such a reassessment tool are evident:

1. unnecessary maintance can be avoided;
2. it can be predicted when a maintenance intervention will be necessary, so that the repair intervention can be properly planned;
3. life-extensions of the existing unit can be justified.

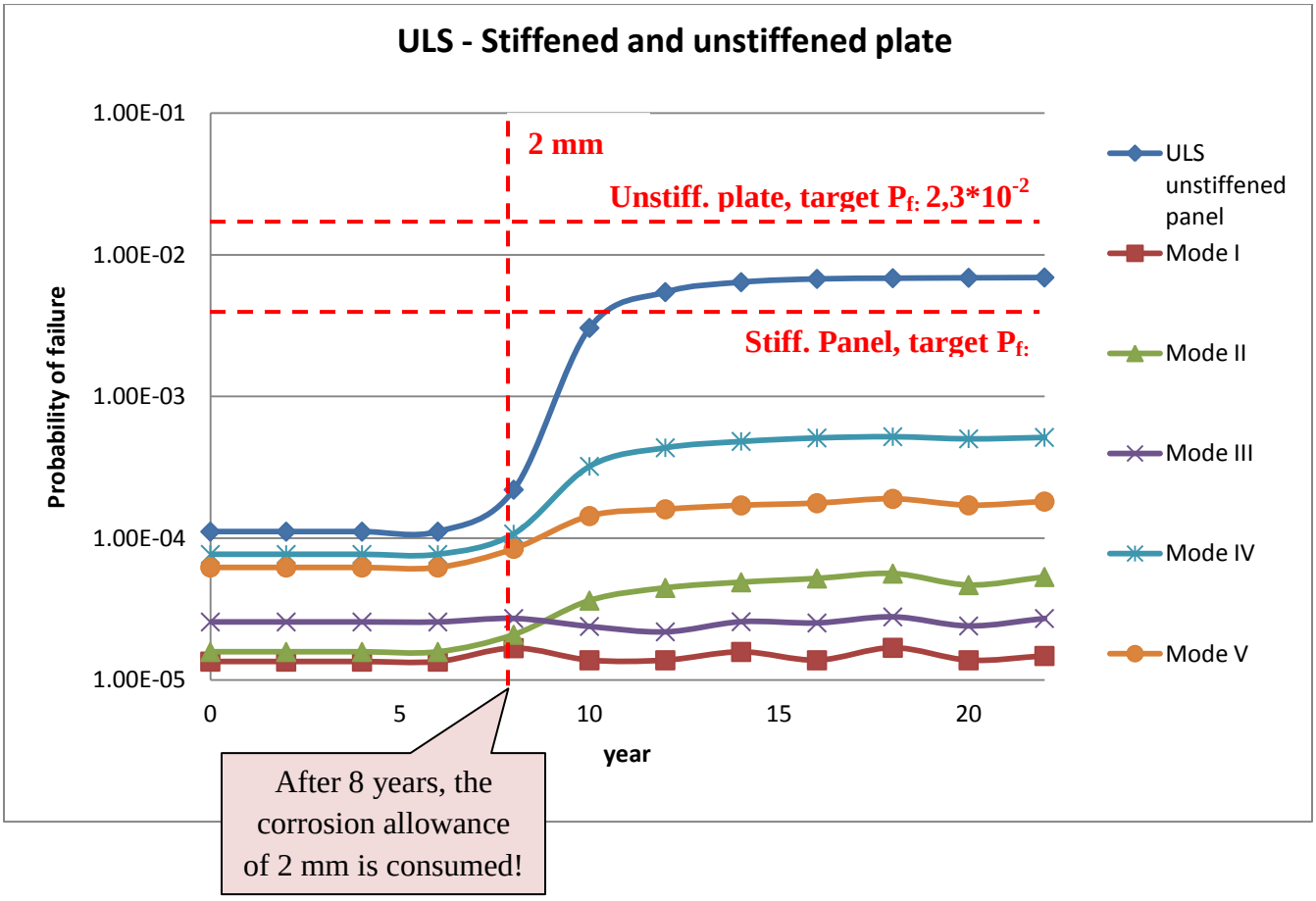

Figure 8 – Time-dependent reliability analysis

7.2 Comparison with some target reliability indices

Defining some target reliability levels is not an easy task. Several variables have to be taken into account, including some economic variables. The target reliability levels used in this paragraph have been taken from Mansour et al. ([5]). These values are based on the review of proposals made by various regulatory bodies and analysis of the results of reliability analyses performed for 30 years on traditional vessels. Even if they cannot be considered valid for FPSOs, here they

can be used to give a first idea. In paragraph 8.2.2 a way to derive some target reliability indices suitable for the reassessment of a corroded FPSO is briefly introduced.

Results are listed in table 6. For each failure mode and each load combination method , the obtained reliability level is beyond the target level. All these reliability indices have been calculated considering the real loads and the real thicknesses, thus a quite large number of samples was generated ($6*10^8$). They are all annual target reliability indices. For the ULS of stiffened panel we have only one value since the lowest reliability level among the 5 failure modes has been considered. Analogously, for the yielding limit states, the lowest reliability indices between the hogging and sagging condition have been reported.

Table 6 – Comparison with some target reliability levels

	Peak coincidence	SRSS	Turkstra	Target reliability
	β	β	β	$\boldsymbol{\beta}$
Yielding unstiff. plate	4.93	4.90	4.92	**3.7**
Yielding stiff. panel	5.00	4.96	4.99	**4.1**
ULS unstiff. plate	4.41	4.40	4.39	**2.0**
ULS stiff. panel	4.44	4.46	4..54	**2.5**
Fracture	4.23	4.24	4.12	**4.1**

In table 6 we notice that the reliability indices are higher for the yielding limit states than for the ultimate limit states, especially for the target reliability levels. The reason for that is to be found in the criteria which classification societies traditionally used for the design of new vessels. The initial yield criterion, for many years, it has been the main criterion used in the classification society. Consequently, in an effort to avoid the other failures, they deliberately required very high safety coefficients for the yielding failure ([4]).

It is also possible to see that the reliability indices for the stiffened panel are always larger than for the unstiffened plate. This is consistent with the structural hierarchy introduced in chapter 1.

Finally, we notice that the differences between the three load combination methods is very small (even if modelling uncertainties from table 4 have been included). This is because the real loads have been used, and so the wave induced loads have not been multiplied times 3, as it was done in all the other paragraphs of this chapter.

References

[1] J. K. Paik, A. K. Thayamballi, B. J. Kim, “Large deflection orthotropic plate approach for ultimate strength formulation for stiffened panels under combined biaxial compression/tension and lateral pressure”, Thin-Walled Structure 39, 2001

[2] G. Wang, J. Spencer, H. Sun, “Assessment of corrosion risks to aging ships using an experience database”, International Conference on Offshore Mechanics and Arctic Engineering, 2003

[3] DNV-OS-C102, “Structural Design of Offshore Ships”, October 2012

[4] Dominique Beghin, Bureau Veritas, “Reliability-based structural design”, Ship structural analysis and design (Chapter 5), SNAME 2010

[5] A. E. Mansour, P. Wirsching, M. Luckett, A. Plumpton, “Assessment of reliability of ship structures”, Report SSC-398, 1997

8

Conclusions and recommendations

This last chapter of the thesis is divided into two main paragraphs.

In the first one some conclusions on the work done are drawn. In the second one some guidelines and recommendations for eventual future devolpments are given.

8.1 Main findings

In this thesis a way to reassess the strength of a corroded FPSO, using a probability-based approach, has been proposed. In particular, the model is able to check inspected unstiffened plates and stiffened panels. If properly combined with a corrosion prediction model, this tool can be used to avoid unnecessary maintainance or to justify some extra maintainance.

The reassessment procedure has been applied to evaluate the strength of the deck of a real FPSO. The thickness measurements processing showed that the best way to model the corroded thicknesses distribution for the FPSO deck was by using a truncated exponential distribution (for both the plating and the stiffeners). For the loads, it was found out that the gamma distribution and the normal distribution give the best approximation of the empirical distributions for the wave-induced bending moments and the still water bending moment, respectively. No correlation was seen between the HWBM and the VWBM.

The sensitivity analysis showed that – for the considered load condition – the reliability of the structure is much more sensitive to the corrosion of the plating rather than to the corrosion of the stiffeners.

Furthermore, the model is also able to predict the most likely failure mode. For example, during the case study it was found that the most likely failure mode for the deck of the inspected FPSO is the one induced by the web buckling of the stiffeners. On the other hand, some failure modes showed no sensitivity to the corrosion of both the plating and the stiffenerse. This type of knowledge can be used to optimize the maintainace intervention.

It was also found that the analytical model proposed for the calculation of the ultimate strength (large deflection analysis with membrane stress-based method) is giving unreliable results if a

proper way to model and include the initial imperfections (initial deflection and residual stresses) is not adopted. Alternatively, the empirical Johnson-Ostenfeld formula can be used.

Finally, results also showed a great sensitivity of the results to the way the modelling uncertainties for the load combinations methods are modelled.

8.2 Future developments

This last paragraph is further divided into three sub-paragraphs.

In the first one the "weak points" of the proposed reassessment model are given, and some methods to correct them are introduced. In the second sub-paragraph it is explained what still needs to be done in order to implement the reassessment model and to make the reassessment tool fully operative. Finally, some ideas to use the model in a different way (that is, from a "research point of view" rather than for practical purposes) are written down.

8.2.1 Further improvements

During this work, many assumptions were necessary. Most of them are quite acceptable, some of them are not. Here a list of the least reasonable assumptions, which requires further investigation, is given.

1. ***Modelling uncertainties:*** in chapter 3 it has been shown how the modelling uncertainties have been modelled for all the random variables of interest. For all of them a literature research was carried out and – since there is not a lot of material about FPSO – most of the time the modelling uncertainties for commercial vessels (preferably for oil tankers) have been assumed to be valid also for FPSOs. This assumption seems to be quite reasonable. However, we should mention that these modelling uncertainties are supposed to be used during the design of a new vessel. The point is that we have at the momen of the reassessment some extra data which are not available during the design of a new vessel: the MONITAS monitored loads. Therefore the actual modelling uncertainties are surely lower than the values which have been used. On the other hand these modelling uncertainties are not zero. Hence, a new – less conservative – possible way to model these type of uncertainties should eventually be studied.

2. ***Load combination methods:*** results from chapter 7 showed a great sensitivity of the reliability indices to the way the modelling uncertainties were modelled for any of the three load combination methods. The problem is that we are using three deterministic methods to combine loads in a stochastic approach. This does not necessarily produce bad results, provided that the modelling uncertainties are properly modelled. Alternatively, probabilistic methods to combine loads can be used (e.g. Ferry-Borges and Castenheta [1] and Moan and Jiao [2] methods). In 1984 Guedes Soares demonstrated that stochastic methods provide exact solutions for combining still-water and wave-induced bending moments [3].

3. ***Initial imperfections:*** the ALPS/ULSAP theory from professor Paik has been used to write down the failure functions for the ultimate limit states. This is an analytical theory which allows to write down the failure functions in a closed-form expression. This is a great advantage if these limit state functions have to be used in a stochastic approach. However, they require a proper way to model the initial imperfections, which is something that has not been done in the present study, but which needs to be done in the future.

4. ***Grouping thickness measurements:*** in chapter 2 – when thickness measurements from a real FPSO have been processed – all the measurements which gave $t_{corr} \leq 0$ were not considered (a negative corroded thickness is possible since there are always some points on a new plate which have an actual thickness higher than the nominal thickness). The reason for this choice was that considering all measurements from a plate (or from a stiffener web or from a stiffener flange) all together may led to optimistic results, since not all the locations on a plate experience the same corrosion. Indeed, there are always some parts of a plate with a corrosion more severe than the average one. Disregarding the measurements which gave $t_{corr} \leq 0$ is giving some conservativity to the proposed reassessment procedure, but it does not guarantee both that the results will be conservative and – if it will be conservative – that it will not be *too* conservative. A way to solve this problem is given in the following paragraph.

8.2.2 Implementation of the reassessment procedure

In order to make this reassessment method ready to be implemented on a real FPSO, some extra work has to be done.

1. For an FPSO stiffened panel, the most general loading case is a combination of: longitudinal stress, transverse stress, shear stress and lateral pressure. Equations given in chapter 4 always neglect the shear stress. For the case study of chapter 6 (deck plate with longitudinal axial load) this was not a problem but if those equations pretend to be used also for other load cases than this assumptions is no more valid.

2. Since the final purpose of this tool is – from an operator point of view – avoiding superfluous maintenance, this reassessment procedure should be able to convince Class Socities about its validity. Therefore it is necessary to get approval from Class Socities, in particular with respect to:
   - the way a probability distribution is obtained from a set of measured data;
   - the way the loads are calculated from the MONITAS data;
   - the way the modelling uncertainties are modelled;
   - the theory used to write down the limit state functions.

   Furthermore, it must be underlined that this analysis only focuses on ultimate strength. For CSs, accidental limit state will also be of importance.

3. The results of a reliability analysis are strongly sensitive to the way the input random variables are modelled (i.e. to the probability distributions used to model the uncertainties). Of course, the more data are available, the more precise the fitting of the empirical data with a probability distribution function will be. In chapter 2, during the thickness processing, some difficulties have been encountered in modelling the statistical uncertainties of the corroded thickness for the stiffeners, due to a limited number of measurements. If this reassessment tool is going to be implemented on a real FPSO, then it is recommended that a "large enough" number of measurements is taken. The amount of measurements to be taken needs to be discussed with an FPSO operator/surveyor, since it has to be a compromise between the necessity of making the structural reassessment as precise as possible, and the necessity of making the inspections not too difficult and/or too long. A possible solution may be: first, a visual inspection of the stiffened panel is made. Some plates and stiffeners which showed the most severe corrosion are selected. Then thickness measurements are carried out: for the non-selected plates/stiffeners, in the traditional way; for the selected stiffeners and plates, the number of measurements is increased. In this way we are also able to solve the problem from point 4, paragraph 8.2.1 (about grouping thickness measurements). Indeed, in this way, it is possible to consider *all* the measurements but *only* from the selected stiffeners/plates. In so doing, we can guarantee the efficiency of the estimation of the probability distribution (since for the selected structural elements the number of thickness measurements carried out is "large enough"), and at the same time be sure that we are not acting on the optimistic side, since the selected elements have been properly chosen as the most corroded ones.

4. Some target reliability indices need to be identified. A possible way to do that is to use as inputs the deterministic rule-based corrosion allowance, for the corroded thickness, and the rule-based loads, and to calculate the reliability indices using the procedure described in the present study.

5. An efficient corrosion prediction model for FPSO still does not exist. In the literature there exist several corrosion prediction models, but their validity for FPSO needs to be verified by a comparison with some measured thicknesses. Due to the high number of variables affecting the corrosion rate, a large amount of inspection reports (preferably relative to different tanks of the same unit, differents units from the same ocean area, and different ocean areas) has to be analyzed. It is not possible to guarantee that one of the existing corrosion prediction model will fit the empirical data in a satisfactory manner, and therefore there may be the necessity to set up a completely new corrosion prediction model. The eventuality of tuning different models for different units/tanks should also be taken in onsideration.

8.2.3 *Utilization of the model for research purposes*

The great advantage of the MONITAS system is its capability to also say *why* the calculated fatigue lifetime is different from the design-predicted fatigue lifetime. This is done calculating the fatigue lifetime several times, replacing each time one input variable with the design-predicted variable, to see the effects that the assumed value of the input component has on the results. Furthermore, in order to study the effcts of the fatigue tool itself on the calculated fatigue damage, the calculated fatigue lifetime is compared with the so-called measured fatigue lifetime, which is computed directly from the stresses measured by some strain gauges.

The same philosophy can be applied also to the present structural reliability analysis. In particular, we can distinguish three components which combined together are able to calculate the reliability of the corroded structure (see figure 1): the thickness measurements, the monitored loads and the limit state functions.

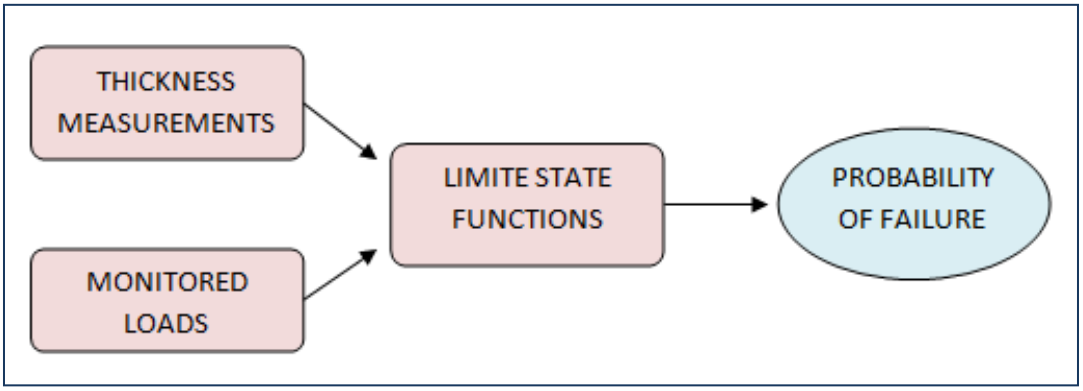

Figure 1 – Probability-based structural reassessment of a corroded FPSO

If we replace any of the three components (pink boxes in figure 1) with the design-predicted value, and if we compare the new obtained probability of failure with the "original" probability of failure, it is possible to investigate:

- the influence of the design-assumed extreme loads on the reliability;
- the influence of the corrosion allowance on the reliability;
- the influence of the class societies formulae for the dimensioning of stiffened and unstiffend plates on the reliability.

Another interesting topic of research may be the coupling between the two degradation mechanisms for FPSO which have been described at the very beginning of the present thesis: fatigue and corrosion. In particular, it would be interesting to include the effects of the corrosion on the calculated stresses (that is, on the fatigue loads). Let us consider, for instance, a strain gauge located on the side shell close to the neutral axis (which is a typical location for a strain gauge in the MONITAS system). The deformation in that area is dominated by one dominant load mechanism (lateral pressure). If a corrosion prediction model have been validated, and if a comparison between the mean stresses in the plate and the corrosios loss of thickness in the plate is made over a sufficiently long period, it should be noted a similar trend between these two

variables. Indeed, the stresses in the plate are expected to grow with the reduction of the thickness (note that we are talking about local load-induced stresses!). If this analogy is found, then the precision of the calculated fatigue lifetime can be further increased if the prediction of the stresses in the future takes into account the thickness reduction due to corrosion.

Therefore, the present study – besides providing FPSO operators with an useful tool to evaluate the structural reliability of their corroded unit – can also be seen as a starting point for many research topics.

References

[1] J. Ferry-Borges, M. Castanheta, “Structural safety”, Lisbon: Laboratoria Nacional de Engenhera Civil, 1971

[2] T. Moan, G. Jiao, “Characteristic still water load effect for production ships”, Report MK/R 104/88, Trondheim: The Norwegian Institute of Technology, 1988

[3] C. Guedes Soares, “Probabilistic models for load effects in ship structures”, Report UR-84-38, Trondheim: Dept. of Marine Technology, Norwegian Institute of Technology, 1984

9

Annex A

9.1 Kolmogorov-Smirnov tables

Number of trials, n	Level of significance			
	0.10	0.05	0.02	0.01
1	0.95000	0.97500	0.99000	0.99500
2	0.77639	0.84189	0.90000	0.92929
3	0.63604	0.70760	0.78456	0.82900
4	0.56522	0.62394	0.68887	0.73424
5	0.50945	0.56328	0.62718	0.66853
6	0.46799	0.51926	0.57741	0.61661
7	0.43607	0.48342	0.53844	0.57581
8	0.40962	0.45427	0.50654	0.54179
9	0.38746	0.43001	0.47960	0.51332
10	0.36866	0.40925	0.45662	0.48893
11	0.35242	0.39122	0.43670	0.46770
12	0.33815	0.37543	0.41918	0.44905
13	0.32549	0.36143	0.40362	0.43247
14	0.31417	0.34890	0.38970	0.41762
15	0.30397	0.33760	0.37713	0.40420
16	0.29472	0.32733	0.36571	0.39201
17	0.28627	0.31796	0.35528	0.38086
18	0.27851	0.30936	0.34569	0.37062
19	0.27136	0.30143	0.33685	0.36117
20	0.26473	0.29408	0.32866	0.35241
21	0.25858	0.28724	0.32104	0.34427
22	0.25283	0.28087	0.31394	0.33666
23	0.24746	0.27490	0.30728	0.32954
24	0.24242	0.26931	0.30104	0.32286

[a] Values of $d_\alpha(n)$ such that $p(\max)|F^n(x) - F(x)|d^\alpha(n) = \alpha$.

[b] $N > 40 \approx \frac{1.22}{N^{1/2}}, \frac{1.36}{N^{1/2}}, \frac{1.51}{N^{1/2}}$ and $\frac{1.63}{N^{1/2}}$ for the four levels of significance.

Number of trials, n	Level of significance, α			
	0.10	0.05	0.02	0.01
25	0.23768	0.26404	0.29516	0.31657
26	0.23320	0.25907	0.28962	0.31064
27	0.22898	0.25438	0.28438	0.30502
28	0.22497	0.24993	0.27942	0.29971
29	0.22117	0.24571	0.27471	0.29466
30	0.21756	0.24170	0.27023	0.28987
31	0.21412	0.23788	0.26596	0.28530
32	0.21085	0.23424	0.26189	0.28094
33	0.20771	0.23076	0.25801	0.27677
34	0.20472	0.22743	0.25429	0.27279
35	0.20185	0.22425	0.26073	0.26897
36	0.19910	0.22119	0.24732	0.26532
37	0.19646	0.21826	0.24404	0.26180
38	0.19392	0.21544	0.24089	0.25843
39	0.19148	0.21273	0.23786	0.25518
40[b]	0.18913	0.21012	0.23494	0.25205

[a]Values of $d_\alpha(n)$ such that $p(\max)|F^n(x) - F(x)|d^\alpha(n) = \alpha$.

[b]$N > 40 \approx \frac{1.22}{N^{1/2}}, \frac{1.36}{N^{1/2}}, \frac{1.51}{N^{1/2}}$ and $\frac{1.63}{N^{1/2}}$ for the four levels of significance.

10

Annex B

10.1 Statistical uncertainties for FPSO with AHMS

Random variable	Mean value	c.o.v.	Distribution	Source
Yield strength, ordinary steel	Bias 1.11	0.068	Lognormal	Design value
Yield strength, high strength steel	Bias 1.22	0.089	Lognormal	Design value
Poisson's ratio	-	-	Deterministic	Nominal value for steel 0.3
Elastic modulus	Bias 1.024	0.0179	Normal or lognormal	Nominal value for steel 210 GPa
Crack length for the SCF	-	-	Deterministic	Rules
Critical stress intensity factor	-	-	Deterministic	Rules
Main dimensions and constructional parameters	-	-	Deterministic	Design values
SWBM	-	-	To be determined	Load master
VWBM	-	-	To be determined	MONITAS LBSG
HWBM	-	-	To be determined	MONITAS LBSG
Static sea pressure	-	-	To be determined	MIONITAS: draft times ρg
Static cargo/ballast pressure	Bias 1	0.05	Normal	Design value
Dynamic sea pressure on sides	-	-	To be determined	MONITAS data for the relative wave height
Inertia cargo/ballast loads	-	-	To be determined	MONITAS accelerations (for the density use a normal distribution, with bias 1 and c.o.v. 0.05)
Sloshing impact pressure	-	-	Deterministic	Design value
Corroded thicknesses	-	-	To be determined	Inspections

10.2 Modelling uncertainties for FPSO with AHMS

Random variable	Mean value	c.o.v.	Distribution
SWBM	*Neglected*		
Static sea pressure	*Neglected*		
Static cargo pressure	*Neglected*		
Load combination - Peak coincidence method	0.72	0.11	Normal
Load combination - SRSS	1.01	0.12	Normal
Load combination - Turkstra	1.17	0.11	Normal
Dynamic sea pressure on the side	1	0.1	Normal
Dynamic cargo/ballast loads	1	0.1	Normal

11

Annex C

11.1 Generation of uncorrelated random variables

If $\boldsymbol{V}$ is a generated sample of uniform uncorrelated random variables, then to generate a non-uniform distributed sample of random variables $\boldsymbol{X}$, the transformation to apply is ([1]):

$$\boldsymbol{X} = F_X^{-1}(\boldsymbol{V})$$

Where F_X is the cumulative distributin function for the random variables $\boldsymbol{X}$.

If X is a lognormal distributed random variable (such as, for example, the yielding stress), then:

$$F_X(X) = \frac{1}{2} + \frac{1}{2}\operatorname{erf}\left(\frac{\log X - \mu}{\sigma\sqrt{2}}\right) \tag{12.1}$$

and :

$$X = \exp\left\{\sigma\sqrt{2}\,\operatorname{erf}^{-1}[2F_X(X) - 1] + \mu\right\} \tag{12.2}$$

where μ and σ are the mean value and standard deviation of the associated normal distribution, respectively.

If X is a normal distributed random variable (such as, for example, the SWBM), then:

$$F_X(X) = \frac{1}{2} + \frac{1}{2}\operatorname{erf}\left(\frac{X - \mu}{\sigma\sqrt{2}}\right) \tag{12.3}$$

and :

$$X = \sigma\sqrt{2}\,\operatorname{erf}^{-1}[2X - 1] + \mu \tag{12.4}$$

where μ and σ are the mean value and standard deviation, respectively.

If X is a gamma distributed random variable (such as, for example, the VWBM), then:

$$F_X(X) = gammainc\left(\frac{X}{\theta}, k\right) \tag{12.5}$$

and :

$$X = \theta * gammainc^{-1}(X, k) \tag{12.6}$$

$gammainc\left(\frac{X}{\theta}, k\right)$ is the lower gamma incomplete function, whose definition is given by (2.39). k is the shape parameter and θ the scale parameter of the gamma distribution.

11.2 Generation of correlated random variables

The corroded thicknesses are correlated truncated-exponentially distributed random variables. To generate them, at first we need to generate a set of uncorrelated standard-normally distributed variables $\boldsymbol{U}$ from a set of uniformly distributed random variables $\boldsymbol{V}$ ([1]).This is done by the (12.7).

$$U = \sqrt{2}\,\mathrm{erf}^{-1}[2X - 1] \tag{12.7}$$

To generate correlated non-uniformly distributed random variables $\boldsymbol{X}$, the following transformation has to be applied ([1]):

$$X = F_X^{-1}[\Phi(L_U, U)] \tag{12.8}$$

L_U is given by the (lower) Cholesky decomposition of the correlation matrix R_{UU} ([1]):

$$L_U = chol(R_{UU}) \tag{12.9}$$

If $\boldsymbol{X}$ are truncated random variables, then the (12.8) becomes the (12.10):

$$X = F_X^{-1}\{\Phi(L_U, U)[F_X(b) - F_X(a)] + F_X(a)\} \tag{12.10}$$

where a and b are the truncation values. $F_X(X)$ is the non-truncated exponential CDF:

$$F_X(X) = 1 - \exp(-\lambda X) \tag{12.11}$$

Hence:

$$X = -\frac{1}{\lambda}\log\{1 - \Phi(L_U, U)[\exp(-\lambda b) - \exp(-\lambda a)] - 1 + \exp(-\lambda a)\} \tag{12.12}$$

The elements of the R_{UU} are not the same of R_{XX}. That is, the correlation coefficients between the standard normally-distributed random variables are not the same of the truncated exponentially-distributed random variables (although they are always quite close, [1]).

The correlation coefficients $\rho_{U_iU_j}$ can be expressed as a function of $\rho_{X_iX_j}$ using the following ([2]), which is only valid if both X_i and X_j are both exponentially distributed:

$$\rho_{U_i U_j} = \rho_{X_i X_j}\left[1.229 - 0.367 * \rho_{X_i X_j} + \left(\rho^2_{X_i X_j}\right) 0.153\right] \quad (12.13)$$

References

[1] D. Straub, “Lecture notes in structural reliability”, TU Munchen, 2012

[2] O. Ditlevsen, H. O. Madsen, “Structural reliability methods”, Technical university of Denmark, 2007

12

Annex D

12.1 Results

12.1.1 *Analytical method vs. Jonshon-Ostenfeld formula*

	Analytical method	Jonshon-Ostenfeld	Elastic buckling
t_p [mm]	P_f	P_f	P_f
10	2.89E-04	6.80E-03	6.80E-03
12	8.86E-05	8.82E-04	8.46E-04
14	1.84E-05	1.62E-04	8.30E-05
16	5.80E-06	5.62E-05	7.80E-06
18	4.50E-06	2.94E-05	2.00E-07
20	3.60E-06	1.87E-05	0 (*)

Number of samples: 10^7

(*) The elastic buckling strength for such a stocky plate is meaningless

12.1.2 *Effects of the initial corroded thickness on the structural reliability*

ULS unstiffened plate – Peak coincidence method		
	Analytical method	*Jonshon-Ostenfeld*
f	P_f	P_f
0	8.00E-08 (*)	1.80E-06
0.5	1.10E-07 (*)	2.10E-06
1	1.30E-07 (*)	1.70E-06
1.5	1.50E-07 (*)	4.90E-06
2	5.00E-07 (*)	4.05E-05
2.5	1.00E-06	2.00E-04
3	3.10E-06	6.40E-04
3.5	4.70E-06	1.51E-03
4	9.70E-06	2.80E-03
4.5	1.20E-05	4.57E-03
5	1.73E-05	6.69E-03
5.5	2.06E-05	9.12E-03

6	2.84E-05	1.19E-02

Number of samples: 10^7 (unless otherwise specified)

(*) For these probabilities of failure the number of samples has been increased to 10^8

ULS stiffened panel - Peak coincidence method							
	Mode I	*Mode II*	*Mode III*	*Mode IV (**)*	*Mode IV (***)*	*Mode V (**)*	*Mode V (***)*
f	P_f	P_f	P_f	P_f	P_f	P_f	P_f
0	8.00E-08 (*)	8.00E-08 (*)	1.50E-07 (*)	7.20E-07 (*)	2.80E-06	2.40E-07 (*)	1.70E-06
0.5	7.00E-08 (*)	1.10E-07 (*)	1.90E-07 (*)	6.30E-07 (*)	4.40E-06	1.90E-07 (*)	2.80E-06
1	1.00E-07 (*)	1.30E-07 (*)	1.90E-07 (*)	8.80E-07 (*)	4.10E-06	3.00E-07 (*)	2.30E-06
1.5	1.30E-07 (*)	1.40E-07 (*)	2.00E-07 (*)	1.22E-06 (*)	5.30E-06	4.40E-07 (*)	3.00E-06
2	1.00E-07 (*)	2.10E-07 (*)	1.60E-07 (*)	2.23E-06 (*)	1.12E-05	6.70E-07 (*)	3.00E-06
2.5	7.00E-08 (*)	2.60E-07 (*)	1.80E-07 (*)	4.60E-06	3.28E-05	8.00E-07	9.70E-06
3	1.10E-07 (*)	4.00E-07 (*)	2.00E-07 (*)	1.03E-05	6.51E-05	1.80E-06	1.28E-05
3.5	8.00E-08 (*)	4.60E-07 (*)	1.50E-07 (*)	1.40E-05	1.12E-04	2.40E-06	1.66E-05
4	1.00E-07 (*)	6.40E-07 (*)	1.70E-07 (*)	2.21E-05	1.87E-04	3.70E-06	2.42E-05
4.5	1.20E-07 (*)	1.02E-06 (*)	2.00E-07 (*)	3.10E-05	2.87E-04	5.00E-06	3.31E-05
5	1.20E-07 (*)	1.26E-06 (*)	1.80E-07 (*)	4.68E-05	3.92E-04	5.20E-06	3.99E-05
5.5	8.00E-08 (*)	1.62E-06 (*)	1.90E-07 (*)	5.36E-05	5.13E-04	5.10E-06	4.93E-05
6	8.00E-08 (*)	2.15E-06 (*)	1.90E-07 (*)	6.94E-05	6.51E-04	6.40E-06	5.34E-05

Number of samples: 10^7 (unless otherwise specified)

(*) For these probabilities of failure the number of samples has been increased to 10^8

(**) Analytical method

(***) Jonshon-Ostenfeld formula method

ULS unstiffened plate – SRSS		
	Analytical method	*Jonshon-Ostenfeld*
f	P_f	P_f
0	2.50E-06	2.67E-05
0.5	3.60E-06	2.95E-05
1	4.50E-06	3.60E-05
1.5	3.20E-06	4.39E-05

2	8.60E-06	1.15E-04
2.5	1.15E-05	3.66E-04
3	2.00E-05	9.81E-04
3.5	3.36E-05	2.11E-03
4	5.37E-05	3.76E-03
4.5	8.18E-05	6.03E-03
5	1.15E-04	8.58E-03
5.5	1.40E-04	1.15E-02
6	1.78E-04	1.48E-02

Number of samples: 10^7

ULS stiffened panel - SRSS							
	Mode I	*Mode II*	*Mode III*	*Mode IV (*)*	*Mode IV (**)*	*Mode V (*)*	*Mode V (**)*
f	P_f	P_f	P_f	P_f	P_f	P_f	P_f
0	2.40E-06	2.50E-06	3.60E-06	6.70E-06	1.96E-05	2.60E-06	1.53E-05
0.5	3.00E-06	3.60E-06	5.50E-06	7.80E-06	2.22E-05	2.70E-06	1.73E-05
1	4.20E-06	4.40E-06	6.40E-06	9.20E-06	2.88E-05	4.60E-06	2.10E-05
1.5	2.20E-06	2.90E-06	3.80E-06	8.50E-06	2.34E-05	3.40E-06	1.63E-05
2	3.90E-06	5.80E-06	6.70E-06	2.04E-05	4.20E-05	1.04E-05	2.70E-05
2.5	2.70E-06	5.40E-06	4.80E-06	3.37E-05	6.81E-05	1.50E-05	3.18E-05
3	2.50E-06	6.30E-06	4.40E-06	5.82E-05	1.16E-04	2.21E-05	3.99E-05
3.5	2.20E-06	9.20E-06	5.30E-06	8.82E-05	2.01E-04	2.70E-05	5.21E-05
4	2.60E-06	1.11E-05	5.00E-06	1.24E-04	3.01E-04	3.57E-05	6.23E-05
4.5	2.50E-06	1.45E-05	4.20E-06	1.66E-04	4.33E-04	4.20E-05	7.53E-05
5	2.90E-06	2.02E-05	4.80E-06	2.19E-04	5.95E-04	5.47E-05	9.41E-05
5.5	2.60E-06	2.39E-05	4.80E-06	2.59E-04	7.52E-04	5.64E-05	1.08E-04
6	2.00E-06	2.87E-05	4.70E-06	3.15E-04	9.70E-04	6.33E-05	1.27E-04

Number of samples: 10^7

(*) Analytical method

(**) Jonshon-Ostenfeld formula method

ULS unstiffened plate – Turkstra's rule		
	Analytical method	*Jonshon-Ostenfeld*
f	P_f	P_f
0	1.58E-05	1.12E-04
0.5	1.72E-05	1.15E-04
1	1.83E-05	1.34E-04
1.5	2.21E-05	1.61E-04
2	2.88E-05	2.98E-04
2.5	4.58E-05	7.48E-04
3	7.61E-05	1.76E-03
3.5	1.14E-04	3.58E-03

4	1.63E-04	6.20E-03
4.5	2.24E-04	9.57E-03
5	2.88E-04	1.36E-02
5.5	3.61E-04	1.80E-02
6	4.38E-04	2.27E-02

Number of samples: 10^7

ULS stiffened panel – Turkstra's rule							
	Mode I	*Mode II*	*Mode III*	*Mode IV (*)*	*Mode IV (**)*	*Mode V (*)*	*Mode V (**)*
f	P_f	P_f	P_f	P_f	P_f	P_f	P_f
0	1.35E-05	1.58E-05	2.57E-05	3.32E-05	7.70E-05	1.67E-05	6.23E-05
0.5	1.45E-05	1.72E-05	2.51E-05	3.38E-05	7.83E-05	1.64E-05	6.08E-05
1	1.50E-05	1.79E-05	2.61E-05	3.89E-05	9.25E-05	1.74E-05	7.49E-05
1.5	1.58E-05	1.92E-05	2.62E-05	4.42E-05	9.59E-05	2.52E-05	7.54E-05
2	1.51E-05	2.17E-05	2.39E-05	6.62E-05	1.21E-04	3.54E-05	8.68E-05
2.5	1.32E-05	2.40E-05	2.44E-05	1.11E-04	1.73E-04	5.39E-05	1.08E-04
3	1.59E-05	3.34E-05	2.63E-05	1.73E-04	2.47E-04	7.81E-05	1.25E-04
3.5	1.57E-05	4.37E-05	2.78E-05	2.55E-04	3.47E-04	1.03E-04	1.46E-04
4	1.66E-05	5.01E-05	2.57E-05	3.43E-04	4.83E-04	1.26E-04	1.71E-04
4.5	1.31E-05	6.04E-05	2.52E-05	4.35E-04	6.57E-04	1.48E-04	2.04E-04
5	1.29E-05	7.34E-05	2.60E-05	5.22E-04	8.37E-04	1.65E-04	2.23E-04
5.5	1.62E-05	8.89E-05	2.63E-05	6.26E-04	1.03E-03	1.83E-04	2.58E-04
6	1.57E-05	9.70E-05	2.88E-05	7.46E-04	1.28E-03	2.14E-04	2.90E-04

Number of samples: 10^7 (unless otherwise specified)

(*) Analytical method

(**) Jonshon-Ostenfeld formula method

ULS stiffened panel – Turkstra's rule				
	Mode I	*Mode III*	*Mode IV*	*Mode V*
hw	P_f	P_f	P_f	P_f
0 %	1.03E-02	6.23E-01	1.42E-04	1.42E-04
10 %	4.30E-03	3.82E-01	1.30E-04	1.30E-04
20 %	8.09E-04	4.31E-02	1.21E-04	1.21E-04
30 %	7.44E-05	2.86E-03	1.16E-04	1.15E-04
40 %	1.50E-05	3.31E-04	1.19E-04	1.17E-04
50 %	1.62E-05	1.17E-04	1.18E-04	1.13E-04
60 %	1.62E-05	6.27E-05	1.09E-04	1.02E-04
70 %	1.35E-05	4.11E-05	1.09E-04	9.70E-05
80 %	1.45E-05	3.44E-05	1.11E-04	9.40E-05
90 %	1.59E-05	2.76E-05	1.11E-04	8.70E-05
100 %	1.51E-05	2.39E-05	1.10E-04	8.68E-05

Number of samples: 10^7 (unless otherwise specified)

12.1.3 *Effects of the load combinations method on the structural reliability*

	Peak coincidence	SRSS	Turkstra
	P_f	P_f	P_f
Hogging unst. plate	3.69E-06	2.85E-05	8.54E-05
Hogging stiff. panel	2.86E-06	2.55E-05	7.76E-05
Sagging unst. plate	3.00E-07	3.60E-06	1.72E-05
Sagging stiff. panel	2.00E-07	3.30E-06	1.62E-05
Fracture	6.17E-05	2.64E-04	6.21E-04

Number of samples: 10^8

ULS unstiffened plate – Anlytical method			
	Peak coincidence	*SRSS*	*Turkstra*
f	P_f	P_f	P_f
0	8,00E-08 (*)	2,50E-06	1,58E-05
0.5	1,10E-07 (*)	3,60E-06	1,72E-05
1	1,30E-07 (*)	4,50E-06	1,83E-05
1.5	1,50E-07 (*)	3,20E-06	2,21E-05
2	5,00E-07 (*)	8,60E-06	2,88E-05
2.5	1,00E-06	1,15E-05	4,58E-05
3	3,10E-06	2,00E-05	7,61E-05
3.5	4,70E-06	3,36E-05	1,14E-04
4	9,70E-06	5,37E-05	1,63E-04
4.5	1,20E-05	8,18E-05	2,24E-04
5	1,73E-05	1,15E-04	2,88E-04
5.5	2,06E-05	1,40E-04	3,61E-04
6	2,84E-05	1,78E-04	4,38E-04

Number of samples: 10^7 (unless otherwise specified)

(*) For these probabilities of failure the number of samples has been increased to 10^8

ULS unstiffened plate – Johnson Ostenfeld			
	Peak coincidence	*SRSS*	*Turkstra*
f	P_f	P_f	P_f
0	1,80E-06	2,67E-05	1,12E-04
0.5	2,10E-06	2,95E-05	1,15E-04
1	1,70E-06	3,60E-05	1,34E-04
1.5	4,90E-06	4,39E-05	1,61E-04
2	4,05E-05	1,15E-04	2,98E-04
2.5	2,00E-04	3,66E-04	7,48E-04
3	6,40E-04	9,81E-04	1,76E-03
3.5	1,51E-03	2,11E-03	3,58E-03
4	2,80E-03	3,76E-03	6,20E-03
4.5	4,57E-03	6,03E-03	9,57E-03
5	6,69E-03	8,58E-03	1,36E-02

5.5	9,12E-03	1,15E-02	1,80E-02
6	1,19E-02	1,48E-02	2,27E-02

Number of samples: 10^7

ULS stiffened panel – Mode I			
	Peak coincidence	*SRSS*	*Turkstra*
f	P_f	P_f	P_f
0	8,00E-08 (*)	2,40E-06	1,35E-05
0.5	7,00E-08 (*)	3,00E-06	1,45E-05
1	1,00E-07 (*)	4,20E-06	1,50E-05
1.5	1,30E-07 (*)	2,20E-06	1,58E-05
2	1,00E-07 (*)	3,90E-06	1,51E-05
2.5	7,00E-08 (*)	2,70E-06	1,32E-05
3	1,10E-07 (*)	2,50E-06	1,59E-05
3.5	8,00E-08 (*)	2,20E-06	1,57E-05
4	1,00E-07 (*)	2,60E-06	1,66E-05
4.5	1,20E-07 (*)	2,50E-06	1,31E-05
5	1,20E-07 (*)	2,90E-06	1,29E-05
5.5	8,00E-08 (*)	2,60E-06	1,62E-05
6	8,00E-08 (*)	2,00E-06	1,57E-05

Number of samples: 10^7 (unless otherwise specified)

(*) For these probabilities of failure the number of samples has been increased to 10^8

ULS stiffened panel – Mode II			
	Peak coincidence	*SRSS*	*Turkstra*
f	P_f	P_f	P_f
0	8,00E-08 (*)	2,50E-06	1,58E-05
0.5	1,10E-07 (*)	3,60E-06	1,72E-05
1	1,30E-07 (*)	4,40E-06	1,79E-05
1.5	1,40E-07 (*)	2,90E-06	1,92E-05
2	2,10E-07 (*)	5,80E-06	2,17E-05
2.5	2,60E-07 (*)	5,40E-06	2,40E-05
3	4,00E-07 (*)	6,30E-06	3,34E-05
3.5	4,60E-07 (*)	9,20E-06	4,37E-05
4	6,40E-07 (*)	1,11E-05	5,01E-05
4.5	1,02E-06 (*)	1,45E-05	6,04E-05
5	1,26E-06 (*)	2,02E-05	7,34E-05
5.5	1,62E-06 (*)	2,39E-05	8,89E-05
6	2,15E-06 (*)	2,87E-05	9,70E-05

Number of samples: 10^7 (unless otherwise specified)

(*) For these probabilities of failure the number of samples has been increased to 10^8

ULS stiffened panel – Mode III

	Peak coincidence	*SRSS*	*Turkstra*
f	P_f	P_f	P_f
0	1,50E-07 (*)	3,60E-06	2,57E-05
0.5	1,90E-07 (*)	5,50E-06	2,51E-05
1	1,90E-07 (*)	6,40E-06	2,61E-05
1.5	2,00E-07 (*)	3,80E-06	2,62E-05
2	1,60E-07 (*)	6,70E-06	2,39E-05
2.5	1,80E-07 (*)	4,80E-06	2,44E-05
3	2,00E-07 (*)	4,40E-06	2,63E-05
3.5	1,50E-07 (*)	5,30E-06	2,78E-05
4	1,70E-07 (*)	5,00E-06	2,57E-05
4.5	2,00E-07 (*)	4,20E-06	2,52E-05
5	1,80E-07 (*)	4,80E-06	2,60E-05
5.5	1,90E-07 (*)	4,80E-06	2,63E-05
6	1,90E-07 (*)	4,70E-06	2,88E-05

Number of samples: 10^7 (unless otherwise specified)

(*) For these probabilities of failure the number of samples has been increased to 10^8

ULS stiffened panel – Mode IV – Analytical method			
	Peak coincidence	*SRSS*	*Turkstra*
f	P_f	P_f	P_f
0	7,20E-07 (*)	6,70E-06	3,32E-05
0.5	6,30E-07 (*)	7,80E-06	3,38E-05
1	8,80E-07 (*)	9,20E-06	3,89E-05
1.5	1,22E-06 (*)	8,50E-06	4,42E-05
2	2,23E-06 (*)	2,04E-05	6,62E-05
2.5	4,60E-06	3,37E-05	1,11E-04
3	1,03E-05	5,82E-05	1,73E-04
3.5	1,40E-05	8,82E-05	2,55E-04
4	2,21E-05	1,24E-04	3,43E-04
4.5	3,10E-05	1,66E-04	4,35E-04
5	4,68E-05	2,19E-04	5,22E-04
5.5	5,36E-05	2,59E-04	6,26E-04
6	6,94E-05	3,15E-04	7,46E-04

Number of samples: 10^7 (unless otherwise specified)

(*) For these probabilities of failure the number of samples has been increased to 10^8

ULS stiffened panel – Mode IV – Johnson Ostenfeld			
	Peak coincidence	*SRSS*	*Turkstra*
f	P_f	P_f	P_f
0	2,80E-06	1,96E-05	7,70E-05
0.5	4,40E-06	2,22E-05	7,83E-05
1	4,10E-06	2,88E-05	9,25E-05

1.5	5,30E-06	2,34E-05	9,59E-05
2	1,12E-05	4,20E-05	1,21E-04
2.5	3,28E-05	6,81E-05	1,73E-04
3	6,51E-05	1,16E-04	2,47E-04
3.5	1,12E-04	2,01E-04	3,47E-04
4	1,87E-04	3,01E-04	4,83E-04
4.5	2,87E-04	4,33E-04	6,57E-04
5	3,92E-04	5,95E-04	8,37E-04
5.5	5,13E-04	7,52E-04	1,03E-03
6	6,51E-04	9,70E-04	1,28E-03

Number of samples: 10^7

ULS stiffened panel – Mode V – Analytical method			
	Peak coincidence	*SRSS*	*Turkstra*
f	P_f	P_f	P_f
0	2,40E-07 (*)	2,60E-06	1,67E-05
0.5	1,90E-07 (*)	2,70E-06	1,64E-05
1	3,00E-07 (*)	4,60E-06	1,74E-05
1.5	4,40E-07 (*)	3,40E-06	2,52E-05
2	6,70E-07 (*)	1,04E-05	3,54E-05
2.5	8,00E-07	1,50E-05	5,39E-05
3	1,80E-06	2,21E-05	7,81E-05
3.5	2,40E-06	2,70E-05	1,03E-04
4	3,70E-06	3,57E-05	1,26E-04
4.5	5,00E-06	4,20E-05	1,48E-04
5	5,20E-06	5,47E-05	1,65E-04
5.5	5,10E-06	5,64E-05	1,83E-04
6	6,40E-06	6,33E-05	2,14E-04

Number of samples: 10^7 (unless otherwise specified)

(*) For these probabilities of failure the number of samples has been increased to 10^8

ULS stiffened panel – Mode V – Johnson Ostenfeld			
	Peak coincidence	*SRSS*	*Turkstra*
f	P_f	P_f	P_f
0	1,70E-06	1,53E-05	6,23E-05
0.5	2,80E-06	1,73E-05	6,08E-05
1	2,30E-06	2,10E-05	7,49E-05
1.5	3,00E-06	1,63E-05	7,54E-05
2	3,00E-06	2,70E-05	8,68E-05
2.5	9,70E-06	3,18E-05	1,08E-04
3	1,28E-05	3,99E-05	1,25E-04
3.5	1,66E-05	5,21E-05	1,46E-04
4	2,42E-05	6,23E-05	1,71E-04

4.5	3,31E-05	7,53E-05	2,04E-04
5	3,99E-05	9,41E-05	2,23E-04
5.5	4,93E-05	1,08E-04	2,58E-04
6	5,34E-05	1,27E-04	2,90E-04

Number of samples: 10^7

12.1.4 Corrosion of the plate vs. Corrosion of the stiffeners

Corrosion of the plate						
	ULS unst. plate	*Mode I*	*Mode II*	*Mode III*	*Mode IV (*)*	*Mode V (*)*
f	P_f	P_f	P_f	P_f	P_f	P_f
0	1.12E-04	1.68E-05	1.79E-05	2.74E-05	8.00E-05	6.62E-05
1	1.33E-04	1.38E-05	1.58E-05	2.40E-05	8.97E-05	7.19E-05
2	2.99E-04	1.40E-05	1.95E-05	2.22E-05	1.13E-04	8.09E-05
3	1.76E-03	1.58E-05	3.24E-05	2.55E-05	1.97E-04	1.11E-04
4	6.18E-03	1.38E-05	5.04E-05	2.53E-05	3.39E-04	1.52E-04
5	1.35E-02	1.71E-05	7.85E-05	2.74E-05	4.93E-04	2.02E-04
6	2.27E-02	1.36E-05	8.94E-05	2.34E-05	6.27E-04	2.19E-04

Number of samples: 10^7

Turkstra's rule to combine loads

(*) Jonshon-Ostenfeld formula method

Corrosion of the stiffeners						
	ULS unst. plate	*Mode I*	*Mode II*	*Mode III*	*Mode IV (*)*	*Mode V (*)*
f	P_f	P_f	P_f	P_f	P_f	P_f
0	1.35E-04	1.56E-05	1.80E-05	2.76E-05	8.91E-05	7.02E-05
1	1.27E-04	1.25E-05	1.56E-05	2.33E-05	8.82E-05	6.73E-05
2	1.34E-04	1.65E-05	1.82E-05	2.66E-05	8.82E-05	6.73E-05
3	1.28E-04	1.34E-05	1.62E-05	2.37E-05	8.85E-05	6.77E-05
4	1.33E-04	1.55E-05	1.73E-05	2.69E-05	9.12E-05	7.28E-05
5	1.34E-04	1.46E-05	1.75E-05	2.67E-05	9.46E-05	7.51E-05
6	1.36E-04	1.59E-05	1.83E-05	2.73E-05	1.02E-04	7.75E-05

Number of samples: 10^7

Turkstra's rule to combine loads

(*) Jonshon-Ostenfeld formula method

12.1.5 Effects of the correlation coefficients on the structural reliability

ULS stiffened and unstiffened plates						
	ULS unst. plate	*Mode I*	*Mode II*	*Mode III*	*Mode IV (*)*	*Mode V (*)*
f	P_f	P_f	P_f	P_f	P_f	P_f
0	2.98E-04	1.68E-05	2.17E-05	2.72E-05	1.15E-04	8.79E-05
0.33	3.03E-04	1.38E-05	2.03E-05	2.39E-05	1.17E-04	8.79E-05
0.66	2.99E-04	1.38E-05	1.95E-05	2.23E-05	1.15E-04	8.16E-05
1	2.92E-04	1.56E-05	2.24E-05	2.60E-05	1.18E-04	8.29E-05

Number of samples: 10^7
Turkstra's rule to combine loads
(*) Jonshon-Ostenfeld formula method

12.1.6 Time-dependent reliability analysis

ULS stiffened and unstiffened plates								
			ULS unsifft. plate	*Mode I*	*Mode II*	*Mode III*	*Mode IV (*)*	*Mode V (*)*
Year	t_{corr} *plate*	t_{corr} *stiffeners*	P_f	P_f	P_f	P_f	P_f	P_f
0	0.000	0.000	1.12E-04	1.35E-05	1.58E-05	2.57E-05	7.70E-05	6.23E-05
2	0.000	0.000	1.12E-04	1.35E-05	1.58E-05	2.57E-05	7.70E-05	6.23E-05
4	0.000	0.000	1.12E-04	1.35E-05	1.58E-05	2.57E-05	7.70E-05	6.23E-05
6	0.000	0.000	1.12E-04	1.35E-05	1.58E-05	2.57E-05	7.70E-05	6.23E-05
8	1.088	0.226	2.20E-04	1.68E-05	2.09E-05	2.72E-05	1.07E-04	8.44E-05
10	2.050	0.426	3.05E-03	1.38E-05	3.64E-05	2.39E-05	3.22E-04	1.44E-04
12	2.356	0.490	5.46E-03	1.38E-05	4.47E-05	2.19E-05	4.36E-04	1.60E-04
14	2.454	0.510	6.42E-03	1.58E-05	4.90E-05	2.58E-05	4.82E-04	1.71E-04
16	2.485	0.517	6.76E-03	1.38E-05	5.21E-05	2.53E-05	5.11E-04	1.77E-04
18	2.495	0.519	6.84E-03	1.69E-05	5.64E-05	2.79E-05	5.21E-04	1.90E-04
20	2.499	0.520	6.89E-03	1.38E-05	4.68E-05	2.41E-05	5.03E-04	1.71E-04
22	2.500	0.520	6.92E-03	1.48E-05	5.34E-05	2.72E-05	5.15E-04	1.82E-04

Number of samples: 10^7
Turkstra's rule to combine loads
Corroded thicknesses in mm
(*) Jonshon-Ostenfeld formula method

12.1.7 Comparison with some target reliability indices

	Peak coincidence	**SRSS**	**Turkstra**
	P_f	P_f	P_f
Yielding unstiff. plate – Hogging	4.20E-07	4.76E-07	4.22E-07
Yielding unstiff. plate – Sagging	1.29E-07	1.01E-07	1.56E-08
Yielding stiff. panel – Hogging	2.87E-07	3.51E-07	3.09E-07
Yielding stiff. panel – Sagging	9.44E-08	8.22E-08	6.67E-09
ULS unstiff. Plate (*)	5.15E-06	5.45E-06	5.64E-06
ULS stiff. panel – Mode I	0	0	6.67E-09
ULS stiff. panel – Mode II	0	0	1.89E-08
ULS stiff. panel – Mode III (*)	0	0	2.86E-06
ULS stiff. panel – Mode IV (*)	4.46E-06	4.08E-06	2.86E-06
ULS stiff. panel – Mode V (*)	2.86E-06	2.62E-06	1.60E-06
Fracture	1.16E-05	1.14E-05	1.87E-5

Number of samples: $3*10^8$
(*) Jonshon-Ostenfeld formula method

References for figures

All the figures without the reference have been produced by the author.

Cover picture

The cover picture is unrelated to the project

http://www.equatorialoil.com/Oil_production.html

Chapter 1

Figure 1 – http://www.modec.com/fps/fpso_fso/projects/stybarrow.html

Figure 2 – http://www.corrosionlab.com/Failure-Analysis-Studies/29173.fatigue-cracking.crude-unit.htm and http://www.lemschout.net/psc/$cthickm.htm

Figure 5 – http://www.amteccorrosion.co.uk/corrosionresistantship.html and http://www.ndt.net/article/v07n07/ginzel_r/ginzel_r.htm

Figure 6 – http://www.supremeship.com/utm.htm

Figure 7 – M. Kaminski, slide from the "Numerical Methods" course, TU Delft, 2012

Figure 9 – http://www.viking-systems.net/industries/topsides-module-supports

Chapter 3

Figure 1 – Universities of Glasgow and Strathclyde, "Structural Reliability Framework for floating production, storage and offloading vessels/floating surface units", Research Report 429, 2006

Chaper 4

Figure 4 – O. Huges, J. B. Caldwell, "Plate bending", Ship Structural Analysis and Design (chapter 9), SNAME, 2010

Figure 5 – http://www.nptel.ac.in/courses/Webcourse-contents/IIT-ROORKEE/strength%20of%20materials/lects%20&%20picts/image/lect9/lecture9.htm

Figure 7 – J. K. Paik, "Large deflection behaviour and ultimate strength of plates", Ship Structural Analysis and Design (chapter 13), SNAME, 2010

Figure 8 – J. K. Paik, "Large deflection behaviour and ultimate strength of plates", Ship Structural Analysis and Design (chapter 13), SNAME, 2010

Figure 9 – J. K. Paik, "Large deflection behaviour and ultimate strength of plates", Ship Structural Analysis and Design (chapter 13), SNAME, 2010

Figure 11 – D. Beghin, “Reliability-based structural design”, Ship Structural Analysis and Design (chapter 5), SNAME, 2010

Figure 12 – D. Beghin, “Reliability-based structural design”, Ship Structural Analysis and Design (chapter 5), SNAME, 2010

Figure 13 – J. K. Paik, “Large deflection behaviour and ultimate strength of stiffened panels”, Ship Structural Analysis and Design (chapter 15), SNAME, 2010

Figure 14 – J. K. Paik, “Large deflection behaviour and ultimate strength of stiffened panels”, Ship Structural Analysis and Design (chapter 15), SNAME, 2010

Figure 15 – J. K. Paik, “Large deflection behaviour and ultimate strength of stiffened panels”, Ship Structural Analysis and Design (chapter 15), SNAME, 2010

Figure 16 – J. K. Paik, “Large deflection behaviour and ultimate strength of stiffened panels”, Ship Structural Analysis and Design (chapter 15), SNAME, 2010

Figure 17 – J. K. Paik, “Large deflection behaviour and ultimate strength of stiffened panels”, Ship Structural Analysis and Design (chapter 15), SNAME, 2010

Figure 18 – J. K. Paik, “Large deflection behaviour and ultimate strength of stiffened panels”, Ship Structural Analysis and Design (chapter 15), SNAME, 2010

Figure 19 – Y. Okumoto, Y. Takeda, M. Mano, T. Okada, “Design of ship hull structures, A practical guide for engineers”, Springer, 2009

Figure 20 – Y. Okumoto, Y. Takeda, M. Mano, T. Okada, “Design of ship hull structures, A practical guide for engineers”, Springer, 2009

Figure 21 – J. Paik, “Ultimate Strength of Plates and Stiffened Panels”, Presentation given at the LRET Research Collegium, Southampton, 11 July – 2 September 2011

Figure 22 – J. Paik, “Ultimate Strength of Plates and Stiffened Panels”, Presentation given at the LRET Research Collegium, Southampton, 11 July – 2 September 2011

Chapter 5

Figure 1 – P. Aalberts, J. van der Cammen, M. L. Kaminski, “The Monitas system for the Glas Dowr FPSO”, OTC 20873, 2010

Chapter 6

Figure 2 – Bruno Vasconcelos de Farias, Theodor Antoun Netto, “FPSO hull structural integrity evaluation via Bayesian updating of inspection data”, Ocean engineering, 2012

Figure 3 – Bruno Vasconcelos de Farias, Theodor Antoun Netto, “FPSO hull structural integrity evaluation via Bayesian updating of inspection data”, Ocean engineering, 2012